Beatriz María Almarza Galdón

An evaluation of in situ measurement methods of K'$_o$ in sensitive clays

With focus on push-in earth pressure cells and hydraulic fracturing

Master's thesis in Geotechnics and Geohazards
Supervisor: Steinar Nordal

July 2020

Master's thesis

NTNU
Norwegian University of Science and Technology
Faculty of Engineering
Department of Civil and Environmental Engineering

NTNU
Norwegian University of
Science and Technology

Beatriz María Almarza Galdón

An evaluation of in situ measurement methods of K_0' in sensitive clays

With focus on push-in earth pressure cells and hydraulic fracturing

Trondheim, July 2020

MASTER THESIS: TBA4900
Main supervisor: Prof. Steinar Nordal
Co-supervisor: Dr. Jean-Sébastien L'Heureux

Department of Civil and Environmental Engineering
Norwegian University of Science and Technology (NTNU)

NTNU – Trondheim
Norwegian University of
Science and Technology

NORWEIGAN UNIVERSITY OF SCIENCE AND TECHNOLOGY
DEPARTMENT OF CIVIL AND ENVIRONMENTAL ENGINEERING

Report title: An evaluation of in situ measurement methods of $K_0^{'}$ in sensitive clays. With focus on push-in earth pressure cells and hydraulic fracturing	Date: 01.07.2020 Number of pages (incl. Appendices):			
	Master' thesis	X	Project's thesis	
Name: Beatriz Almarza Galdón				
Professor in charge/supervisor: Steinar Nordal (NTNU)				
Other external professional contacts/supervisors: Jean-Sébastien L'Heureux (NGI)				

Abstract:

The coefficient of earth pressure at rest is an important geotechnical parameter for both laboratory testing and design. A literature review on in situ determination of $K_0^{'}$ is presented with main focus on push-in earth pressure cells and hydraulic fracturing.

A testing program with push-in cells and a new hydraulic fracturing device was performed at Tiller-Flotten ''Norwegian Geo-Test Sites'' (NGTS), located outside the city of Trondheim. The test site is characterized by the presence of quick clay below 8 m depth. Data from previous investigations by other in situ investigation methods at the same site are collected and compared to the results obtained in the current study by using push-in cells and hydraulic fracturing. The main finding is that the K-0 values from the earth pressure cells fit well with what is expected to be correct values, while the hydraulic fracturing values are more uncertain, and the procedure remains a challenge.

Key words:	
1.	Earth pressure at rest
2.	Hydraulic fracturing
3.	Total stress cells
4.	In situ testing
5.	Quick clay

(sign.)

Preface

This master thesis is written under the Master Program in Geotechnics and Geohazards at NTNU. The topic was proposed by Dr. Jean-Sébastien L'Heureux and has been carried out in collaboration with NGI as a part of the Norwegian Geo-Test Site (NGTS) program. One of the main research activities under the NGTS project is the determination of lateral stress coefficient at rest (K_o') by in situ field measurements. This project thesis is focused on evaluation of hydraulic fracturing and push-in total stress cells as reliable methods for evaluation of K_o' fro in situ measurements.

Trondheim, July 1st, 2020

Beatriz Almarza Galdón

Acknowledgment

I would like to express my gratitude to my supervisor Professor Steinar Nordal for his support during the development of this master thesis project, but also for the trust put on me during the three years I have been part of Geotechnical division at NTNU. Special acknowledgment to Dr. Jean-Sebastian L'Heureux for proposing this topic and giving me the opportunity to enter in contact with NGI.

Secondly, I would like to thank technical staff form NTNU, Karl Ivar Volden Kvisvik, Espen Andersen, Frank Stæhli and Per Asbjørn Østensen, for their help to accomplish all the practical work. Thank for your infinite patience.

Aleksander Sæthereng Gundersen, project engineer at NGI, has contributed to this master thesis with guidance during the interpretation of test results.

To all study fellows, professors and colleagues at the Geotechnical Division who have contributed to make my return to university one of the best decisions I made in the last years.

Finally, this master thesis is dedicated to my family, especially those who have "suffer" most my implication in this master's degree: my husband Tono for supporting me, and my two little ladies, Celia and Dácil, who remind me that we never should forget to look life through child eyes.

Summary and conclusions

The determination of the in situ stress state within the frame of any geotechnical problem is crucial. The coefficient of earth pressure at rest (K_0') is an important parameter for numerical analysis and laboratory test design. In situ vertical stress is easily calculated by knowing depth and specific gravity of the material forming the soil. However, the determination the in situ horizontal stress is a challenging task as it has been stated by numerous authors work as found in the literature review fulfilled within this master thesis. The determination of K_0' is still a pending task within geotechnical engineering since both in situ or laboratory testing induce, in major or minor degree, a disturbance on the original soil stress state. The repeatability and reliability of the results outcasted by in situ and laboratory methods seems not to be enough.

Hence many efforts have been made to define an empirical relationship between soil parameters, (which determination is reliable by well establish field and laboratory methods) and the coefficient of earth pressure at rest. Nevertheless, it is difficult to define a general expression or equation since there is a high degree of dependence on soil properties and local conditions as stress history or time. The uncertainty is then larger in the case of overconsolidated soils.

A general description of Tiller-Flotten Geo-Test Site is presented. A summary of strength and index parameters from previous work found in literature are summarized and used as input to determine K_0' by mean of correlation methods.

Push-in earth pressure cells have been installed to measure lateral total stress as well as in situ pore pressure. Each cell has been installed at the same borehole to draw a profile. In total 4 measurement have been performed, two at 5 m in the overconsolidated Unit IIa, and two at 7.5 m in the transition zone from Unit IIa to Unit IIb where the consolidation grade begins to decrease. The installation of the cells is uncomplicated, and no disturbance of the instrument is observed after removal from ground. In general, in situ lateral stress derived from push-in cells show low scatter and fit well with expected values at investigated depths. Pore pressure registered are close to the in situ estimated pore pressure at that investigation depth, but values may be taken with precaution. Unfortunately, the logging compliance failed at the end of the second installation maybe due to condensation inside the box. The equipment was sent to repair and due to COVID-19 crisis, the repairing

of the electronic compliance of push-in earth pressure cells suffered a big delay, precluding the availability of the equipment inside this master thesis schedule. Hence the testing program had to be cancelled. Results from push-in earth pressure cells show that the method is potentially reliable and stable.

Hydraulic fracturing test is presented as a potential method for the in situ measurement of horizontal stress. The literature suggests good results in normally consolidated clay deposits, but no previous experiences are available in Norwegian high sensitive clays. A detailed description of the equipment and the procedure followed during the execution of the test are presented. A deep review of the collected data by the author during spring of 2019 is done. These data were taken at 6 different boreholes with investigation depths going from 5 to 17 m, including a second test attempt at same investigation depth for depths 5, 10 and 15 m. In general, K_0' obtained by hydraulic fracturing are between 20 and 40% higher than those previously reported from dilatometer, CPTU or by the empirical correlation for Norwegian clays. Those higher values could indicate that perhaps the horizontal stress is not being measured, i.e. no vertical cracks open when injecting the fluid in the ground. Cracks could be opened following weak horizontal or inclined surfaces thus the closing pressured register would not correspond to the horizontal stress.

The hydraulic fracturing set up was modified by adding a new syringe pump to avoid stopping the injection cycling for refilling. Also, two injection spade shaped nozzles (designed at NTNU) were tested, looking to create a preferential vertical plane to contribute to the formation of a vertical crack during the injection. It is difficult to extract any reliable conclusion from results obtained since no evidence of what is the mechanism is taking place around injection nozzles.

Contents

CONTENTS

List of figures

LIST OF FIGURES

LIST OF FIGURES

List of tables

List of Abbreviations and Symbols

Acronyms

Symbol	Description	Units
$CPT(U)$	Cone Penetration Test (with pore pressure measurements	
CRS	Constant Rate of Strain Oedometer test	
DMT	Dilatometer	
NGI	Norwegian Geotechnical Institute	
$NGTS$	Norwegian Geo-Test Sites	
OCR	Overconsolidation ratio	
$SCPT$	Seismic Cone Penetration Test	
$UNIS$	The University Centre in Svalbard	

Greek Symbols

Symbol	Description	Units
β	Soil type parameter, dilatometer -	-
γ	Unit weight	kN/m^3
ϕ'	Drained friction angle	°
σ_h'	Effective horizontal stress	kPa
σ_h	Total horizontal stress	kPa
σ_v'	Effective vertical stress	kPa
σ_v	Total vertical stress	kPa
σ_t	Tensile strength	kPa
σ_{h0}'	Initial effective horizontal stress	kPa
σ_{v0}'	Initial effective horizontal stress	kPa
σ_θ	Tangential stress	kPa
σ_r	Radial stress.	kPa
σ_1	Major principal total stress	kPa
σ_3	Minor principal total stress	kPa
σ_1'	Major principal effective stress	kPa
σ_3'	Minor principal effective stress	kPa
σ_p'	Vertical pre-consolidation pressure	kPa
ν	Poison modulus	-

LIST OF ABBREVIATIONS AND SYMBOLS

Roman symbols

Symbol	Description	Units
a	Attraction	kPa
c	Cohesion	kPa
C_α	secondary compression index	
C_c	compression index	
E	Elastic modulus	kPa
E_d	Dilatometer modulus	kPa
G	Shear modulus	kPa
I_d	Material index, dilatometer	-
I_L	Liquidity index	-
I_P	Plasticity index	%
K_o	Coefficient of earth pressure at rest for total stresses	-
K_o'	Coefficient of earth pressure at rest for effective stresses	-
K_D	Lateral stress index, dilatometer	-
K_{oNC}'	Coefficient of earth pressure at rest for normally consolidated clay	-
K_{oOC}'	Coefficient of earth pressure at rest for overconsolidated clay	-
p_0	Initial pressure value, dilatometer	kPa
p_1	Inflated pressure value, dilatometer	kPa
p_2	Deflated pressure value, dilatometer	kPa
$P_{closure}$	Fracture closing pressure	kPa
$P_{fracture}$	Fracturing or breakdown pressure	kPa
P_o	External pressure outside a cavity	kPa
P_i	internal pressure inside a cavity	kPa
p_{wi}	Initial excess water pressure	kPa
r_e	External radius of a cavity	m
r_i	Inner radius of a cavity	m
s_u	Undrained shear strength	kPa
u_0	Initial pore pressure	kPa
w	Water content	%
w_L	Liquid limit	%

Chapter 1

Introduction

1.1 Background and Problem Formulation

For any geotechnical problem, assessing the stress state of the soil is crucial. The more knowledge about the stress state, the bigger chance to improve investigation methods, actuation, soil model constructions, pile foundation systems, retention structures, slope stability analyses and better input for numerical simulations (Ku and Mayne, 2015).

The in situ stress state could be expressed into a horizontal and a vertical stress component. The ratio between horizontal and vertical stress is referred as K_0'. The vertical stress component is assumed to be well defined by the overburden. On the other hand, the determination of the horizontal stress component is affected by several uncertainties and it still represents a challenge in Geotechnical Engineering. These uncertainties are related, first to the fact there is a poor understanding of the factors affecting the in situ stress state of the soil and secondly, in situ and laboratory methods usually alter the stress situation, hence the measured horizontal stress is not the real in situ horizontal stress (Hamouche *et al.*, 1995; Lindgård and Ofstad, 2017). In this report, push-in earth pressure cells and hydraulic fracturing would be evaluated as reliable in situ method for measuring K_0'.

The initial stress condition is a result of stress history. Stress history affects the overconsolidation level, the K_0' and the undrained strength. Initial stress values are the result of gravitational loading, tectonic activity, weathering, erosion and other processes

like diagenetic swelling of minerals (Chowdhury, 1978; J. H. Schmertmann, 1985)(J. Schmertmann, 1985). In the case of erosional or ice removal unloading, considerable strain energy will be stored in the clays as reported in Brooker and Ireland (1965). The stored strain energy subsequently will be released if the bonds are destroyed as a result of weathering (Bjerrum, 1967b; Yang, 1987). A high K_0' condition may cause progressive movements which can result in reaching residual shear strength conditions and progressive failures (Bjerrum, 1967b; Leroueil, 2004).

In situ stress state values are also of quite importance when approaching slope stability analysis by finite elements method. If excavated slopes are to be modelled, the initial stress distribution in the horizontal ground before excavation is clearly defined by the K_0' condition (Hwang, Dewoolkar and Ko, 2002). It seems that K_0' values influences the calculated shear strength values in a direct proportion and the higher lateral stresses take place at the toe of the slope (Duncan, J.M.; Dunlop, 1968; Hwang, Dewoolkar and Ko, 2002). An analysis carried out on excavated slopes with strength anisotropy by mean of finite elements method is presented in Hwang, Dewoolkar and Ko (2002), showing that relationship between horizontal and vertical stresses increases significantly at the toe of the slope (Figure 1- 1). Palladino and Peck (1972) reported a study on slope failure during a highway construction on overconsolidated clay materials. Slopes were gentle and failing in the short-term due to the high initial stress within the soil mass. Constructions methods applied had to accomplish to minimize disturbance of the soil mass and provide confinement at the same time to avoid lateral deformation caused by release of lateral stress.
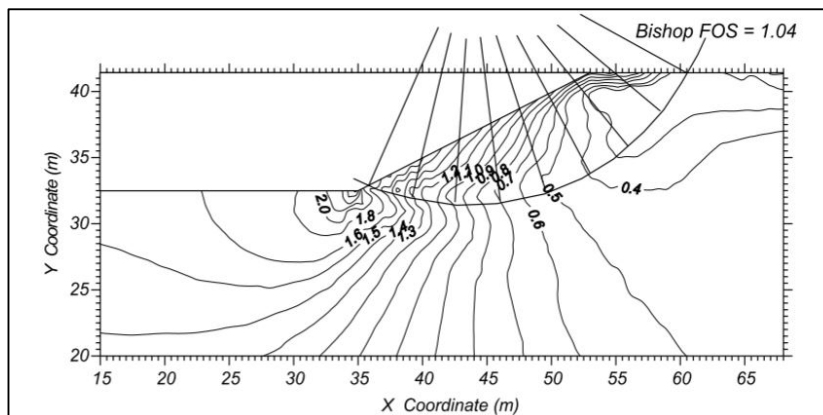
Figure 1- 1 Stress ratio distribution at an excavation depth of 9 m (Hwang, Dewoolkar and Ko, 2002)

Assumptions regarding Ko' has a significant influence on results from advanced numerical analysis of deformations under footings, embankments and in connection with excavations. Improving our ability to measure and determine K0' is also for this reason an important challenge for Geotechnical engineering.

This chapter goes through the motivation and objectives of the problem as well as for the limitations during the elaboration of the present report. Later the selected approach to the problem is described. Finally, the structure of the report is presented.

1.2 Objectives

The objectives of the present project are summarized below:

a) Present a literature review on the concept of coefficient lateral earth pressure at rest (K_0') and the processes affecting its evolution along the geological history of the soil.

b) Provide a general presentation on the difference in situ, laboratory and empirical methods to determine K_0'. A more extensive description of hydraulic fracturing method and lateral earth pressure cells is presented.

c) Present a general geotechnical description and classification of the Tiller-Flotten geo-test site.

d) Test a new hydraulic fracturing set-up, designed to open a preference zone to formation of vertical cracks. The prototype will be tested at Flotten test site and results will be compared with previous pilot experiments.

e) Perform and evaluate in situ measurements by earth pressure cells and compare with previous results at Tiller-Flotten geo-test site.

f) Make a review about the methods suitable of being applied to determine K_0' from in situ measurement in the case of sensitive clays.

1.3 Limitations

Main limitation within the accomplishment of the objectives presented above has been related to time .All work at NTNU was stopped from March to May 2020 which made difficult to perform previous test at the laboratory to test the new injection nozzles for

hydraulic fracturing set up. Finally, just a quick test on ambient conditions was performed to check the equipment before setting it up at field. Thus, the new injection nozzles are only quickly tested on field.

A second limitation was the unfortunate failure of logging compliance of push-in cells set up. It took longer than two months for the provider to propose a solution to fix the electronics and finally, NGI decided to send the logging box back to UK for repairing at the beginning of June of 2020.

1.4 Problem Formulation and Approach

To accomplish objectives from (a) to (c) in previous list, a deep study on technical literature related to the topic has been carried out. Main sources employed for the literature review has been NTNU and NGI libraries.

Objective (d) will be approached by performing and evaluating field investigation with hydraulic fracturing device owned by NGI. The equipment was previously tested in spring og 2019 and, based on obtained results, a modification on the geometry of the injection tips is done by NTNU. A deep study on the different formulations governing hydraulic fracturing mechanism is also presented.

Results obtained from pilot studies are to be analysed and compared with previous investigation on K_0' by different techniques. A comparative chart will be presented with data available from literature and previous work done on K_0' determination at Tiller-Flotten site and data obtained in field work.

Objective (e) is related to earth pressure cells field test. A new device borrowed from NGI is tested at Tiller-Flotten geo-test site. A complete profile from 5 to 12 m depth is planned in order to compare results with the Götzl earth cell pressure tests by Lindgård and Ofstad (2017). Finally, and based on obtained results, a review on report published by NGI (Lunne and L'Heureux, 2016) on recommendations for in situ determination of horizontal stresses on quick clays is proposed.

1.5 Structure of the report

The present report is divided in six chapters. Chapter 2 is focused on definition of K_0' and the processes governing its evolution. Moreover, a wide literature review is presented, focused on previous research on in situ, laboratory, and correlation methods for the determination of K_0'. For that purpose, a technical description of the methods and background formulation are also presented. Focus is set on hydraulic fracturing and push-in earth pressure cells.

Chapter 3 presents a detailed description of the Tiller-Flotten test site based on literature review.

Chapter 4 is dedicated to the pilot experiments program performed during 2019 and 2020 at Tiller-Flotten test site. A detailed description on the procedure followed is presented. Chapter 5 is a summary of the results obtained on field testing. All results are compared with previous data from in situ and empirical methods for determining K_0' reported under NGTS project. NGI has published the data via DataMaps web (*https://www.geocalcs.com/datamap*). More info about this data base and data published by NGI is found on J.P.Dohertya *et al.* (2018) and L'Heureux and Lunne, (2020) Discussion of the presented results is to be presented on Chapter 6. Finally, Chapter 7 is a summary of main important findings and the recommendation of further work on the topic.

Chapter 2

Theory and background

2.1 Introduction

The following chapter is divided in two different sections. A first one in which definition of "earth pressure coefficient at rest" (K_0') is given together with a deep literature research on processes governing the evolution of K_0'. Secondly, a review of different methods for determining K_0' is developed, including field, laboratory, and empirical approaches.

2.2 Definition of K_o'

The coefficient of lateral earth pressure at rest is an important geotechnical parameter that defines the static stress state of a soil mass. The concept of an at rest state earth coefficient was reported for first time by Donath in 1891 (Hamouche *et al.*, 1995). This coefficient is defined as the ratio between effective horizontal stress and effective vertical stress (Das and Sobhan, 2012) as expressed in equation (2. 1):

$$K_o' = \frac{\sigma_h'}{\sigma_v'} = \frac{\sigma_h - u_o}{\sigma_v - u_o} \tag{2.1}$$

Where σ_v' is the effective vertical stress, σ_h' is the effective horizontal stress, σ_v is total vertical stress, σ_h is total horizontal stress and u_o is the in situ pore pressure.

It worth to mention that K_0' is defined for vertical loading and zero lateral strains conditions.

2.3 Processes governing the evolution of K_o'

In situ stress conditions of the soil varies with time, affecting structure and properties of the soil. These changes play an important role in the evolution of the value for K_0' (Sivakumar *et al.*, 2004). In this section, a review on the different processes governing the evolution of K_0' is presented.

2.3.1 Stress history

Numerous studies confirm that the relationship between vertical and horizontal stress values in a soil is dependent on the stress history of the soil itself (Brooker and Ireland, 1965; Mayne and Kulhawy, 1982) as it is schematically represented in Figure 2- 1.
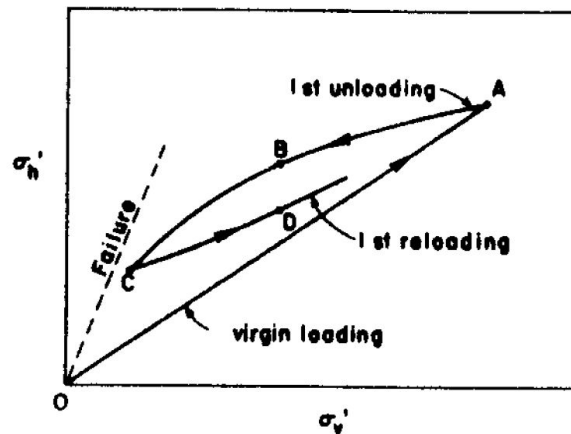
Figure 2- 1 Simplified stress history of a soil (Mayne and Kulhawy, 1983)

From Figure 2- 1 it is possible to define two types of soil depending on stress history. Soils suffering only primary loading or virgin loading (branch OA) are defined as normally consolidated soils. If soil suffers vertical unloading (branch ABC) it is named as overconsolidated soil. In this case, the soil has suffered a higher vertical stress condition

than the actual one. The maximum vertical load experienced by the soil during its geological history is called pre-consolidation pressure (σ_p'). The ratio relating pre-consolidation pressure and the actual in situ vertical stress is called overconsolidation ratio and is expressed in equation (2. 2).

$$OCR = \frac{\sigma_p'}{\sigma_v'}$$
(2. 2)

The geological process corresponding to the first loading and unloading branch in Figure 2- 1, could be related to erosional processes, glacial melting or rising of groundwater level by which soil becomes overconsolidated. In the particular case of Scandinavia and Canada, this it related to the glaciation and posterior ice melting (Reite, A.J.; Sveian, H.; Erichsen, 1999; L'Heureux, Lindgård and Emdal, 2019).
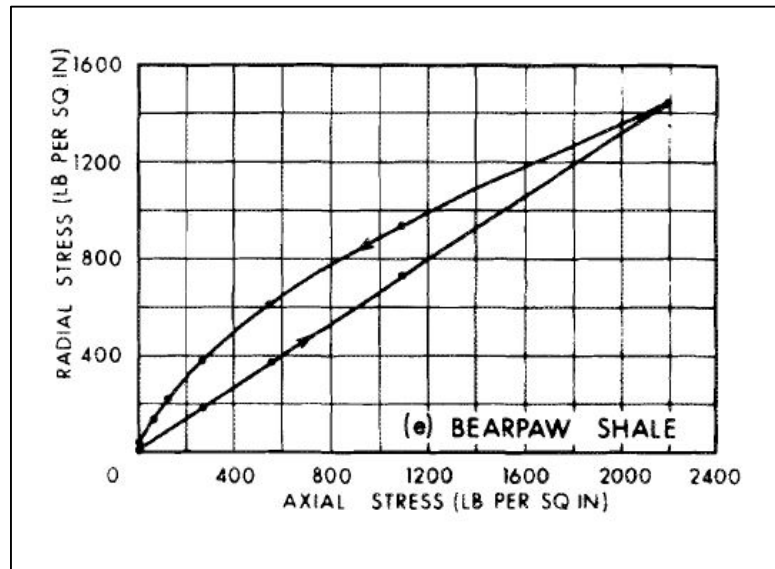
Figure 2- 2 Relationship between axial and radial stress (Brooker and Ireland, 1965)

Brooker and Ireland (1965) performed an experimental study on five different clay specimens to confirm K_0' dependency with stress history. A series of compression tests were completed in an apparatus which allowed to measure and adjust lateral pressures to satisfy zero lateral strains condition. A first loading and unloading cycle was applied for each clay and the relationship between vertical and horizontal stress plotted. Results showed in Figure 2- 2 correspond to the OAC branch in Figure 2- 1. Relationship between σ_v' and σ_h' is linear during the virgin curve (first loading), thus K_0' is renamed as K_{NC0}' to

indicate that it is related to a normally consolidated soil. During vertical unloading phase, it could be observed that the relationship between vertical and horizontal stress is no longer linear, and horizontal stress decreases slower than vertical stress does. This situation corresponds to ABC branch in Figure 2- 1 and in this case, $K_0^{'}$ is renamed as $K_{oOC}^{'}$ to denote the soil is overconsolidated. It could be observed that first overconsolidation process leads in higher values of K_{oOC}' than K_{oNC}'.

This dependency of $K_0^{'}$ with stress history presented by Brooker and Ireland (1965) was the starting point to define empirical correlations based on overconsolidation ratio of soils as it will be presented in section 2.6.

2.3.2 Ageing

As previously mentioned, the evolution of K_0' is dependant on *OCR*, i.e. of pre-consolidation stress (Brooker and Ireland, 1965; Mayne and Kulhawy, 1982; Hamouche *et al.*, 1995) which is mainly related to the mechanical unloading. However, it is possible that normally consolidated soils present slightly overconsolidated characteristics even when no mechanical unloading has taken place during the geological history of the soil deposit (Bjerrum, 1967a) (Figure 2- 3). In these cases, the pre-consolidation effect is referred as apparent pre-consolidation or quasi-consolidation (Won and Chang, 2007; Ma, Muhunthan and Xie, 2014).

These mechanisms are a combination of time-volumetric strains at a constant effective stress, alteration clay minerals, ions in pore water due to changes in concentration and/or valence, precipitation/cementation, and mineral leaching/internal erosion. Secondary compression is to be the dominant mechanism in the development of the apparent pre-consolidation pressure (Bjerrum, 1967a; Hanzawa and Kakuichiro, 1983; Ma, Muhunthan and Xie, 2014).
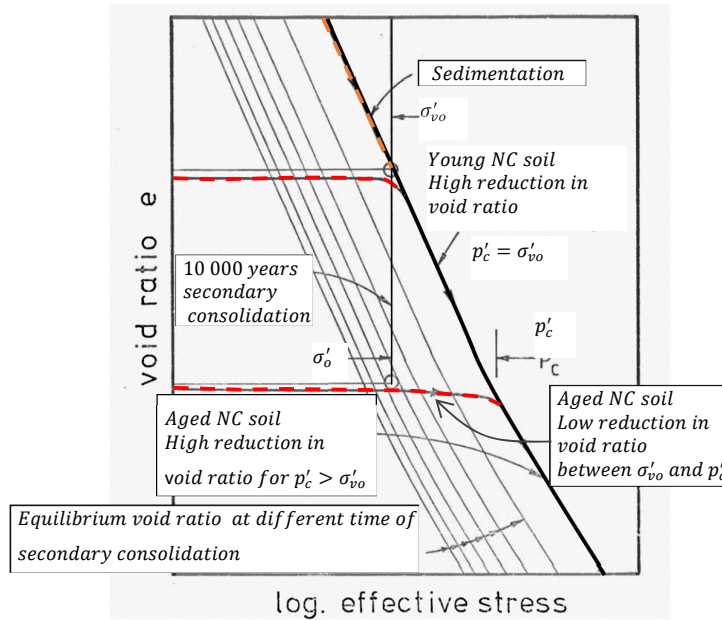
Figure 2- 3 Geological history and compressibility of "young" and "aged" normally consolidated soil (after Bjerrum (1967), slightly modified by the author)

Secondary consolidation

Secondary consolidation, also referred as secondary compression or creep, is the process of compression of the soils under constant vertical load after the completion of primary consolidation. This process consists in a slow rearrangement of grain particles to reach a more stable configuration under a vertical constant load acting during hundreds or thousands of years (Bjerrum, 1967a). Whereas the rate of primary consolidation is controlled by hydrodynamics, the rate of secondary compression is controlled by the viscous resistance of the soil structure (Soga, 2005). The one-dimensional compression test or odometer test is the mean to simulate soil consolidation process since non lateral stress is allowed. But how is the evolution of horizontal stress under these conditions was stated by Schmertrmann in his technical note of 1983 (Schmertmann, 1983).

Some authors report a hardening of the soil and the subsequent increase in shear strength or cohesion due to bonding as reported by Bjerrum, (1967a), Yasuhara and Syunji (1983) and Brown (1985). Consequently, less lateral stress is supported by the soil and $K_0^{'}$ decreases. On the other hand, some authors refer to the structural composition of a clay as an alternation clay minerals and bonded water layers. Under constant vertical loading conditions, this structure leads to a softening of the soil and it will be less capable to support

the vertical load with increasing of lateral stress, i.e. $K_0^{'}$ will increase. Results confirming this phenomenon are reported by Kavazanjian and Mitchell (1984) and Soydemir (1984)as mentioned in Brown (1985). As a third approach, the soil could be considered as an elastic medium under one-consolidation process since Poisson's ratio is constant (Schmertmann, 1983) although no evidence is reported.

Further, some authors as Kavazanjian and Mitchell (1984) set the hypothesis that the evolution of stress state in a soil should converge to the minimum energy state, i.e. $K_0^{'}=1$. This leads to different behaviour of lateral earth pressure for normally and overconsolidated soils. After a thorough analysis of data from testing program in San Francisco Bay mud and kaolinite specimens, Lacerda (1976) could not confirm this statement, but it was conclude that for a young, normally consolidated soil, $K_0^{'}$ does increase with time. Posterior studies were published in order to estimate in what degree $K_0^{'}$ increases during secondary compression for normally consolidated soils. Holtz, Jamiolkowski and Lancellotta (1987) presented results from a temperature-controlled compression test program but no significative variation in $K_0^{'}$ were found.

Mesri and Hayat (1993) presented a study on evolution of $K_0^{'}$ along different compression stages from laboratory experiments performed on undisturbed specimens of clays deposits as well as granular soils. In order to evaluate the evolution of $K_0^{'}$ during secondary compression, 11 clays were tested in triaxial and oedometer cells, under laterally constrained conditions. Under the assumption of a reduction of void ratio occurs during secondary compression (see Figure 2- 4), a $K_0^{'}$ expression based on C_α/C_c was led as expressed in eq. (2. 3)

$$K_o = K_{oNC} \left(\frac{t}{t_p} \right)^{C_\alpha/C_c} \tag{2. 3}$$

where K_{oNC} is the coefficient of earth pressure after primary consolidation is over, t_p is the time required to reach the end of primary consolidation, $C_\alpha = \Delta e/(\Delta \log t)$ is secondary compression index, $C_c = \Delta e/(\Delta \log \sigma_v')$ is the compression index. The use of C_α/C_c to evaluate secondary compression in one-dimensional compression lab-test was first introduced by Mesri and Castro (1989) due to its low variability for different soil types. The comparison between computed and measured values of $K_0^{'}$ showed a scatter mainly related to long term effects during testing, although a small reduction in $K_0^{'}$ is derived from σ_h' *versus* σ_v' slope.

11
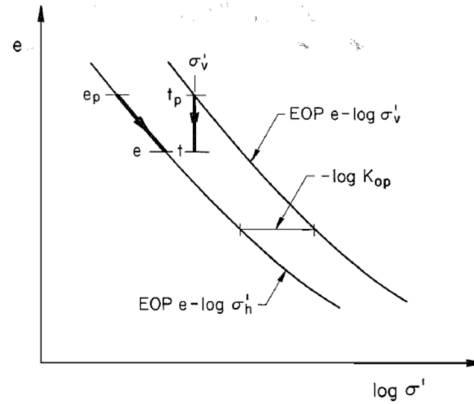
Figure 2- 4 Soil behaviour assumed in formulation of eq.(2. 3). e_p is void ratio at the end of primary consolidation (after Mesri and Hayat, 1993)

Chemical bonding

As pointed by Bjerrum (1967a), secondary compression is not the only mechanism that could lead to a reduction of compressibility. Historically, the most accepted theory used to explain ageing effects is the interparticle bonding. Terzaghi originally referred to a bond strength in connection with the presence of an apparent pre-consolidation pressure in the field (Schmertmann, 1991). Generally, this mechanism has been thought of as type of cementation, which would increase the cohesion of a soil without affecting its friction angle (Soga, 2005).Several authors reported a strengthen of clay samples in the laboratory under unchanged stress conditions, as well as an increase in brittleness (Bjerrum, 1967a; Leroueil and Vaughan, 1991). This is shown in Figure 2- 5 where increase on shear strength from S_{uB} to S_{uP} is due to soil structure.

This phenomenon could be only related to the development of cohesive bonds between particles caused by a variety of processes lumped together under the concept of chemical bonding (Bjerrum, 1967a; Terzaghi, Peck and Mesri, 1996). The suggested processes involved with chemical bonding in clays include weathering, leaching, divalent cation adsorption, cold welding, exchange of cations and precipitation of agents (Bjerrum, 1967b; Won and Chang, 2007; Quigley, 2008). Following Bjerrum's criteria, in the present work, three main processes are described for young Norwegian clays:

1. cold-welding of mineral contact points between particles

2. exchange of cations

3. precipitation of cementing agents
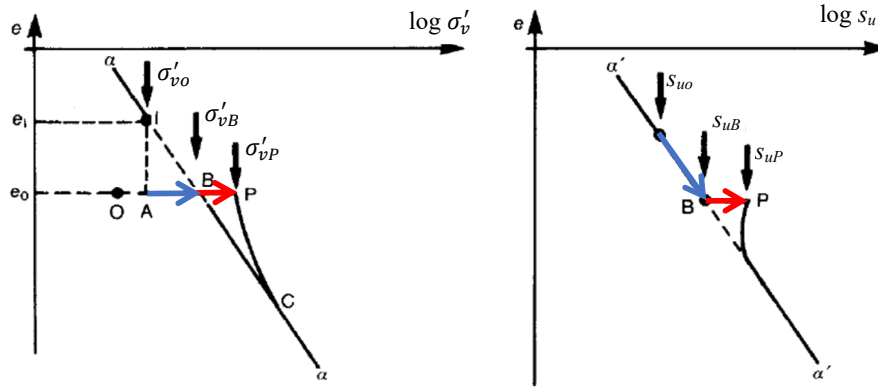
Figure 2- 5 Normal consolidation of clay soil and the effects of secondary compression (blue arrow) and structure (red arrow) on void ratio, pre-consolidation pressure and undrained shear strength (edited from Leroueil and Vaughan, (1991))

From the three processes listed above, exchange of cations is the most important in the case of Norwegian clays (Bjerrum, 1967a). Clay is composed by flake-shaped phyllosilicates which have a negative surface charge due to isomorphous substitution and/or charged mineral edges. In the case of Norwegian clays, chlorite and illite are the most common clay minerals and they are characterized by a t-o-t structure or octahedral sheet. Cations present in pore water, as potassium (K^+), sodium (Na^+) or calcium (Ca^{+2}) neutralize negative surface charge of clay particles and work as bond between t-o-t sheets. Clay suffer transformations due to ionic exchange originated by variation in the relative concentration of ions in pore water. This could lead to a change in the composition of clay minerals and, in consequence, in the geotechnical properties of the clay in terms of plasticity, compressibility and strength. In the case of marine clays, Na^+ acts as bonding cation. If the soil deposit is subjected to percolating rainwater flow, Na^+ will be removed gradually in a process called leaching. Concurrently, O_2 and CO_2 dissolved in rainwater reduce the value of pH of pore water arising the disintegration of clay minerals in a process called hydrolysis. In Norwegian clays, rich in felspar and mica, release of K^+ from mineral lattice is dominant. The substitution of Na^+ by K^+ induces an increase of strength of soils and a reduction of compressibility as described in laboratory test on lean clay treated with KCl presented by Bjerrum, (1967a).

Cementation is the third of the processes related to chemical bonding. Cementation is the process of lithification of loose unconsolidated sediments. It is related to the strengthen or creation of bonds in the clay structure and not related to the alteration in mineral

composition it-self. As remarked by Bjerrum (1967a), this is not the common case in Norwegian clays, but post-glacial soft clays from eastern Canada, which geotechnical properties as plasticity, water content, sensitivity and mineralogy are similar, show higher shear strength. Fischer, Andersen and Moum, (1978) reported a test program on Drammen clays summited to artificial cementation by calcium carbonate precipitation. An increase on apparent OCR of about 1.7 for soil samples was observed in samples that had an increase in $CaCO_3$ between 2.2 and 3.9%. *OCR* values of 1.6 is reported by Bjerrum, (1967a) as well as $CaCO_3$ up to 3.1%. The effect of cementation in undrained shear strength is increased by 40% in the Drammen clay as reported by Fischer et al. (1978).

Change of static groundwater level

Important overconsolidation effects may be induced by changes in groundwater level. These effects are in general smaller than the effects due to secondary consolidation and may be insignificant (Parry, 1975). A soil submitted to groundwater changes is presented in Figure 2- 6.
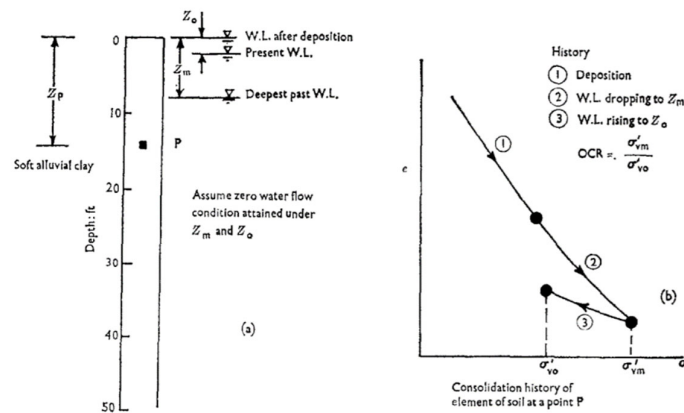
Figure 2- 6 Variation of consolidation history due to change in groundwater level

If z_o is water level at the time of deposition, z_m is the maximum water table in the past and z_p is depth of point A of the soil element to be analysed. In figure curve 1 represent the evolution of effective vertical stress and void ratio during deposition phase. If water level is drawn until z_m, the effect stresses follows line 2 until it reaches σ'_{vm}. If water level rises, effective stresses will decrease until present effective stress level, σ'_{vo}. From it could be led a led a function of *OCR* equation dependant on changes in effective stresses due to groundwater levels variation:

$$OCR = \frac{\sigma'_{vm}}{\sigma'_{vo}} = \frac{z_A(\gamma - \gamma_W)}{z_A\gamma - z_o\gamma_W} \qquad (2.4)$$

Desiccation

The effect of drying is mainly present on the shallowest levels of the soil deposits. Desiccation could be related to evaporation of water from the soil due to vegetation or to the thawing-freezing cycles (Jamiolkowski *et al.*, 1985). During the cycles of drying and wetting soil experiences non-negligible stress in a micro-scale level, being theses stresses related to suction (Tomás *et al.*, 2010). The reduction in water saturation degree of the soil generates changes in the effective vertical stress of the soil. If the excess pore pressure dissipates then the soil is submitted to a primary consolidation. Stress history for this kind of deposits is highly erratic and in situ stress conditions can deviate from K'_0 (Jamiolkowski *et al.*, 1985). Effective stresses are dependent on pore pressure and the effect of variation with pore pressure is may be derived from equation (2.1) as presented in Massarsch (1975)

$$\Delta K'_o = \frac{\sigma_h - u}{(\sigma_v - u)^2} \Delta u \qquad (2.5)$$

and the normalized expression

$$\frac{\Delta K'_o}{K'_o} = \frac{K'_o - 1}{K'_o(\sigma_v - u)} \Delta u \qquad (2.6)$$

A small variation in pore pressure may lead in large variation ok K'_0, specially in the shallowest layers, which are specially under desiccation conditions.

2.4 Field methods for determining K'_0

In this section, a review over the most common field method for determine ing K'_0 is presented, with special detail on total stress cells and hydraulic fracturing which are the equipment to be used in the present project.

2.4.1 Hydraulic fracturing

Hydraulic fracturing is the process of creating a fracture or a fracture system in a porous medium by injecting a fluid under pressure through a wellbore. The main purpose is to overcome native stresses and to cause material failure (Howard and Fast, 1970). Hydraulic fracturing is a well-developed technique applied in the oil and gas industry and it is mainly focused on enhancing the production of oil and gas from underground reservoirs (Yew and Weng, 2015).

In the 1960s, hydraulic fracturing was introduced as a method for measuring stress state in deep rock masses formation and since then it has become widely used technique for in situ stress measurements (Baumgärtner and Zoback, 1989).
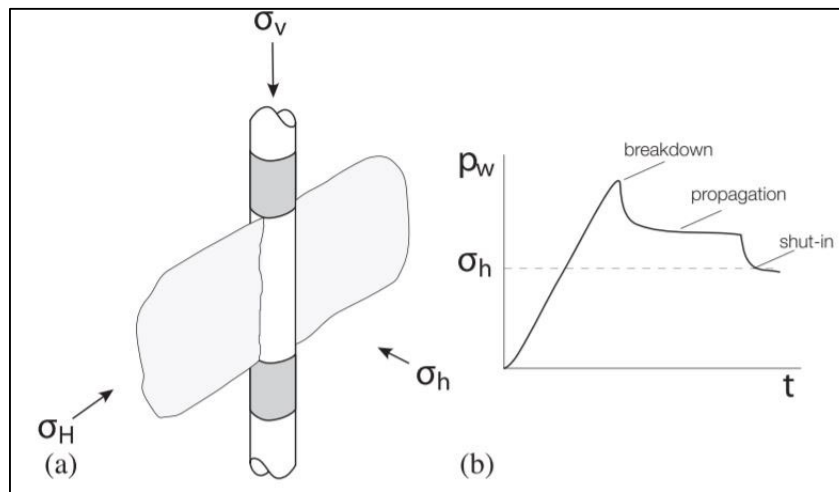
Figure 2- 7 (a) Hydraulic fracturing stress test. (b) Typical pressure–time record on the first injection/shut-in cycle (Lakirouhani, Detournay and Bunger, 2016)

In 1972, Bjerrum *et al.*, considered hydraulic fracturing as a way to set limits when performing permeability test in soils to avoid the creation of fracture in the ground. This investigation derived in the application of hydraulic fracturing for determining the stress state in soils. In 1978, Massarsch (Massarsch, 1978) presented hydraulic fracture as and approach for fracturing created while pile driving and driven sand drains. Hydraulic fracturing has been pointed out as possible main mechanism of failure in clay cores of earth and rock fills. This was presented in the report published by an independent panel (US. Department of the Interior - State OF Idaho, 1976) where a deep analysis of the Teton dam failure occurred in 1976 was carried out, proving that hydraulic fracture was behind dam

failure. Furthermore, this technique has been proposed to evaluate formation damage caused by hydraulic fracturing pressure in off-shore installation as for example during well completions (Andersen *et al.*, 1994). Hydraulic fracturing is also applied in the design of injection parameters in processes related to soils strengthen by cement injection (Mori and Tamura, 1987). Finally, hydraulic fracturing is a technique applied to improve effectiveness of most in situ remediation methods for contaminated sites underlain with unfavourable low-permeability soils (Alfaro and Wong, 2011).

This sub-section presents a detailed description of hydraulic fracturing method as a technique for in situ measurement of stress state in soils. A review of the proposed governing theories of material fracturing applicable to hydraulic fracturing is also presented. Finally, a review of the different interpretation methods is developed since it is relevant for the interpretation of data obtained in field testing.

Hydraulic Fracturing Testing Set-up

Theoretical background of hydraulic fracturing is simple. It consists on the injection of a fluid into a borehole until a fracture is created in the soil surrounding the injection tip. The pressure at which the cracks open is called "fracturing pressure" or "breakdown pressure", $P_{fracture}$.

The initial investigations on hydraulic fracturing as a technique to determine stress state in cohesive materials are reported in Bjerrum and Anderson, (1972). During a permeability test campaign, it was noticed that permeability increased abruptly when injection pressure reached a certain value of overburden. This was interpreted as an indicator of water might be leaking through fractures opened by hydraulic fracturing, as a result of induced increase on water pressure when performing permeability test. It was concluded that hydraulic fracturing is likely to occur in almost all cohesive soils and the excess critical water pressure required to produce a fracture in the soil is related with the in situ effective stress state. Therefor the equipment used at that time is based on falling head field permeameters and it is illustrated in Figure 2- 8. It was basically composed of a common piezometer copper filter installed in a borehole and connected by a hose tube screwed to a pump and to a mercury manometer. A pressurized fluid is injected through the piezometer into the ground. Pressure and injection rate are recorded manually. Later, in 1974, Bozozuk (Bozozuk, 1974) made an improvement of the original apparatus by adding a pressure transducer and a chart recorder. In that way the mercury manometer

could be avoided and the evolution of the pressure with time could be logged. Due to technical background, hydraulic fracturing is limited to fine grained cohesive soils with low permeability. Injection fluid could be water based although more viscous fluids like glycerine are recommended for more permeable formations as silts (Bjerrum and Anderson, 1972; Bozozuk, 1974).
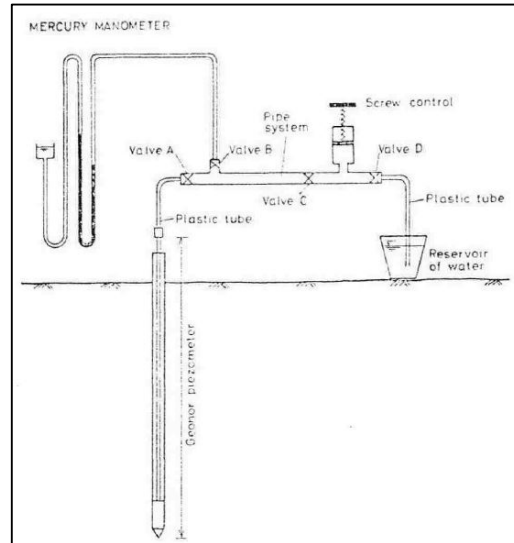
Figure 2- 8 Sketch of equipment employed for hydraulic fracturing testing

(Bjerrum and Anderson, 1972)

As other in situ techniques, hydraulic fracturing produces a degree of disturbance in the soil, mainly during the installation of the piezometer. This effects may introduce uncertainty when determining in situ stress by the water pressure needed to fracture the soil (Bjerrum and Anderson, 1972). Lefebvre *et al.* (1991) performed an exhaustive study to determine local disturbances on soil strength properties during installation of piezometer. Non-disturbance in strength properties was observed at a distance in radial direction between 30 and 40 mm away from the piezometer rod. For practical purposes, it is recommended to allow dissipation of excess pore pressure generated during installation before starting the test (Hamouche *et al.*, 1995).

No further development of the technique has been done. Only the possibility of performing hydraulic fracturing test using the BAT probe (Lunne and L'Heureux, 2016) as mentioned in subsection 2.4.6.

Fracture theories

This review is focused on the different approaches proposed in the literature for assessing the pressures state at the initiation of a fracture around a well. Fracturing model prediction is presented in literature under two different modes: (a) tensile failure mode (Bjerrum and Anderson, 1972; Andersen *et al.*, 1994), and (b) shear failure mode (Mori and Tamura, 1987; Panah and Yanagisawa, 1989). These two failure modes are presented in Figure 2- 9. As the target soil to be studied is mainly composed by clay, undrained conditions are assumed during fracturing process.
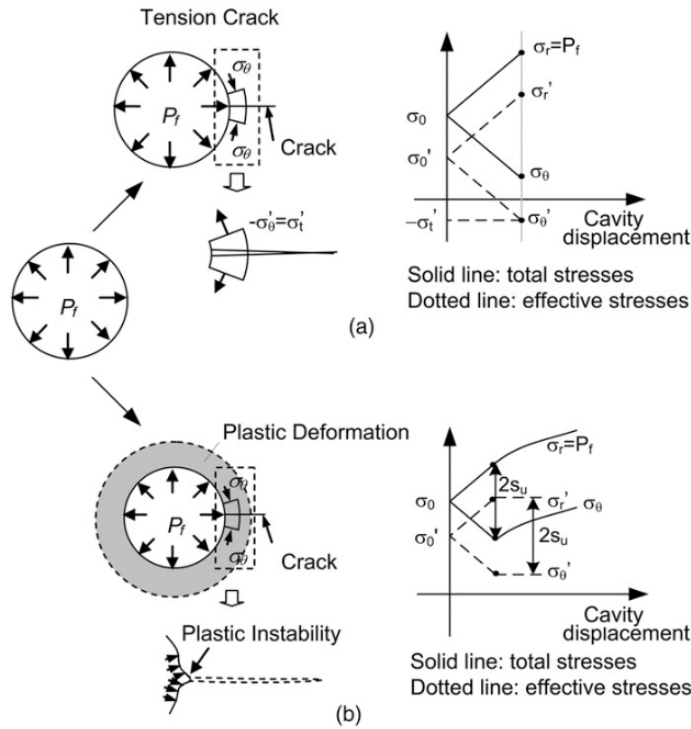
Figure 2- 9 (a) Tensile fracturing and (b) shear-induced fracturing modes of an injection fluid into a cylindrical cavity in undrained conditions (Marchi, Gottardi and Soga, 2013)

Considering tensile fracturing mode, hydraulic fracturing occurs in an elastic and isotropic media when the minor principal effective stress, σ_3', becomes tensile and reaches a value larger than the tensile strength of the soil, σ_t' (Andersen *et al.*, 1994), i.e. when

$$\sigma_3' \ + \ \sigma_t' \leq 0 \tag{2. 7}$$

The minor stress will be the first becoming negative, i.e., tensile. Assuming elastic properties of the soil, the problem approach may be done by thick-wall geometry cylinder (Figure 2- 10). If a circular hole is made in a stressed plate, the stress distribution around the hole will be changed (Timoshenko and Goodier, 1951). In the same manner, as a borehole is drilled, the soil surrounding the hole must carry the force previously carried by the removed soil. When the material is assumed to be elastic, the radial and tangential stresses to the cylinder wall are given by Lamé's formulas (equations (2. 8) and (2. 9)) and tensile fracture occurs:
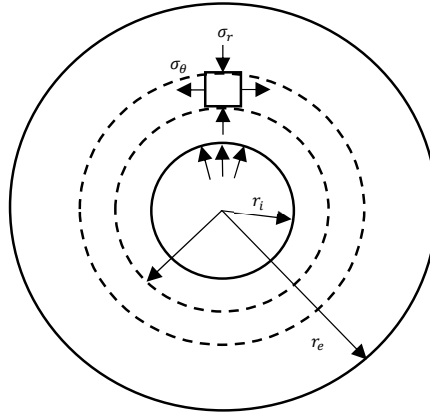
Figure 2- 10 Equilibrium of an infinitesimal element in a thick-walled pipe (Howard and Fast, 1970)

$$\sigma_\theta = \frac{P_i r_i^2}{(r_e^2 - b^2)}\left(1 + \frac{r_e^2}{r^2}\right) - \frac{P_o r_e^2}{(r_e^2 - r_e^2)}\left(1 + \frac{r_i^2}{r^2}\right) \qquad (2.\ 8)$$

$$\sigma_r = \frac{P_i r_i^2}{(r_e^2 - r_i^2)}\left(1 - \frac{r_e^2}{r^2}\right) - \frac{P_o r_e^2}{(r_e^2 - r_i^2)}\left(1 - \frac{r_i^2}{r^2}\right) \qquad (2.\ 9)$$

where, P_i is the internal pressure, P_o is the external pressure, σ_θ is the tangential stress and σ_r is the radial stress, r_e is the external radio and r_i is the internal radio.

If the external radio is much larger than the internal radio ($a \gg b$), the expression of the stresses on the contour wall of a borehole ($r = b$) may be written as:

$$\sigma_\theta = P_i - 2P_o \qquad (2.\ 10)$$

$$\sigma_r = -P_i \tag{2.11}$$

Renaming P_i as P_f (fracturing pressure), P_o as σ_{3o} (initial in situ lateral total stress prior to drilling), and σ_θ as σ_t (tensial strength of the soil) the total pressure inside a borehole when fracturing occurs can be expressed as:

$$P_f = 2\sigma_{3o} + \sigma_t = 2\sigma'_{3o} + u_o + \sigma_t \tag{2.12}$$

Considering that the tensile stress in a cohesive soil is generally negligible (Andersen *et al.*, 1994; Overy and Dean, 1986), equation (2.12) could be expressed as:

$$P_f = \sigma'_{3o} + u_o \tag{2.13}$$

As addressed by Jaworski, Bolton Seed and Duncan (1981), the soil is not an elastic rather a plastic media. To undertake the plastic behaviour of soil material, an empirical formula derived from the classical formula of hydraulic fracturing in rocks given by Haimson (1968) and based on laboratory testing proposed by Jaworski, Bolton Seed and Duncan (1981) (referred in Marchi, Gottardi and Soga, 2013). This formulation is more adequate to elasto-plastic materials as cohesive soils (Overy and Dean, 1986):

$$P_f = m\sigma_3 + \sigma_{ta} \tag{2.14}$$

where σ_{ta} is the apparent tensile stress and m is an empirical factor.

As addressed by Marchi, Gottardi and Soga, (2013), Jaworski, Bolton Seed and Duncan (1981) proposed values for σ_{ta} between zero and the cavity expansion pressure. The empirical factor m was found to lead in a range between 1.5 and 1.8. Empirical factor m is influenced by several factors as shear strength of the soil, overconsolidation ratio, boundary conditions and flow conditions (Andersen *et al.*, 1994), so the findings of this study suggest that empirical formulas should be defined on the base of representative condition for the actual case.

Andersen *et al.*, (1994) introduced a new formulation where nonlinearity of strain-stress properties of the soil and pore pressure induced by variation in mean stress and by

dilatancy during shearing were included. A relationship between variation of tangential stress, $\Delta\sigma_\theta$, and internal pressure, Δp_m, in the borehole was defined as:

$$P_f = \Delta p_m + \sigma_\theta \qquad (2.15)$$

where Δp_m is governed by $\Delta\sigma_\theta' = -(\sigma_3' + u_o + \sigma_t)$.

Results from the implementation of this model for measured undrained shear strength from DDS triaxial test from Drammen clay, shows an improvement between model prediction and fracturing pressures obtained from laboratory test. Alfaro and Wong, (2011) also observed that the failure mechanism for cohesive soils appears to be a tensile mode failure enhanced by the increase in pore pressure at the soil around the cylindrical cavity during shearing as consequence of the increase of the difference between radial and tangential stress during the fluid injection.
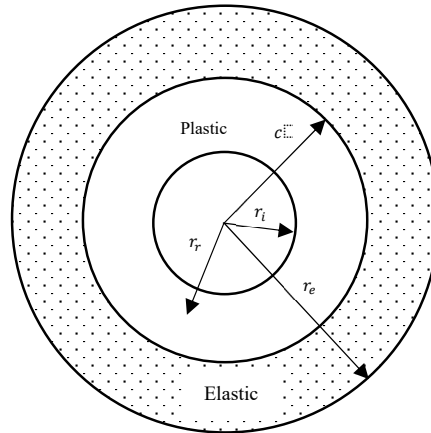
Figure 2- 11 Partial yielding of a thick-walled cylinder (Howard and Fast, 1970)

If the material is assumed to be plastic, the material may yield partially within a plastic region surrounded by a stressed region in elastic behaviour (Howard and Fast, 1970) as shown in Figure 2- 11. This means that the soil may reach shear failure before tensile failure (Soga, 2005; Marchi, Gottardi and Soga, 2013).

Some studies suggest that plastic yielding is the mechanism governing shearing fracturing (Panah and Yanagisawa, 1989; Marchi, Gottardi and Soga, 2013). Yielding criteria for cohesive undrained materials is given by Tresca failure criterion:

$$\sigma_r - \sigma_t = 2s_u \tag{2.16}$$

Equation (2. 16) could be rearranged if radial stress is linked to fracturing pressure and tangential stress is linked to lateral in situ stress so the failure criterion for an elastic material with initial yielding criterion can be expressed as:

$$P_f = \sigma_3' + u_o + 2s_u \tag{2.17}$$

A formulation for shear fracturing criterion based on cavity expansion theory was proposed by Vesic (1971) and Massarsch (1978), and solved even for K'_o values over the unity. The problem geometry is assumed to be that corresponding to an infinite thick wall of a well (see Figure 2- 10 and Figure 2- 11). When injecting a fluid into the well, the cavity walls will try to expand, and vertical fractures will appear. The pressure needed for this expansion in a plastic deforming material is given by equation (2. 18):

$$P_f = \sigma_3 + s_u \left(1 + \log\frac{G}{s_u}\right) \tag{2.18}$$

where P_f is the pressure for cavity expansion, σ_3 is lateral total stress, s_u is undrained shear strength and G is the soil shear modulus which can be expressed as:

$$G = \frac{E}{2(1+v)}. \tag{2.19}$$

Andersen *et al.*, (1994) proposed a varying value for shear modulus, G, in order to introduce the nonlinearity of strain stress properties of the soil into the cavity expansion theory. Main concern about cavity expansion formulation is that it represents the pressure when large radial displacement occurs. However, fracturing may occur before large radial displacements take place, and the fracture pressure will be in that cases lower than the cavity-expansion pressure, thus an overestimation of the fracturing pressure is expected as it was reported by some authors in field test results (Overy and Dean, 1986; Andersen *et al.*, 1994; Marchi, Gottardi and Soga, 2013). Overy and Dean (1986) concluded that shear failure lay between initial plastic yielding and cavity expansion as it was demonstrated by Andersen *et al.*, (1994) in the case of Drammen clays.

Hydraulic fracturing test results ok

Initially pressure vs. flow rate diagrams were used for interpretation of test results (Bjerrum and Anderson, 1972) as is shown in Figure 2- 12. This interpretation method is based on Cubic Law for steady state laminar flow between two parallel plates. Head loss, dP, along the fracture can be expressed as a function of the rate of flow into the fracture (q), the width of the fracture (H), the length of the fracture (x) and the viscosity of the injection fluid (μ):

$$dP = \frac{3\mu q}{H^3} dx \qquad (2.20)$$
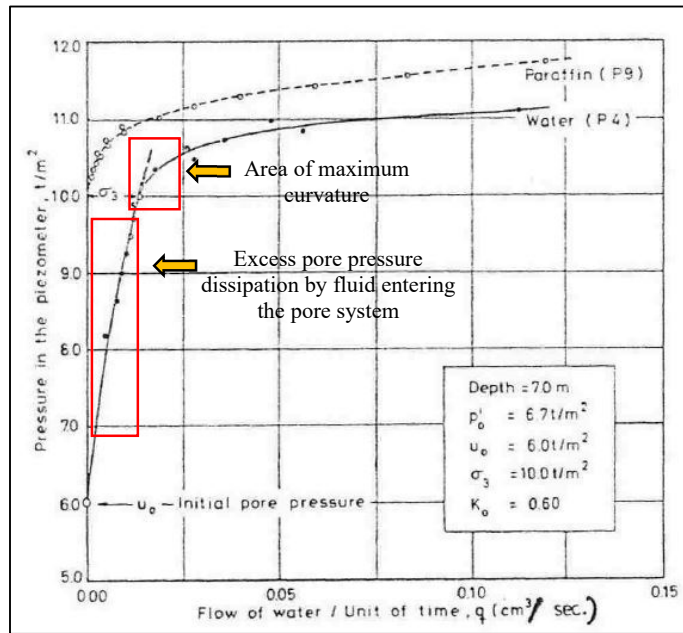
Figure 2- 12 Relationship between pressures in the piezometer and flow rate (Bjerrum and Anderson, 1972)

As addressed by Bjerrum and Anderson (1972), if the opening width, H, is related to the excess pressure, $P - \sigma_3$, from equation (2. 20) it is possible to state that the flow rate is proportional to $(P - \sigma_3)^4$. This means that when the pressure in the piezometer decrease to a value near to total horizontal stress, the flow entering in the fracture is zero.

However, as Bjerrum and Anderson (1972) remarked, the flow during the test may be unsteady and it could be the reason the data showed in Figure 2- 12 cannot be adjusted by lineal interpolation but with a slightly curved fitting. It can also be observed that the value of total lateral stress is not interpreted when the flow rate is zero but when the fitting line shows its maximal curvature. This corresponds to the pore pressure dissipation where the measured pressure is larger the pore pressure thus the injection fluid will flow into the soil

24

pore system. This fact was also confirmed in the work presented by Bjerrum and Anderson (1972) by injecting a non-penetrating fluid (paraffin) into the pore system. In that case, the flow dropped to zero when total lateral stress was reached (Figure 2- 12).

Later, after the introduction of pressure logging system in the equipment, determination of lateral in situ stress was evaluated by using pressure vs. time curves as shown in Figure 2- 13. It seems that this representation of data is less scattered compared to the pressure vs. flow rate charts presented by Bjerrum and Anderson (1972) and the interpretation of the breaking point to determine the minor principal stress is easier. In consequence, it has become the most widely analysis method (Bozozuk, 1974; Lefebvre *et al.*, 1991; Hamouche *et al.*, 1995).

Figure 2- 13 presents a schematic pressure vs. time curve typical from hydraulic fracturing test. The fluid is injected at constant rate and the pressure is registered by the pressure transducer. At the initial section of the curve, the pressure increases due to the low permeability of the soil until fracturing takes place. At that point, the pressure is named as breakdown pressure or fracturing pressure ($P_{fracture}$). Pumping continues and, in some cases, pressure is kept stable at fracturing pressure or it decays slightly. Injection is stopped when pressure starts to increase again, which indicate fracture propagation and pressure dissipation is allowed. Then, pressure drops rapidly as the injection fluid flows out from the fracture and when the fracture closes again, the pore water flows into the soil pores. The dissipation of the pressure is much slower from that point as it could see in the pressure-time curve. The inflection point between the two sections of the curve is usually interpreted as the pressure at which fractures close (Bozozuk, 1974; Gronseth, 1982; Lefebvre *et al.*, 1991; Hamouche *et al.*, 1995; Papanastasiou, 2000).
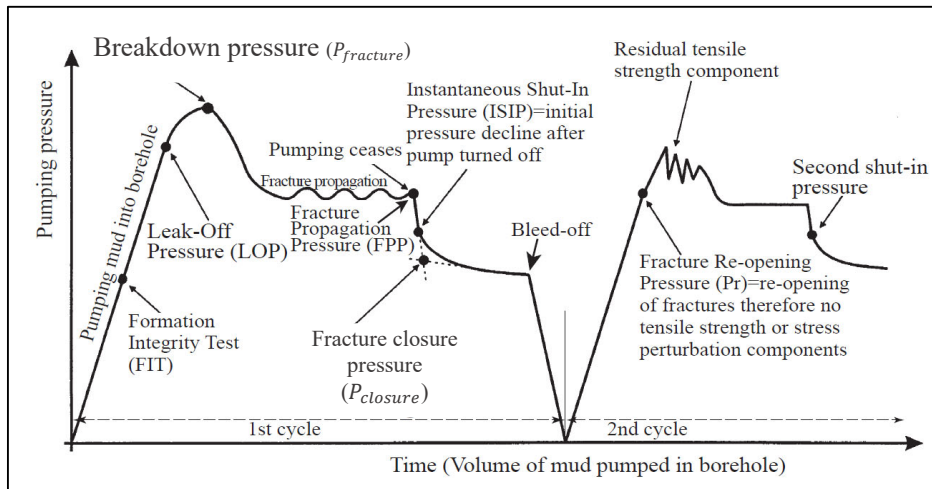
Figure 2- 13 Idealized relationship between pumping pressure and time or volume of injected fluid (slightly modified from Lin et al., 2008)

The intersection point is found as the intersection of two tangents, one drawn to initial or primary section of the curve, and another one drawn on the later or secondary part of the decay curve (see Figure 2- 13). The pressure value at that intersection is called fracture closure pressure ($P_{closure}$). This interpretation is related to the assumption that the curve from hydraulic fracturing test is lineal. All deviations from this model are due to non-uniform
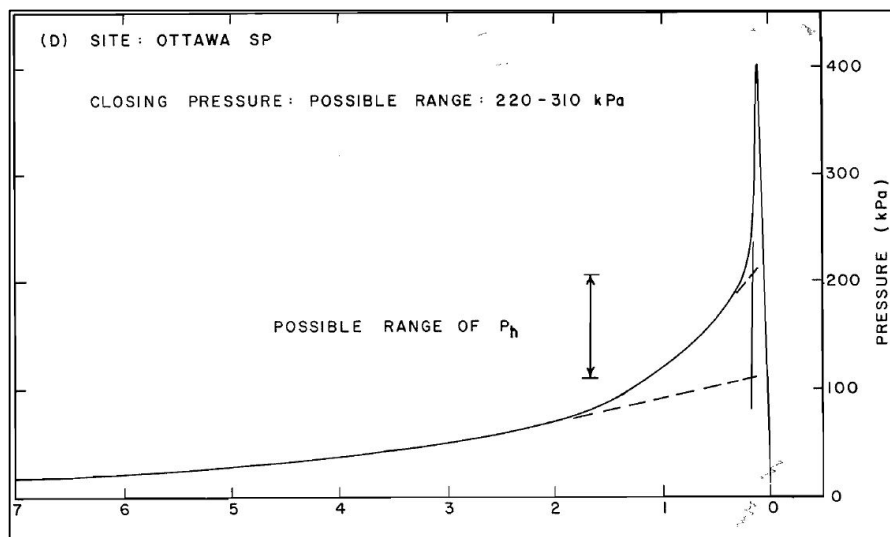
Figure 2- 14 Hydraulic fracturing tests reported by Lefebvre et al., (1991) where it is possible to observe the possible upper and lower limit of closure pressure

closure of the fractures, the possible presence of air bubbles in the fluid, and compliance of the system (Bozozuk, 1974; Lefebvre *et al.*, 1991). The greater this deviation, the larger the curvature between the tangents and more inaccurate and subjective will be the determination closure pressure, ($P_{closure}$). An example of this kind of deviation has been reported by some authors (Gronseth, 1982; Lefebvre *et al.*, 1991) as shown in Figure 2- 14. Closing pressure upper and lower limit is about 100 kPa which could affect the calculation of K_0' by 60%.

Despite of all discussed above, it is necessary to assume that the cracks formed are perpendicular to the minor stress direction, the presence of the crack does not alter the total stress acting across it and time dependant properties of the soil are not critical (Overy and Dean, 1986).

Hydraulic fracturing and K_0'

As the minor principal stress will be the first to become tensile, the cracks will develop perpendicularly to the minor principal stress direction. If the minor principal stress is horizontal, i.e. tangential to the borehole boundaries, vertical cracks will form. In the opposite case, a horizontal crack will form if the minor effective stress is vertical. Given the coefficient of lateral stress at rest (K_o') as the relationship between principal stresses (see equation (2. 1)), a vertical crack will form if K_0' is below one, and the crack will grow horizontally if K_o' is larger than one, i.e. if minor principal stress is in the vertical direction (Bjerrum and Anderson, 1972). The case presented by Bjerrum and Anderson (1972), corresponded to this situation where K_o' is below one. As consequence, the authors limited the measurement of horizontal stress by hydraulic fracturing technique to clay soils where $K_0'<1$, i.e. to normally consolidated. In opposition to this premise, Lefebvre *et al.*, (1991) showed that the orientation of fractures is more dependant of injection tip geometry than overconsolidation grade of the soil. For piezometer tips with a ratio length-diameter ratio over 10, it was observed vertical fractures even for K_0' over the unit.

Following with the studies accomplish by Lefebvre *et al.* (1991) and Hamouche *et al.* (1995), K_0' values calculated from hydraulic fracturing were compared with the empirical correlation for estimating proposed by Mayne and Kulhawy (1982).
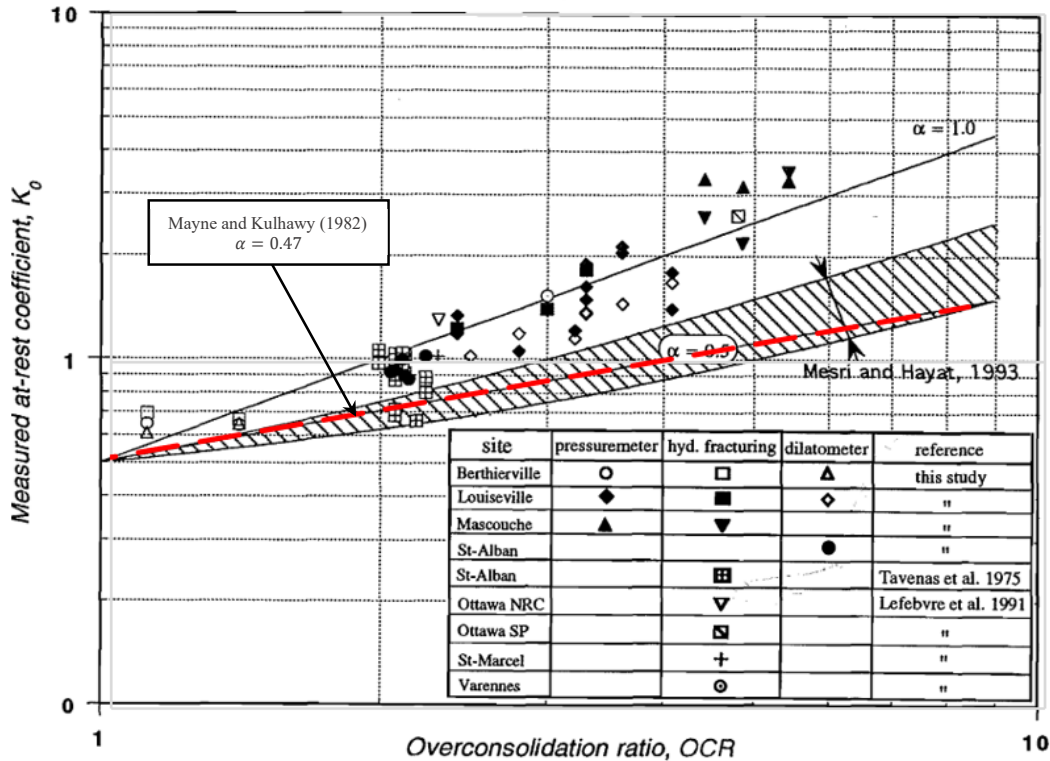
Figure 2- 15 Evaluation of K_0' values from different in situ techniques from Eastern Canada clays. Slightly modified from (Hamouche et al., 1995).

The α exponent ($\alpha = sin\varphi$) obtained was much higher than that suggested in the literature (Brooker and Ireland, 1965; Mayne and Kulhawy, 1982). These results were also reported by Hamouche *et al.* (1995) who accomplish a test program consisting in hydraulic fracturing, self-boring pressuremeter and dilatometer on eastern Canada clays (Figure 2-15). This higher measured K_0' values than predicted shows a that horizontal stress decreases slowly under unloading. As pointed in Lefebvre *et al.* (1991), this is due to the particular property of tested clays, which present bonded structure. This leads to a low relaxation of the horizontal stress during unloading processes and subsequent higher measured K_0' values than those predicted by the empirical relationships.

2.4.2 Push-In Earth Pressure Cells

Push-in pressure cells are a geotechnical instrument for in situ measurements of stress state in soils. They may be applied to monitor changes in stress state (both lateral and vertical stresses) during construction, excavation or tunnelling. They may be used also to

monitor lateral stress increase during pile driving or in soil structures compaction. However, it seems that push-in earth pressure cells are not so widely employed as expected, perhaps due to lack of knowledge in their real potential and reliability, especially as a test for site characterization. The present section intends to give a detailed description of the push-in earth pressure cells, as well as present some relevant previous experiences of the method for both instrumentation and in situ testing.

Background and previous experiences

The principle of the push-in earth pressure cells, similar to the flat jack, is to introduce a thin pressure cell into the ground with a minimal disturbance due to installation and monitor the changes in pressure with time until an equilibrium is reached. (Massarsch, 1975) presented the earth pressure cells as an innovative tool for measuring in situ horizontal stress, especially in the case of sensitive soft clays. Other authors have also reported satisfactory results from more stiffer clays.

Spade cells have been widely used to monitor changes in in situ lateral stresses specially for embedded retaining and pile walls constructed in stiff overconsolidated clays (Ryley and Carder, 1995; Richards, Clark and Powrie, 2006), as well as for monitoring support/lining stresses in tunnelling projects (Hoult and Soga, 2014) stress in tunnelling projects. Putting the focus on application of this method in the determination of lateral stress in natural clay deposit, Rankka (1990) performed a campaign for measuring lateral earth pressure along slopes in Scandinavian soft clays by mean of total stress cells. This study compares predicted lateral earth pressure by Janbu's method and measured values of lateral stress cells and dilatometer. Results showed earth pressure cells to be very reliable in soft clays but reported data were far from $K_0^{'}$ condition (no strain).

The most recent experiences for determining $K_0^{'}$ in Scandinavian clays are those performed in Tiller-Flotten (Lindgård and Ofstad, 2017) and Onsøy (Gundersen *et al.*, 2019) test fields in Norway. In both surveys the authors reported elastic bending of the cells during installation inducing permanent deformations in the spade blade. This may explain the high variation between individual measurements in data and uncertain quality.

Description of the equipment and installation

The cell is formed by two rectangular spade-shaped cells welded together, usually with triangular shape bottom edge, but also rectangular geometries are found (Figure 2- 16). The

narrow space between them is filled with oil. The original design by Massarsch was an extensometer inside a thin spade blade filled with oil. The lateral stress is then measured by pressurizing a valve until it reached the pressure at the earth cell. Readings were taken in a manometer (see Figure 2- 16). The old cell system did not include a pore pressure measurement device which implies that piezometer should be installed near the total stress cell (Massarsch, 1975).
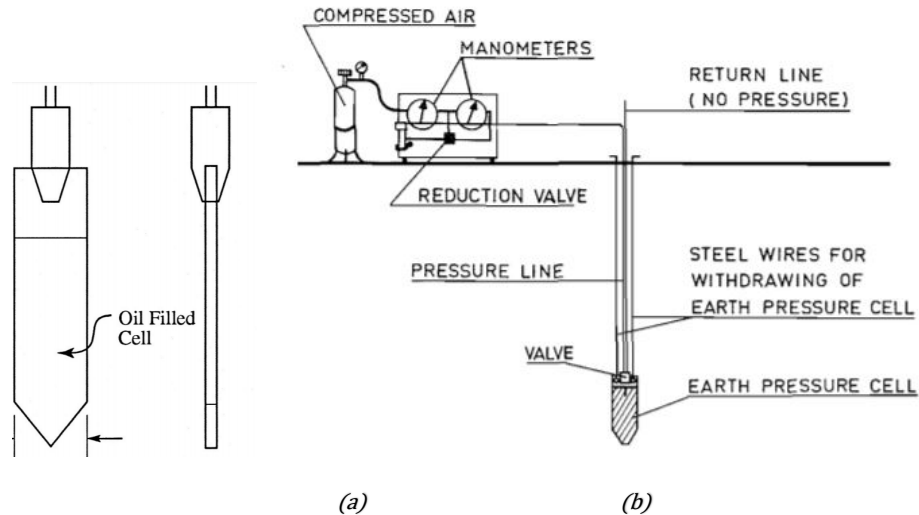
Figure 2- 16 Earth pressure cell set up (Massarsch, 1975)

The most recent devices measure pressure by a vibrating wire sensor connected to the spade blade as well as and a vibrating wire piezometer. The spade is attached to a drilling rod or pipes within which run the data transmission wire into a vibrating readout.

The geometry and material of the cell may ensure enough stiffness to support pushing down process into the ground preventing the spade to bend (as experienced by Lindgård and Ofstad (2017) during the field survey with Göztl cells) but the blade should be sufficiently thin to minimize disruption effects in the soil. Likewise, the cell may not present stiffness in excess to avoid under-reading effects or at least, be of small significance (Richards, Clark and Powrie, 2006). There is no developed standard (as ASTM or ISO) to control the dimensions and geometry of the spade cell therefore it will vary from one manufacturer to other (Lutenegger, 2012).

Push-in earth pressure cells are installed by pushing them into the ground. Previously, a pre-drilled borehole is drilled with the help of a drill rig it reaches level 30-50 cm above desired measurement depth. The cell is then pushed by hand or by help og a drilling rig

into the ground, never driving it but rather keeping the desired orientation of the blade. Some push-in earth pressure cells models have a protective cover to try avoiding damaging of the cell during installation in more stiffer clays as well as in sand deposits. Independently of which of both procedures is to be used, the cell may be pushed down into undisturbed soil the last 30-50 cm above measuring point. Measurement starts once the vertical pushing load is removed.

Push-In Earth Pressure Cells Test Results

The push-in earth pressure cells are an intrusive method which disturbs the stress state of the soil during installation since a built-up in pore pressure occurs due to compaction of the soil against the cell. Pore pressure dissipation may last 4 days in the case of sensitive soft clays (Massarsch, 1975; Lindgård and Ofstad, 2017), or up to one month in the case of deepest installations (Ryley and Carder, 1995). Thanks to the integration of vibrating wire piezometer in the cell, it is possible to monitor the stabilization of both lateral stress and pore pressure with time (Figure 2- 17).
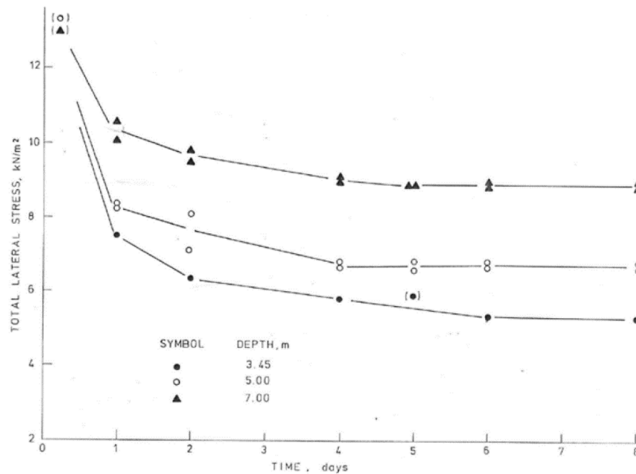
Figure 2- 17 Result of Push-In Earth pressure cells (Lunne and Massarsch, 1979)

Different evolution of the total horizontal stress is expected depending on stiffness of the soil. Lutenegger (2012) defined the reconsolidation lateral stress ratio as:

$$K_c = \frac{\sigma_c - u_o}{\sigma'_{vo}} = \frac{\sigma'_c}{\sigma'_{vo}} \qquad (2.21)$$

31

where σ_c refers to lateral stress measured in the blade after installation and stabilization of pore pressure.

Effective lateral stress (σ_c') is defined as a composition of the initial at-rest horizonal stress and the change in effective stress due to blade insertion in the ground, i.e.

$$\sigma_c' = \sigma_c - u_o = \sigma_{ho}' - \Delta\sigma_h' \tag{2.22}$$

It is excepted than the value of $\Delta\sigma_h'$ might be large in the case of stiff or overconsolidated soils and negligible for soft or normally consolidated soils. For normally consolidated soils Massarsch (1979) suggested a dependency of K_0' from in situ measurements with a correlation based on plasticity index (PI) indicating that slight disturbance is caused in the soil during installation of the cells. On the other hand, in stiffer overconsolidated larger disturbance effect on measured lateral stress are observed (Tedd and Charles, 1981; Ryley and Carder, 1995; Lutenegger, 2012). The effect of this disturbance seems to over-estimate the measurements of horizontal stress, i.e. overestimation of K_0'. Tedd and Charles (1981) and also Ryley and Carder (1995) recommended to subtract a correction factor within the range of 0.5 to 0.8 s_u for the case of London Clay. However Richards, Clark and Powrie (2006) defined a factor of 0.35 from calibration test performed in field test.
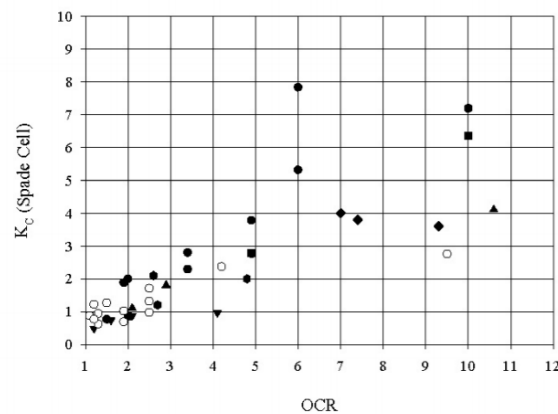
Figure 2- 18 Variation in K_C from Push-In Earth Pressure Cells at Several Sites with OCR from oedometer (Lutenegger, 2012)

It may seem logical to relate the over stresses with undrained shear strength of the soil since an aged and stiff overconsolidated clay will show higher shear resistance against the

insertion of the cell. However, this approach may be misleading since undrained shear strength varies with the test used. The correction factor for overstressed is suggested to be determined for normalized undrained shear strength i.e. s_u/σ'_{vo}. thus, to stress history (Lutenegger, 2012). the calculated K_c from push-in cells shows a dependency with stress history as shown in Figure 2- 18.

2.4.3 Other field methods for determining $K_0^{'}$

In this section a short review on existing methods for in situ evaluation of K_0' is presented.

Stepped blade

The stepped blade was developed for the U.S. Federal Highway Administration to provide a rapid and alternative method to measure lateral in situ stress in soils (Handy *et al.*, 1990). The stepped blade is a flat 64 mm wide and 640 mm long device with three equally increasing thickness that confers the blade a stepped appearance. Thickness goes from 7.5 mm at the top to 3 mm at the tip. There is an expandable Teflon membrane installed at each step, which is connected to a control unit at the ground surface through two pneumatic tubes. in the way that each pressure value is related to one of the pre-defined thickness. For the installation of the blade, a hole is bored slightly above the measuring depth and the blade is pushed into the ground. Lift-off pressure of all membranes are determined at the same depth by successive pushing and inflation steps (Masood and Kibria, 1994) By plotting the measured values at each step, a pressure value for a zero-thickness blade is extrapolated. This pressure values corresponds to the in situ horizontal stress at rest (see Figure 2- 19). The proposed form of the stress-thickness relationship is given in equation (2. 23):

$$P_f = \sigma'_h = \sigma'_{ho} \cdot a \cdot e^{bt} \tag{2. 23}$$

where a and b are empirical regression coefficients and e is the blade thickness.
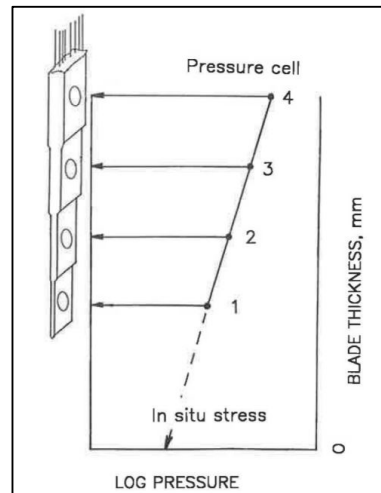
Figure 2- 19 Principle of the stepped blade and the extrapolation of zero blade thickness pressure (Handy et al., 1990).

The stepped blade method presents three main disadvantages. First, although it was developed to be a quick and accurate method, the experience during the investigation carried out at Lierstranda by Masood and Kribia (Masood and Kibria, 1994) shows that the stepped blade was the most time consuming method compared to dilatometer and lateral stress cone. Secondly, the tool has a high vulnerability and could be very easily damaged during installation, even in relatively soft soil (Masood and Kibria, 1994). Finally, the extrapolated stress value at zero blade thickness usually is found not to be so well defined.

Dilatometer

Marchetti introduced the flat dilatometer in 1979 (Marchetti, 1979). The flat dilatometer is a commercial tool, used worldwide in geotechnical investigations and good practice guidelines for gain a more systematic understanding of interpretation and design applications have been recently attempted (Schnaid, 2009). For further information about good practices it is available the proceedings stablished Marchetti *et al.* (2001) and the review on this proceeding in 2015 (Marchetti, 2016).

Nowadays it is possible to follow ASTM standard procedures (ASTM, 2015) (ASTM, 2012). The device is shown in Figure 2- 20. It consists in a stainless-steel blade with a flat circular membrane on one side. This membrane is inflated by flushing compressed gas (nitrogen) after penetrating the device into the soil at desired depth.
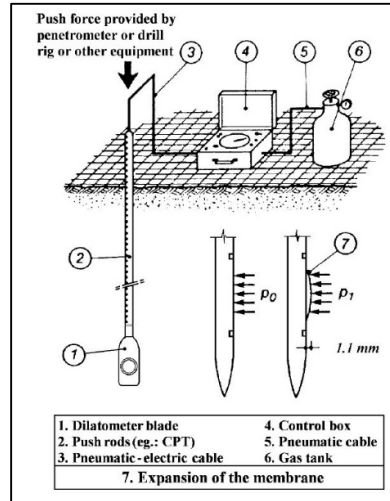
Figure 2- 20 Schematic representation of a dilatometer device (Marchetti, 1979)

Two pressures are measured, first the soil contact pressure, p_o, and secondly the 1 mm expansion pressure, p_1. The difference between these pressures, Δp is used to compute the three "intermediate" parameters, material index (I_D), horizontal stress index (K_D) and dilatometer modulus (E_D) (Marchetti, 1979).

$$I_D = \frac{\Delta p}{p_o - u_o} \tag{2.24}$$

$$K_D = \frac{p_o - u_o}{\sigma'_v} \tag{2.25}$$

$$E_D = 34.7(p_1 - p_0) \tag{2.26}$$

where u_o is the initial pore pressure and σ'_v is the effective overburden pressure.

In general, for the geotechnical characterization of a site, the main contributions that DMT can provide are information on stress history K_D and information about stiffness (via E_D). Equation gives an approximate value of K'_0 in sands (Marchetti, 1979) but it is also applicable for clays (Marchetti, 2016).

$$K'_0 = \frac{K_D}{\beta_k^{0.47}} - 0.6 \tag{2.27}$$

The parameter β_k is depending upon soil type and geological origin (Marchetti, 1979). A value of β_k = 1.5 was proposed by Marchetti (Marchetti, 1979) but later studies conclude than a value of β_k =2 is more reliable for sensitive clays (Hamouche *et al.*, 1995).

Cone Penetration test (CPT)

The initial attempt to derivate $K_0^{'}$ from CPT measurements are from sleeve friction values (Masood and Kibria, 1994). Lately, the lateral stress cone was developed by the University of British Columbia. It consists of a standard UBC 15 cm^2 piezocone unit followed by a lateral stress module. The lateral stress module is located 0.69 m behind the cone tip and is composed by a friction sleeve instrumented to measure hoop stresses in an under-reamed section of the sleeve (Sully and Campanella, 1990). Pore pressure measurements are also performed at the same location that the lateral stress sleeve location. The work presented by Sully and Campanella, (1991) related the effect of lateral stress on pore pressure changes during penetration test performance. A normalized pore pressure parameter was defined as

$$PPD = \frac{u_1 - u_2}{u_o} \qquad (2.28)$$

Where u_1 is the pore pressure measured on face of the cone, u_2 is the pore pressure measured behind the cone tip, and u_o is the in situ pore pressure. However, it was a large scatter when plotting PDD values and $K_0^{'}$ values from different sites and it was no possible to define a linear relationship between PPD and $K_0^{'}$.

Self-boring pressuremeter test

A pressuremeter is a cylindrical device designed to apply uniform pressure to the wall of a borehole by inflating three membranes. Both pressure and deformation of the cavity wall are recorded. The pressuremeter provides also other geomechanical parameters such shear modulus, undrained shear strength in clay, internal friction angle and dilation angle in sands (see Figure 2- 21)

First version of this device was developed by Ménard in 1955. Some aspects to be improved in the first version of the pressuremeter were related to the need of testing in a pre-drilled borehole with consequent soil disturbance. As a solution, the self- boring pressuremeter was developed simultaneously by Baguelin, Jézéquel and Shields, (1978)

and Wroth and Hughes, (1973)who developed the Camkometer which is designed to measure pore pressure also. The working principle of the method is similar to the previous version of the pressuremeter. The main improvement is the installation, at the end of the probe, of a rotating cutter bit encased by a cutting-shoe. The removed material by the cutter bit is flushed up to the surface using a water flushing system. On the other hand, this technique shows some disadvantages such as the boring technique should achieve the minimum disturbance from drilling the surrounding soil. Also, the combination of balance thrust, speed of the cutter, pressure and flow require of skilled operators and makes the self-boring pressuremeter technique time consuming and expensive (Schnaid, 2009).

(a)   (b)
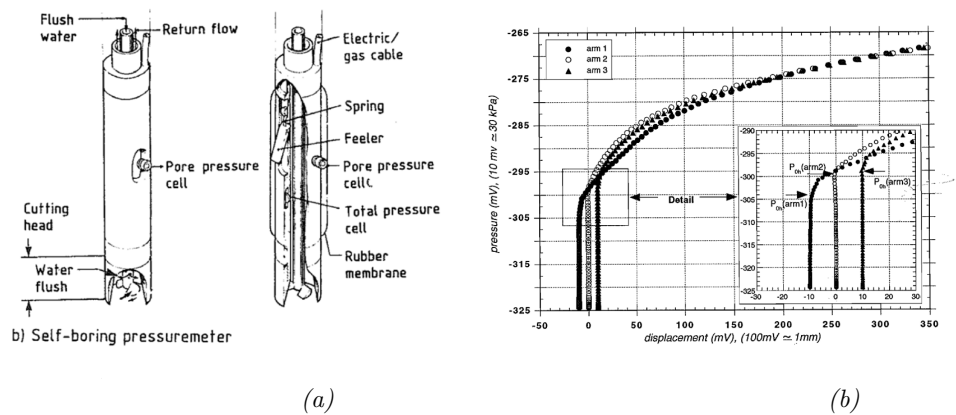
Figure 2- 21 Principle of the self-boring pressuremeter (a) and typical self-pressuremeter results (b) from (Hamouche et al., 1995)

The evaluation in situ horizontal stress is done by the recording of expansion curves. Different interpretation methods are presented by Lacasse and Lunne (1983) and concluded that some uncertainties related to the interpretation method chosen and the results from each of them may be compared to determine horizontal stress. Some authors reported reliable values in soft clay with *OCR* below 4 (Lacasse and Lunne, 1983; Hamouche *et al.*, 1995).

Self-boring pressuremeter seems to be the most adequate method to measure in situ horizontal stress in clays, as the disturbance when inserting the device in the ground is minimum (Lacasse and Lunne, 1983). It simulates the expansion of a cylindrical cavity, is the only in situ device which works with well-defined boundary conditions and therefore permits a more rigorous theoretical analysis than for other in situ tests (Jamiolkowski *et*

al., 1985). The main disadvantages of this method are the requirement of high qualified and trained personal to operates.

Field Vane

Vane test are used to determine the undrained shear strength s_u of saturated clay deposits. The field vane test consists in a group of four rectangular blades assembled at 90° to each other. This device is pushed into the ground to the desired depth, rotated and the torque required to produce rotation of the blade set is measured. Torque is converted to a value of undrained shear strength. Intact and remoulded shear strength is then estimated and with this values Ass et. al (1986) developed a method to estimate K_0' (Lunne and L'Heureux, 2016). The value of K_0' is obtained from graphical construction from stress path from CAUC triaxial test (see Figure 2- 22).
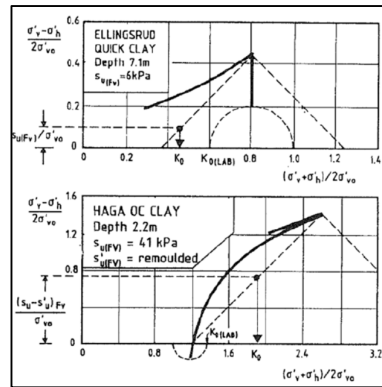
Figure 2- 22 Graphical construction to determine K_0' from field vane test. Original figure from Aas et al. (1986) (Lunne and Rad, no date)

BAT-prove

The BAT-probe was originally designed for ground water monitoring. The device consists in a filter tip which is connected to a pipe (see Figure 2- 23). The main functions are collecting of groundwater, measurement of pore pressure, in situ hydraulic conductivity and tracer test monitoring of groundwater. Its application in the in situ measurement of lateral stress is similar to the hydraulic fracturing. Injection fluid in water container is pressurized and when in contact with the filter, the fluid flows out and the soil fractures. The pressure, which is measured in the container, drops suddenly until the fracture closes.

At that point is the hydraulic conductivity which domain the pressure dissipation. The measured pressure at this transition point may be taken as the minor principal stress (Rad et al., 1988). A test program was carried out at Onsøy test site with very satisfactory results which correlated well form other measurements as it is shown in Figure 2- 23.

(a)   (b)
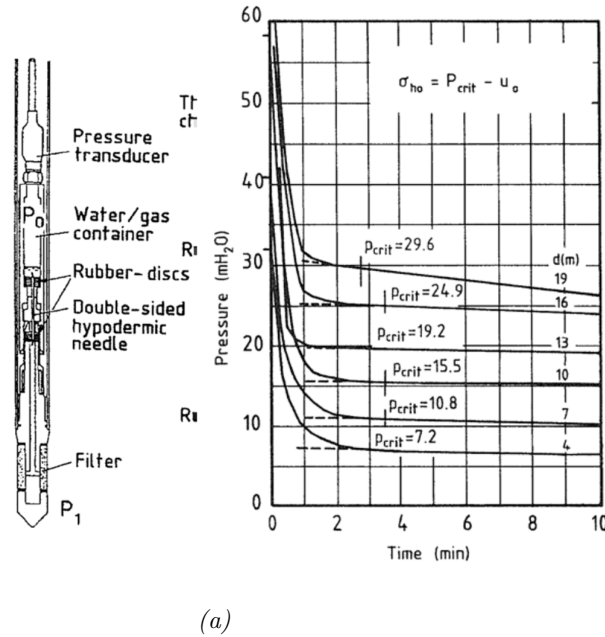
Figure 2- 23 Principle of BAT probe (a) and results of BAT probe performed in Onsøy (After Rat et al. 1988)

Shear wave velocity measurements

The use of shear waves velocity is presented as a valuable in situ method to evaluate $K_0^{'}$ (Sully and Campanella, 1995; Fioravante *et al.*, 1998). One of the main advantages seismic geophysical testing presents is a low grade of disturbance, similar to the self-boring penetrometer. It is possible to classify seismic methods in invasive and non-invasive. Invasive methods include up-hole, down-hole, cross-hole and rotary cross-hole tomography as well as special techniques as seismic piezocone (SCPTU) and seismic dilatometer (SDMT). Figure 2- 24 presents the different possible test configurations and the shear wave velocity that can be recorded.

UH, DH and SCPTU with a lateral source is employed to measure $V_{s,VH}$; CH is used to determine $V_{s,HV}$ after applying a vertical source; and rotary CH is used to generate and register $V_{s,HH}$ but in that case a rotary or torsional source is used.

(a)

(b)

(c)
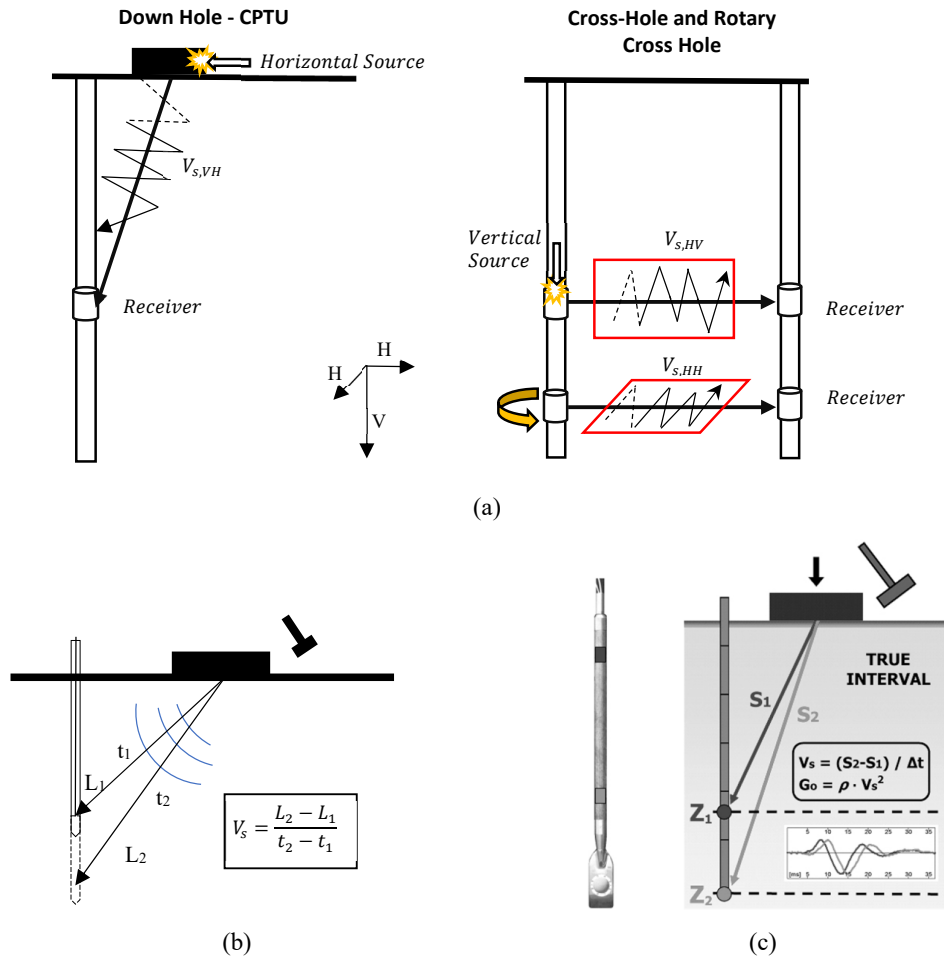
Figure 2- 24 General illustration (a) of intrusive methods for measuring V_s from drilled holes (from Ku and Mayne, 2013) and detailed set up for (b) seismic piezocone (SCPTU) (modified from Sully and Campanella, 1995) and (c) seismic dilatometer (SDTM) (Marchetti et al., 2008)

Shear wave velocity is dependent on soil inherent structure and stress state so the general expression for V_s is

$$V_s \ = \ C_s(\sigma')^n \tag{2.29}$$

where C_s is a coefficient dependent os soil state and n is the stress-dependent exponent (Sully and Campanella, 1995; Ku and Mayne, 2013), ranging from 0.10 to 0.15 and having a low impact on the accuracy of the calculated results.

Soils are structurally anisotropic by nature so different soil coefficients can be defined depending on wave direction and particle movement directions and by definition of lateral earth pressure coefficient at rest presented in eq.(2. 1).

$$V_{sVH} = C_{sVH} \cdot (\sigma'_v)^n (K'_0)^{n/2} \tag{2. 30}$$

$$V_{sHV} = C_{sHV} \cdot (\sigma'_v)^n (K'_0)^{n/2} \tag{2. 31}$$

$$V_{sHH} = C_{sHH} \cdot (\sigma'_v \cdot K'_0)^n \tag{2. 32}$$

Solving for K'_0, (Ku and Mayne, 2013) derived a semi-empirical formula, assuming the empirical factor α equivalent to $\left(C_{VH} / C_{HH} \right)^{2/n}$ or $\left(C_{HV} / C_{HH} \right)^{2/n}$

$$K'_0 = \alpha \cdot \left(\frac{V_{s,HH}}{V_{s,VH}} \right)^\beta = \alpha \cdot \left(\frac{V_{s,HH}}{V_{s,HV}} \right)^\beta \tag{2. 33}$$

A feasibility and sensitivity analysis were presented by Ku and Mayne (2015) on this semi-empirical formula, where different shear waves from 16 well documented sites, comprising normal and over consolidated clays, silt and sandy soils. The conclusion confirmed the site dependency of parameters α and β.

An alternative approach to the evaluation of K'_0 is based on the estimation of in situ soil properties as shear modulus from high-quality field measurement of dynamic properties. Based on wave propagation theory, shear modulus in a linear elastic media is defined by the mass density and the shear wave velocity, as seen in eq.(2. 34).

$$G_{0,ij} = \rho_t \cdot (V_{sij})^2 \tag{2. 34}$$

where subscripts i and j denote propagation and polarization direction respectively, and shear wave velocity should be generated at shear strain amplitudes of 10^{-4} or less Sully and Campanella, 1995). Ku and Mayne (2015) published an statistical study where the relation

41

of K_0', overconsolidation difference (OCD) and shear stiffness anisotropy (i.e. $G_{0,ij}$ values at different soil planes) is evaluated from data base from well-documented test sites. The OCR can be expressed in terms of shear moduli anisotropy as

$$OCD = \alpha \cdot (\sigma_{atm}) \left({G_{0,HH}} \middle/ {G_{0,VH}} \right)^\beta \qquad (2.35)$$

where OCD is the difference between pre-consolidation stress and in situ vertical stress thus overconsolidation ratio (OCR) can be also related to shear stiffness anisotropy:

$$OCR = \alpha \cdot (\sigma_{atm}) \left({G_{0,HH}} \middle/ {G_{0,VH}} \right)^\beta + 1 \qquad (2.36)$$

Setting equation (2.36) in the proposed semiempirical equation (2.37) by Mayne and Kulhawy (1982) an expression for lateral stress coefficient at rest for overconsolidated soils can is derived as:

$$K_{oOC}' = (1 - \sin\phi') \cdot OCR^{\sin\phi'} \qquad (2.37)$$

$$K_{oOC}' = (1 - \sin\phi') \left[\alpha \cdot (\sigma_{atm}) \left({G_{0,HH}} \middle/ {G_{0,VH}} \right)^\beta + 1 \right]^{\sin\phi'} \qquad (2.38)$$

These equations are valid in uniform soil deposits where reflection and refraction effects are negligible (Fioravante *et al.*, 1998).

As mentioned above, the main disadvantage of all these methods is the need of penetrating into the ground which derives in a soil disturbance during the installation and consequent lack og accuracy. Non-invasive geophysical methods include spectral analysis of surface waves (SASW), multichannel analysis (MASW), Continuous surface waves (CSW), frequency wavenumber methods (f-k methods), seismic refraction, and seismic reflection (L'Heureux and Long, 2017). Spectral analysis of surface waves (SASW) was introduced by Nazarian and Stokoe (1984) (as referred in L'Heureux and Long, 2017) as a reliable method for estimating shear moduli from Rayleigh waves. It consists in an impulsive source and a couple pair of receivers to register the arriving of dispersed surface waves (Figure 2- 25). Multichannel analysis (MASW) is an enhancement of the SASW method where the coupled pair of receivers is substituted by a multichannel acquisition system in order to reduce acquisition time consumption (Park, Miller and Xia, 1999).
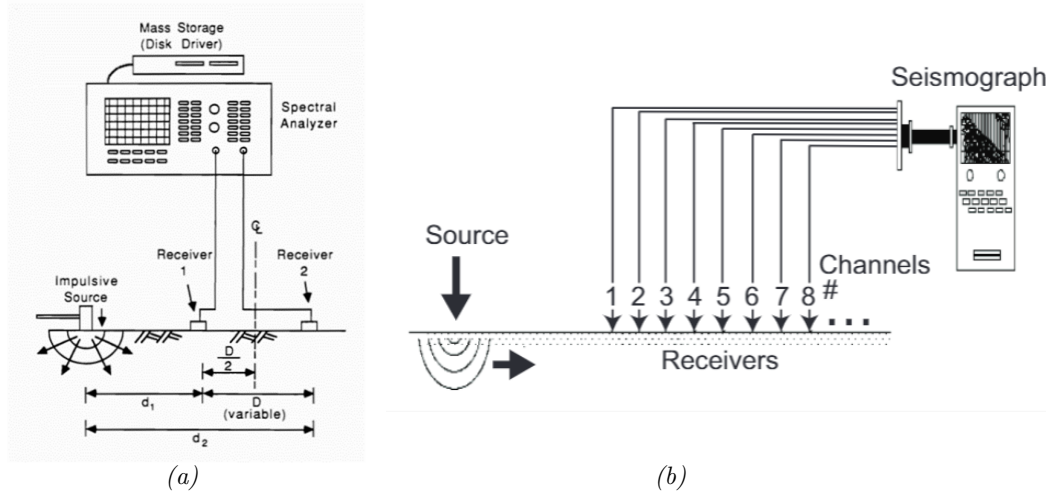
Figure 2- 25 General set-up for (a) SAWS and (b) MASW and CSW seismic geophysical prospection methods

Care is needed when planning field surveys and source offset distance, geophone spacing, array length, source frequency content, and the sampling time can all influence the results (L'Heureux and Long, 2017). Methodical uncertainties also arise when attempting to localize the global estimate of the dispersive characteristics, as well as the inverted vertical S-wave velocity profile relative to the mid-spread position. Performing surface wave measurements in both directions of the array line is recommended (Steinel *et al.*, 2014).

The continuous shear wave (CSW) set up includes a variable-frequency source with a range from 5 to 600 Hz which allows to vary the investigation depth since in most soils, Rayleigh waves travel at a depth of between a half and a third of a wavelength (Matthews, Hope and Clayton, 1996).

From the above mentioned non-destructive methods it is possible to define a mean shear wave velocity profile, V_s , which is dependent on soil inherent properties as particle stiffness and soil structure but also on effective stress conditions (Ku and Mayne, 2013) as expressed in eq.(2. 29). An K_0' estimation based in mean effective stress and mean shear wave velocity values is given by (Ku and Mayne, 2013):

$$K_o' = \left[\left(\frac{3}{\sigma_v'}\right)\left(\frac{V_s}{C_s}\right)^{1/n} - 1\right]/2 \qquad (2.39)$$

2.5 Laboratory methods for determining $K_0^{'}$

In this section a short review on literature of different work done by laboratory investigations to determine $K_0^{'}$.

2.5.1 $K_o^{'}$ - triaxial test

$K_0^{'}$-triaxial test or oedotriax is a special test set up to allow consolidation of soil simples with no lateral strains. The main target is to reset the soil specimen into in situ stress condition. For that purpose, cell pressure increases slowly while vertical stress is applied intermittently, when lateral deformation intends to occur. First set up was presented by Bishop and Henketl (1968) and later in 1972 a new device was presented by Campanella and Vaid (1972). Some disadvantages are related to this test procedure. First one is that it requires long time to achieve the $K_0^{'}$ consolidation curve, up to 2 weeks as reported in Campanella and Vaid (1972).

The second is the possible cell water compliancy which is negligible if compared with large consolidation occurring in normally consolidated soils but significant for low compressibility of overconsolidated soils.

The test is executed under drained conditions. The axial load in increased inducing am axial deformation (δ) into the soil specimen. The cell pressure is simultaneously changed to keep the volume change (water expelled) equal to the volumetric deformation, i.e. equal to $\delta \times specimen\ area$. The inclination of the $K_0^{'}$-line in the NTNU plot is given by is given by equation (2. 40)

$$\tau = \frac{\sigma_1^{'} - \sigma_3^{'}}{2} = \frac{\sigma_3^{'}}{2}\left(\frac{1}{K_o^{'}} - 1\right) \qquad (2.\,40)$$

So, the $K_0^{'}$ from oedotriax consolidation may be expressed as

$$K_o^{'} = \frac{1}{2\dfrac{\tau}{\sigma_3^{'}} + 1} \qquad (2.\,41)$$

However, the definition of $K_0^{'}$ presented in equation above is not that one corresponding the natural or geological $K_0^{'}$ value.

2.5.2 Split-ring oedometer

Splint ring oedometer was designed and developed by Geotechnical Division at NHT (now NTNU) and presented in Senneset (1989). The main difference with a usual oedometer is the possibility of monitor lateral stresses. The oedometer ring is a split ring divided in three equal sections. The sample is built up by clamping the three sections accurately into the sample. The apparatus records precisely any change in lateral deformation by LVDT pressure sensor attached to each ring section. Senneset and Janbu (1994) performed a survey on two different Norwegian clays with satisfactory results by interpreting both effective stress theory paths and stress ratios. It was also defined a dependency of K_0' with wáter content. However, latter test performed by (Lunne, Long and Forsberg, 2003) on clay from Onsøy test site did not follow this relationship.

2.5.3 Oedometer test - work criterion

Becker *et al.* (1987) presented a new interpretation method of results from conventional oedometer testing based on work per unit volume as criterion for defining both in situ stress and yielding stresses. The technique was proved by performing oedometer test on artificially slurry samples, previously load as simulating in situ conditions. Testing was performed on horizontally and vertically trimmed simples. The purpose was to identify both vertical and horizontal pre-consolidation stresses suffered by slurry samples. Thus, this approach is intended to define previous lateral stress suffered by the soils. If in situ vertical stress is then possible to calculate K_0'.

The work per unit volume can be expressed in terms of stress tensor acting ($\overline{\overline{\sigma}}$) and consequent strains ($d\varepsilon_i$)

$$W = \int (\sigma_1 d\varepsilon_1 + \sigma_2 d\varepsilon_2 + \sigma_3 d\varepsilon_3) \qquad (2.42)$$

As the lateral strains in the oedometer are restrained in the conventional oedometer test, the expression above may be expressed in terms of incremental strains as:

$$\Delta W_{oed} = \left[\frac{\sigma_i' + \sigma_{i+1}'}{2}\right](\varepsilon_{i+1} - \varepsilon_i) \qquad (2.43)$$

To find the yielding stresses, work per unit volume is plotted against axial effective stress as shown in Figure 2- 26.
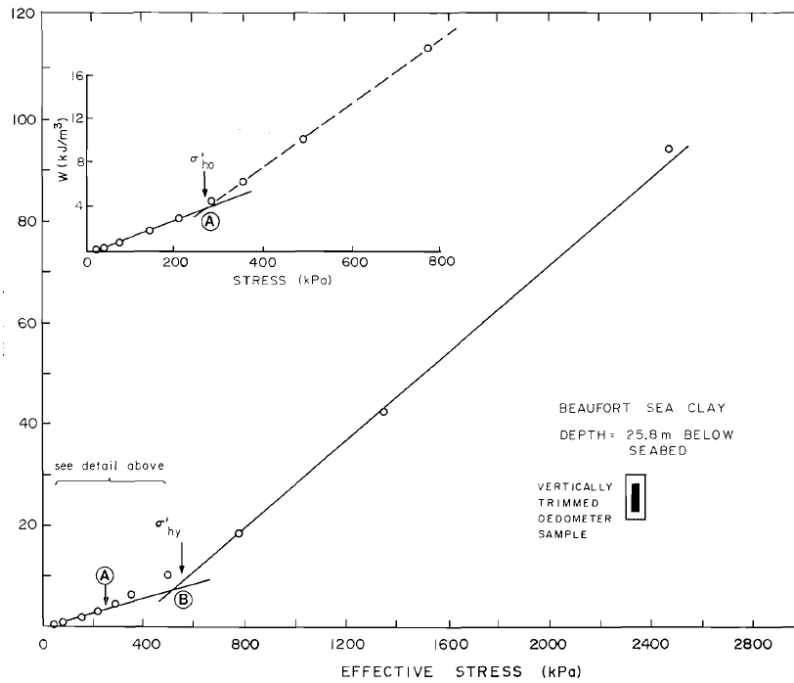
Figure 2- 26 Work per unit volume interpretation in a vertical trimmed sample (from Becker et al., 1987)

Previous experiences with work criterion in oedometer testing on samples from Tiller-Flotten was reported by Lindgård and Ofstad (2017). CRS oedometer test was performed on horizontal trimmed simples. The authors reported difficulties to determine in situ vertical stress from work criterion due to por quality of sample and limited amount of data.

2.6 Empirical methods for determining K'_o

Many investigations have been carried out in order to define an empirical relationship for K'_0. Main motivation is the high cost of performing field and laboratory testing (Ku and Mayne, 2015). Most of these studies conclude that for normal consolidated deposits, K'_0 (or K'_{oNC}) is constant for a given soil type (Sivakumar *et al.*, 2004). This is not applicable to the case of highly overconsolidated deposits where an anisotropy in soil parameters is observed, hence the empirical relationships are no longer valid. It is accepted that this anisotropy is generally the result of factors such as stress history, age of deposit, creep and depositional environment (Mayne and Kulhawy, 1982; Sivakumar *et al.*, 2004).

46

2.6.1 Empirical correlations for normally consolidated soils

Jáky (1948) proposed an empirical equation for estimating K'_0. This empirical expression is shown in equation (2. 44):

$$K'_{oNC} = 1 - \sin \phi' \qquad (2. 44)$$

where K'_{oNC} is the lateral earth pressure at rest for normally consolidated soils and ϕ' is the effective stress friction angle.

The validity of this empirical equation has been reviewed by several authors by analysing results from laboratory. Brooker and Ireland (1965) performed a test program on 5 samples and confirmed the relationship between K'_o and friction angle (see Figure 2- 27).
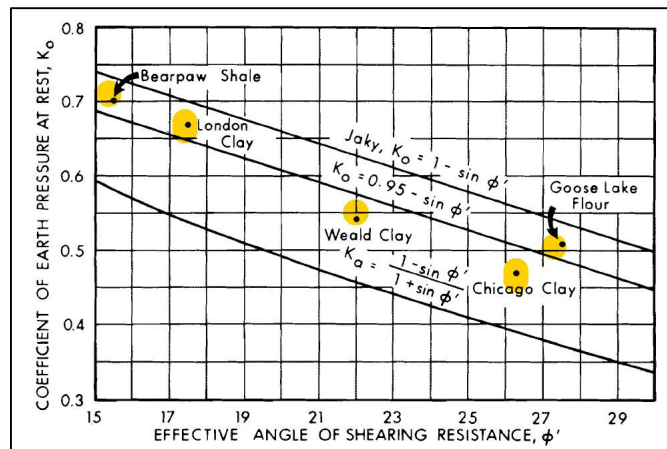
Figure 2- 27 Relationship between K'_0 and $\sin \phi'$ for normally consolidated cohesive soils (Brooker and Ireland, 1965)

Moreover, it was observed a dependency of K'_0 and plasticity index, i.e. cohesiveness of soil and the dependence of this relationship on stress history (or OCR) as shown in Figure 2- 28.
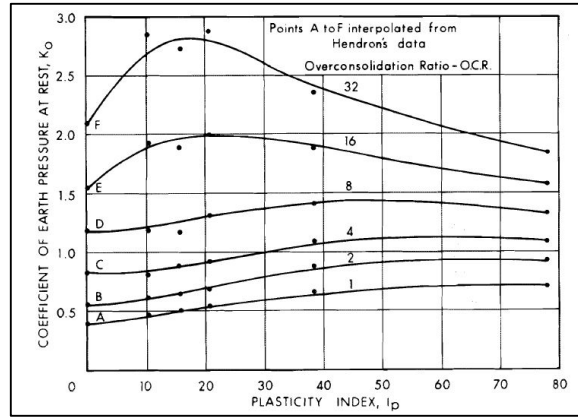
Figure 2- 28 K'_o dependency on OCR (Brooker and Ireland, 1965)

Mayne and Kulhawy (1982) made a review over laboratory data from more than 170 soils in order to evaluate the proposed empirical method for predicting K'_0 by Jáky (1948). As main conclusion, the study reveals than the relationship in equation (2. 44) is in general valid for cohesive normally consolidated soils under first unloading. This is also pointed out by Hamouche *et al.* (1995) on in situ measurements in soils with an *OCR* near to 1. It was concluded that for cohesive and cohesionless soils, the empirical relationship between K'_o and $\sin \varphi'$ is given by equations (2. 45) and (2. 46) respectively (Mayne and Kulhawy, 1982):

$$K'_{oNC} = 1 - 0.987 \sin \phi' \qquad (2. 45)$$

$$K'_{oNC} = 1 - 0.998 \sin \phi' \qquad (2. 46)$$

2.6.2 Empirical correlations for overconsolidated soils

As previously mentioned, Brooker and Ireland (1965) confirmed the dependency of K'_0 on stress history. From the results presented in their investigation, Schmidt proposed an empirical formula for K'_0 in overconsolidated soils

$$K'_{ooc} = K'_{ooc} OCR^{\alpha} = (1 - sin\phi')OCR^{sin\phi'} \qquad (2. 47)$$

This equation evaluated with in situ data form different reports. Lefebvre *et al.* (1991) reported higher K'_0 values than expected from equation (2. 47) from hydraulic fracturing test. Data showed a better fitting with equation (2. 44), pointing out the effect of clay structuration bounding is not accounted in the exponent $sin\phi'$, so higher values of K'_0 are to be expected from in situ measurements. Lately, Hamouche *et al.* (1995) reported data from several in situ testing on sensitive Eastern Canada clays, reporting a good fitting for an exponent $sin\phi' = 0.98$. It was also suggested that the sensitivity of the clay may influence on the α exponent.

For the case of Norwegian soft clays, L'Heureux *et al.*(2017) published a new empirical relationship between stress history and K'_0 including the plasticity as it done by Brooker and Ireland (1965). This regression was based on high quality laboratory data from Norwegian clays. A new regression for *OCR* values lower than 8 and cohesive material (Ip>0), obtaining the following empirical relation:

$$K'_0 = 0.48I_p^{0.043} \cdot OCR^{0.47}$$

(2. 48)

The influence of the plasticity index is negligible and has a little influence on K'_0 values. The comparison of regression lines calculated by equation (2. 48) with data from in situ measurements gives a good fitting for normally overconsolidated to slightly overconsolidated clay sites.

As a general conclusion, the empirical correlations for estimating K'_0 should be always supported by high quality laboratory and field data, and considering the conditions in which these empirical relations were established (Lefebvre *et al.*, 1991; Hamouche *et al.*, 1995; Ku and Mayne, 2015; L'Heureux *et al.*, 2017).

Chapter 3

Tiller-Flotten Geo Test Site

3.1 Introduction

The Tiller-Flotten research site is a part of the Norwegian GeoTest Site (NGTS) project. This project is part of a research program supported by The Research Council of Norway infrastructure and led by the Norwegian Geotechnical Institute (NGI). In total there are five testing fields within the project in Norway, which are chosen to represent five different relevant types of soils: soft clay in Onsøy, silt in Halten, sand in Øysand, quick clay in Tiller-Flotten and permafrost in Svalbard. In this chapter a description of the Tiller-Flotten test site is presented, including location, brief geological description as well as geotechnical parameters.

3.2 Location and description

The Tiller-Flotten geo-test site is located 15 km south the city of Trondheim (Figure 3- 1). The test field is emplaced in a farming area with and adjacent non-cultivated area covered by a ditched marsh. Clay deposit is estimated to be found 2 m under the marsh area. The average height above sea level of the test field is around 125 m.
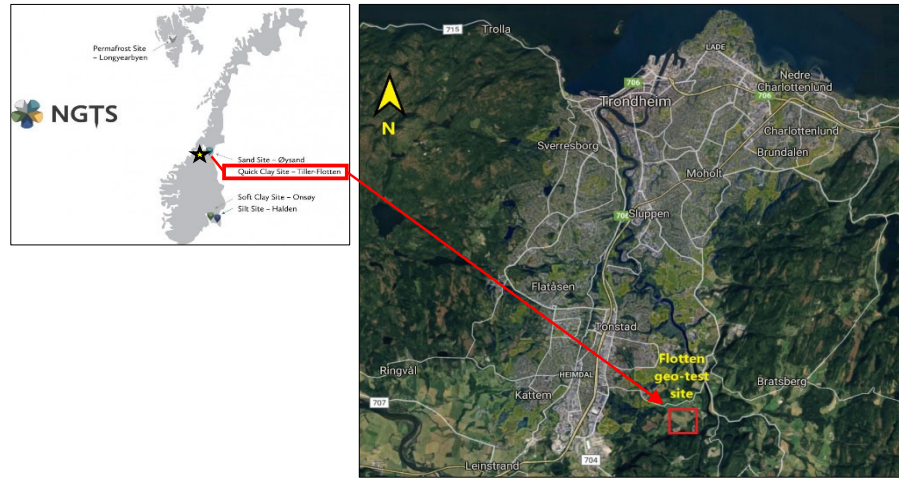
Figure 3- 1 Location of Tiller-Flotten test site (source: www.ngi.no *and* www.ngu.no*)*

This field test has been studied for more than 30 years and it is of special interest due to the presence of thick marine sediments, including quick clay. The ground surface of surrounding area of Flotten Geo-Test Site is characterized by ravines and old slide scars that reveals a landslide past activity related to quick clay. Available LIDAR image (Figure 3- 2) shows that Tiller-Flotten test site is located only few meters form the Tiller landslide occurred in 1816 and it is suggested that a pre-historic landslide scars is located only 500 m north from testing location (L'Heureux, Lindgård and Emdal, 2019). The area drains towards east to the Nidar river which is found at 72 m over sea level as shown in Figure 3- 2.

In Figure 3- 4, a general quaternary geological map of Trondheim area and the detailed quaternary geological map of Tiller site are presented. The soil deposits formed during the Quaternary period are due to glacial processes. Last ice melting period started around 10600 years ago. Figure 3- 5 represents a schematic situation of Trondheim area at that period. A glacial covered the southern area of the region and the sea level was higher than the sea level nowadays.
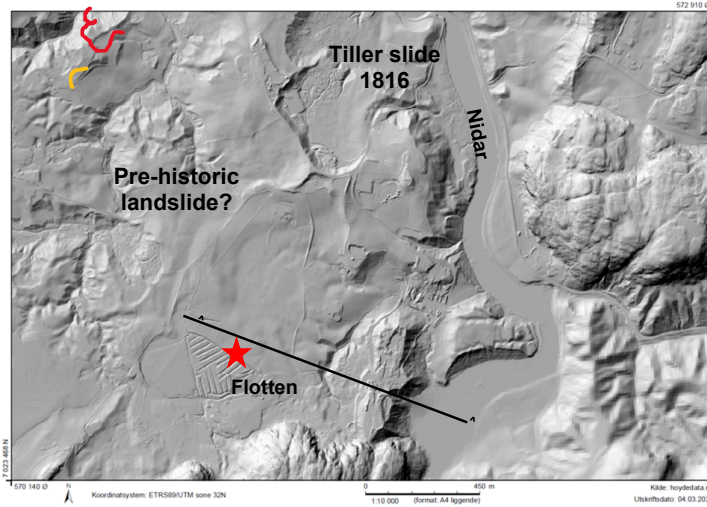
Figure 3- 2   Lidar data for Tiller (L'Heureux, Lindgård and Emdal, 2019)
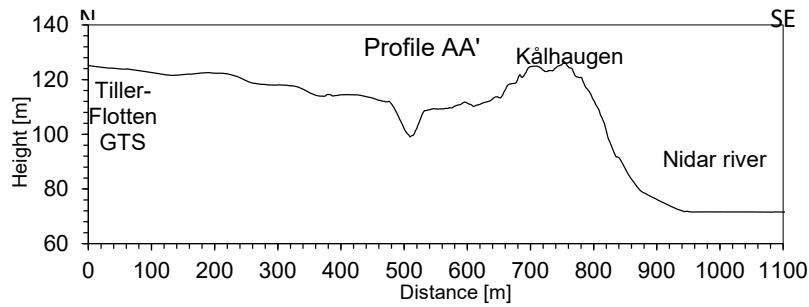
Figure 3- 3   Ground elevation of profile A-A' (Source: www.hoydedata.no)
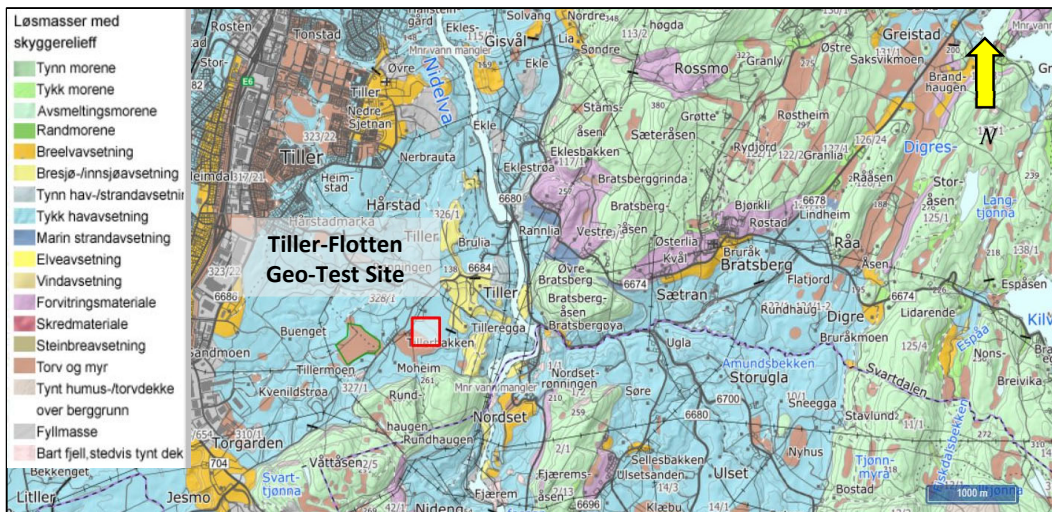
Figure 3- 4   Quaternary geology surrounding Tiller-Flotten Geotechnical site (source NGU)

The advance of the ice cover formed a terminal moraine deposit which extends form Estenstadmarka at north-east to Vassfjellet in the south, passing by Tiller and Heimdal areas (Reite, A.J.; Sveian, H.; Erichsen, 1999; L'Heureux, Lindgård and Emdal, 2019)**Error! Reference source not found.**. When the deglaciation period started around 10600 years ago, the glacial cover retreated backwards following south-east direction. An ablation moraine was formed and fluvioglacial sediments were deposited there where the melting water run to the sea. Tiller basin was filled with fine material supplied from the river. This fine material was deposited on the sea bottom forming up to 100 m thick clay deposit (Reite, A.J.; Sveian, H.; Erichsen, 1999).
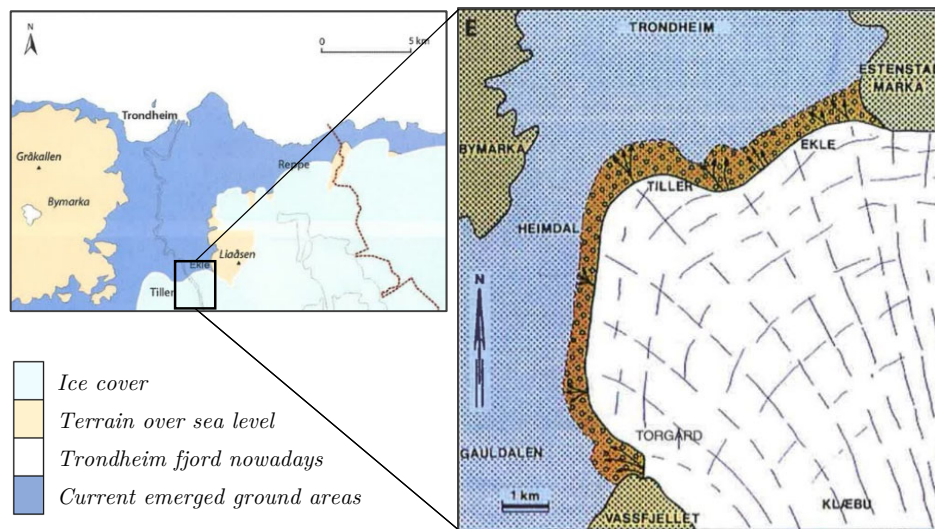
Figure 3- 5 Map over glacial and glacial free areas in Trondheim 10600 years ago and maximum extension of ice cover over the Tiller basin (modified from (Reite, A.J.; Sveian, H.; Erichsen, 1999)

Most of the depositional material was derived from glacial erosion from the bedrock, consisting mostly on greenstones, meta-sediments and volcanic material. Clay minerals, consisting mostly on quartz, feldspars and phyllosilicates as illite and chlorite were deposited under sea level (Gylland *et al.*, 2013). The flat shaped clay mineral grains are bounded by Van der Waals forces (Solberg, 2019). During the crustal rebound, after retreat of ice cover, Tiller basin emerged from sea level and marine clay deposits were exposed to fresh groundwater percolation. This process is known as leaching and consists on the removal of the salt ions holding the Van der Waals bonding between mineral grains. The result is a stable clay structure which is named as "house of cards" (Figure 3- 6) but upon a small mechanical disturbance collapse occurs (Gylland *et al.*, 2013). The clay at this state

53

is referred as "quick". During the isostatic crust up-lift, the water broke of the terminal moraine forming a fluvial channel which nowadays is Nidar river.
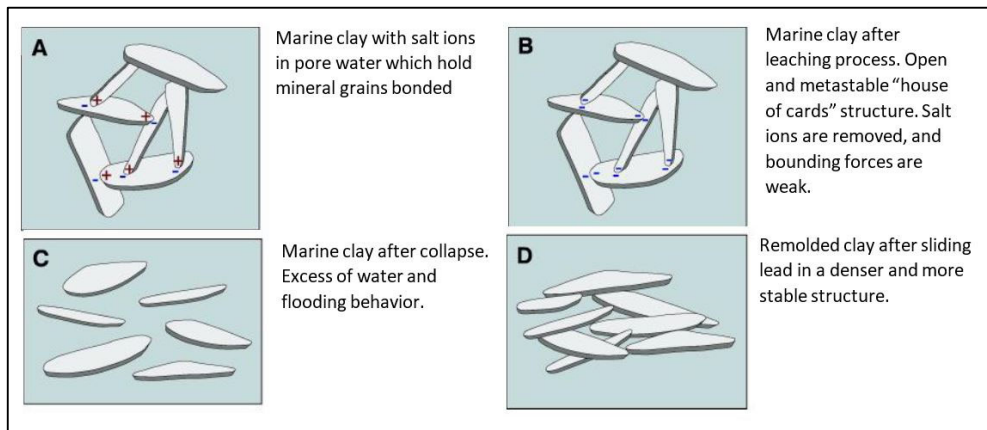
Figure 3- 6   Quick clay formation process by salt ion leaching (Reite, A.J.; Sveian, H.; Erichsen, 1999)

Fluvioglacial sediments consisting on sand and gravel covered marine clay deposits. Most of this coarse material was removed in the past decades to be used as aggregate material, however it is possible to see some remains of these fluivoglacial material between Tiller-Flotten and Nidar river.

3.3 Geotechnical settings

3.3.1 Stress history

As mentioned on chapter 2, the evolution of lateral earth pressure at rest coefficient (K_0') is dependent on stress history of the soil. Therefore, a short review of the stress history of Tiller-Flotten site is presented in this section.

Groundwater flow conditions have been conditioned (in a geological scale of time) by the formation of Nidar river valley by fluvio-erosional processes, as a consequence of the progressive emergence of the region during the Holocene. The variation of groundwater conditions contributes with changes on stress history and lead in an apparent pre-consolidation (L'Heureux, Lindgård and Emdal, 2019). Currently, the groundwater level is at a location of 2 m depth and pore pressure is under hydrostatic condition but with increasing trend with depth (Figure 3- 7).
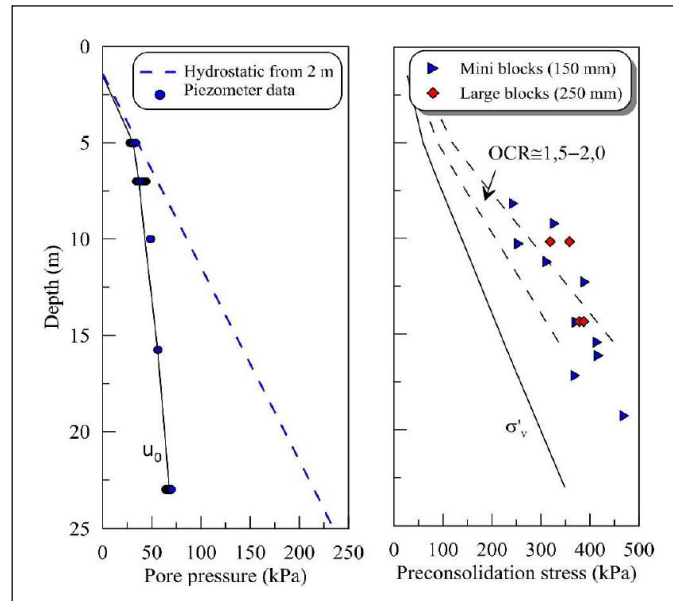
Figure 3- 7 In situ piezometric and pre-consolidation stress profiles (L'Heureux, Lindgård and Emdal, 2019)

3.3.2 Soil profiling and Index Parameters

The study published by L'Heureux, Lindgård and Emdal (2019) provides an exhaustive and detailed soil profiling as shown in Figure 3- 8. Soil is divided in three units: Unit I at the top, comprising the first 2 m and corresponding to the dry crust; Unit IIa, from 2 to 7.5 m depth, mainly composed of low to medium sensitive clay; and Unit IIa, from 7.5 m and containing very sensitive clay. Index parameters are quite uniform along the soil profile with exception of water content of around 50% in average at Unit IIa and dropping to 40% in Unit IIb. In addition, liquid limit is around 50% at Unit IIa while it decreases suddenly to 30% at the transition to Unit IIb. Plastic limit is higher in Unit IIa, with a value of 30% and it reduces to 20% in the clays at Unit IIb. Plasticity index ranges from 10 to 21%, decreasing with depth. Clay content is fairly the same at both clay units and it is in average of 50%.
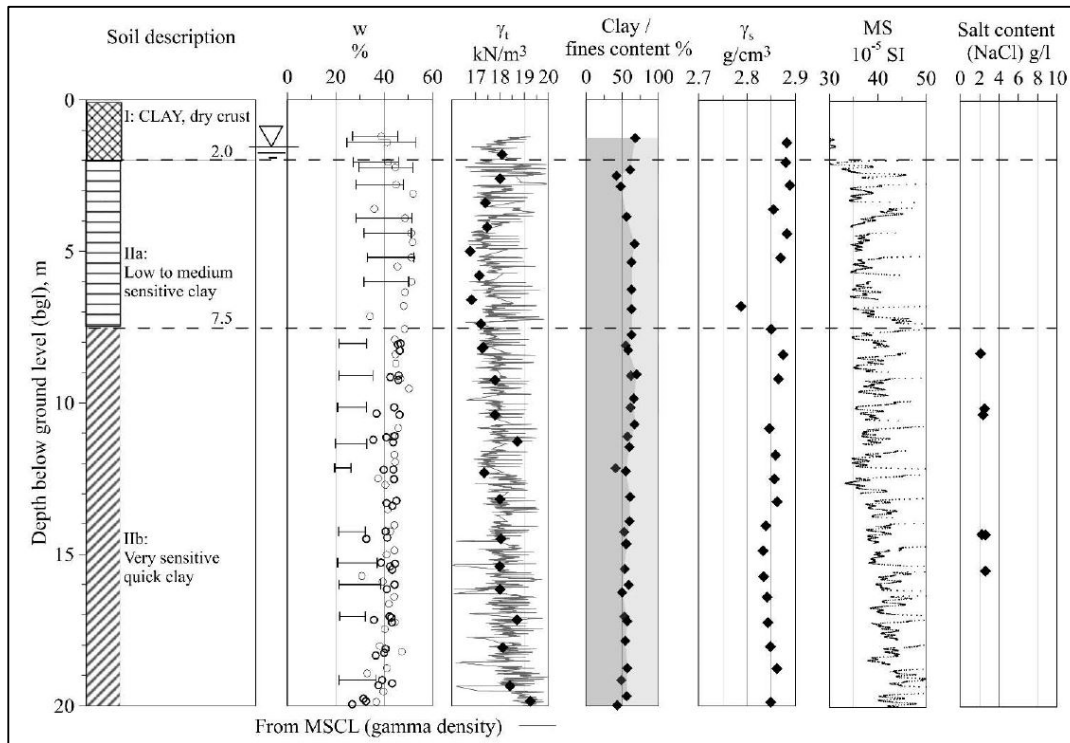
Figure 3- 8 Soil profile, stratigraphy and index properties at the Tiller-Flotten site (L'Heureux, Lindgård and Emdal, 2019).

3.3.3 Overconsolidation ratio and in situ horizontal stress

Several studies have been performed in order to evaluate pre-consolidation pressure (σ'_p) as well as constrained modulus (M), coefficient of consolidation (C_v) and creep number (r_s). L'Heureux, Lindgård and Emdal (2019) presented the results of this investigation program to determine stiffness and consolidation properties of the Tiller clay. CRS oedometer test program was performed on samples from mini- and large blocks taken at depths between 8 to 20 m depth. Results reported are summarized in Figure 3- 9. The value of σ'_p is above the actual vertical stress, σ'_v and *OCR* value is estimated as 5 in average within the first 7 m, and between from 1.5 to 2 from 7 m and below. A slightly apparent pre-consolidation is observed on the CRS oedometer results as a result of glacial front re-advance, groundwater fluctuations, secondary consolidation creep and chemical changes (L'Heureux, Lindgård and Emdal, 2019). From the geological history of the Tiller-Flotten area, only normal sedimentation process can be reported. These high *OCR* values are related to groundwater fluctuations which may have induced some changes in stress

history. *OCR* profiles reported are derived from dilatometer and CPTU based on equation presented in Mayne (1988) also match quite well with CRS oedometer data.
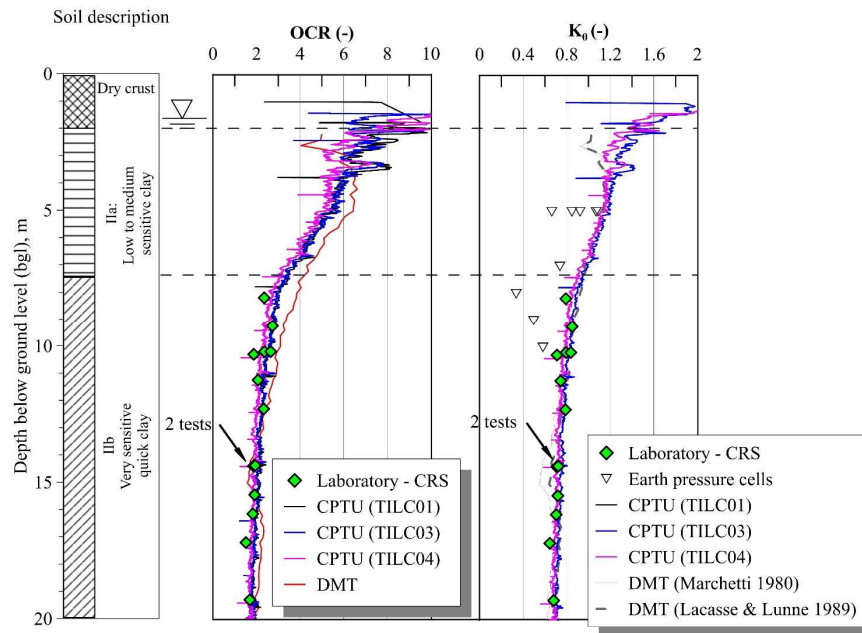
Figure 3- 9 Overconsolidation ratio (OCR) and coefficient of earth pressure at rest (K′₀) with depth (L'Heureux, Lindgård and Emdal, 2019)

As seen in Figure 3- 9, several surveys have been carried out in order to determine coefficient of earth pressure at rest (K'_0) on Tiller-Flotten. Several testing methods has been employed as dilatometer (DMT), earth pressure cells and hydraulic fracturing. Most reliable data were reported by Lindgård and Ofstad (2017) and L'Heureux, Lindgård and Emdal (2019). As seen in Figure 3- 9, correlational equation (2. 31) proposed by L'Heureux et al. (2017) fits with DTM data interpreted both with Marchetti and Lacasse and Lunne correlation parameters. As expected, values of K'_0 fall in a range between 1 and 2 for the upper level and decrease with depth converging to a value of K'_0 of 0.7.

3.3.4 Strength properties

Undrained shear strength (s$_u$)

L'Heureux, Lindgård and Emdal (2019) reported and exhaustive study of undrained shear properties of Tiller-Flotten clay. Based on field and laboratory testing on high quality samples a summary of undrained shear properties is presented in Figure 3- 10. Values are

obtained from falling cone, uniaxial compression test, anisotropic consolidated in extension and in compression triaxial test.
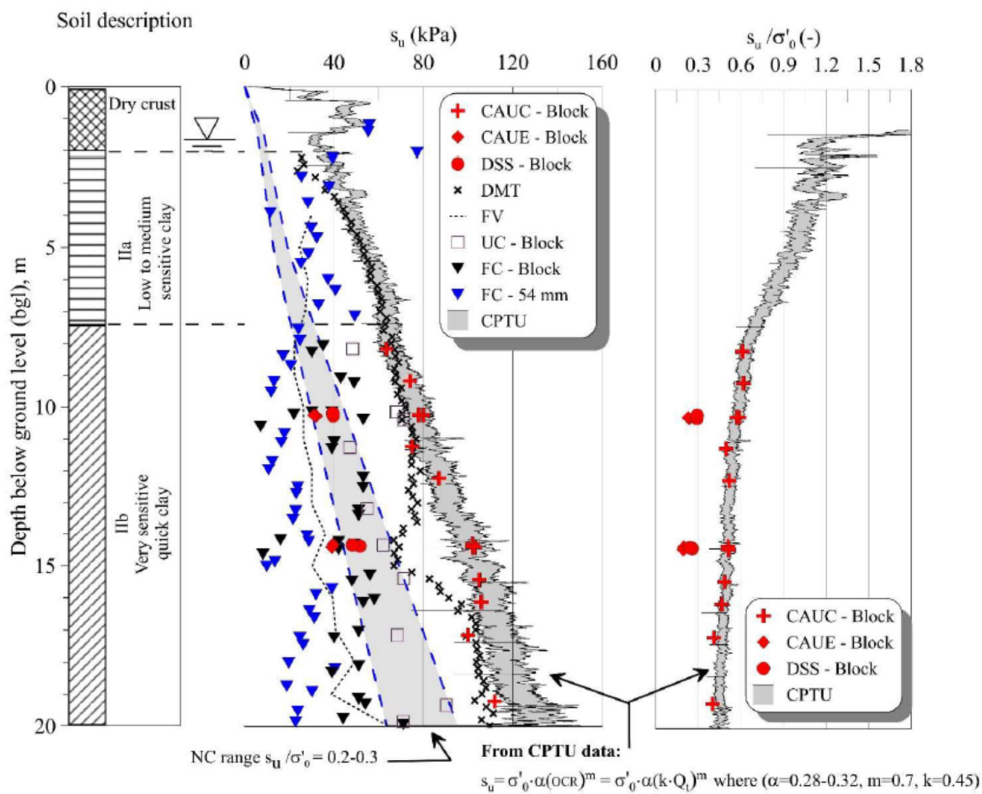
Figure 3- 10 Undrained shear strength profile (from L'Heureux, Lindgård and Emdal, 2019)

Drained strength properties (a, φ)

Results from CAUC and CAUE triaxial test reported in [16] are presented in Figure 3-11. Failure line was defined for a friction angle in the range of 29 and 32°of and a cohesion of 5 kPa.

Friction angle, ϕ [°]	29-32
Cohesion, c [kPa]	5
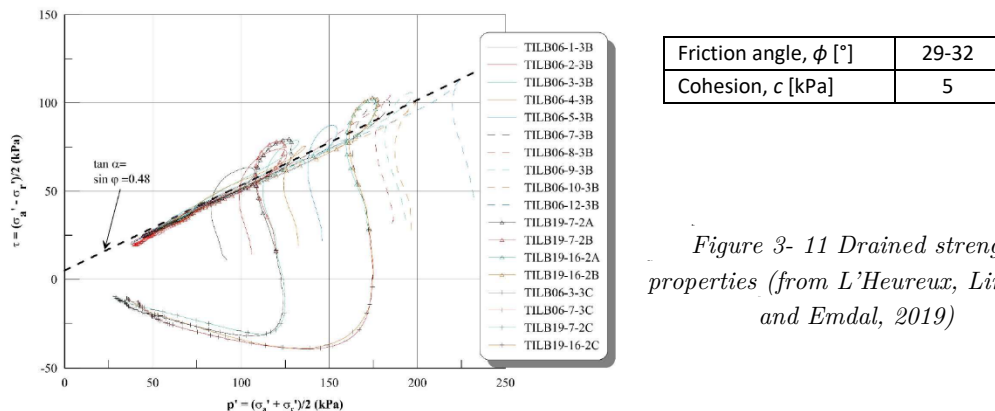
Figure 3- 11 Drained strength properties (from L'Heureux, Lindgård and Emdal, 2019)

Chapter 4

Field testing

4.1 Introduction

In this chapter, a description of field work executed in Tiller-Flotten test site is presented. Two different field-test program were planned: a field-testing program with push-in total earth pressure cells, which started on December 2019 and finished in April 2020; a new round of hydraulic fracturing testing with two new injections tips to be performed during spring 2020.

4.2 Push-in total stress cells

Two push-in earth pressure cells were employed for field testing. The instruments were manufactured by Soil Instruments and acquired by NGI to be tested on NGTS project. The device set up is consist in a spade shaped cell with dimensions 50 cm length and 10 cm width (see Figure 4- 1).
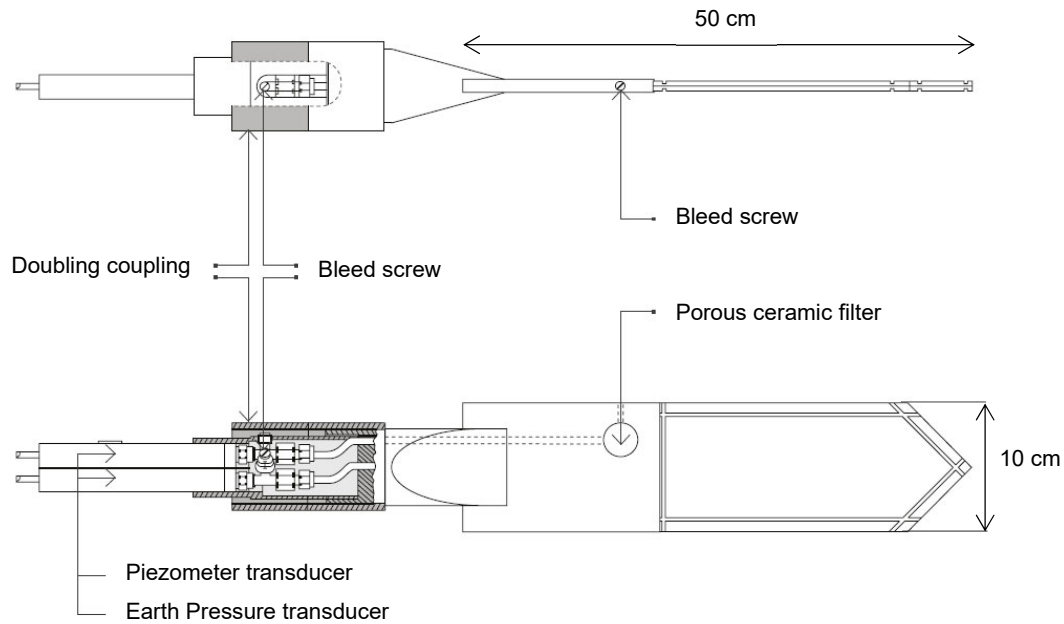
Figure 4- 1 Schematic of the VW Push-In Pressure Cell (source: www.soilinstrumets.co.uk*)*

Push-in cells are wired to a logging system composed by a vibrating wire analyser unit, a multiplexer which multiply number of sensors to be connected, and a datalogger which steer the analyser and collect data. Data logger is connected to a peripheral SIM modem which transfer the collected data to a data base, accessible via Internet.

The initial proposal was to make four installations along two boreholes, one for each push-in cell. The aim was to obtain two parallel profiles, in which the lateral pressure is registered at the same depth levels. In that way, it is possible to compare registered lateral stress values and evaluate the spread and the reliability of the results. As mentioned in Chapter 2, previous investigations in Tiller Flotten with push-in cells shows a large scatter for measurements taken at same depths, specially at 5 m., within in the unit IIa where an *OCR* between 5-6 is reported (see Figure 3- 9). It was planned to make four measurements on each borehole: at 5, 7.5, 10 and 12.5 m depth, with the aim of make measurements at the level with high *OCR*, at the transition between units IIa and IIb and two measurements in unit IIb (very sensitive/ quick-clay levels). Installation at 5 m were performed on December 9th, 2019 and installation at 7.5 m was performed on February 13th, 2020. Unfortunately, the logging system failed on February 26th and the test was stopped. The cells remained on the ground, holding for the appliance to be repaired. Finally, the logging

box was sent to NGI Oslo at the end of April and further test were discarded inside this master thesis project.

The location of the boreholes is given in Table 4- 1 and a location map is available in Appendix A. Boreholes were decided to be placed in perpendicular alignment with the limit of the marsh located at the SW corner of the geo-test site.

Table 4- 1 Coordinates of the installed earth pressure cells

Borehole ID	Earth pressure sensor ID	Pore pressure sensor ID	WGS84 EUREF UTM32/NN2000		
			X [m]	Y [m]	Z [m]
EP36	064036	064032	7023912.520	571100.312	123.000
EP37	064037	064033	7023914.213	571101.039	122.894

Cells were located near 3 piezometers in order to compare pore pressure values registered by push-in cells with those from piezometers. Installations were performed by the help of NTNU engineers Karl Ivar Volden Kvisvik and Espen Andersen. The author was involved in both installation and removal of the equipment.

Before installation, the push-in cells should be prepared in the lab. It is recommended to register zero readings before installation and after removal of the push-in cells from the ground. Zero readings are given in Table 5- 1. The filters for pore pressure measurement should be saturated by submerging the push-in cell in degassed and deionized water before installation. That step was not performed for installations at 5 and 7.5 m.

The boreholes were previously augered with a 12 cm diameter auger drill. The dimension of the auger drill was conditioned by the dimension of the push-in cells (Figure 4- 1). Drilling stopped 40 cm above desired measurement depth, as recommended by NGI from previous experience with this equipment at Onsøy geo-test site and forthwith, push-in cells were pushed through 40 cm of undisturbed soil. This process is done manually by two people. The measurement range for the cells goes from 0 to 300 kPa.

4.2.1 Installation at 5 m depth

First installation was performed on December 3rd, 2019. A 12 cm diameter auger was performed to pre-drill both boreholes until 4.60 m depth. Further, the cells were pushed by hand along the last 40 cm above the target measurement depth. This method was followed based on previous experiences within installation of push-in cells (Massarsch, 1975;

Lindgård and Ofstad, 2017) and also from more recent recommendations from NGI with this equipment. No main difficulties were observed during the installation beside those derived from first experience with the equipment. Once the push-in cells were in place, the borehole was filled with bentonite pellets.

During installation, the push-in cells were connected to the logger to monitor the pressure increase and subsequent decay stabilization. In this phase, the logging frequency was set to 1 minute. One day after installation the reading frequency was set down to 8 hours (3 points per day).

The push-in cells logged until December 21st when logging stopped due to low battery power. Cold temperatures experienced during this period of the year at Tiller-Flotten had a great influence in the battery performance. Nevertheless, enough data were collected, and stabilization line was achieved. A battery with more capacity was also installed to avoid this problem in future installations. It was also possible to make additional readings before the extraction of the cells to confirm stabilization of the lateral pressure values (see Figure B- 1). Push-in cells were removed on February 10th with the help of a tractor. No evident signs of damage in the cells were observed.

Figure 4- 2 Cell extraction procedure for first installation at 5 m
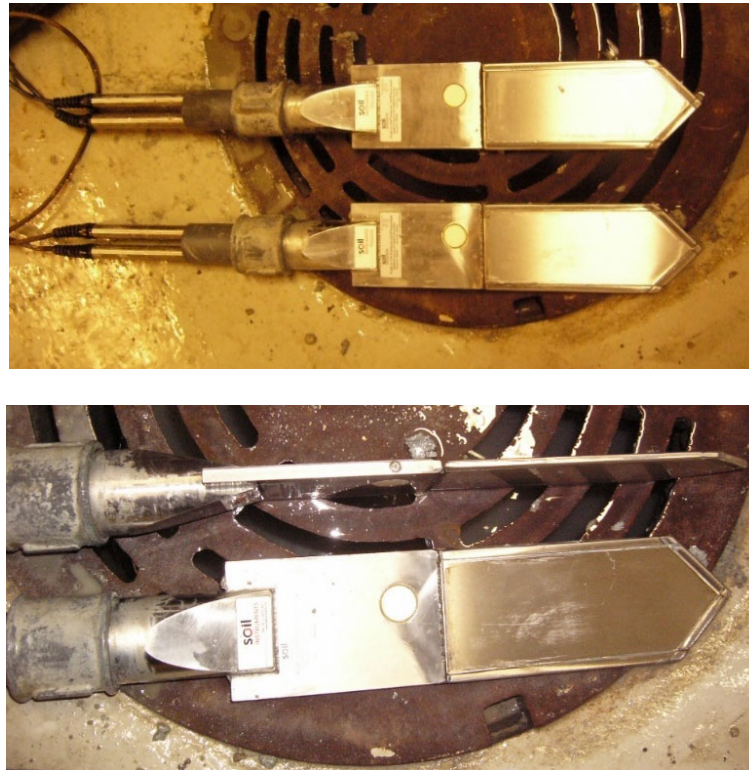
Figure 4- 3 State of the cells after extraction from 5 m

4.2.2 Installation at 7.5 m depth

Installation at 7.5. m was executed on two different steps. First, the borehole was pre-drilled with an auger until it reached 7.10 m. The day after, the push-in cells were installed by pushing them manually. Thereafter, the borehole was filled with bentonite pellets to avoid water entering in contact directly with the push-in cell. This installation occurred with no incidents and the work dynamic was more fluent due to gained experience from first installation.

Reading frequency was set to one minute during installation and reduced to 10 min for stabilization period. Despite the efficient installation process, some issue was reported with logging system. Unfortunately, the logging scrip were not correctly activated after reducing the reading frequency. It was re-started 5 days after installation and, in consequence, pressure decay line could not be registered.

On February 26th it was observed that registered values from data logger were those corresponding to default values (as if no sensor were connected to the analyser unit), indicating a failure in the logging compliance. Condensation was observed inside the logging box which could lead into an electrical failure of electronics components. The box

containing the logging system was placed in a dry place at NTNU installations, while the push-in cells were left in the ground, holding for logging system to be repaired. The components were allowed to dry for few days. It was then decided to remove push-in cell installed at EP37 and use it for testing the logging system at NTNU dependencies. After several testing, it was concluded that data logger and analyser units were working properly but the condensation could have affected the multiplexer.

Push-in cell EP36 was left at 7.5 m depth while the logging device was in repair. After verifying that the analyser unit AVW200 was reading right values, it was decided to take a last measurement on borehole EP36 by connecting the push-in cell directly to the analyser (instead of the multiplexer). As the analyser unit is configured for only reading one sensor, it was decided to only connect lateral pressure sensor 064036 and let it read lateral pressure values during almost one day. This last measurement was taken to verify the stability of the pressure sensor with time. Once some reading values were taken, the box containing logging system was sent to NGI Oslo to repair and installation at 10 and 12.5 m cancelled.

4.3 Hydraulic fracturing – Geonor filter tip

4.3.1 Location and installation of piezometers

As mentioned in section 2.4.1, the first step is the installation of the piezometers in the ground. In total, six piezometers filters were installed by NGI operators in November 2018. Filter tip is a common Casagrande filter tip provided by Geonor (see Figure 4- 4) connected to a 63 mm rubber hose and saturated with the injection fluid. Table 4- 2 summarizes coordinates and installation depths for the piezometers.

Figure 4- 4 Geonor hydraulic npiezometer tip

Table 4- 2 Coordinates and installation depths of the six piezometers during spring 2019

Piezometer ID	EUREF89/UTM32		NN2000
	Northing	Easting	Height
TILH01	7023918.190	571091.100	123.42
TILH02	7023919.390	571089.500	123.45
TILH03	7023917.000	571096.000	123.04
TILH04	7023918.200	571094.400	123.22
TILH05	7023919.400	571092.800	123.42
TILH06	7023920.600	571091.200	123.44

4.3.1 Experimental set-up

The equipment is based on the first settings presented by Bjerrum and Anderson, (1972) and Bozozuk (1974). A general overview is presented in Figure 4- 5 and a basic description of the equipment is presented in diagram in Figure 4- 6. The device is a prototype designed by NGI and tested by the author in the Tiller-Flotten test site in during spring of 2019. Main components are: electronically steered pump, electronic pressure transducer, bladder accumulator, burette, reservoir with injection fluid, rubber hoses, injection tips, logging software, laptop, valves, wheelbarrow to hold the accumulator and place pump and tools, a portable electric generator for power supply, cord and electrical connexions, and a photographic camera.

Figure 4- 5 General overview of the test set-up

Two main improvements have been introduced regarding the prototypes presented in the literature (Bjerrum and Anderson, 1972; Bozozuk, 1974). First improvement in the

experimental set-up is the addition of a an electronically steered pump, facilitating an accurate and constant flow rate. The pump is a pressure/volume controller from GDS Instruments, has a capacity of 200 mm^3 and is equipped with an integral pressure transducer.
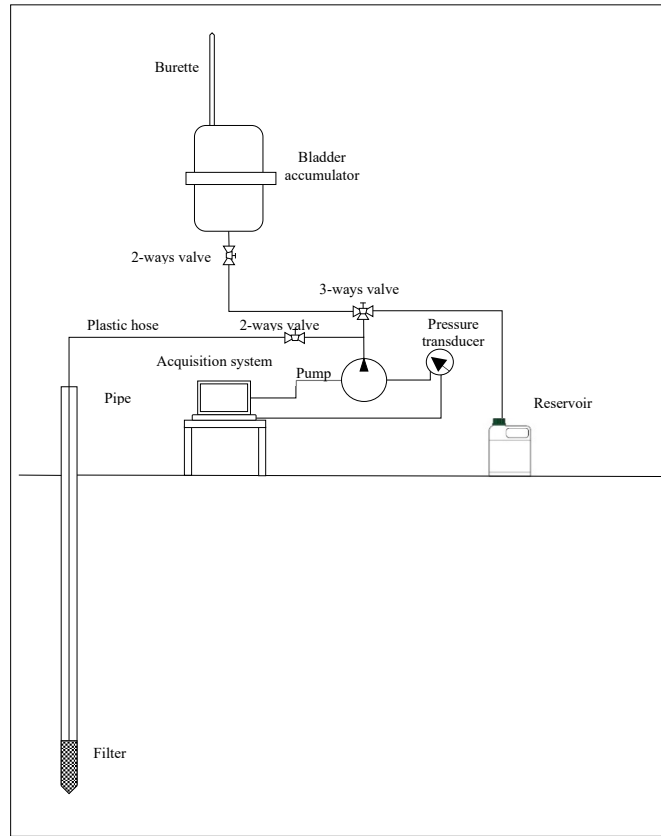
Figure 4- 6 Schematic diagram of hydraulic fracturing test set-up

Pressure working range goes up to 2 MPa with a resolution of 1 kPa. The pressure controller presents the advantage of having portable size, with dimensions 620 × 100 × 400 mm following manufacturer information, and 10 kg weight (see Figure 4- 7). It is a widely instrument used in geotechnical laboratory testing of soils, and it allows the registration of injection parameters as volume and pressure. It is possible to screw an external electronic pressure transducer to the pump if a higher resolution is required.

The second improvement consists in a bladder accumulator. The bladder accumulator is a vessel that holds hydraulic fluid and a compressible gas (see Figure 4- 8). The housing or shell of the accumulator is made of stainless steel and, inside, a flexible rubber bladder separates the oil from the gas. In this case, the bladder accumulator is filled with injection

fluid in both chambers. The rubber bladder is a thin-walled long-stroke rolling diaphragm, made from highly elastic material. It does not present any additional resistance when a change in direction of movement of the fluids occurs inside the accumulator.
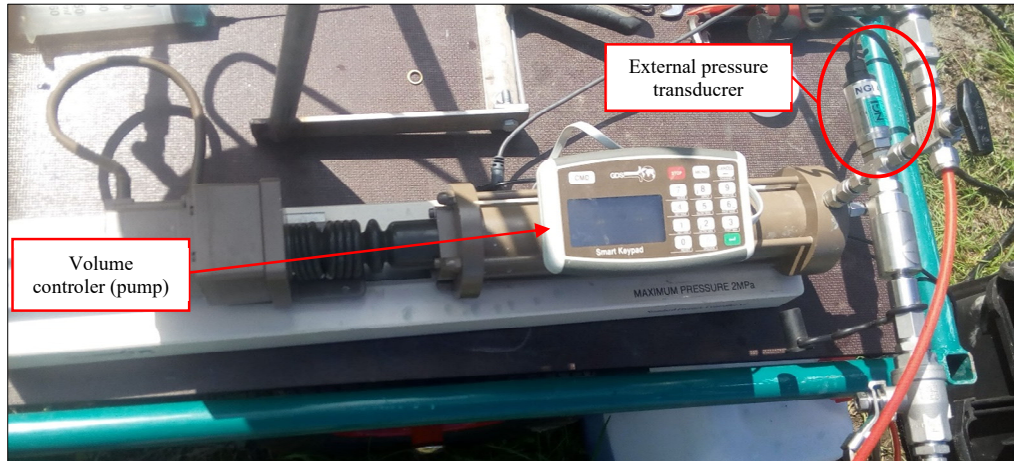
Figure 4- 7 Detail picture of volume controller (pump) and external pressure transducer
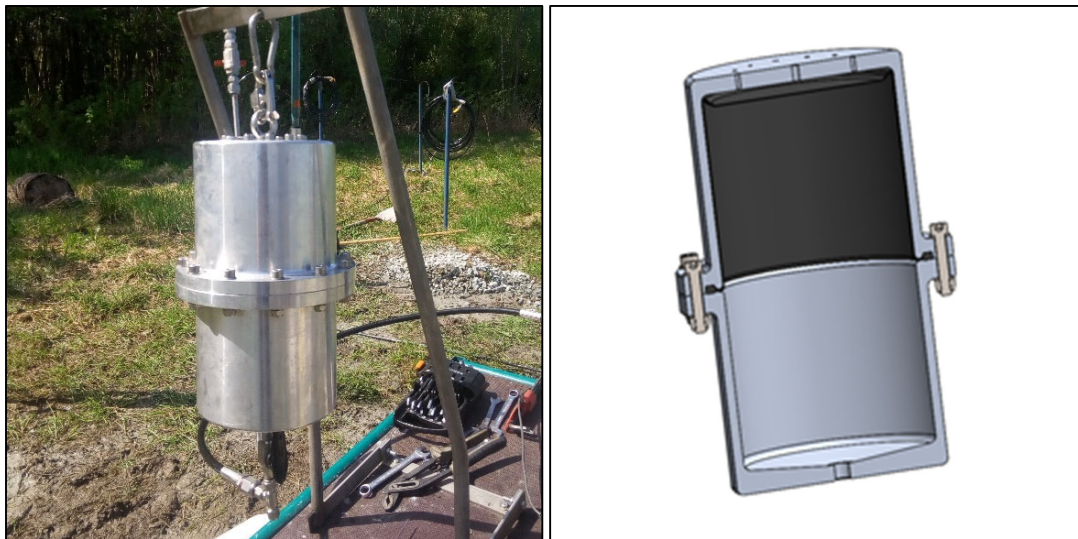
Figure 4- 8 Detail picture of the accumulator bladder and internal configuration of the diaphragm (courtesy of NGI).

The upper chamber of bladder accumulator is open to atmosphere to allow water column to flow freely as in a falling head permeability set up. This is the main function of the accumulator, since the GDS pressure controller works as a blind plug when it is

switched off, thus the entire water column would be suspending, and it would not be possible for the injection fluid to flow without restrictions.

A burette is connected to the upper chamber of the accumulator, in order to monitor the flow rate of the water column during the test. Moreover, the burette acts as an air bleed for the accumulator and hose connecting pump and the piezometer system. When the injection is stopped, the level in the burette is registered every 10 seconds and flow rate is calculated later.

4.3.2 Preparing the test and general proceeding

The experimental setting is easy and do not requires much space. It could be done by one operator. The accumulator is hanging in the rack and the water filled burette is set on the upper outlet as shown in Figure 4- 9. The pore pressure transducer is screwed to one of the pumps outlets. The pressure transducer is connected to the logging system which is connected to a laptop via USB connection. The lines are connected as shown in the diagram on Figure 4- 6 with exception of the piezometer line. The height of the piezometer casing and the pressure transducer to the ground level are measured. A camera is placed on a tripod to record the changes in the burette level.

Figure 4- 9 Filled burette connected to upper outlet of the accumulator

Degassing the system

First step is to purge all the system. No air bubbles should be inside the pump, pressure transducer, bladder accumulator or hoses. Air is a compressible fluid and in the case of being present in the system, the recorded pressure then would be lower than expected.

Pump should be purged in first place by emptying and filling it again with the injection fluid. It is important that the feeding hose of the pump is always below the injection fluid free surface in the reservoir. Once the pump is purged, it also necessary to purge the accumulator bladder. For that purpose, injection fluid is then slowly pumped through the bottom inlet of the accumulator, expanding the membrane upward and pushing out the air through the upper outlet and the burette. The accumulator bladder is purged when no air bobbles are observed flowing out from the upper inlet and when the fluid level in the burette is stable. It is possible that small bubbles continue flowing out from the accumulator but if the level in the burette is constant, it will be assumed that the accumulator system is purged. At that point, the pressure in the pump may be high due to the pressure accumulated in the bladder (it is recommended not go over 100 kPa). The pressure is then reduced to 20-30 kPa and the bottom in the accumulator is closed.

The hose connected to the piezometer tip should be fully saturated also with injection fluid before starting the test. This is done by injecting injection fluid by the help of a syringe until no air bubbles are observed coming out from the hose. After completion of this step, the piezometer hose is connected to the pump.

Finally, air should be removed from the external pressure transducer connected to the pump. For that purpose, it is necessary to partially unscrew the pressure transducer and pump out some fluid until no air is observed flowing out. Screw pressure sensor again and stop the pump.

Zeroing the pressure sensor

Once the pressure sensor is fastened again to the pump, zero level pressure is to be set in the logging system. In the ModLab software it is necessary to follow the next sequence:

| ZERO READING | → | PRESSURE SENSOR | → | START | Read for 5 seconds → | STOP | → | APPLY VALUE |

Pressure values registered both on pressure transducer and integrated pressure transducer in the pump should coincide.

Test procedure

After zeroing the pressure sensor, the piezometer hose is connected to the injection pump and the equipment is ready to perform the test. It is recommendable to check that the pump is completely full before starting the test. Logging is started a few minutes before switching on the pumping. Once the pumping rate is fixed, the pump is activated and right away the valves against piezometer and accumulator should be opened. If the water level at the burette falls suddenly at that point, it is a clear symptom that there is air in the system.

During the test, the pressure rises until pressure breakdown where a pressure drop is expected (and observed as it will be described in next section). After pressure dropping, injection was continued until it begins to increase again, indicating that the fracture is fully open. At that point, the pump is shut down in and the pressure allowed for dissipation for 30 minutes. Flow in the burette should be recorded.

At the end of the test, valves in the piezometer and in the accumulator are closed and the data file saved. It is also recommended to take a print screen with logged pressure.

4.3.3 February 2019 – Geonor filter tip - 5, 10 and 15 m depth

Installation of six piezometers was done in November 2018 by operators from NGI. Piezometers filters TILH01 and TILH04 were installed at 5 m, TILH02 and TILH05 were installed at 10 m depth, and TILH03 and TILH06 were installed at 15 m depth. During the first round, in February 2019, two different injections rate, 15 and 20 ml/min, were used (see Table 4- 3) although no evidence of influence of the test results is described Bozozuk (1974). No remarkable issues to be mentioned during the first testing round. Table 4- 3 summarizes installation depths and injection rate for the testing performed in February 2019. A period of two months elapsed between the installation of the piezometers and the hydraulic fracturing test, ensuring the total stabilization of pore pressure (Bjerrum *et al.*, 1972).

During the first attempt at 10 m in borehole TILH02, three more injection sequences were performed after first injection-pressure dissipation cycle. The main target was to observe the behaviour of pressure in the ground after a first breakdown. This is a common practice in hydraulic fracturing in rock mass since the closure and reopening pressures are

controlled by the minimum principal compressive stress (Nolen-Hoeksema, 2013). In general, it is advisable to conduct a second cycle additional pressurization cycles beyond the second cycle (after first breaking-closing cycle) to confirm that values of fracture closure pressure (P_f) has been achieved (Lin *et al.*, 2008). Flow rate was the same as during the first cycle, but less dissipation time was left between successive pumping sequences during the second cycle. Results are presented in Appendix C.

Table 4- 3 Installation and injection rates for testing round in February 2019

Piezometer ID	Depth [m]	Injection rate [ml/min]	Comments
TILH01	5	20	No flow record after shut-in
TILH02	10	20	4 injection sequences, pump refilling, No flow record after shut-in
TILH03	15	15	No flow record after shut-in
TILH04	5	15	No flow record after shut-in
TILH05	10	20	No flow record after shut-in
TILH06	15	20	Pump refilling

If it is worth to mentioning, the pump capacity in some cases was not enough to reach breakdown pressure. In these cases, the valve to the piezometer filter was closed to preserve the pressure level, and the pump set for refilling. Later, the test was started again with no evidence of big variation in recorded pressure. It is important to mention that there was no registration of the level in the burette.

4.3.4 May 2019 - Geonor piezometers at 5, 10 and 15 m depth

The second round was performed in May 2019 at the same depth levels. Main purpose was to check the repeatability of the test. It is not expected to reach the same pressure values due to reconsolidation occurred in the clay after the first injection cycle. After reviewing the test procedure with NGI, the variation of the level in the burette was recorded by taking pictures every 10 seconds. The injection rate was set to 20 ml/min for the six piezometers. For piezometer TILH04, TILH03 and TILH06 the syringe pump had to be stopped for refilling (see Table 4- 4).

Table 4- 4 Installation and injection rates for testing round in May 2019

Piezometer ID	Depth [m]	Injection rate [ml/min]	Comments
TILH01	5	20	
TILH02	10	20	
TILH03	15	20	Test stopped due to pump refilling
TILH04	5	20	Test stopped due to pump refilling
TILH05	10	20	
TILH06	15	20	Test stopped due to pump refilling

4.3.5 June 2019 - Geonor piezometers at 7, 12, and 17 m depth

The piezometer filters were pushed down the 23rd May by NTNU operators. Each filter was pushed down 2 m, so the new reached depths were 7, 12 and 17 m. New depths and flow rate are presented in Table 4- 5. To allow stabilization of pore pressure, two weeks' time were left before starting the new injections and a new round of test were performed the 6th June. An injection rate of 20 ml/min was used on each test. With the help of a photographic camera, the fluid level at the burette was also registered.

Table 4- 5 Installation and injection rates for testing round in June 2019

Piezometer ID	Installation depth [m]	Injection rate [ml/min]	Remarks Comments
TILH01	7	20	-
TILH02	12	20	Test stopped due to pump refilling
TILH03	17	20	Test stopped due to pump refilling
TILH04	7	20	No logfile, only print screen
TILH05	12	20	-
TILH06	17	20	Test stopped due to pump refilling, leakage after re-starting the test

There was an issue during the execution of test at borehole TILH04 where no data were recorded during the test but fortunately, a screenshot of the logged could be saved. It was also recorded a leakage during testing in piezometer TILH06. Also test performed in piezometers TILH02 and TILH03 were stopped to refill the pump.

4.4 Hydraulic fracturing – Preference fracturing tips

After the previous injection tests performed during spring 2019, it was decided to introduce some modification in the test set up. First, as it was decided to use a second pump to increase available injection fluid volume to 400 ml. As it was observed during pilot testing, the GDS cylinder volume capacity was not enough to reach fracturing pressure and the test should be stopped for refilling. For that purpose, an additional GDS cylinder was attached to the pumping system

The second modification to the original NGI's set up is to use a new injection tip to avoid cylindrical geometry and consequent cavity expansion of plasticized soil. As it was observed from previous pilot testing, high lateral stress values were registered than expected. It was also possible to examine an increase in the opening pressure during testing on piezometer TILH02 (Figure C- 2), where three successive injection sequences were performed. It was then hypotized that the affected material was not fracturing in a crack or flat crack shape but behaving as an expanding cavity which allows for higher injection pressures before failing for each injection sequence.
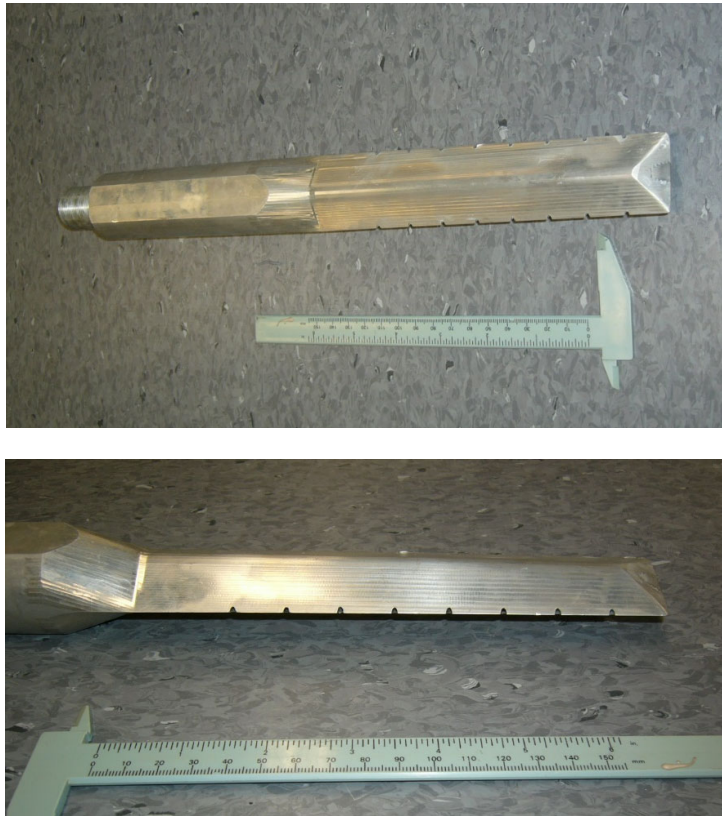
Figure 4- 10 Nozzle A- Thin spade

The idea was then to create a weakness plane in the injection area as simulating a vertical crack, by cutting or pre-cutting the soil before injection. Two tips were then designed in collaboration with engineer by Frank Særthli at NTNU. Tips are shown in Figure 4- 10 and Figure 4- 11 . It was planned to create an inner geometry, similar to those which is found in a normal piezometer tip, with a pocket and a filter but it was technically difficult. Finally, it was decided to avoid filter and the pocket.
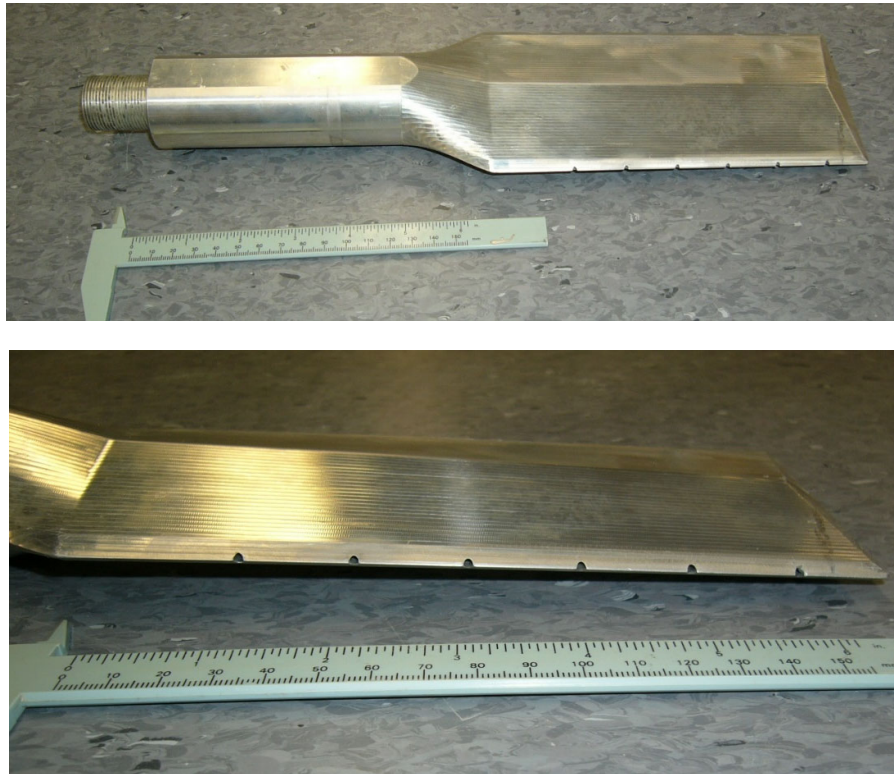
Figure 4- 11 Nozzle B – Wide spade

Lastly, as for the test program for spring 2020 there was no availability to use NGI's logging system, engineer Per Asbjørn Østensen form NTNU developed a simple volume/pressure logging system with LabView.

4.4.1 June 2020 – New injection nozzle A at 8.30 m

The installation of injection nozzle A was performed on June 11th. The procedure for the setting up of the equipment is presented in previous sections except for no pressure sensor transducer is employed for this test. It was necessary to auger with an 8 cm diameter auger drill rod down to 7 m. Thereafter, it was planned to push the rod by hand the last meter. However, it was only possible to push the though 10 cm and the rest was pushed down with the help of a drill rig. During this process, the main challenge was to avoid the obturation of the injection holes with clay. It was decided then to use one of the pumps as a pressure controller. A target pressure of 25 kPa was set during pushing down the injection nozzle. This will also help to remove remaining air in the injection nozzle.

The logging started before pushing down the injection nozzle into the ground. Once the injection nozzle was at the desired investigation depth, the injection was started with a rate of 30 ml/min, and valves against accumulator and piezometer opened. During the test, the registered pressure values were erratic, and it was difficult to decide when to stop the pump for stabilization. Therefore, pumping was stopped when a drop in pressure was registered. Four cycles of injection were performed. It is remarkable that the level at the burette was constant after shutting down of the pump.

4.4.2 June 2020 – New injection nozzle B at 9.30 m

The installation of injection nozzle was performed on June 17th. The setting up of the equipment is similar to the one employed for the installation ofthin spade (nozzle A).

The procedure for the setting up of the equipment is presented in previous sections except for no pressure sensor transducer is employed for this test. It was necessary to auger the bore hole again with a 10 cm diameter auger drill due to the dimensions of the injection nozzle. The auger was then driven down to 8 m and the injection nozzle pushed down until reaching 9.30 m depth. This last step was also performed by the help drill rig. From previous experience during the installation of nozzle A, the borehole was partially filled with water to ensure fully saturation of the injection tip and avoid the entry of clay fines in the injection holes. The pressure applied during the introduction of the injection nozzle into the ground was set to 100 kPa.

The logging started before pushing down the injection nozzle into the ground. The pressure controller needed some minutes to reach the flushing pressure so one-third way of the pushing down of the nozzle was done while building up of pressure. The logging system failed when the nozzle was halfway to installation depth so there is no data recorded from that point to the start of the test.

Once the injection nozzle was at the desired investigation depth, the pumping was started with a rate of 30 ml/min and valves against accumulator and injection hose opened. The initial pressure at the injection tip was recorded before starting the test. Three injection cycles were performed. Results are presented in Appendix C. During the first injection test, the pump was stopped after pressure dropped. It was left to stabilization, but pressure values showed erratic behaviour. Hence, a second injection test was started with no satisfactory results. After refilling the pumps, always with the valves at piezometer and accumulator closed, a third injection cycle was started. Pressure dropped when reaching

201.5 kPa and the curve shape was similar to those registered in previous experiences in 2019. It was then decided to continue pumping until pressure increases again and pump shut in thereafter. Stabilization was allowed for 10 minutes.

Both injection nozzles were recovered by the help of a drilling rig. Clay obstructing the openings was found after flushing both nozzle with air and water. Enough marine clay to tight the outlets was collected (see Figure 4- 12). It is difficult to confirm if the clay came into the nozzle during installation or removing process.

Figure 4- 12 Collected clay from nozzle A (left) and nozzle B (right)

Chapter 5

Results

5.1 Introduction

In this chapter the results from the field testing are presented. The results are presented in the same order as the methods were presented in Chapter 4. At the end of this chapter, $K_0^{'}$ values derived from field testing within this master thesis project are compared with previous $K_0^{'}$ values reported from different field methods surveys at Tiller-Flotten.

5.2 Push-in Total Stress Cells

Table 5- 1 presents an overview of the results obtained from push-in cells installed at Tiller-Flotten test site. For push-in cell EP36, lateral pressure sensor has id. 064036 and pore pressure sensor with id. 064032. Push-in cell EP37 contains lateral pressure sensor with id. 064037 and pore pressure sensor with id. 064033. Parameters presented in Table 5- 1 are:

- σ_{ho} is the *in situ* horizontal total stress derived from the stabilized value of pressure sensor without corrections from air pressure.
- u_{EP} is pore pressure value measured from pore pressure sensor integrated in the push-in cell (these two parameters are calculated from calibration functions attached in Appendix B).

- σ'_{vo} is the best estimation of effective vertical stress calculated assuming an average unit weight $\gamma = 18.5 \frac{kN}{m^3}$

- σ'_{ho} is the *in situ* horizontal effective stress, calculated by subtracting u to σ_{ho}; and finally K'_0 is calculated by equation (2. 1).

- If available, zero readings before and after the installation of the push-in cells are given.

Table 5- 1 Overview of earth pressure cell testing at Tiller-Flotten. Zero readings are relative to atmospheric pressure (100 kPa)

Date	Depth	Borehole	Sensor	σ_{ho}	u_{EP}	σ'_{ho}	σ'_{vo}	K'_0	Zero readings	
									Before installation	After installation
	[m]	ID	[m]	[kPa]	[kPa]	[kPa]	[kPa]	[-]		
08.12.2019	5	EP36	064036	98.30	-	69.97	64.17	1.09	5942.075[a]	5265.655[b]
			064032	-	28.33				6389.280[a]	6149.519[b]
		EP37	064037	102.30	-	69.58	59.77	1.16	5925.897[a]	5217.707[b]
			064033	-	32.73				6444.901[a]	6220.993[b]
26.02.2020	7.5	EP36	064036	104.37	-	59.46	92.99	0.64	5925.687[a]	-
			064032	-	45.76				6391.658[a]	-
		EP37	064037	100.81	-	59.24	97.18	0.61	5897.122[a]	-
			064033	-	41.57				6448.842[a]	-

a.   *Zero reading taking at test site*

b.   *Zero reading taken at NTNU dependencies*

As mentioned in subsection 4.2.2, there was a last measurement taken on borehole were push-in cell EP36 was installed at 7.5 m depth, performed 30th April 2020. It was only possible to record lateral pressure form sensor 064036. Values are presented in Table 5- 2.

Table 5- 2 Control measurement for lateral pressure in EP36 push-in cell

Date	Depth [m]	Borehole ID	Sensor [m]	σ_{ho} [kPa]	u [kPa]	σ'_{ho} [kPa]	σ'_{vo} [kPa]	K'_0 [-]
30.04.20	7.5	EP36	064036	103.84	45.76*	58.08	89.24	0.65

* From last measurement on February 2020

Figure 5- 1 presents the evolution of measured in situ effective horizontal stress versus depth and derived K'_0 values from push-in cells measurements are summarized in Figure 5-2.
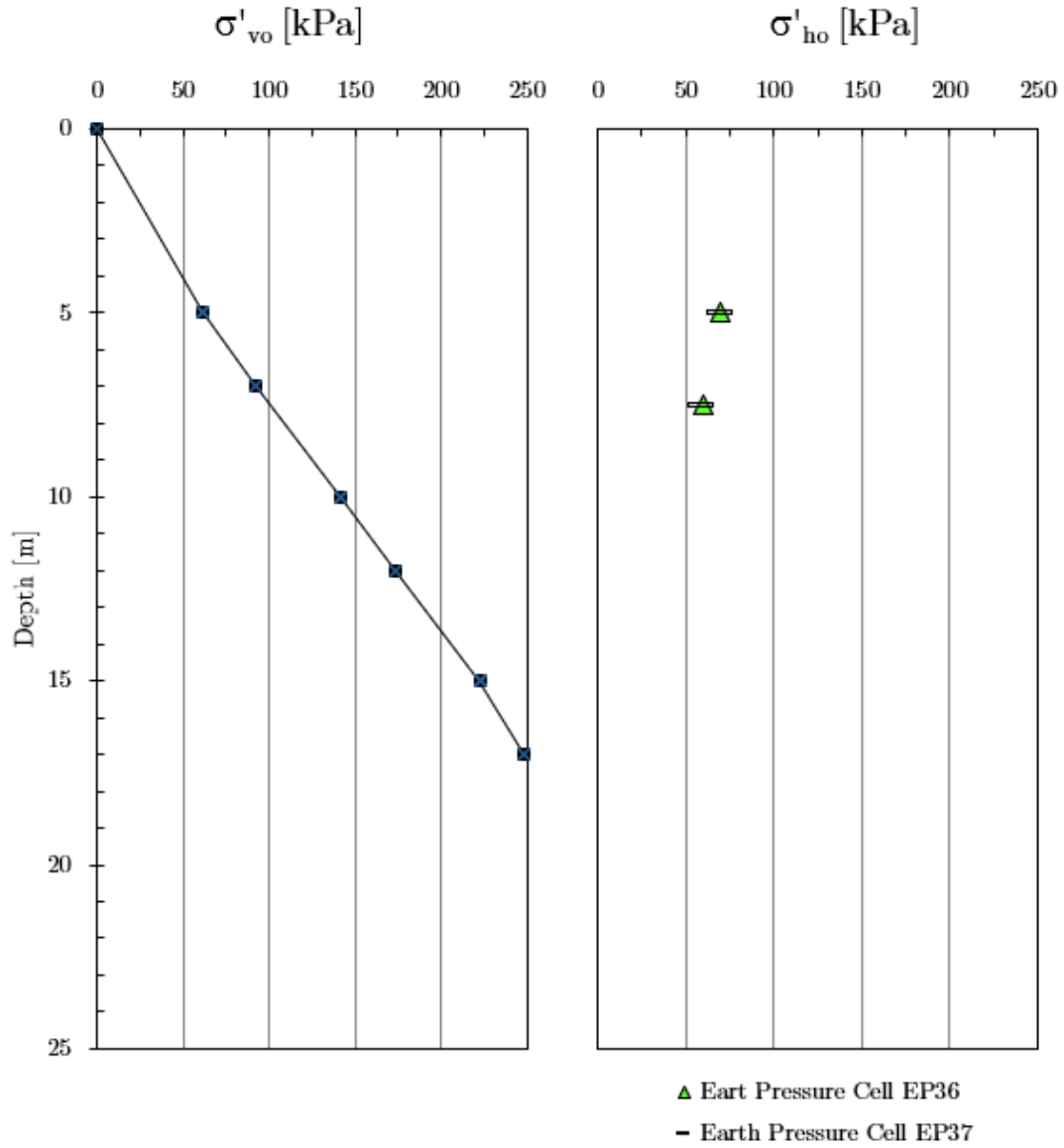
Figure 5- 1 Left: effective vertical stress (σ_v') profile; right: effective vertical stress (σ_h') profile obtained from push-in earth pressure cells at Tiller-Flotten by the author during spring 2020
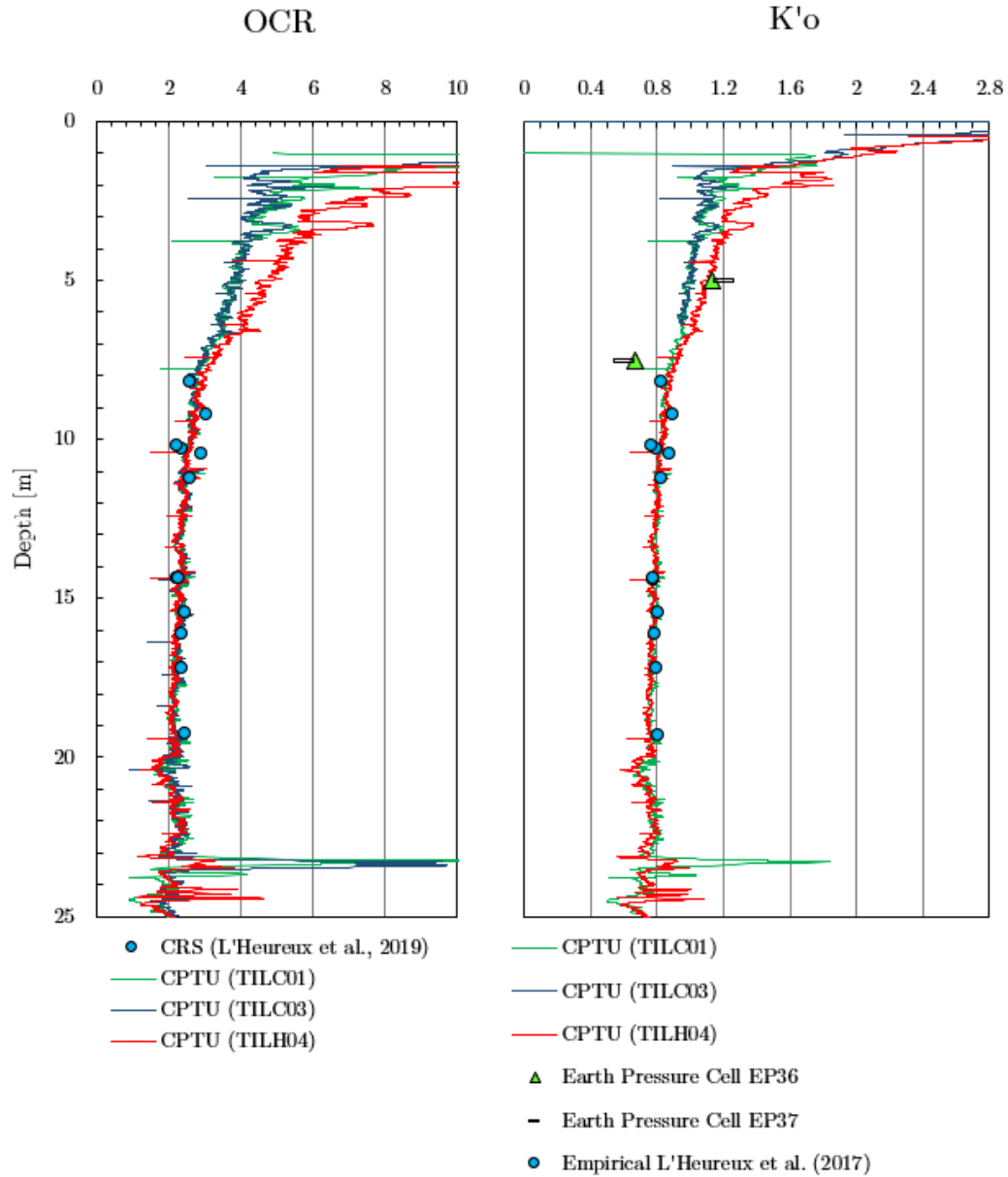
Figure 5- 2 Left: OCR profile vs. depth from CRS oedometer test and CPTU sounding (from L'Heureux, Lindgård and Emdal, 2019); right: derived K_0' values from push-in earth pressure cells (performed during spring 2020 by the author) and previously reported K_0' values from empirical correlations from CPTU data and from CRS oedometer test (from L'Heureux, Lindgård and Emdal, 2019)

In Appendix B, raw data with the evolution of earth pressure and pore pressure throughout installation time is presented. Derived values of K_0' from push-in cells are presented together with K_0' other in situ and empirical methods in **Error! Reference source not found.** at the end of this chapter.

5.3 Hydraulic fracturing – Geonor piezometer

During spring 2019 and within the specialization project thesis reported by the author, the acquired field data from hydraulic fracturing test have been processed by the methodology described in Bozozuk (1974). Data treatment and analysis were made with the help of Excel spreadsheet. An average unit weight of $\gamma = 18.5 \, kN/m^3$ is assumed along the whole profile. Groundwater level is assumed to be at 2 m depth.

For the completion of this master thesis, reported data in 2019 are reviewed with the help of Aleksander S. Gundersen (NGI). There is an initial water head over pressure transducer equivalent to the height between the top of the accumulator and the pressure sensor. This distance is 0.65 m which is equivalent to 6.5 kPa (Y). A value for Y between 3 and 10 kPa is acceptable (personal communication with Aleksander S. Gundersen). If not, probably the accumulator might have been pressurized during air bleeding. Hence, raw data should be corrected for possible drift.
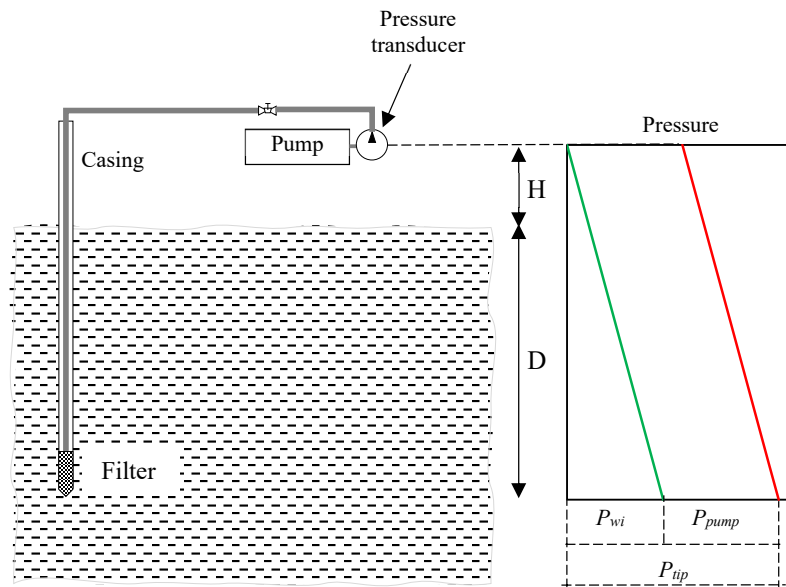
Figure 5- 3 Schematic representation of initial excess water pressure at measurement point due to water column (P_{wi}) and total pressure at the injection tip (P_{tip})

As the pressure sensor is not installed at measurement depth (Figure 5- 3), the pressure due to water column between pressure itself and injection tip. This is called initial excess

water pressure (P_{wi}). Excess water pressure is dependent on the length of the casing from ground or investigation depth (D) and the height of pressure sensor to ground surface (H), as showed in Figure 5- 3.

$$P_{wi} = (D + H) \cdot \gamma_w \qquad (5.1)$$

Thus, the pressure at injection tip is expressed as:

$$P_{tip} = P_{pump} + P_{wi} \qquad (5.2)$$

The determination of the closure pressure ($P_{closure}$) is approached by the assumption of stabilization of the dissipation curve is reached after approximate 30 minutes, despite for most of the cases the final decay values of pressure are higher than the in situ pore pressure (u_o). This approach agrees with most of the methods found on literature (Bjerrum and Anderson, 1972; Bozozuk, 1974; Lefebvre *et al.*, 1991; Hamouche *et al.*, 1995). Closing pressure is defined as the intersection point between the tangents to the pressure decay and pressure dissipation branches on pressure versus time plot (see Figure 5- 4). From closing pressure (P_c) it is possible then to calculate total horizontal stress as:

$$\sigma_h = P_{closure} + P_{wi} \qquad (5.3)$$
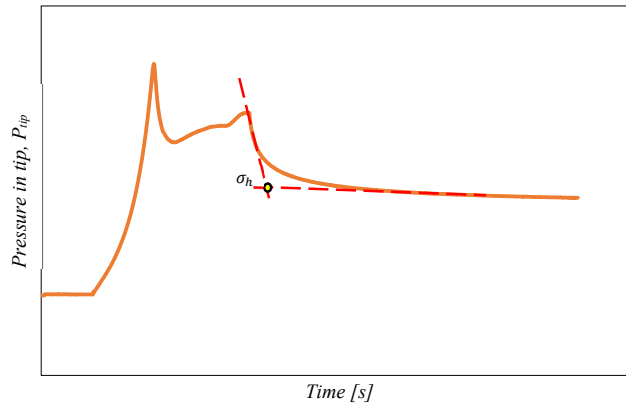
Figure 5- 4 Schematic representation of the determination of in situ total horizontal (σ_h) stress from pressure at the filter tip, (P_{tip}). P_{tip} curve is calculated by adding initial excess pressure (P_{wi}) to pressure in the pump versus time logging from hydraulic fracturing injection test (drawn by the author)

The graphical representation of pressure variation with time is presented in Appendix C. Table 5- 3 shows a summary of following parameters:

u_o: in-situ pore pressure (from L'Heureux, Lindgård and Emdal, 2019)

σ'_v: in situ effective vertical stress calculated from $\gamma = 18.5 \ kN/m^3$

P_{wi}: excess pressure at filter tip due to water column (see also Figure 5- 4)

$P_{fracture}$: maximum pressure registered during hydraulic fracturing test

$P_{closure}$: read closing pressure form pressure vs. time charts

σ_h : in situ total horizontal stress calculated from equation (5. 3)

σ'_h: in situ effective horizontal stress calculated as $\sigma_h - u_o$

K'_o: coefficient of lateral earth pressure at rest, calculated from equation (2. 1).

Table 5- 3 Overview of hydraulic fracturing testing results at Flotten Geo-Test Site.

Depth [m]	Borehole ID	Date	u_o [kPa]	σ'_v [kPa]	P_{wi} [kPa]	$P_{fracture}$ [kPa]	$P_{closure}$ [kPa]	σ_h [kPa]	σ'_h [kPa]	K'_o [-]	Comments
5	TILH01	25.02.2019	31	61.5	55.5	195.5	103.5	159.0	128.0	2.08	
5	TILH01	21.05.2019	31	61.5	55.5	139.2	79.7	135.2	104.2	1.69	
5	TILH04	26.02.2019	31	61.5	55.5	176.1	97.6	153.1	122.1	1.99	
5	TILH04	22.05.2019	31	61.5	55.5	150.0	104.3	159.8	128.8	2.09	
7	TILH01	06.06.2019	37	92.5	75.5	136.7	78.3	153.9	116.9	1.26	
7	TILH04	06.06.2019	37	92.5	75.5	161.6	94.8	170.3	133.3	1.44	No logged data
10	TILH02	25.02.2019	43	142.0	105.5	207.4	113.4	218.9	176.0	1.24	
10	TILH02	21.05.2019	43	142.0	105.5	188.0	89.3	194.8	151.8	1.07	
10	TILH05	26.02.2019	43	142.0	105.5	205.3	128.0	233.5	190.5	1.34	
10	TILH05	22.05.2019	43	142.0	105.5	196.0	120.0	225.5	182.5	1.29	
12	TILH02	06.06.2019	48	174.0	125.5	211.0	154.0	279.5	231.5	1.33	Pump refilling
12	TILH05	06.06.2019	48	174.0	125.5	236.7	138.4	236.9	215.9	1.24	
15	TILH03	25.02.2019	55	222.5	155.5	188.3	87.6	218.9	188.1	0.85	Pump refilling
15	TILH03	21.05.2019	55	222.5	155.5	326.0	188.9	344.4	289.4	1.30	Pump refilling
15	TILH06	26.02.2019	55	222.5	155.5	268.0	163.6	319.1	264.1	1.19	
15	TILH06	22.05.2019	55	222.5	155.5	266.5	158.2	313.7	258.7	1.16	Pump refilling
17	TILH03	06.06.2019	66	248.5	175.5	297.4	211.0	386.5	320.5	1.29	Pump refilling
17	TILH06	06.06.2019	66	248.5	175.5	301.2	284.2	359.6	293.6	1.18	Pump refilling

Figure 5- 5 shows a depth profile of effective vertical stress calculated (σ'_v) as well as the evolution of horizontal effective stress (σ'_h) resulting from hydraulic fracturing test performed at Tiller-Flotten by the author in spring 2019. Derived K'_0 values from measured effective horizontal stress by hydraulic fracturing are also presented in Figure 5- 5. These values are plotted together with K'_0 values previously reported in L'Heureux, Lindgård and Emdal (2019), derived from CPTU and OCR from CRS oedometer test.
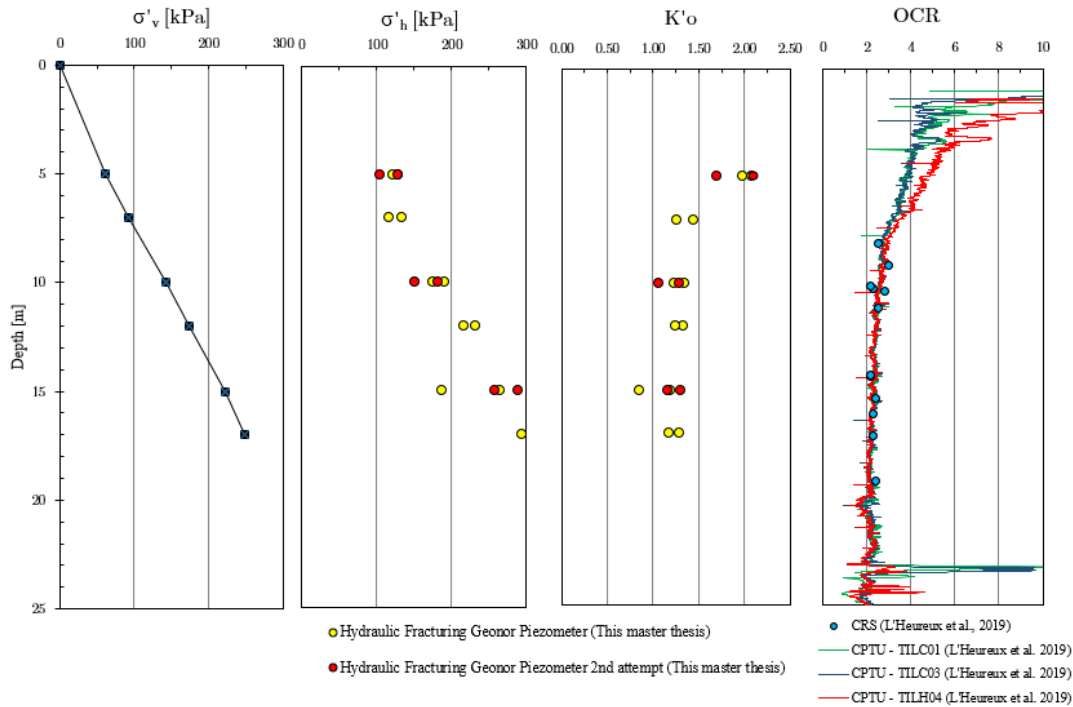
Figure 5- 5 From left to right: effective vertical stress (σ'_v) profile; effective horizontal stress (σ'_h) profile obtained from hydraulic fracturing testing in Tiller-Flotten; K'_0 profile derived from horizontal stress obtained from hydraulic fracturing OCR profile at Tiller-Flotten derived from CRS oedometer testing and CPTU sounding (from L'Heureux, Lindgård and Emdal, 2019)

As mentioned in chapter 4, during the first injection attempt at 10 m in borehole TILH02, a second injection cycle was performed in order to measure the re-opening fracture pressure. Results are presented in Table 5- 4. An increase in re-opening fracture pressure is observed. From results reported in Table 5- 4 above, and regarding the high horizontal stress obtained by hydraulic fracturing, it might be interesting to look deeply into the fracture pressures in order to assess the governing fracture mechanism when a fluid is injected into the clay at Flotten-Tiller.

Table 5- 4 Re-opening fracture pressure values for TILH02 at 10 m depth

Pump sequence	Re-opening fracture pressure [kPa]
Initial	207.4
2nd	190.0
3rd	197.2
4th	199.0

Figure 5- 6 present a depth profile with measured pressure fractures and those calculated theoretically from shear failure mode and cavity expansion mode. Only data from test performed for first time have been included. Pressure fracturing values have been corrected by adding the initial excess pressure (P_{wi}) corresponding to each depth.

In order to obtain theoretical fracturing pressures, total horizontal values are derived from theoretical $K_0^{'}$ equation from L'Heureux *et al.*, (2017)

$$K_o^{'} = 0.52 \cdot OCR^{0.47} \tag{5.3}$$

Shear failure mode is calculated as:

$$P_{failure} = \sigma_h - 2s_u \tag{5.4}$$

Cavity expansion falilure mode is calculated as:

$$P_{failure} = \sigma_h + s_u \left[1 + ln\left(\frac{G}{s_u}\right)\right] \tag{2.49}$$

Input parameters are summarized in Table and a plot with measured and theoretical fracture pressure values is found in Figure 5- 6.

Table 5- 5 Input parameters for determination of theoretical fracture pressure

Depth [m]	OCR [-]	$K_0^{'}$ [-]	σ_h [kPa]	G_{50} [kPa]	s_u^{DSS} [kPa]
5	4.4	1.04	95.2	30000	17
7	3.1	0.86	94.0	30000	22
10	1.7	0.67	118.9	37500	40
12	1.6	0.65	118.9	37500	42
15	1.5	0.63	137.4	50000	52
17	1.5	0.63	137.4	50000	57

Figure 5- 6 Comparison between fracturing pressures (P$_{fracture}$) obtained from hydraulic fracturing and theoretical pressure fractures from shear failure and cavity expansion mechanisms

5.4 Hydraulic fracturing – Preference fracturing opening

Results from pilot testing with the new nozzles are presented in Figure C- 19 and Figure C- 20 in Appendix C. It is not possible to define an opening fracture pressure neither a closing pressure from results obtained during testing performed with nozzle A (thin spade on Figure 4- 10). During the third injection cycle performed in the testing with nozzle B (wide spade on Figure 4- 11), a well-defined pressure vs. time lime was registered. Table 5- 6 presents the results derived from raw data and from applying the same methodology previously described in this section. Results are also plotted in Figure 5- 7.

Table 5- 6 Derived K_0'-values from pilot test with preference fracture opening direction nozzles

Depth [m]	Borehole ID	Date	u_o [kPa]	σ_v' [kPa]	P_{wi} [kPa]	$P_{fracture}$ [kPa]	$P_{closure}$ [kPa]	σ_h [kPa]	σ_h' [kPa]	K_O' [-]	Comments
8.3	TILH07	11.06.2020	39	114.6	88.5	-	-	-	-	-	Thin spade
9.3	TILH07	17.06.2020	41	131.1	98.5	203	68.9	167.4	126.4	0.96	Wide spade
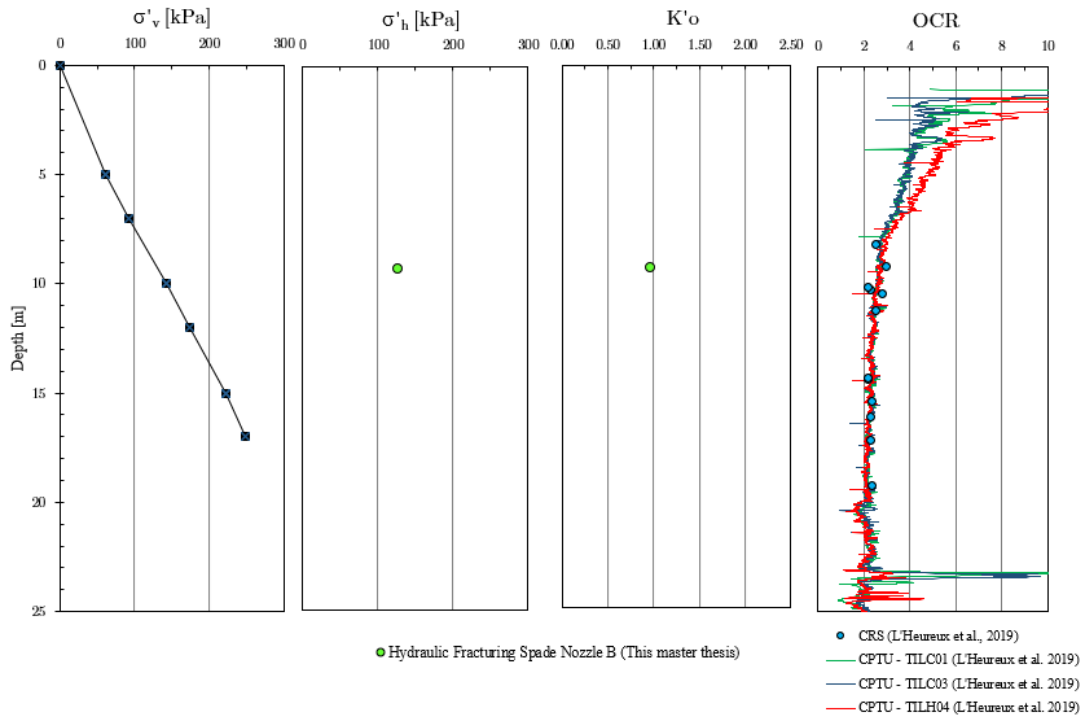
Figure 5- 7 From left to right: effective vertical stress (σ_v') profile; effective horizontal stress (σ_h') profile obtained from hydraulic fracturing with new injection spade B in Tiller-Flotten; K_0' profile derived from measured horizontal stress; OCR profile at Tiller-Flotten derived from CRS testing and CPTU sounding (from L'Heureux, Lindgård and Emdal, 2019)

5.5 Evaluation with previous investigations and correlation methods

Previous investigations have been performed at Tiller-Flotten test site related to the determination of K_o'. Lindgård and Ofstad (2017) designed and executed a field test program for the measurement of in situ stress state determination. Methods employed were dilatometer, earth pressure cells and field vane test. Data from CPTU is also available in the publication from L'Heureux, Lindgård and Emdal (2019), and will be included in the discussion of the results. Results are also compared with the values obtained by correlation methods mentioned in section 2.6, in line with work done presented by Lindgård and Ofstad

(2017) and to complement the work presented in their master thesis. The input parameters for the correlation methods and the calculated K_0'-values are summarized in Table 5- 7.

Table 5- 7 Input parameters use on correlation methods and K_0'-values (Lindgård and Ofstad, 2017; L'Heureux et al., 2019)

Depth [m]	Friction angle [°]	OCR [-]	K_0' L'Heureux (2017) [-]
5	31	4.4	1.04
7	31	3.1	0.89
7.5	28	2	0.72
9.3	28	1.6	0.65
10	28	3.1	0.67
12	28	3.1	0.65
15	28	1.5	0.63
17	28	1.5	0.63

○ Hydraulic Fracturing Geonor Piezometer (This master thesis)

● Hydraulic Fracturing Geonor Piezometer 2nd attempt (This master thesis)

○ Hydraulic Fracturing Spade Nozzle B (This master thesis)

△ Earth Pressure Cell EP36 (this master thesis)

− Earth Pressure Cell EP37 (this master thesis)

— CPTU - TILC01 (L'Heureux et al. 2019)
— CPTU - TILC03 (L'Heureux et al. 2019)
— CPTU - TILH04 (L'Heureux et al. 2019)
� Earth Pressure Cells (Lindgård and Ofstad, 2017)
✗ Empirical L'Heureux et al. (2017)
● CRS (L'Heureux et al., 2019)

Figure 5- 8 from left to right: effective vertical stress (σ_v') profile; effective horizontal stress (σ_h') profile obtained from in situ testing performed by the author compared with results from previous investigations in Tiller-Flotten; K_0' profile derived from horizontal stress obtained from in situ testing performed by the author compared with K_0' from previous investigations; OCR profile at Tiller-Flotten derived from CRS testing and CPTU sounding (from L'Heureux, Lindgård and Emdal, 2019)

Chapter 6

Discussion

6.1 Introduction

In this chapter, attained results by the two in situ methods for determining $K_0^{'}$ at Tiller-Flotten test site, push-in cells and hydraulic fracturing, will be discussed. The aim of this chapter is to discuss and learn from experience during conduction of the test, and relate observations done in field with background theory.

6.2 Push-in Total Stress Cells

6.2.1 Setting-up and test execution

The installation of push-in cells is discussed in this section. There are some systematic error sources related to calibration. A quick check of the calibration constants provide by manufacturer should be taken before starting any investigation program. Secondly, the zero reading might be taken before and after execution of the test to control possible drift. Likewise, zero reading should be measured at testing conditions and for enough time to ensure stabilization of the sensors. An important source of error is related also to the fully saturation of the porous filter to measure pore pressure. The manufacturer recommends

submerging the cell in water covering the ceramic filter. This process does not ensure the completely removal of air from system. It is worth to mention previous investigations with Götzl push-in cells at Tiller-Flotten reported by Lindgård and Ofstad (2017), where the data spreading was large specially at 5 m, and the decision of one $K_0^{'}$ value was not trivial. This fact was related to damaging of the stress cells during installation as well as to installation effects in the soil (disturbance) when pushing down the total stress cells. There was not observed damages in the installations preformed in Tiller-Flotten within this master project. As no bending of the spades is observed, it may be assumed that no bending moment is affecting the lateral pressure values.

6.2.2 Evaluation of lateral stress measurements

During installation, an increase in lateral stress is registered but the stabilization begins few minutes after pushing the cell into the ground. The stabilization takes only few days as it may be observed in data from installation at 5 m (see Figure B- 1 in Appendix B). This is in accordance with previous investigations performed with push-in cells in sensitive soils (Ryley and Carder, 1995; Lindgård and Ofstad, 2017). The pressure values are quite constant after stabilization is reached as shown in the logging charts in Figure B- 1.

The calculated $K_0^{'}$ values from push-in total stress cells are presented in Figure 6- 1 together with $K_0^{'}$ values reported from previous in situ investigations preformed at Tiller-Flotten test site. The values of lateral pressure registered from both cells EP36 and EP37 are quite similar on both investigation depths (5 and 7.5 m).

As mentioned in Chapter 3, Tiller-Flotten test site is in general a deep and homogeneous deposit of marine sediments. This is reported from different sounding performed by Lindgård and Ofstad (2017). Ground morphology is rather flat with no abrupt geographical events. Based on this premise, it may be assumed a quite homogeneous initial stress state throughout the test site, except for a recession delimiting a marsh in the southwest corner of the test site. In this area it is expected a rotation on the principal stresses. Thus, the push-in cells were installed perpendicular to the recession slope so that measured lateral stresses have parallel direction to the recession crest. The cells were located aligned with them self, with 2 m between them. Cell EP37 is located at 2.5 m distance to recession and EP 36 is located at 4.5 m to recession. Lateral stress measured in both push-in cells are quite similar for both installation depths (5 and 7.5 m).
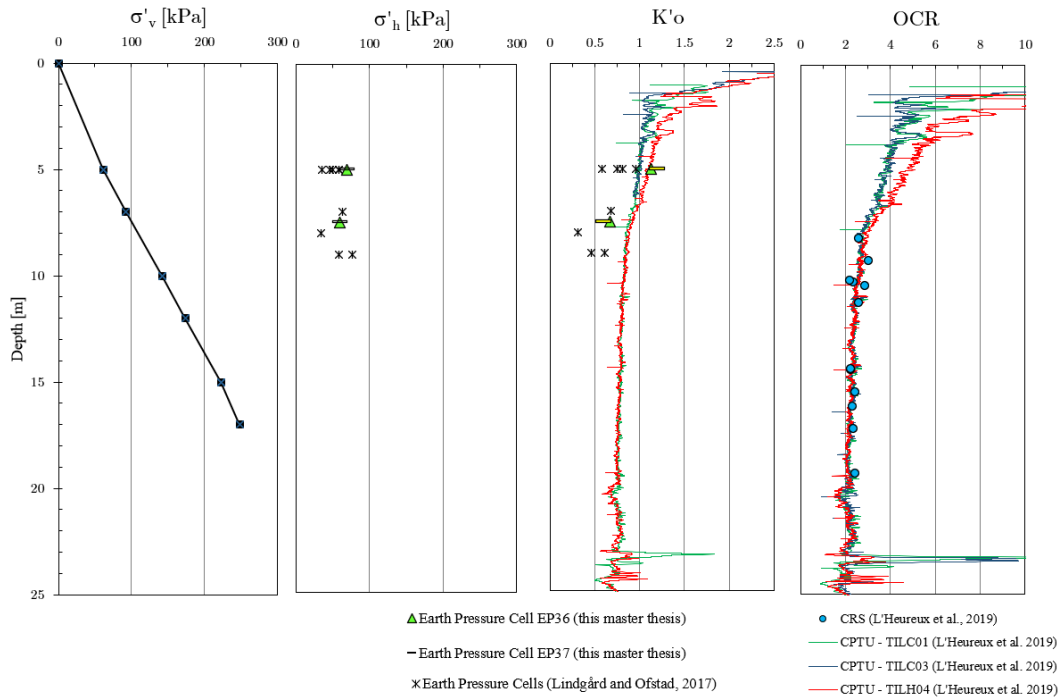
Figure 6- 1 From left to right: effective vertical stress (σ'_v) profile; effective horizontal stress (σ'_h) profile obtained from earth pressure cells performed by the author compared with results from previous investigations in Tiller-Flotten; K'_0 profile derived from horizontal stress obtained from in situ testing performed by the author compared with K'_0 from previous investigations; OCR profile at Tiller-Flotten derived from CRS testing and CPTU sounding (from L'Heureux, Lindgård and Emdal, 2019)

At 5 m depth, the reported K'_0 values are larger than expected based on previous in situ investigation methods performed at Tiller-Flotten. This overestimation is registered at Unit IIa, corresponding to the overconsolidated and stiff clay, as described in Chapter 3. Therefore, and in agreement with previous experiences reported by some authors (Tedd and Charles, 1981; Ryley and Carder, 1995; Lutenegger, 2012), this overestimation of the lateral stress is expected. Contrary, lateral stresses measured at 7.5 m (in the transition from Unit IIa to Unit IIb) are lower than those estimated from other methods. Lindgård and Ofstad (2017) also reported this behaviour. At this level, although *OCR* is slightly below 3, the sensitivity of the material is greater and therefore, the rigidity against the driving of the cell is less. However, the installation of the cell may cause remoulding and the measured lateral pressure after the material reconsolidation is lower than the initial horizontal stress.

It is difficult to evaluate if these values are directly related to horizontal stress and are not also related to any disturbance effects during installation. Pre-boring with auger may also contribute to change in initial in-situ stress, as pointed out by Lindgård and Ofstad

(2017). It may compact the soil between the rod and the measurement depth so the horizontal stress registered will be larger. However, the contrary effect may also occur, and soil may displace upwards, reducing the measured lateral stress values.

6.2.3 Evaluation of pore pressure measurements

There are several piezometers installed in Tiller-Flotten which allowed to define an accurate pore pressure profile with depth, as described in Chapter 3. Under groundwater level, the pore pressure profile is under hydrostatic. Figure 6- 2 presents both measured values from vibrating wire piezometer and the pore pressure measured by installed piezometers. The pore pressure from push-in cells are quite similar at 5 m. However, pore pressure measure at 7.5 m is over the estimated pore pressure value from piezometers, deviating around 20% at borehole EP36 from values reported in L'Heureux, Lindgård and Emdal (2019).
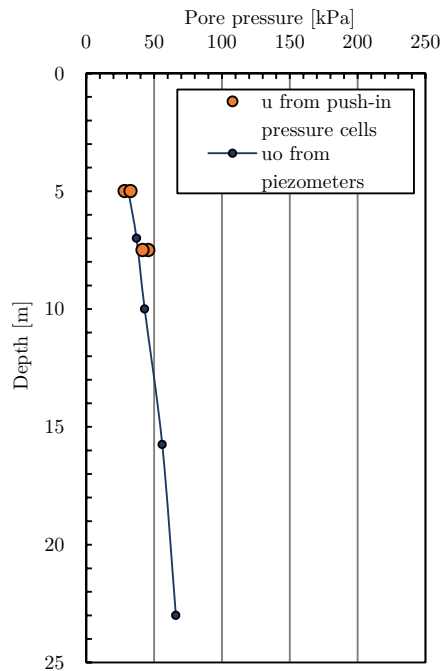
Figure 6- 2 Comparison of estimated pore pressure from piezometer measurements and vibrating wiring piezometers installed in push-in cells

Looking at raw data, the pore pressure values are erratic during the stabilization, fluctuating in the same way for both piezometers in cells EP36 and EP37 (see Figure B- 1 in Appendix B). During installation of push-in cells, pore pressure increases and stabilizes in the same manner as lateral pressure does. Plotting measured pore pressure data with

atmospheric pressure it seems that the fluctuations in pore pressure are influenced by the fluctuation in air atmospheric pressure (see Figure 6- 3).
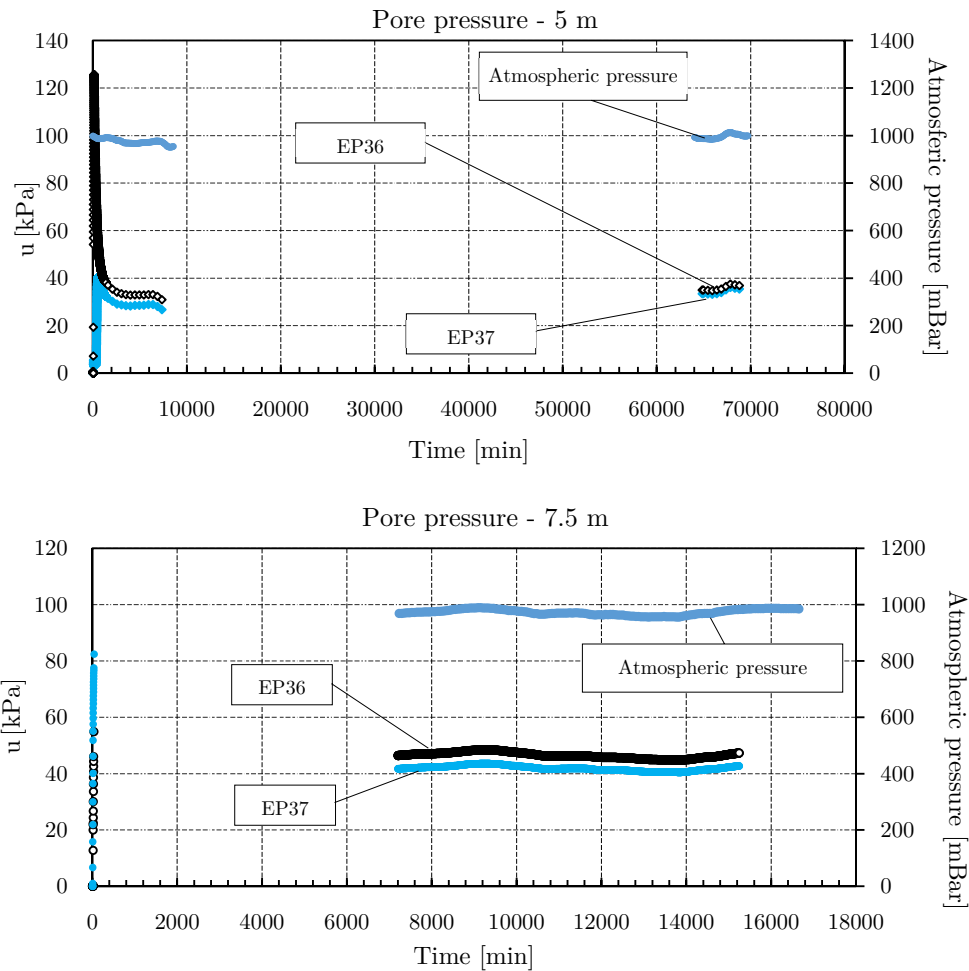
Figure 6- 3 Influence of variation in atmospheric pressure on pore pressure measurements by piezometers in push-in cells installed at 5 and 7.5 m depth

6.3 Hydraulic fracturing – Geonor Filter tip

6.3.1 Setting-up and test execution

The hydraulic fracturing prototype developed by NGI is easy to set up and to steer. Once the piezometer filters are installed at target depth, one day work is enough for executing the test on six boreholes. However, some issues related to the configuration of

the setting-up could induce uncertainties during the execution of the test. First one is the stabilization of pore pressure after installation of the filter tips. There is no measurement of pore pressure and could be interesting to verify the pore pressure value at the investigated depth before starting the test. Since the in situ ground water pressure is low the water in a standpipe would not rise to the level of the pressure transducer. In our case the pressure transducer needs to measure a suction to determine the in situ pore pressure. Such a measurement was not performed. For calculation method, the pore pressure is assumed to be as the one measured in the piezometers installed in the vicinity.

Secondly, the volume capacity of the pump is not enough in some test. Consequently, the test should be stopped and re-started again after refilling of the pump. Although no big variation on pressure values just before shutting-up and after resumption of injection is observed, it is a source of uncertainty.

Other source of uncertainty is related to the fact that the measurement of pressure is done on surface and not in bottom-hole, so the pressure of the column of water in the hose should be added to the measured pressure values. These assumptions may lead to uncertainty in the calculation of in situ lateral stress from pressure vs. charts diagrams.

In this report the friction of fluid against the sleeve has not been taken in account. A potential improvement to equipment could be to install a pressure measurer inside the filter tip in order to measure the bottom-hole pressure.

A significant concern is related to the geometry of the filter tip and how it could influence to the creation of vertical cracks. A systematic study on this line was reported by Lefebvre *et al.* (1991). A field test program was conducted on Champlain clays in East Canada. Each test site presented different consolidation states with *OCR* values in the range between 1.6 to 4.8. Reported K'_0 values are ranging from 1.6 to 4. To evaluate the orientation of formed cracks after hydraulic fracturing tests, large block samples were jacked-out at the depth where the piezometer tips were installed. Two main conclusions were reported by Lefebvre *et al.* (1991). First conclusion, vertical cracks were observed even at levels where high values of K'_0 were measured. This happened when longer piezometer tips were used. Thus, the shape of the cavity created by the piezometer tip influences on the formation and orientation of the formed cracks. After several attempts, it was suggested to use a piezometer filter with a length to diameter ratio of 10 or more in order to obtain vertical oriented cracks (Lefebvre *et al.*, 1991; Hamouche *et al.*, 1995). The Geonor filter tip employed at Tiller-Flotten has a length of 120 mm and a diameter of 32

mm, leading a length to diameter ratio of 3.75, far from recommendation for over consolidated soils.

6.3.2 Results

Measured in situ effective horizontal stresses (σ'_h) values at Tiller-Flotten by hydraulic fracturing are in general higher than those expected, reported in previous experience from other in situ tests (L'Heureux, Lindgård and Emdal, 2019) as is presented in Figure 6- 4.
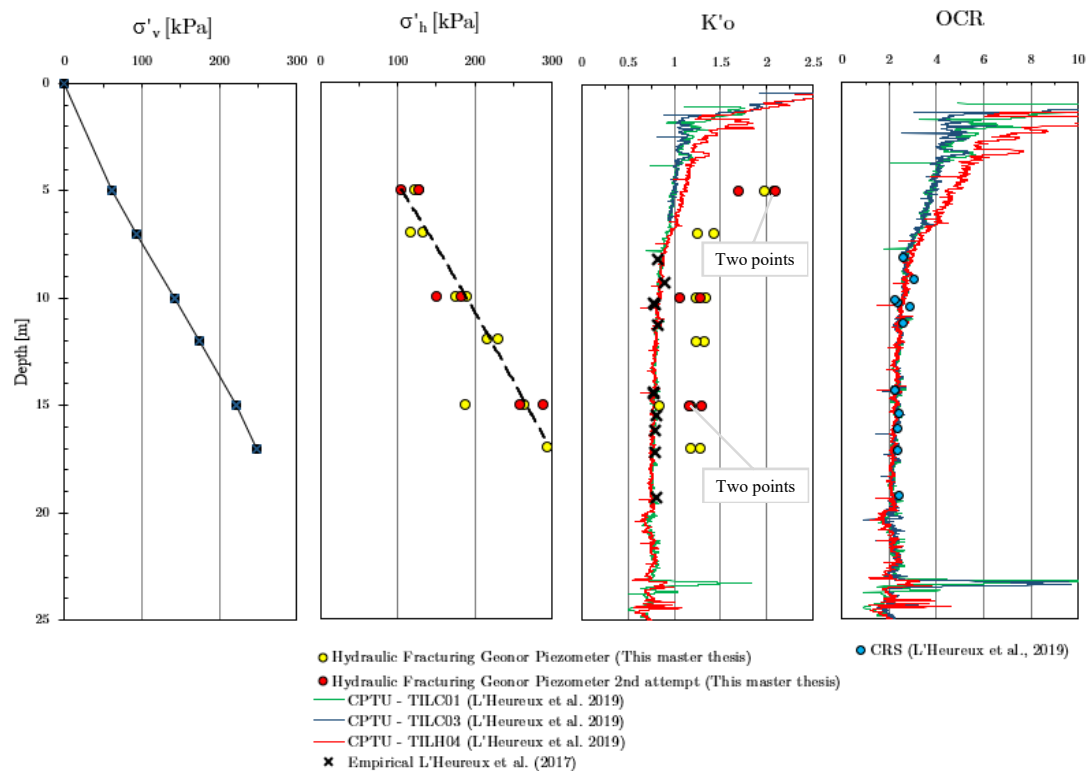
Figure 6- 4 Comparison of effective lateral stress derived from hydraulic fracturing and empirical correlation based on OCR and CPTU soundings

The trend is an almost lineal increasing behaviour of with depth σ'_h, and a K'_0 profile decreasing in the same manner as for previously reported K'_0 profiles. Nevertheless, hydraulic fracturing overestimate in situ lateral stress, derived K'_0 values are rather larger than those derived from earth pressure cells, empirical correlations based on CPTU soundings and CRS oedometer test (see Figure 6- 5).
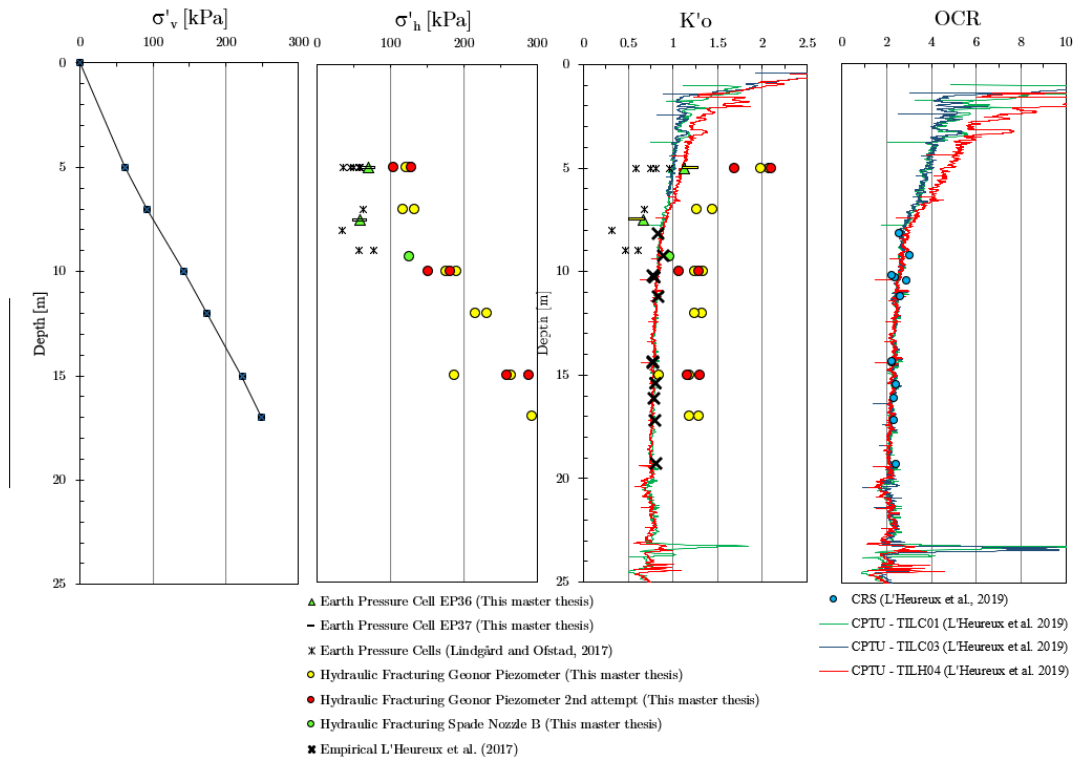
Figure 6- 5 Calculated K_0' values from field in situ measurements within this master thesis (hydraulic fracturing and earth pressure cells), compared with K_0' data from in situ and empirical methods previously reported by L'Heureux, Lindgård and Emdal (2019)

One might think about the origin of so high values. First question to pose is related to the assumption that the cracks or fractures formed are perpendicular to the horizontal stress. The high K_0' values suggest that perhaps the orientation of created fractures is not horizontal. This is one of the main discussed hypothesis in hydraulic fracturing (Lefebvre *et al.*, 1991). Some authors have reported a series of laboratory testing in order to show that vertical cracks are formed when K_0' is less than one and confirmed the previous assumption that fracture closes when water pressure decrease to the value of minor principal stress (Bjerrum and Anderson, 1972; Andersen *et al.*, 1994). But later investigations programs within hydraulic fracturing in cohesive material have reported K_0' values higher than one (Bozozuk, 1974; Lefebvre *et al.*, 1991; Hamouche *et al.*, 1995). Bozozuk (1974) arguments the creation of vertical fracture in deposits with K_0' larger than one to the fact that tensile strength due to cementation could be larger along the horizontal plane than in vertical plane thus cracks are forming along the vertical direction. There is no a clear evidence on cementation structures in Tiller-Flotten clay rather that the results of triaxial testing presented in L'Heureux, Lindgård and Emdal (2019).

97

A second hypothesis to work with is the fracture mechanism, that may be related with cavity expansion rather than shear failure. It worth discuss the results presented Figure 5-6. At borehole TILH02 various injection sequences were performed. During the second injection cycle, the fracture re-opening pressure increases. As the soil tested is a plastic media, the reaction of the material to fluid injection is a deformation before fracturing. This phenomenon points out to the cavity expansion as mechanism conducting to fracturing, since it is necessary a higher pressure to re-open the fracture. Displacement distribution around piezometer tip, development of plastic radii and cavity pressure are parameters governing cavity expansion (Mo, Marshall and Yu, 2014) which could influence in the fracturing mechanism and in the in situ horizontal stress values calculated from pressure measurements. Some authors have related the cavity expansion mechanism with hydraulic fracturing. Lefebvre *et al.* (1991) concluded from the results obtained in their work that the applied pressure in the cavity boundaries governs the creation of a fracture in the soil. This is in good agreement with the results reported by Jaworski et al. (1981), as referred in (Lindgård and Ofstad, 2017), and with the work of Massarsch (1978), who published a study of hydraulic fracturing during pile driving. In cohesive soils some authors relate the closing pressure to the octahedral stress (Overy and Dean, 1986).

In general, K_0'-values derived from hydraulic fracturing testing at Tiller-Flotten test site are higher than those estimated by in situ and empirical methods. During the procedure, the in situ piezometric pressure with fully saturated system was not measured, introducing a high uncertainty related to how the column of water is affecting the real pore pressure value at filter tip during the injection test.

6.4 Hydraulic fracturing – Modified NGI set-up

6.4.1 Setting-up and test execution

Insertion of the new injections spade were challenging. The main difficulty was related to the fact that there is no filter stone installed on the outlets. It means the test should be started after installation of injection spade and no time to pore pressure dissipation and filling of the standpipe is allowed. It was observed injection fluid was from spade which

may induce some air entry into the system but is was solved by filling up the borehole with water. A flushing pressure is necessary during the insertion of the spades into the ground. It seems that flushing pressure was not enough in none of the test performed. The maximum pressure reached, around 800 kPa for both tests, may be an indication of tight spades' outlets.

6.4.2 Results

Results from pilot tests for both new nozzles A and B are presented in Figure C- 19 and Figure C- 20 respectively in Appendix C. As no properly pre-testing of the nozzles was done before going to field testing, the pilot test has been the trial and error arena. From both pilot tests, it could be concluded that both nozzles get plugged with clay when pushing them into the ground. It was not enough to hold an outlet pressure of 25 kPa for nozzle A and 100 kPa for nozzle B to avoid the clay occluding the openings. The pressure line versus time reached 806 kPa for nozzle A and 812 kPa for nozzle B and, thereafter, a sudden pressure drop occurs. As previously mentioned, this high pressure values reached during the injection may be due to tightening of the outlets but also it maximum pressure values are quite similar to q_c values from CPTU soundings at investigations depths. To avoid the obstruction of the nozzles, it is necessary to set small filter stones on each injection hole.

After the pressure dropped, the pumping was stopped and started again when the pressure seemed to be stable, despite it was challenging to decide when the pressure stopped decaying. During the second injection cycle on nozzle A it may be observed that the pressure is constant after shutting up the pump. Subsequent injection cycles showed an erratic behaviour of pressure, going up and down. Two may be the reasons for that, the partially obstruction of injection nozzle and/or the geometry of the nozzle itself. If there is not a good tightening between the injection tip and the surrounding soil, injection fluid may migrate upwards when a certain degree of pression is reached. Once the fluid moves, then the pressure drops.

Injection nozzle B showed also and erratic pressure behaviour during the second injection cycle. Reasons may be those addressed for nozzle A. A third injection sequence was then performed and unexpectedly, the pressure dropped at 203 kPa. It is reasonable if compared with previous hydraulic fracturing values registered at 10 m depth which are around 204 kPa on average (see Figure 6- 5). After the pressure became stable at that level, the injection was stopped, and a pressure decay curve registered. The pressure was allowed

to stabilization until it reached 57.5 kPa. This value is far from in situ pore pressure which is estimated to be around 41 kPa at that depth. As previously mentioned, the closure pressure ($P_{closure}$) is calculated in the same manner as for the testing carried out with the Geonor piezometer tip (see Figure 6- 6). The $K_0^{'}$ obtained is a 15% larger than the estimation from L'Heureux (2017) but 15% lower than $K_0^{'}$ values derived from CPTU soundings.
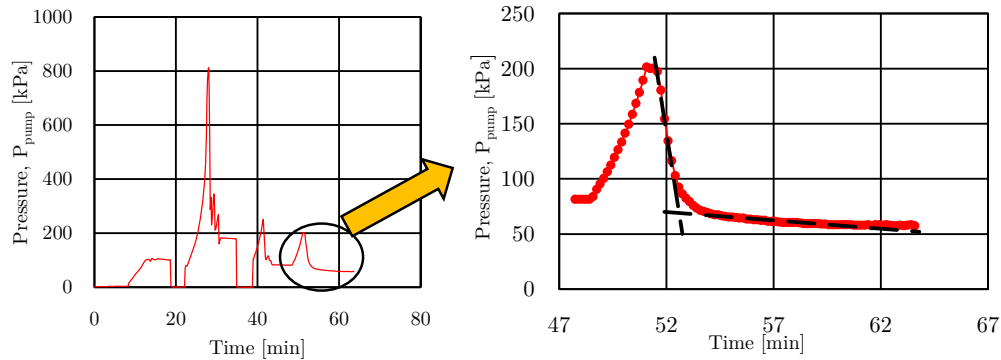
Figure 6- 6 Left: recorded pressure in the pump during test performed at borehole TILH07 (9.3 m depth). Right: Enlarged chart of the 3rd injection cycle used to find closure pressure ($P_{closure}$)

Despite the result obtained with nozzle B seems reasonable and encouraging, the reliability of the measurement is questionable. It is not possible to know if the spade-shape geometry of the nozzle really helped to create a vertical opening and avoid expansion of the sensitive material, or if contrary it contributes to the creation of a expanding cavity, or just a total remoulding of the high sensitive clay found at 8 and 9 m depth in Tiller – Flotten.

Laboratory testing may help to better understand how the geometry of the new injections tips influences the fracture mechanism of the soil. The device could be tested with a down scaled model of the injection tips. The test should simulate the mor realistic in situ conditions, i.e., confined conditions, preferably under no lateral strain conditions. A triaxial test set up could be the base to configure a possible laboratory testing but also a polyaxial box rig . A pore pressure transducer may also be installed near the injection tip to have fully control of pressure build up during injection test. In order to study the fracture pattern, it may possible to use tracers in the injection fluid as previously reported by some authors (Bjerrum and Anderson, 1972; Andersen *et al.*, 1994) In such way it would be possible to study fracturing patterns in hydraulic fracturing test. It may be interesting going

to a larger scale testing, in an artificially build up compacted clay column, but in this case, it would not be possible to test the device in sensitive clay.

Chapter 7

Summary and Further Work

7.1 Summary and Conclusions

As previously exposed, the determination of the in situ stress state within the frame of any geotechnical problem is crucial. Any laboratory testing program or numerical design need as input the soil parameters at in situ stress condition of the soil. The coefficient of earth pressure at rest K_0', is a main input parameter for numerical analysis and laboratory test design. In situ vertical stress is easily calculated by knowing depth and specific gravity of the material forming the soil. However, the determination the in situ horizontal stress is a challenging task as it has been stated by numerous authors work as presented in the literature review on Chapter 2. The determination of $K_0^{'}$ is still a pending task within geotechnical engineering since both in situ or laboratory testing induce, in major or minor degree, a disturbance on the original soil stress state. The repeatability and reliability of the results outcasted by in situ and laboratory methods presented in Chapter 2 seems not to be enough.

Hence many efforts have been made to define an empirical relationship between soil parameters, which determination is reliable by well-established field and laboratory methods, and the coefficient of earth pressure at rest $(K_0^{'})$. Nevertheless, it is difficult to define a general expression or equation since there is a high degree of dependence on soil local conditions and properties as stress history as well as time effects ageing or ageing.

The uncertainty is then larger in the case of overconsolidated soils, confirmed by the spread of K_0' for soil levels with *OCR* larger than one.

In chapter 3 a description of Tiller-Flotten Geo-Test Site is presented. A summary of strength and index parameters from previous work found in literature are summarized and used as input for correlation methods.

Push-in earth pressure cells have been installed to target depth investigations. In total 4 measurement have been performed, two at 5 m in the overconsolidated Unit IIa, and two at 7 m in the transition zone from Unit IIa to Unit IIb where the consolidation grade begins to decrease. K_0' values at 5 m have a slightly scatter and are over those predicted values for Norwegian clays from L'Heureux *et al.* (2017). Contrary, the results obtained at 7 m show no scatter and lay under previously reported K_0' values. The installation of the cells is uncomplicated, and no damages on the spades are observed after removal of the equipment. Pore pressure registered are close to the in situ estimated pore pressure at both investigation depths, but values may be taken with precaution. No evidence on how installation procedure may affect filter stone.

Hydraulic fracturing test is presented as a potential method for the in situ measurement of horizontal stress. The literature suggests good results in normally consolidated clay deposits, but no previous experiences are available in Norwegian high sensitive clays. A detailed description of the equipment and followed procedure during the execution of the test are presented Chapter 4. Two different equipment set-ups have been tested. A first testing was performed with a common Geonor piezometer during spring 2019 within the specialization project thesis submitted by the author. A deep review of the collected data has been carried out, pointing to the fact that no initial pressure at the piezometer was recorded before starting the injection test. Hydraulic fracturing test was performed along 6 different boreholes. Investigation depth goes from 5 to 17 m, covering the 2 main units conforming the soil profile at Tiller-Flotten. In general, the procedure to perform the test is straightforward with only a few steps to complete. Main issue is related to the way of purging a 20 m hose with the only help of a syringe. This is a step to be improved since the presence of air bubbles in the system may induce lower pressure values.

The hydraulic fracturing set up was modified by adding a new syringe pump to avoid stopping the injection cycling for refilling. Also, two injection spade shaped nozzle were tested, looking to create a weak vertical plane and help for vertical fracturing during the injection. Two tests were carried out at 8.30 and 9.30 m on the same borehole for nozzle A

and nozzle B, respectively. It is difficult to extract any reliable conclusion from results obtained. The pressure profile is erratic and suggests to a tightening of injection openings. This may be solved by adding a small filter stone at each injection orifice. Several injection cycles were attempted at each test. Once the pressure is enough to expel the clay from the openings, the pressure profile does not follow a regular pattern. No tightening between the soil and the nozzle may be the reason for it, allowing the injection fluid to migrate upwards.

On the third injection sequence completed with nozzle B, a typical pressure vs. time was registered. In spite of it was possible to define a breaking pressure, closing pressure and effective lateral stress, and these values are in good accordance with correlation methods and CPTU derived $K_0^{'}$ values, the reliability and repeatability of the method is not known.

In chapter 5, results obtained by push-in cells and hydraulic fracturing testing are presented and compared with previous investigations on in situ measurements of horizontal stress. In general, K_0' obtained by hydraulic fracturing are between 20 and 40% higher than those obtained by dilatometer, CPTU or by the empirical correlation for Norwegian clays. These higher values could indicate that perhaps the horizontal stress is not being measured, i.e. no vertical cracks open when injecting the fluid in the ground. Cracks could be opened following a weak horizontal or inclined surface; thus, the closing pressured register would not correspond to the horizontal stress. Results from push-in earth pressure cells show that the method is potentially reliable and stable.

7.2 Further Work

Further work is recommended to be done with push-in earth pressure cells. The values obtained seem to be reliable and repeatable. It may be interesting to investigate deeper into the very sensitive material of Unit IIb to complete the profiles along boreholes EP36 and EP37. It might be interesting to investigate along several profiles to confirm the repeatability of the method and maybe stablish a correlation with collected data and the different evaluation methods for $K_0^{'}$ presented in **Error! Reference source not found.**.

Technically, and regarding very adverse climatic conditions at Tiller-Flotten test site with very cold temperatures on winter season, it is necessary to isolate better the logging box to avoid condensation and failure of electronics components.

Preparation of the equipment before installation is also on great importance. The pore pressure ceramic filter is to be saturated by submerging the cell in deionized and degassed water. However, this procedure does not ensure saturation of the smaller pores in the ceramic filter. Zero readings may be taking during at least 4 hours before and after installation at site conditions. A calibration of the equipment is also recommended before installation since the calibration sheets provided by the manufacturer were defined within different ambient conditions. This calibration might be just a checking of the calibration sheet values.

There are still some possible improvements that may be done on hydraulic testing device. The bladder accumulator is a source of uncertainty and the pressure may be better be measured at desired investigation depth. Installation of a pressure transducer in the filter tip could be one of the most interesting steps to acquire more reliable pressure measurements. A logging device may be also connected to the system to monitor the evolution of the pore pressure after performing the test. In these low permeable soils, the duration of the dissipation process is longer than the 30 minutes allowed during the field testing. It could be interesting to get the in situ pore pressure value before starting a test and after finalizing it. In that way a drift may be established.

Further understanding on fracturing mechanism yielding hydraulic fracturing in sensitive clays is necessary to be analysed and studied, specially the cavity expansion theory approach. Numerical simulations could be helpful on that purpose as well as laboratory simulation of hydraulic fracturing on quick clays. From the results obtained from hydraulic fracturing, it could be concluded that probably the pressure values measured do not satisfy the assumption of formation of horizontal cracks. For practical purposes, it could be interesting to sample mini-block samples there where the hydraulic fracturing test has been performed to analyse the fracture or net of fractures created. A suggested procedure for this purpose is presented in Lefebvre et al. (Lefebvre *et al.*, 1991).

The influence on the injection tip geometry on hydraulic fracturing testing may be better be understood by laboratory testing, under proper confining conditions.

Numerical simulations might be of great interest to better understand the disturbances originated in the soil by the installation of equipment for in situ measurements, especially for push-in cells.

Oedometer testing program on high quality vertical trimmed samples might be also interesting to verify if the work criterion is adequate for soil samples from Tiller-Flotten.

Finally, there are still some methods that could be tested at Tiller-Flotten geo-test site as pressuremeter and, specially, seismic wave velocity analysis as it is a non-intrusive method to determine in situ lateral stress.

References

Alfaro, M. C. and Wong, R. C. (2011) 'Laboratory studies on fracturing of low-permeability soils', *Canadian Geotechnical Journal*, 38(2), pp. 303–315. doi: 10.1139/t00-096.

Andersen, K. H. *et al.* (1994) 'Estimation of hydraulic fracture pressure in clay', *Canadian Geotechnical Journal*, 31(6), pp. 817–828. doi: 10.1139/t94-099.

ASTM (2012) 'Standard Test Method for Performing the Flat Plate Dilatometer', i, pp. 1–5. doi: 10.1520/C0944.

Baguelin, F., Jézéquel, J.-F. and Shields, D. H. (1978) *The pressuremeter and foundation engineering*. Clausthal: Trans Tech Publications.

Baumgärtner, J. and Zoback, M. D. (1989) 'Interpretation of hydraulic fracturing pressure-time records using interactive analysis methods', *International Journal of Rock Mechanics and Mining Sciences and*, 26(6), pp. 461–469. doi: 10.1016/0148-9062(89)91422-8.

Becker, D. E. *et al.* (1987) 'Work as a criterion for determining in situ and yield stresses in clays', *Canadian Geotechnical Journal*, 24(4), pp. 549–564. doi: 10.1139/t87-070.

Bjerrum, L. (1967a) 'Engineering geology of norwegian normally-consolidated marine clays as related to settlements of buildings', *Geotechnique*, 17(2), pp. 83–118. doi: 10.1680/geot.1967.17.2.83.

Bjerrum, L. (1967b) 'Third Terzaghi Lecture: Progressive failure in slopes of overconoslidated plastic clay and clay shales.', *'Journal of Soil Mechanics & Foundations Div'*. American Society of Civil Engineers, 93, pp. 1–49.

Bjerrum, L. *et al.* (1972) 'Hydraulic fracturing in field permeability testing', *Géotechnique*, 22(2), pp. 319–332. doi: 10.1680/geot.1972.22.2.319.

Bjerrum, L. and Anderson, K. (1972) 'In-situ measurement of lateral pressures in clay', *Norwegian Geotechnical Institute*, pp. 11–19. Available at: http://trid.trb.org/view.aspx?id=125847.

Bozozuk, M. (1974) 'Minor principal stress masurements in marine clay with hydraulic fracture tests', in *Proceeding in Engineering foundation Conference on Subsurface Exploration for Underground Excavation and Heavy Construction*. Ottawa, pp. 333–349.

Brooker, E. W. and Ireland, H. O. (1965) 'Earth Pressures at Rest Related to

Chapter 7 References

Stress History', *CANADIAN GEOTECHNICAL JOURNAL*, II(1), pp. 1–15.

Brown, R. W. (1985) *Ko-Behaviour if normally consolidated fone-grained soils during one dimensional secondary compression aging and the quantitative prediction of the quasi-preconsolidation effect.*

Campanella, R. G. and Vaid, Y. P. (1972) ' A Simple K o Triaxial Cell ', *Canadian Geotechnical Journal*, 9(3), pp. 249–260. doi: 10.1139/t72-029.

Chowdhury, R. . (1978) *Slope analysis. Developments in geotechnical engineering, volume 22.*

Das, B. M. and Sobhan, K. (2012) *Principles of Geotechnical Engineering.* 8th edn. Cengage Learning.

Duncan, J.M.; Dunlop, P. (1968) *Slopes in Stiff-Fissured Clays.* Berkeley.

Fioravante, V. *et al.* (1998) 'Assessment of the coefficient of the earth pressure at rest from shear wave velocity measurements', *Géotechnique*, 48(5), pp. 657–666. doi: 10.1680/geot.1998.48.5.657.

Fischer, K. P., Andersen, K. H. and Moum, J. (1978) 'Properties of an Artificially Cemented Clay.', *Canadian Geotechnical Journal*, 15(3), pp. 322–331. doi: 10.1139/t78-030.

Gronseth, J. M. (1982) 'Determination of the instantaneous shut in pressure from hydraulic fracturing data and its reliability as a measure of the minimum principal stress', in *Ihe 23rd U.S Symposium on Rock Mechanics (USRMS).* Berkeley, California: American Rock Mechanics Association, pp. 183–189. doi: 10.1016/0148-9062(83)91564-4.

Gundersen, A. *et al.* (2019) 'Characterization and engineering properties of the NGTS Onsøy soft clay site', *AIMS Geosciences*, 5(3), pp. 665–703. doi: 10.3934/geosci.2019.3.665.

Gylland, A. *et al.* (2013) 'Characterisation and engineering properties of Tiller clay', *Engineering Geology.* Elsevier B.V., 164, pp. 86–100. doi: 10.1016/j.enggeo.2013.06.008.

Hamouche, K. *et al.* (1995) 'In situ evaluation of Ko in eastern Canada clays', *Canadian Geotechnical Journal*, 32(4), pp. 677–688. doi: 10.1139/t95-067.

Handy, R. L. *et al.* (1990) 'Field Experience with the Back-Pressured K0 Stepped Blade', *Transportation Research Record*, (1278), pp. 125–134.

Hanzawa, H. and Kakuichiro, A. (1983) 'Overconsolidation of Alluvial Clays', *Soils and Foundations*, 23(4). Available at: http://www.mendeley.com/research/geology-volcanic-history-eruptive-style-yakedake-volcano-group-central-japan/.

Holtz, R., Jamiolkowski, B. and Lancellotta, R. (1987) 'LESSONS FROM OEDOMETER TESTS ON HIGH QUALITY SAMPLES', 112(8), pp. 768–776.

Hoult, N. A. and Soga, K. (2014) *Sensing solutions for assessing and monitoring tunnels*, *Sensor Technologies for Civil Infrastructures*. Woodhead Publishing Limited. doi: 10.1533/9781782422433.2.309.

Howard, G. C. and Fast, C. R. (1970) 'Hydraulic Fracturing', in *Monograph Volume 2 Henry L. Doherty Series*. New York: Society of Petroleum Engineers of AIME.

Hwang, J., Dewoolkar, M. and Ko, H.-Y. (2002) 'Stability analysis of two-dimensional excavated slopes considering strength anisotropy', *Canadian Geotechnical Journal*, 39(5), pp. 1026–1038. doi: 10.1139/t02-057.

J.P.Dohertya, J. . *et al.* (2018) 'A novel web based application for storing, managing and sharing geotechnical data, illustrated using the national soft soil field testing facility in Ballina, Australia', *Computers and Geotechnics*, 93, pp. 3–8.

Jáky, J. (1948) 'Pressure in silos', *Proceedings of the 2nd International Conference on Soil Mechanics and Foundations Engineering*, 1, pp. 103–107.

Jamiolkowski, M. *et al.* (1985) 'New developments in field and laboratory testing of soils', in *Procedings of the 11th International Conference on Soil Mechanics and Foundation Engineering*. San Francisco: A.A. Balkema, pp. 57–153.

Jaworski, G., Bolton Seed, H. and Duncan, J. (1981) 'Laboratory Study of Hydraulic Fracturing', *Journal of the Geotechnical Engineering Division*, 107(6), pp. 713–732.

Kavazanjian, E. and Mitchell, J. K. (1984) 'Time Dependence of Lateral Earth Pressure By , Jr.,1 M. ASCE and', 105(4), pp. 530–533.

Ku, T. and Mayne, P. W. (2013) 'Evaluating the in situ lateral stress coefficient (K0) of soils via paired shear wave velocity modes', *Journal of Geotechnical and Geoenvironmental Engineering*, 139(5), pp. 775–787. doi: 10.1061/(ASCE)GT.1943-5606.0000756.

Ku, T. and Mayne, P. W. (2015) 'In Situ Lateral Stress Coefficient (K0) from Shear Wave Velocity Measurements in Soils', *Journal of Geotechnical and Geoenvironmental Engineering*, 141(12), p. 06015009. doi: 10.1061/(asce)gt.1943-5606.0001354.

L'Heureux, J.-S. *et al.* (2017) 'A revised look at the coefficient of earth pressure at rest for Norwegian Clays', in *Geoteknikkdagen 2017*. Oslo: Norsk Geoteknisk Forening, pp. 35.1-35.11.

L'Heureux, J.-S. and Lunne, T. (2020) 'Characterization and engineering properties of natural soils used for geotesting', *AIMS Geosciences*, 6(1), pp. 35–53.

L'Heureux, J. S., Lindgård, A. and Emdal, A. (2019) 'The Tiller-Flotten research site: Geotechnical characterization of a very sensitive clay deposit', *AMIS Geosciences (submitted)*, pp. 1–37.

Lacasse, S. and Lunne, T. (1983) 'In situ horizontal stress from pressuremeter tests', *Norwegian Geotechnical Institute Publications*, (146), pp. 1–12. doi: 10.1016/0148-9062(84)91167-7.

Lakirouhani, A., Detournay, E. and Bunger, A. P. (2016) 'A reassessment of in situ stress determination by hydraulic fracturing', *Geophysical Journal International*, 205, pp. 1859–1873.

Lefebvre, G. *et al.* (1991) 'Evaluating K o in Champlain clays with hydraulic fracture tests', *Canadian Geotechnical Journal*, 28(3), pp. 365–377. doi: 10.1139/t91-047.

Leroueil, S. (2004) 'Natural slopes and cuts: movement and failure mechanisms', *Géotechnique*, 51(3), pp. 197–243. doi: 10.1680/geot.51.3.197.39365.

Leroueil, S. and Vaughan, P. R. (1991) 'The general and congruent effects of structure in natural soils and weak rocks', *Geotechnique*, 41(2), pp. 281–284. doi: 10.1680/geot.1991.41.2.281.

Lin, W. *et al.* (2008) 'Estimation of minimum principal stress from an extended leak-off test onboard the Chikyu drilling vessel and suggestions for future test procedures', *Scientific Drilling*, (6), pp. 43–47. doi: 10.2204/lodp.sd.6.06.2008.

Lindgård, A. and Ofstad, C. S. (2017) *Field and laboratory investigations to evaluate the coefficient of earth pressure at rest. NGTS Flotten quick clay test site.* NTNU.

Lunne, T. and L'Heureux, J. S. (2016) *Evaluation of Ko in soft lightly OC clays from in situ tests SP8 – Geotekniske dimensjoneringsparametere (GEODIP)*.

Lunne, T., Long, M. and Forsberg, C. F. (2003) 'Characterisation and Engineering Properties of Onsøy clay', in Tan, T. S. et al. (eds) *Characterisation and Engineering Properties of Natural Soils*. A.A. Balkema Publishers, pp. 395–427.

Lunne, T. and Rad, N. S. (no date) 'developments in in-situ testing - Part 1 : All tests except SPT Pore pressure , u Point resistance , qc'.

Lutenegger, A. J. (2012) 'Field response of Push-In earth pressure cells for instrumentation and site characterization of soils', *Geotechnical Engineering*,

43(4), pp. 24–33.

Ma, B., Muhunthan, B. and Xie, X. (2014) 'Mechanisms of Quasi-preconsolidation stress development in clays: A rheological model', *Soils and Foundations*. Elsevier, 54(3), pp. 439–450. doi: 10.1016/j.sandf.2014.04.012.

Marchetti, S. (1979) 'Journal of the Engineering Division', *Geotechnical Engineering*, 105(May), pp. 655–670.

Marchetti, S. *et al.* (2001) 'The flat dilatometer test (DMT) in soil investigations. A report by the ISSMGE Committee TC 16.', *Proc. Int. Conf. on In Situ Measurement of Soil Properties (IN-SITU 2001)*, pp. 95–131.

Marchetti, S. (2016) 'TC16: Some 2015 Updates to the TC16 DMT Report 2001', *International Conference On In situ Measurement of Soil Properties*, pp. 1–23. Available at: http://www.marchetti-dmt.it/conference/dmt15/papers DMT 2015 (pdf)/Marchetti - keynote.pdf#page=1.

Marchi, M., Gottardi, G. and Soga, K. (2013) 'Fracturing Pressure in Clay', *Journal of Geotechnical and Geoenvironmental Engineering*, 140(2), p. 04013008. doi: 10.1061/(asce)gt.1943-5606.0001019.

Masood, T. and Kibria, S. (1994) 'Estimation of in-situ lateral stresses by full displacement methods', in *XIII International Conference on Soil Mechanics and Foundation Engineering*. New Delhi, pp. 689–694.

Massarsch, K. R. (1975) 'New Method for Measurement of Lateral Earth Pressure in Cohesive Soils', *Canadian Geotechnical Journal*, 12(1), pp. 142–146. doi: 10.1139/t75-013.

Massarsch, K. R. (1978) 'New aspects of soil fracturing in clay', *International Journal of Geotechnical Engineering Division, Proceedings of the American Society of Civil Engineers*, 104(GT8), pp. 1109–1123. doi: 10.1016/0148-9062(79)90790-3.

Massarsch, K. R. (1979) 'Lateral Earth Pressure in Normally Consolidated Clay.', *Proceedings of the European Conference on Soil Mechanics and Foundation Engineering*, 2(January), pp. 245–249.

Matthews, M., Hope, V. and Clayton, C. (1996) 'The use of surface waves in the determination of ground stiffness profiles', in *Proceedings of the Institution of Civil Engineers: Geotechnical Engineering*, pp. 84–95.

Mayne, P. (1988) 'CPT indexing of in situ OCR in clays', *ASCE*, pp. 780–793.

Mayne, P. W. and Kulhawy, F. H. (1982) 'K-OCR relationships in soil', *International Journal of Rock Mechanics and Mining Sciences & Geomechanics Abstracts*, 20(1), p. A2. doi: 10.1016/0148-9062(83)91623-6.

Chapter 7 References

Mesri, G. and Castro, A. (1989) 'Closure - C α/C c concept and K 0 during secondary compression', *Journal of Geotechnical Engineering*, 115(2), pp. 273–277.

Mesri, G. and Hayat, T. M. (1993) 'The coefficient of earth pressure at rest', *Canadian Geotechnical Journal*, 30(4), pp. 647–666. doi: 10.1139/t93-056.

Mo, P. Q., Marshall, A. M. and Yu, H. S. (2014) 'Elastic-plastic solutions for expanding cavities embedded in two different cohesive-frictional materials', *International Journal for Numerical and Analytical Methods in Geomechanics*, 38(9), pp. 961–977. doi: 10.1002/nag.2288.

Mori, A. and Tamura, M. (1987) 'Hydrofacturing pressure of cohesive soils', *Soils and Foundations*, 27(1), pp. 14–22. Available at: http://www.mendeley.com/research/geology-volcanic-history-eruptive-style-yakedake-volcano-group-central-japan/.

Nolen-Hoeksema, R. (2013) 'Elements of Hydraulic Fracturing', *Oilfield Review*, (2), pp. 51–52.

Overy, R. F. and Dean, A. R. (1986) 'Hydraulic Fracture Festing of Cohesive Soil', in *Offshore Technology Conference*. Texas.

Panah, A. K. and Yanagisawa, E. (1989) 'Laboratory studies on hydraulic fracturing criteria in Soil', *Soil and Foundations*, 29(4), pp. 14–22. Available at: http://www.mendeley.com/research/geology-volcanic-history-eruptive-style-yakedake-volcano-group-central-japan/.

Papanastasiou, P. (2000) 'Hydraulic fracture closure in a pressure-sensitive elastoplastic medium', *International Journal of Fracture*, 103(3), pp. 149–161. doi: 10.1023/A.

Park, C. B., Miller, R. D. and Xia, J. (1999) 'Multichannel analysis of surface waves', *Geophysics*, 64(3), pp. 800–808. doi: 10.1190/1.1444590.

Quigley, R. M. (2008) 'Geology, mineralogy, and geochemistry of Canadian soft soils: a geotechnical perspective', *Canadian Geotechnical Journal*, 17(2), pp. 261–285. doi: 10.1139/t80-026.

Rankka, K. (1990) 'Measuring and Predicting Lateral Earth Pressures in Slopes in Soft Clays in Sweden', *Tra*, (1278), pp. 172–182.

Reite, A.J.; Sveian, H.; Erichsen, E. (1999) 'Trondheim fra istid til nåtid-landskapshistorie og løsmasser', *Gråsteinen*. Norges Geologiske Undersøkelse, 5.

Richards, D. J., Clark, J. and Powrie, W. (2006) 'Installation effects of a bored pile wall in overconsolidated clay', *Geotechnique*, 56(6), pp. 411–425. doi: 10.1680/geot.2006.56.6.411.

Ryley, M. D. and Carder, D. R. (1995) 'The performance of push-in spade cells installed in stiff clay', *Geotechnique*, 45(3), pp. 533–539. doi: 10.1680/geot.1995.45.3.533.

Schmertmann, J. (1985) 'Measure and Use of In-Situ Lateral Streses', in *The Practice of Foundation Engineering*. The Department of Civil Engineering, Northwestern University.

Schmertmann, J. H. (1983) 'A Simple Question About Consolidation', 109(1), pp. 119–122.

Schmertmann, J. H. (1985) 'Measure and use of the Insitu Lateral Stress', *The Practice of Foundation Engineering, The Department of Civil Engineering, Northwestern University*, pp. 189–213.

Schmertmann, J. H. (1991) 'The mechanical aging of soils (The twenty-fifth Karl Terzaghi Lecture)', *Journal of Geotechnical Engineering*, pp. 1288–1330.

Schnaid, F. (2009) *In situ testing in geomechanics*. 1st edn. New York: Taylor & Francis.

Senneset, K. (1989) 'A new oedometer with split ring for the measurement of lateral stress', *XII.ICSMFE*, I(I), pp. 115–118. doi: 10.1007/978-3-319-73568-9_174.

Senneset, K. and Janbu, N. (1994) 'Lateral stress and preconsolidation pressure measured by laboratory tests', *XIII International Conference on Soil Mechanics and Foundation Engineering*. New Delhi.

Sivakumar, V. *et al.* (2004) 'Relationship between Ko and overconsolidation ratio: a theoretical approach', *Géotechnique*, 52(3), pp. 225–230. doi: 10.1680/geot.52.3.225.41017.

Soga, K. (2005) *Time Effects Observed in Granular Materials. Lecture notes.* University of Cambridge.

Solberg, I. L. (2019) *'Kvikkleire, skred of kartlegging av kvikkleire.' Forelesningsnotater i Ingeniørgeologi i løsmasser.* NTNU.

Soydemir, C. (1984) 'Discussion of "A Simple Question about Consolidation" by John M. Schmertmann (January, 1983)', *Journal of Geotechnical Engineering1*, 110(5).

Steinel, H. *et al.* (2014) 'Reliability of MASW profiling in near-surface applications', *Near Surface Geophysics*, 12(6), pp. 731–737. doi: 10.3997/1873-0604.2014029.

Sully, J. P. and Campanella, R. G. (1990) 'Measurement of Lateral Stress in Cohesive Soils by Full-displacement in Situ Test Methods', *University of British*

Columbia, Vancouver, B.C., Canada, TRB Record, pp. 1–30.

Sully, J. P. and Campanella, R. G. (1991) 'Effect of Lateral Stress on CPT Penetration Pore Pressures', *Journal of Geotechnical Engineering*, 117(7), pp. 1082–1088.

Sully, J. P. and Campanella, R. G. (1995) 'Evaluation of in situ anisotropy from crosshole and downhole shear wave velocity measurements', *Geotechnique*, 45(2), pp. 238–267. doi: 10.1680/geot.1995.45.2.267.

Tedd, P. and Charles, J. A. (1981) 'In situ measurement of horizontal stress in overconsolidated clay using push-in spade-shaped pressure cells', *Geotechnique*, 31(4), pp. 554–558. doi: 10.1680/geot.1981.31.4.554.

Terzaghi, K., Peck, R. B. and Mesri, G. (1996) *Soil mechanics in engineering practice.* 3rd edn. Edited by G. M. arl Terzaghi, Ralph B. Peck. New York: Wiley.

Timoshenko, S. and Goodier, J. N. (1951) *Theory of Elasticity.* 2nd edn. New York: McGraw Hill.

Tomás, R. *et al.* (2010) 'Cálculo analítico de la presión de preconsolidación del suelo : aplicación a la Vega Baja del río Segura (Alicante) (in Spanish)', *Ingeniería Civil*, 157, pp. 1–11.

Won, J. Y. and Chang, P. W. (2007) 'The causes of apparent overconsolidation in the Namak marine deposit, Korea', *Géotechnique*, 57(4), pp. 355–369. doi: 10.1680/geot.2007.57.4.365.

Wroth, J. and HughesJM (1973) 'An instrument for the in situ measurement of the properties of soft clays', in *Proc. 8th ICSMFE.* Moscow, pp. 487–494.

Yang, J.-F. J. (1987) *Role of lateral stress in slope stability of stiff overconsolidated clays and clayshales.* Iowa State University.

Yasuhara, K. and Syunji, U. (1983) 'Increase in Undrained Shear Strength Due to Secondary Compression', *Soils and Foundations*, 23(3), pp. 50–64.

Yew, C. H. and Weng, X. (2015) *Mechanics of Hydarulic Fracturing.* 2nd edn, *Mechanics of Hydraulic Fracturing.* 2nd edn. Edited by Gulf Professional Publishing. Oxford, UK: Elsevier. doi: 10.1016/B978-0-12-420003-6.09995-X.

Appendix A

Location Map

This appendix contains a summary table with the location of the boreholes where hydraulic fracturing and push-in cells have been installed. A map indicating the position of the boreholes inside the Tiller-Flotten test site is also attached.

Table A. 1 Location coordinates of boreholes at Tiller-Flotten test site

Borehole ID	WGS84 EUREF UTM32/NN2000			Test method
	X [m]	Y [m]	Z [m]	
EP36	7023912.520	571100.312	123.00	Push-in cell
EP37	7023914.213	571101.039	122.89	Push-in cell
TILH01	7023918.190	571091.100	123.42	Hydraulic fracturing Geonor tip
TILH02	7023919.390	571089.500	123.45	Hydraulic fracturing Geonor tip
TILH03	7023917.000	571096.000	123.04	Hydraulic fracturing Geonor tip
TILH04	7023918.200	571094.400	123.22	Hydraulic fracturing Geonor tip
TILH05	7023919.400	571092.800	123.42	Hydraulic fracturing Geonor tip
TILH06	7023920.600	571091.200	123.44	Hydraulic fracturing Geonor tip
TILH07	77023921.607	571086.373	123.49	Hydraulic fracturing Injection spade tip

Appendix B
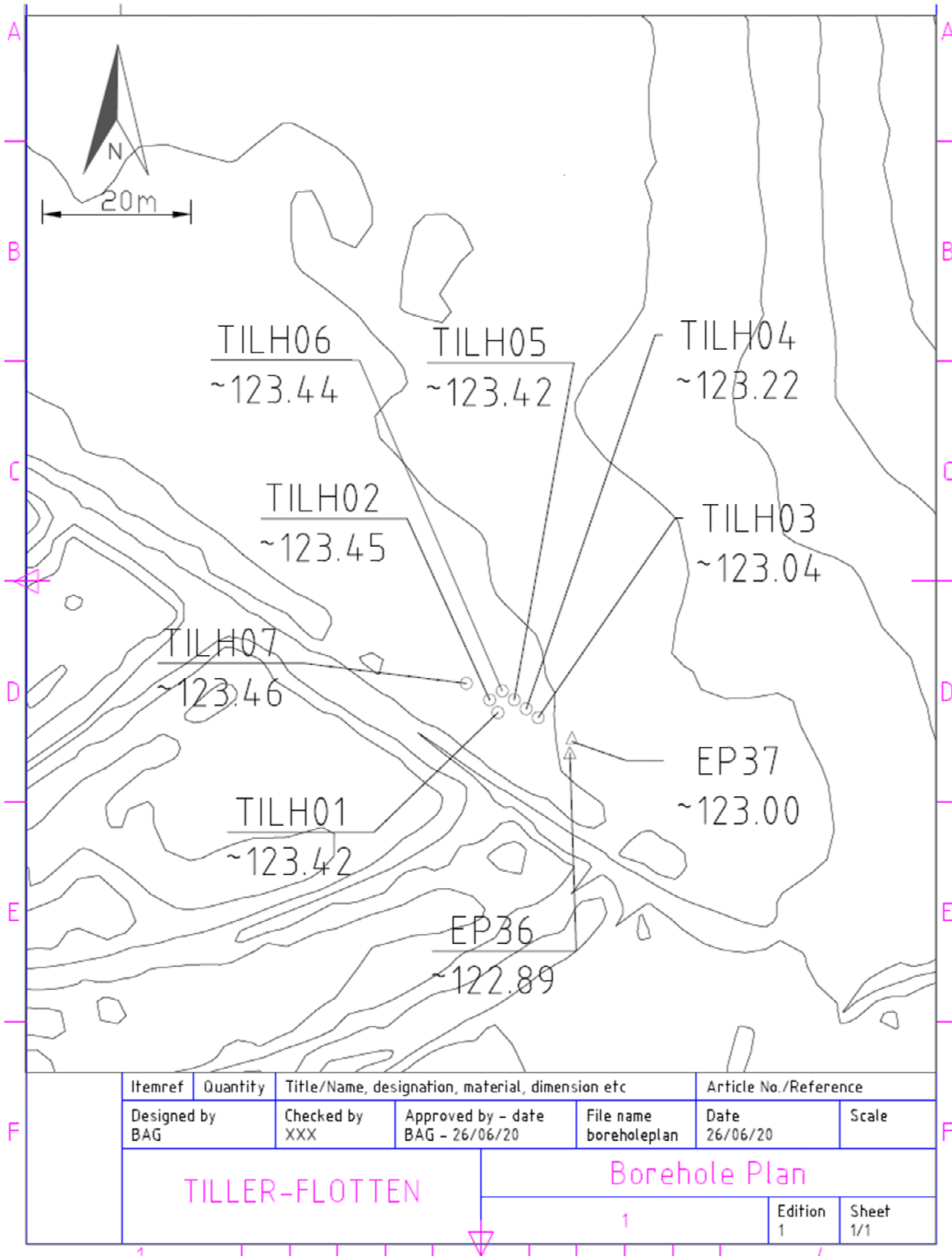
Push-in Total Stress Cells

This appendix contains a description on how the raw data have been processed. Secondly, calculated pressure data are plotted against time. Calibration sheet provided by manufacturer is also attached. A sample of raw data are included at the end of this appendix.

B.1   Calculation method

The raw data have been processed following the instructions given in the calibration sheets. The analyser unit is configured to register data in linear 'engineering' units ($F^2/1000$).

Two regressions lines are proposed, 'lineal' and 'polynomial'. The last one is chosen to calculate measured pressure since the accuracy is better:

$$E = AR_1^2 + BR_1 + C \qquad\qquad (B.1)$$

Where E is the earth or pore pressure in kPa, R_1 is the reading value in 'lineal' engineering units, A and B are calibration constants for each pressure sensor given in the calibration sheet provided by manufacturer, and C is a calibration constant depending on zero reading at the site before installation (R_0).

APPENDIX B: PUSH-IN TOTAL STRESS CELLS

The calibration constant C is given by:

$$C = -(AR_0^2 + BR_0) \qquad \text{(B. 2)}$$

B.2 Calibration sheets

soil
INSTRUMENTS

Bell Lane, Uckfield, East Sussex
TN22 1QL United Kingdom   t: +44 (0) 1825 765044   e: info@soilinstruments.com   w: www.soilinstruments.com
Soil Instruments Limited. Registered in England. Number: 07960087. Registered Office: 3rd Floor, 1 Ashley Road, Altrincham, Cheshire, WA14 2DT, UK

VIBRATING WIRE INSTRUMENTS CALIBRATION CERTIFICATE
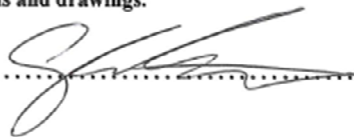
Instrument Type	: W9 Vibrating Wire Piezometer	Serial No.	: 064032

Instrument Range : 0.00 to 300.0 kPa   **Calibration Date** : 17/06/2019

Gauge Factors in kPa   **Ambient Temperature** : 25°C

Period Gauge Factor (K): 1505.6850000   **Barometric Pressure** : 1016 mbar

Linear Gauge Factor (G): (kPa/digit)0.1505700   **Calibration Technician** : Mark Bratton

Polynomial Gauge Factor A: -0.000000655120100   **Calibration Equipment:**
Mensor APC 600

Polynomial Gauge Factor B: -0.1435237000   AVW200 Data Logger

Polynomial Gauge Factor C**: 941.189600   **Regression Zero** : 6375.0

Applied (kPa)	Reading (Period)	Reading F²/1000	Calculated (Linear)	Error %FS (Linear)	Linear Increment	Calculated (Polynomial)	Error %FS (Polynomial)
0.00	3961.4	6372.4	0.383	0.13	0.0	-0.004	0.00
30.00	4024.4	6174.5	30.180	0.06	-197.9	30.026	0.01
60.00	4090.5	5976.5	59.993	0.00	-198.0	60.020	0.01
90.00	4160.0	5778.5	89.806	-0.06	-198.0	89.963	-0.01
120.00	4233.4	5579.9	119.709	-0.10	-198.6	119.944	-0.02
150.00	4311.1	5380.5	149.732	-0.09	-199.4	149.995	0.00
180.00	4393.5	5180.7	179.816	-0.06	-199.8	180.053	0.02
210.00	4480.6	4981.2	209.854	-0.05	-199.5	210.014	0.00
240.00	4573.3	4781.2	239.968	-0.01	-200.0	239.998	0.00
270.00	4672.4	4580.6	270.172	0.06	-200.6	270.019	0.01
300.00	4778.1	4380.1	300.361	0.12	-200.5	299.973	-0.01

Formulae: Linear* $E = G(R0 - R1)$
Polynomial** $E = AR1^2 + BR1 + C$

* The zero reading should be established on site by the user on installation.
** The site value of C must be calculated using the formula $C = -(AR0^2 + BR0)$

The instrument detailed hereon has, as applicable, been tested and calibrated in accordance with procedures, which are part of our ISO 9001:2008 Quality Management System, and unless otherwise indicated, performs within ± 0.10% (Polynomial) as specified. Thus, the instrument conforms in all respects to our relevant specifications and drawings.

Certified: .... Line MANAGER

soil
INSTRUMENTS

Bell Lane, Uckfield, East Sussex
TN22 1QL United Kingdom   t: +44 (0) 1825 765044   e: info@soilinstruments.com   w: www.soilinstruments.com
Soil Instruments Limited. Registered in England. Number: 07960087. Registered Office: 3rd Floor, 1 Ashley Road, Altrincham, Cheshire, WA14 2DT, UK

VIBRATING WIRE INSTRUMENTS CALIBRATION CERTIFICATE

Instrument Type : W9 Vibrating Wire Piezometer		**Serial No.**	: 064033
Instrument Range : 0.00 to 300.0 kPa		**Calibration Date**	: 17/06/2019
Gauge Factors in kPa		**Ambient Temperature**	: 25°C
Period Gauge Factor (K): 1703.4780000		**Barometric Pressure**	: 1016 mbar
Linear Gauge Factor (G): (kPa/digit)0.1703500		**Calibration Technician**	: Mark Bratton
Polynomial Gauge Factor A: -0.000000907761500		**Calibration Equipment:**	
		Mensor APC 600	
Polynomial Gauge Factor B: -0.1602350000		AVW200 Data Logger	
Polynomial Gauge Factor C:** 1071.309000		**Regression Zero**	: 6452.6

Applied (kPa)	Reading (Period)	Reading F²/1000	Calculated (Linear)	Error %FS (Linear)	Linear Increment	Calculated (Polynomial)	Error %FS (Polynomial)
0.00	3937.4	6450.3	0.396	0.13	0.0	-0.024	-0.01
30.00	3991.9	6275.5	30.173	0.06	-174.8	30.004	0.00
60.00	4048.7	6100.4	60.001	0.00	-175.1	60.029	0.01
90.00	4108.2	5925.2	89.846	-0.05	-175.2	90.014	0.00
120.00	4170.4	5749.7	119.742	-0.09	-175.5	119.995	0.00
150.00	4235.7	5573.9	149.689	-0.10	-175.8	149.972	-0.01
180.00	4304.4	5397.2	179.790	-0.07	-176.7	180.045	0.02
210.00	4376.5	5220.9	209.822	-0.06	-176.3	209.994	0.00
240.00	4452.5	5044.3	239.905	-0.03	-176.6	239.937	-0.02
270.00	4533.0	4866.6	270.176	0.06	-177.7	270.010	0.00
300.00	4618.1	4688.9	300.447	0.15	-177.7	300.025	0.01

Formulae: Linear* $E = G(R0 - R1)$
                  Polynomial** $E = AR1^2 + BR1 + C$

* The zero reading should be established on site by the user on installation.
** The site value of C must be calculated using the formula $C = -(AR0^2 + BR0)$

The instrument detailed hereon has, as applicable, been tested and calibrated in accordance with procedures, which are part of our ISO 9001:2008 Quality Management System, and unless otherwise indicated, performs within ± 0.10% (Polynomial) as specified. Thus, the instrument conforms in all respects to our relevant specifications and drawings.

Certified: .... Line MANAGER

soil
INSTRUMENTS

Bell Lane, Uckfield, East Sussex
TN22 1QL United Kingdom   t: +44 (0) 1825 765044   e: info@soilinstruments.com   w: www.soilinstruments.com
Soil Instruments Limited. Registered in England. Number: 07960087. Registered Office: 3rd Floor, 1 Ashley Road, Altrincham, Cheshire, WA14 2DT, UK

VIBRATING WIRE INSTRUMENTS CALIBRATION CERTIFICATE

Instrument Type : Vibrating Wire Pressure Cell	**Serial No.** : 064036
Instrument Range : 0.00 to 300.0 kPa	**Calibration Date** : 17/06/2019
Gauge Factors in kPa	**Ambient Temperature** : 25°C
Period Gauge Factor (K): 1484.1250000	**Barometric Pressure** : 1016 mbar
Linear Gauge Factor (G): (kPa/digit)0.1484100	**Calibration Technician** : Mark Bratton
Polynomial Gauge Factor A: -0.000000618067800	**Calibration Equipment:**
Polynomial Gauge Factor B: -0.1419964000	Mensor APC 600 AVW200 Data Logger
Polynomial Gauge Factor C**: 904.223800	**Regression Zero** : 6203.1

Applied (kPa)	Reading (Period)	Reading F²/1000	Calculated (Linear)	Error %FS (Linear)	Linear Increment	Calculated (Polynomial)	Error %FS (Polynomial)
0.00	4016.0	6200.4	0.409	0.14	0.0	0.028	0.01
30.00	4082.5	5999.9	30.165	0.06	-200.5	30.010	0.00
60.00	4152.6	5799.2	59.952	-0.02	-200.7	59.972	-0.01
90.00	4226.5	5598.1	89.797	-0.07	-201.1	89.944	-0.02
120.00	4304.8	5396.3	119.747	-0.08	-201.8	119.970	-0.01
150.00	4387.9	5193.7	149.815	-0.06	-202.6	150.065	0.02
180.00	4475.9	4991.6	179.809	-0.06	-202.1	180.035	0.01
210.00	4569.5	4789.3	209.833	-0.06	-202.3	209.984	-0.01
240.00	4669.5	4586.3	239.960	-0.01	-203.0	239.985	0.00
270.00	4776.8	4382.6	270.192	0.06	-203.7	270.039	0.01
300.00	4891.5	4179.4	300.349	0.12	-203.2	299.968	-0.01

Formulae: Linear* $E = G(R0 - R1)$
             Polynomial** $E = AR1^2 + BR1 + C$

* The zero reading should be established on site by the user on installation.
** The site value of C must be calculated using the formula $C = -(AR0^2 + BR0)$

The instrument detailed hereon has, as applicable, been tested and calibrated in accordance with procedures, which are part of our ISO 9001:2008 Quality Management System, and unless otherwise indicated, performs within ± 0.50% (Polynomial) as specified. Thus, the instrument conforms in all respects to our relevant specifications and drawings.

Certified: .... Line MANAGER

soil
INSTRUMENTS

Bell Lane, Uckfield, East Sussex
TN22 1QL United Kingdom   t: +44 (0) 1825 765044   e: info@soilinstruments.com   w: www.soilinstruments.com
Soil Instruments Limited. Registered in England. Number: 07960087. Registered Office: 3rd Floor, 1 Ashley Road, Altrincham, Cheshire, WA14 2DT, UK

VIBRATING WIRE INSTRUMENTS CALIBRATION CERTIFICATE

Instrument Type : Vibrating Wire Pressure Cell	**Serial No.** : 064037
Instrument Range : 0.00 to 300.0 kPa	**Calibration Date** : 17/06/2019
<u>Gauge Factors in kPa</u>	**Ambient Temperature** : 25°C
Period Gauge Factor (K): 1477.5510000	**Barometric Pressure** : 1016 mbar
Linear Gauge Factor (G): (kPa/digit)0.1477600	**Calibration Technician** : Mark Bratton
Polynomial Gauge Factor A: -0.000000414417200	<u>Calibration Equipment:</u>
	Mensor APC 600
Polynomial Gauge Factor B: -0.1435396000	AVW200 Data Logger
Polynomial Gauge Factor C**: 891.133400	**Regression Zero** : 6102.5

Applied (kPa)	Reading (Period)	Reading $F^2/1000$	Calculated (Linear)	Error %FS (Linear)	Linear Increment	Calculated (Polynomial)	Error %FS (Polynomial)
0.00	4048.6	6100.8	0.259	0.09	0.0	0.002	0.00
30.00	4117.4	5898.7	30.120	0.04	-202.1	30.017	0.01
60.00	4189.8	5696.7	59.967	-0.01	-202.0	59.982	-0.01
90.00	4266.2	5494.3	89.872	-0.04	-202.4	89.974	-0.01
120.00	4347.2	5291.5	119.837	-0.05	-202.8	119.990	0.00
150.00	4433.2	5088.2	149.876	-0.04	-203.3	150.046	0.02
180.00	4524.4	4885.2	179.870	-0.04	-203.0	180.024	0.01
210.00	4621.5	4682.1	209.879	-0.04	-203.1	209.982	-0.01
240.00	4725.2	4478.7	239.932	-0.02	-203.4	239.950	-0.02
270.00	4837.0	4274.2	270.148	0.05	-204.5	270.045	0.02
300.00	4956.5	4070.5	300.246	0.08	-203.7	299.989	0.00

Formulae: Linear* $E = G(R0 - R1)$
            Polynomial** $E = AR1^2 + BR1 + C$

* The zero reading should be established on site by the user on installation.
** The site value of C must be calculated using the formula $C = -(AR0^2 + BR0)$

The instrument detailed hereon has, as applicable, been tested and calibrated in accordance with procedures, which are part of our ISO 9001:2008 Quality Management System, and unless otherwise indicated, performs within ± 0.50% (Polynomial) as specified. Thus, the instrument conforms in all respects to our relevant specifications and drawings.

Certified: .... Line MANAGER

B.3 Raw data and results

TILLER - FLOTTEN	Push-in earth pressure cells	
Date: 19.12.2019	Borehole: EP36	Depth: 5 m

Specific weight, γ [KN/m3]	18.5	u_o [kPa]		31.0	σ'_v [kPa]	61.5	σ'_h [kPa]	69.97
Depth, D [m]	5.0	u_{EP} [kPa]		28.33	σ_h [kPa]	98.30	K'_0 [kPa]	1.02
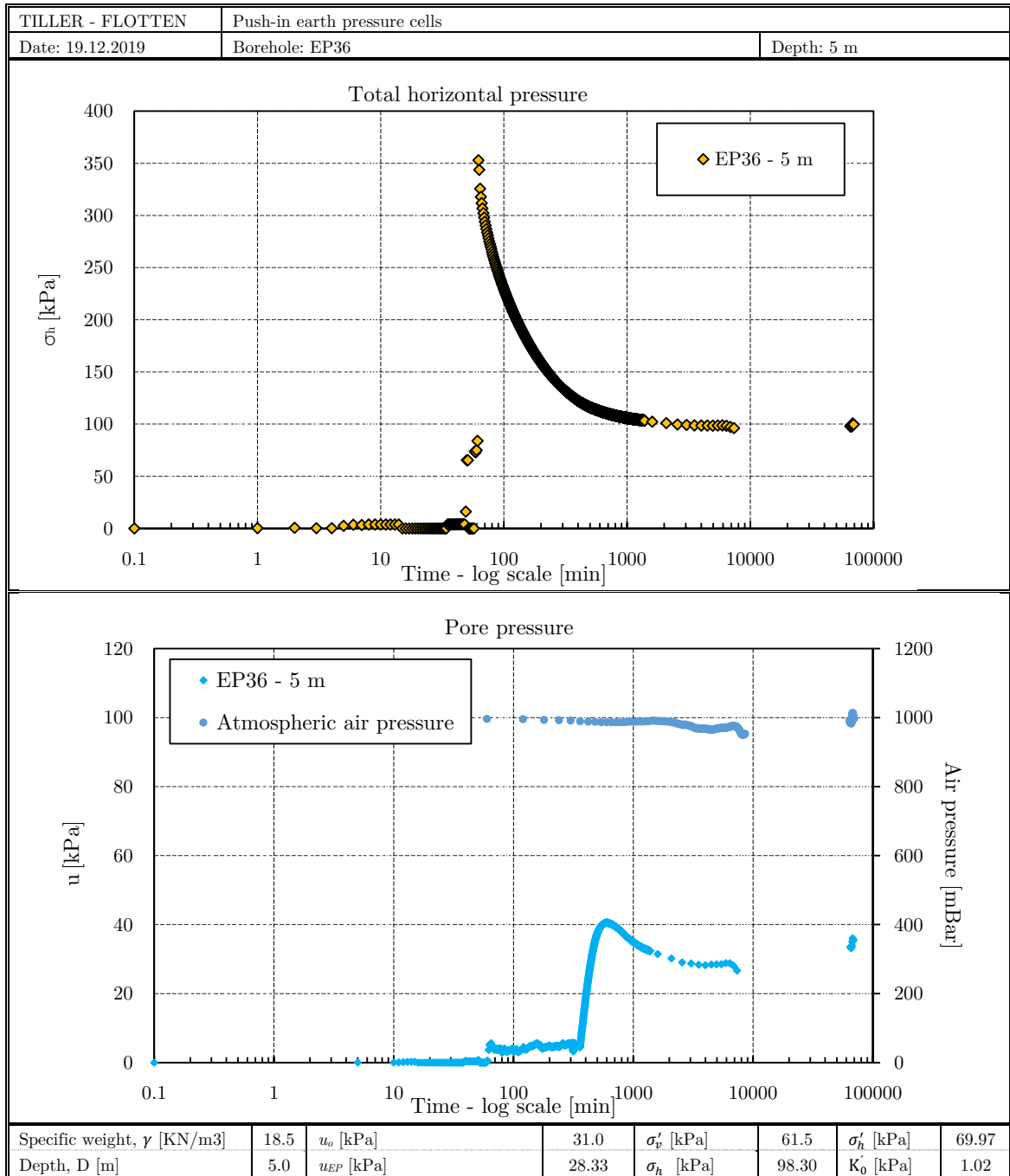
Figure B- 1 Total horizontal stress and pore pressure plotted versus logarithmic time at from at borehole EP36 (5 m depth). u_{EP} is pore pressure obtained by pore pressure sensor installed in the push-in cell and is the pore pressure used to calculate vertical and horizontal effective stresses.

APPENDIX B: PUSH-IN TOTAL STRESS CELLS

TILLER - FLOTTEN	Push-in earth pressure cells	
Date: 19.12.2019	Borehole: EP37	Depth: 5 m

Specific weight, γ [KN/m3]	18.5	u_o [kPa]	31.0	σ_v' [kPa]	59.77	σ_h' [kPa]	69.58
Depth, D [m]	5.0	u_{EP} [kPa]	32.73	σ_h [kPa]	102,31	K_0' [kPa]	1.16
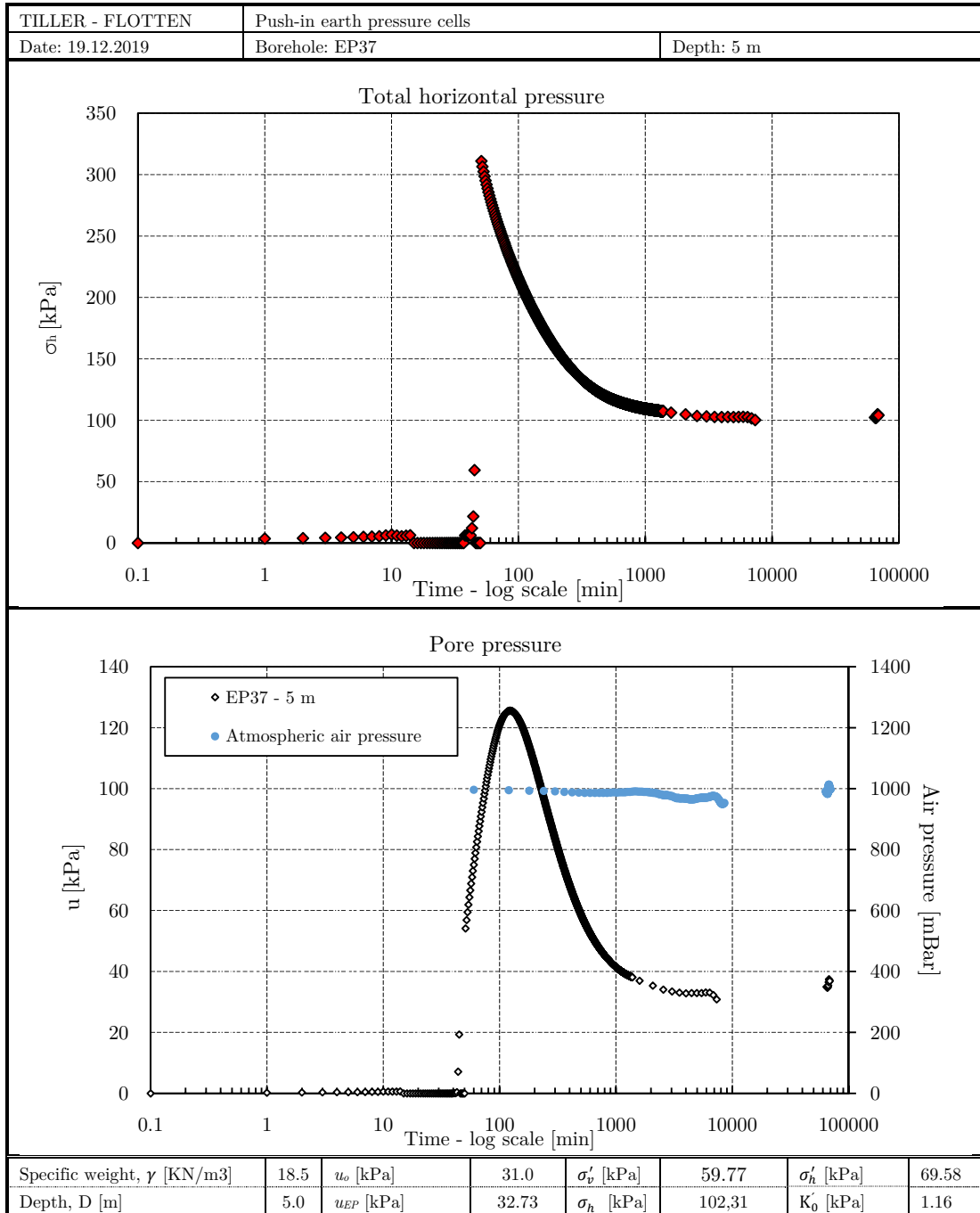
Figure B- 2 Total horizontal stress and pore pressure plotted versus logarithmic time at from at borehole EP37 (5 m depth). u_{EP} is pore pressure obtained by pore pressure sensor installed in the push-in cell and is the pore pressure used to calculate vertical and horizontal effective stresses.

TILLER - FLOTTEN	Push-in earth pressure cells	
Date: 28.02.2019	Borehole: EP36	Depth: 7.5 m

Specific weight, γ [KN/m3]	18.5	u_o [kPa]	37	σ'_v [kPa]	92.99	σ'_h [kPa]	59.46
Depth, D [m]	7.5	u_{EP} [kPa]	45.76	σ_h [kPa]	104.37	K'_0 [kPa]	0.64
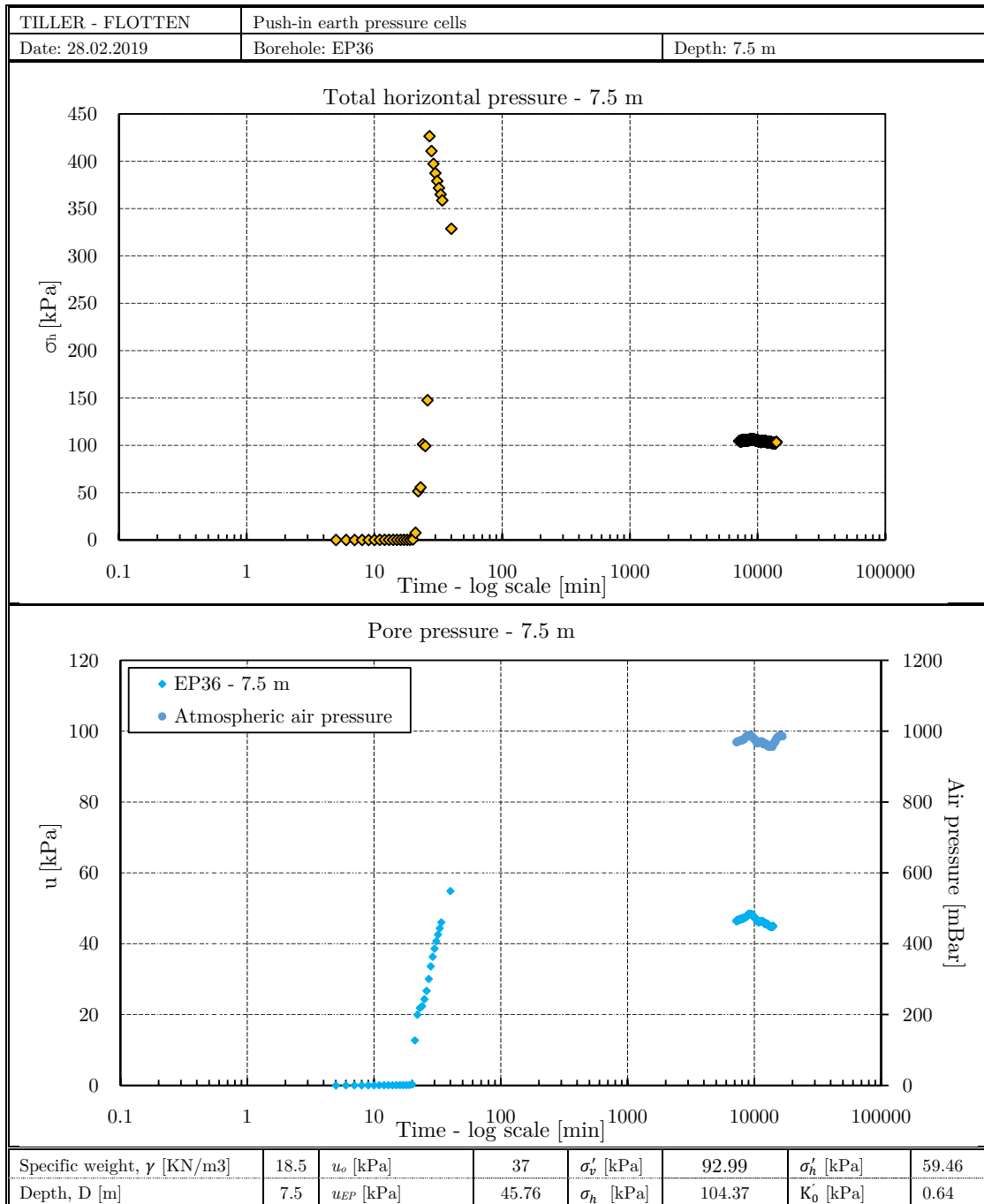
Figure B- 3 Total horizontal stress and pore pressure plotted versus logarithmic time at from at borehole EP36 (7.5 m depth). u_{EP} is pore pressure obtained by pore pressure sensor installed in the push-in cell, and is the pore pressure used to calculate vertical and horizontal effective stresses

APPENDIX B: PUSH-IN TOTAL STRESS CELLS

TILLER - FLOTTEN	Push-in earth pressure cells	
Date: 28.02.2019	Borehole: EP37	Depth: 7.5 m

Total horizontal pressure - 7.5 m

Pore pressure - 7.5 m

Legend:
◇ EP37 - 7.5 m
● Atmospheric air pressure

Specific weight, γ [KN/m3]	18.5	u_o [kPa]	37	σ'_v [kPa]	97.18	σ'_h [kPa]	59.24
Depth, D [m]	7.5	u_{EP} [kPa]	41.57	σ_h [kPa]	100.81	K'_0 [kPa]	0.61
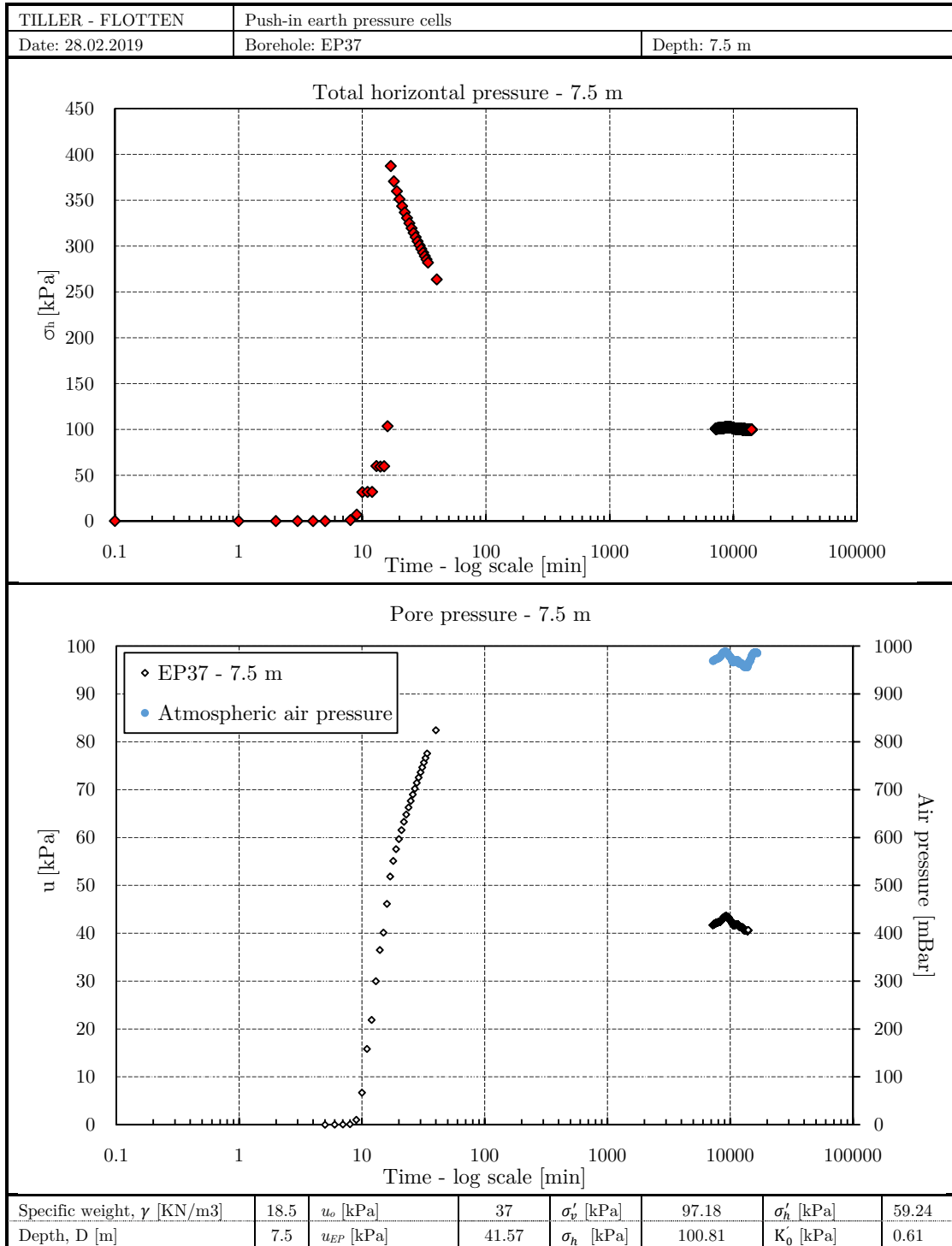
Figure B- 4 Total horizontal stress and pore pressure from the earth pressure cells plotted versus logarithmic time at 7.5 m depth. u_{EP} is pore pressure obtained by pore pressure sensor installed in the push-in cell, and is the pore pressure used to calculate vertical and horizontal effective stresses

Raw data example

Cell ID EP36				
Sensor serial no.	064036	**Sensor serial no.**		064032
Sensor type	Vibrating wire Pressure Cell	**Sensor type**		Vibrating wire Piezometer
Zero reading	5942.075	**Zero reading**		6389.28
Calibration constants	**A** -6.18068E-07	**Calibration constants**	**A**	-6.551E-07
	B -0.1419964		**B**	-0.1435237
	C 865.5761542		**C**	943.757008

Calculated parameters for 5 m depth	
Stabilized earth pressure value [kPa]	98.30
Stabilized earth pressure value [kPa]	28.33
Calculated effective horizontal stress	69.97

Cell ID	EP36	Depth 5 m		
Dato	**Sensor 064036 Reading**	**Sensor 064036 Calculated pressure [kPa]**	**Sensor 064032 Reading**	**Sensor 064032 Calculated pressure [kPa]**
03.12.2019 13:22	5942.075	0.000	6389.28	0.000
03.12.2019 13:23	5940.8	0.190	6389.364	-0.013
03.12.2019 13:24	5938.061	0.599	6389.449	-0.026
03.12.2019 13:25	5940.384	0.253	6389.476	-0.030
03.12.2019 13:26	5940.573	0.224	6389.525	-0.037
03.12.2019 13:27	5925.593	2.461	6389.147	0.020
03.12.2019 13:28	5918.659	3.497	6389.306	-0.004
03.12.2019 13:29	5920.133	3.277	6389.602	-0.049
03.12.2019 13:30	5916.855	3.766	6389.565	-0.043
03.12.2019 13:31	5917.282	3.702	6389.472	-0.029
03.12.2019 13:32	5917.062	3.735	6389.066	0.033
03.12.2019 13:33	5916.95	3.752	6388.595	0.104
03.12.2019 13:34	5916.847	3.767	6388.214	0.162
03.12.2019 13:35	5916.799	3.774	6387.912	0.208
03.12.2019 13:36	5916.801	3.774	6387.69	0.242
03.12.2019 13:37	-9998		6387.504	0.270
03.12.2019 13:38	-9998		-9998	
03.12.2019 13:39	-9998		-9998	
03.12.2019 13:40	-9998		-9998	
03.12.2019 13:41	-9998		-9998	
03.12.2019 13:42	-9998		-9998	
03.12.2019 13:43	-9998		-9998	
03.12.2019 13:44	-9998		-9998	
03.12.2019 13:45	-9998		-9998	
03.12.2019 13:46	-9998		-9998	
03.12.2019 13:47	-9998		-9998	
03.12.2019 13:48	-9998		-9998	
03.12.2019 13:49	-9998		-9998	

03.12.2019 13:50	-9998		-9998	
03.12.2019 13:51	-9998		-9998	
03.12.2019 13:52	-9998		-9998	
03.12.2019 13:53	-9998		-9998	
03.12.2019 13:54	-9998		-9998	
03.12.2019 13:55	-9998		-9998	
03.12.2019 13:56	-9998		-9998	
03.12.2019 13:57	5916.331	3.844	-9998	
03.12.2019 13:58	5916.063	3.884	-9998	
03.12.2019 13:59	5915.864	3.914	-9998	
03.12.2019 14:00	5915.793	3.925	-9998	
03.12.2019 14:01	5915.314	3.996	6386.609	0.406
03.12.2019 14:02	5915.098	4.028	6386.681	0.395
03.12.2019 14:03	5914.9	4.058	6386.681	0.395
03.12.2019 14:04	5914.928	4.054	6386.729	0.387
03.12.2019 14:05	5914.894	4.059	6386.69	0.393
03.12.2019 14:06	5914.938	4.052	6386.734	0.387
03.12.2019 14:07	5914.921	4.055	6386.771	0.381
03.12.2019 14:08	5914.857	4.064	6386.737	0.386
03.12.2019 14:09	5914.957	4.049	6386.713	0.390
03.12.2019 14:10	5915.003	4.043	6386.69	0.393
03.12.2019 14:11	5834.373	16.077	6386.839	0.371
03.12.2019 14:12	5503.106	65.437	6385.496	0.575
03.12.2019 14:13	5503.006	65.452	6384.106	0.786
03.12.2019 14:14	-9998		-9998	
03.12.2019 14:15	-9998		-9998	
03.12.2019 14:16	-9998		-9998	
03.12.2019 14:17	-9998		-9998	
03.12.2019 14:18	-9998		-9998	
03.12.2019 14:19	-9998		-9998	
03.12.2019 14:20	5447.398	73.725	-9998	
03.12.2019 14:21	5452.822	72.918	-9998	
03.12.2019 14:22	5438.329	75.073	6386.554	0.414
03.12.2019 14:23	5379.013	83.893	6385.890	0.515
03.12.2019 14:24	3555.149	352.946	6364.891	3.704
03.12.2019 14:25	3618.473	343.673	6354.999	5.206
03.12.2019 14:26	3741.648	325.623	6354.477	5.286
03.12.2019 14:27	3795.42	317.737	6352.251	5.624
03.12.2019 14:28	3836.018	311.781	6357.891	4.767
03.12.2019 14:29	3870.385	306.737	6358.523	4.671
03.12.2019 14:30	3901.213	302.211	6360.123	4.428
03.12.2019 14:31	3929.855	298.006	6364.612	3.747
03.12.2019 14:32	3956.8	294.048	6363.376	3.934
03.12.2019 14:33	3981.649	290.398	6362.003	4.143
03.12.2019 14:34	4004.559	287.032	6364.998	3.688
03.12.2019 14:35	4026.314	283.834	6365.212	3.655

03.12.2019 14:36	4046.608	280.852	6362.518	4.065
03.12.2019 14:37	4066.135	277.981	6362.788	4.024
03.12.2019 14:38	4084.957	275.213	6365.085	3.675
03.12.2019 14:39	4102.849	272.582	6363.892	3.856
03.12.2019 14:40	4119.585	270.121	6361.675	4.193
03.12.2019 14:41	4135.134	267.833	6367.582	3.296
03.12.2019 14:42	4154.173	265.032	6370.091	2.914
03.12.2019 14:43	4170.407	262.644	6368.582	3.144
03.12.2019 14:44	4185.666	260.398	6368.191	3.203
03.12.2019 14:45	4200.327	258.240	6365.374	3.631
03.12.2019 14:46	4214.343	256.177	6362.236	4.107
03.12.2019 14:47	4227.747	254.204	6364.063	3.830
03.12.2019 14:48	4241.264	252.214	6365.636	3.591
03.12.2019 14:49	4254.512	250.263	6368.820	3.108
03.12.2019 14:50	4267.395	248.366	6369.019	3.077
03.12.2019 14:51	4279.828	246.535	6367.831	3.258
03.12.2019 14:52	4291.926	244.753	6365.625	3.593
03.12.2019 14:53	4303.769	243.008	6365.773	3.570
03.12.2019 14:54	4315.36	241.301	6366.003	3.535
03.12.2019 14:55	4326.628	239.641	6366.415	3.473
03.12.2019 14:56	4337.467	238.043	6366.140	3.515
03.12.2019 14:57	4347.983	236.494	6365.423	3.623
03.12.2019 14:58	4358.253	234.980	6364.423	3.775
03.12.2019 14:59	4368.304	233.499	6363.004	3.991
03.12.2019 15:00	4378.203	232.040	6361.786	4.176
03.12.2019 15:01	4387.929	230.606	6366.570	3.449
03.12.2019 15:02	4397.412	229.208	6367.865	3.253
03.12.2019 15:03	4406.707	227.837	6367.812	3.261
03.12.2019 15:04	4415.801	226.496	6367.136	3.363
03.12.2019 15:05	4424.763	225.175	6366.196	3.506
03.12.2019 15:06	4433.624	223.868	6365.000	3.688
03.12.2019 15:07	4442.378	222.577	6363.606	3.899
03.12.2019 15:08	4450.932	221.315	6363.484	3.918
03.12.2019 15:09	4459.31	220.080	6367.282	3.341
03.12.2019 15:10	4467.476	218.875	6368.581	3.144
03.12.2019 15:11	4475.411	217.704	6368.858	3.102
03.12.2019 15:12	4483.114	216.568	6368.467	3.161
03.12.2019 15:13	4490.707	215.448	6367.931	3.243
03.12.2019 15:14	4498.207	214.341	6367.407	3.322
03.12.2019 15:15	4505.566	213.255	6366.881	3.402
03.12.2019 15:16	4512.788	212.189	6366.316	3.488
03.12.2019 15:17	4519.909	211.138	6365.716	3.579
03.12.2019 15:18	4526.878	210.110	6365.111	3.671
03.12.2019 15:19	4533.716	209.101	6364.528	3.759
03.12.2019 15:20	4540.447	208.107	6363.930	3.850

03.12.2019 15:21	4547.06	207.131	6363.146	3.969
03.12.2019 15:22	4553.639	206.160	6362.456	4.074
03.12.2019 15:23	4560.061	205.212	6359.585	4.510
03.12.2019 15:24	4566.447	204.269	6362.620	4.049
03.12.2019 15:25	4572.801	203.331	6363.778	3.873
03.12.2019 15:26	4579.006	202.415	6363.723	3.882
03.12.2019 15:27	4585.183	201.502	6363.400	3.931
03.12.2019 15:28	4591.246	200.607	6364.042	3.833
03.12.2019 15:29	4597.183	199.730	6364.228	3.805
03.12.2019 15:30	4602.998	198.872	6363.982	3.842
04.12.2019 07:33	5236.255	105.100	6164.767	34.069
04.12.2019 07:34	5236.305	105.093	6164.827	34.060
04.12.2019 07:35	5236.332	105.089	6164.883	34.052
04.12.2019 07:36	5236.396	105.079	6164.938	34.043
04.12.2019 07:37	5236.458	105.070	6164.995	34.035
04.12.2019 07:38	5236.487	105.066	6165.054	34.026
04.12.2019 07:39	5236.561	105.055	6165.109	34.018
04.12.2019 07:40	5236.581	105.052	6165.172	34.008
04.12.2019 07:41	5236.528	105.060	6165.223	34.000
04.12.2019 07:42	5236.603	105.049	6165.277	33.992
04.12.2019 07:43	5236.696	105.035	6165.333	33.984
04.12.2019 07:44	5236.746	105.027	6165.392	33.975
04.12.2019 07:45	5236.798	105.020	6165.451	33.966
04.12.2019 07:46	5236.858	105.011	6165.507	33.957
04.12.2019 07:47	5236.938	104.999	6165.565	33.948
04.12.2019 07:48	5236.991	104.991	6165.623	33.940
04.12.2019 07:49	5237.067	104.980	6165.683	33.931
04.12.2019 07:50	5237.144	104.968	6165.741	33.922
04.12.2019 07:51	5237.187	104.962	6165.799	33.913
04.12.2019 07:52	5237.209	104.959	6165.859	33.904
04.12.2019 07:53	5237.248	104.953	6165.918	33.895
04.12.2019 07:54	5237.336	104.940	6165.974	33.886
04.12.2019 07:55	5237.426	104.927	6166.039	33.877
04.12.2019 07:56	5237.415	104.928	6166.097	33.868
04.12.2019 07:57	5237.434	104.925	6166.151	33.860
04.12.2019 07:58	5237.475	104.919	6166.211	33.851
04.12.2019 07:59	5237.516	104.913	6166.264	33.842
04.12.2019 08:00	5237.585	104.903	6166.319	33.834
04.12.2019 08:01	5237.637	104.895	6166.374	33.826
04.12.2019 08:02	5237.672	104.890	6166.433	33.817
04.12.2019 08:03	5237.735	104.881	6166.484	33.809
04.12.2019 08:04	5237.8	104.871	6166.537	33.801
04.12.2019 08:05	5237.833	104.866	6166.592	33.793
04.12.2019 08:06	5237.828	104.867	6166.648	33.784
04.12.2019 08:07	5237.857	104.863	6166.703	33.776
04.12.2019 08:08	5237.888	104.858	6166.753	33.768

130

04.12.2019 08:09	5237.971	104.846	6166.808	33.760
04.12.2019 08:10	5238.038	104.836	6166.858	33.752
04.12.2019 08:11	5238.061	104.832	6166.914	33.744
04.12.2019 08:12	5238.083	104.829	6166.961	33.737
04.12.2019 08:13	5238.12	104.823	6167.018	33.728
04.12.2019 08:14	5238.167	104.817	6167.071	33.720
04.12.2019 08:15	5238.237	104.806	6167.121	33.713
04.12.2019 08:16	5238.315	104.795	6167.180	33.704
04.12.2019 08:17	5238.369	104.787	6167.236	33.695
04.12.2019 08:18	5238.413	104.780	6167.292	33.687
04.12.2019 08:19	5238.432	104.777	6167.347	33.678
04.12.2019 08:20	5238.479	104.770	6167.400	33.670
04.12.2019 12:21	5247.702	103.401	6175.939	32.376
04.12.2019 12:26	5247.71	103.400	6176.067	32.356
04.12.2019 16:00	5255.218	102.285	6181.989	31.458
05.12.2019 00:00	5264.192	100.952	6190.470	30.172
05.12.2019 08:00	5272.929	99.655	6197.937	29.040
05.12.2019 16:00	5275.476	99.276	6199.973	28.731
06.12.2019 00:00	5278.775	98.786	6202.286	28.381
06.12.2019 08:00	5279.478	98.682	6203.146	28.250
06.12.2019 16:00	5279.479	98.682	6201.744	28.463
07.12.2019 00:00	5280.333	98.555	6201.550	28.492
07.12.2019 08:00	5280.294	98.561	6201.216	28.543
07.12.2019 16:00	5279.228	98.719	6199.190	28.850
08.12.2019 00:00	5281.21	98.425	6199.266	28.839
08.12.2019 08:00	5288.864	97.288	6204.623	28.026
08.12.2019 16:00	5297.1	96.064	6213.481	26.683

Appendix C

Hydraulic Fracturing

In this appendix a description of methodology followed for data interpretation is presented. Secondly, a graphical representation of logged pressure data against time is shown from Figure A.2 to Figure A. Finally, an example of raw data generated by logging system is presented in Table.

C.1   Raw data with Geonor filter tip

TILLER - FLOTTEN	Hydraulic fracturing - Geonor piezometer tip	
Date: 25.02.2019	Borehole: TILH01	Depth: 5 m

Specific weight, γ [KN/m3]	18.5	H [kPa]	5.5	σ_h [kPa]	159.0
Depth, D [m]	5.0	Pwi [kPa]	55.5	σ_h' [kPa]	128.0
GWL, h [m]	2.0	$P_{fracture}$ [kPa]	195.5	σ_v' [kPa]	61.5
u_o [kPa]	31.0	$P_{closure}$ [kPa]	103.5	K_0' [-]	2.08

$$P_{wi} = (D + H) \cdot \gamma_w$$

$$\sigma_h = P_{closure} + P_{wi}$$

$$\sigma_h' = \sigma_h - u_o$$

$$K_o' = \frac{\sigma_h'}{\sigma_v'}$$
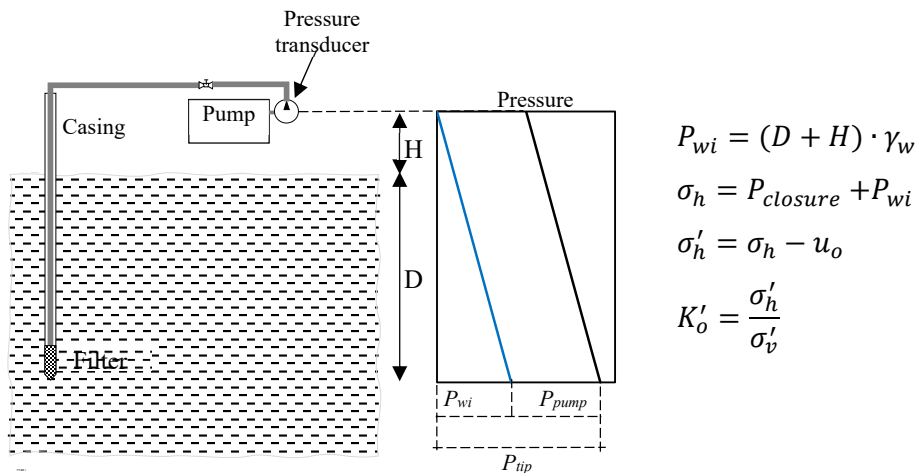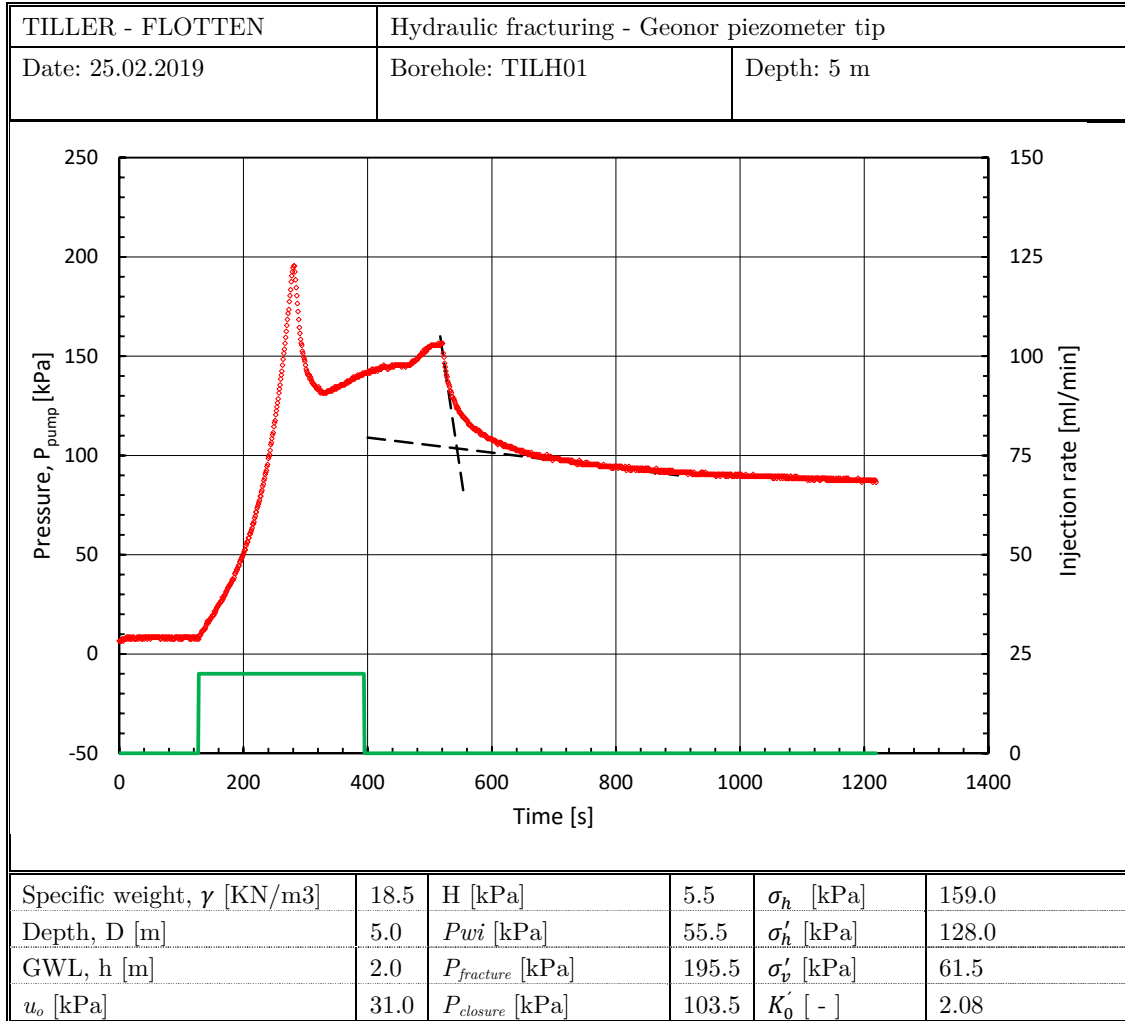
Figure C- 1 Pressure and injection flow rate vs. time record for borehole TILH01 (5m depth)

TILLER - FLOTTEN	Hydraulic fracturing - Geonor piezometer tip	
Date: 25.02.2019	Borehole: TILH02	Depth: 10 m

Specific weight, γ [KN/m3]	18.5	H [kPa]	5.5	σ_h [kPa]	218.9
Depth, D [m]	10.0	Pwi [kPa]	105.5	σ_h' [kPa]	176.0
GWL, h [m]	2.0	$P_{fracture}$ [kPa]	207.4	σ_v' [kPa]	142.0
u_o [kPa]	43.0	$P_{closure}$ [kPa]	113.4	K_0' [-]	1.69

$$P_{wi} = (D + H) \cdot \gamma_w$$

$$\sigma_h = P_{closure} + P_{wi}$$

$$\sigma_h' = \sigma_h - u_o$$

$$K_o' = \frac{\sigma_h'}{\sigma_v'}$$
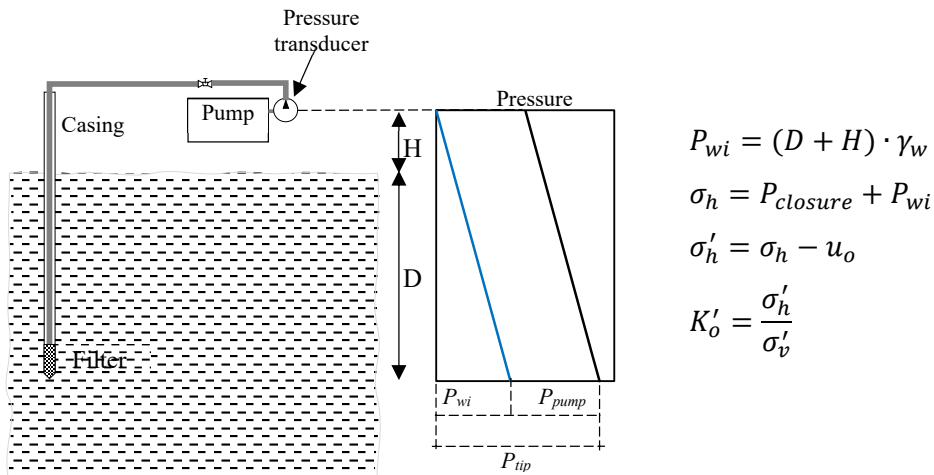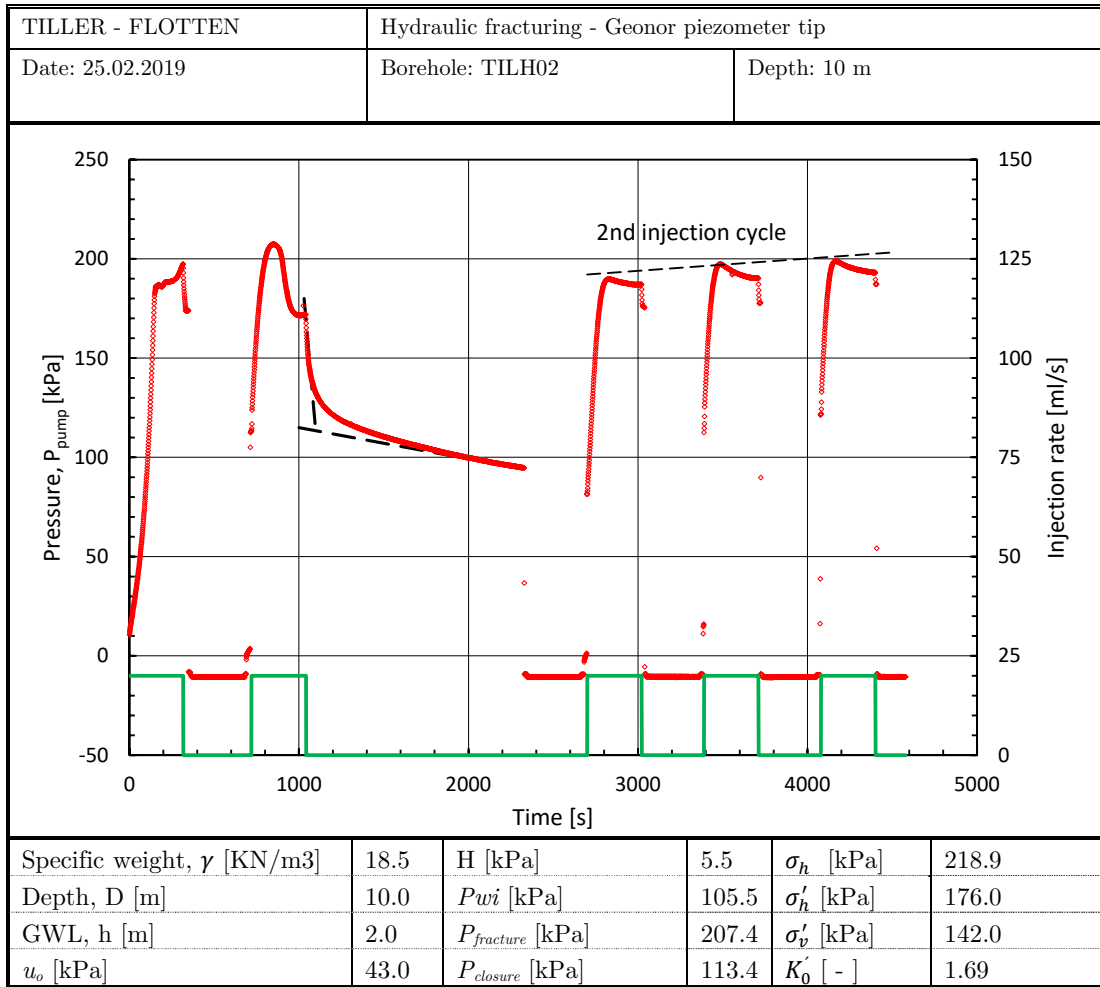
Figure C- 2 Pressure and injection flow rate vs. time record for borehole TILH02 (10m depth)

TILLER - FLOTTEN	Hydraulic fracturing - Geonor piezometer tip	
Date: 25.02.2019	Borehole: TILH03	Depth: 15 m

Specific weight, γ [KN/m3]	18.5	H [kPa]	5.5	σ_h [kPa]	218.9
Depth, D [m]	15.0	Pwi [kPa]	155.5	σ'_h [kPa]	188.1
GWL, h [m]	2.0	$P_{fracture}$ [kPa]	188.3	σ'_v [kPa]	222.5
u_o [kPa]	55.0	$P_{closure}$ [kPa]	87.6	K'_0 [-]	0.85

$$P_{wi} = (D + H) \cdot \gamma_w$$

$$\sigma_h = P_{closure} + P_{wi}$$

$$\sigma'_h = \sigma_h - u_o$$

$$K'_o = \frac{\sigma'_h}{\sigma'_v}$$
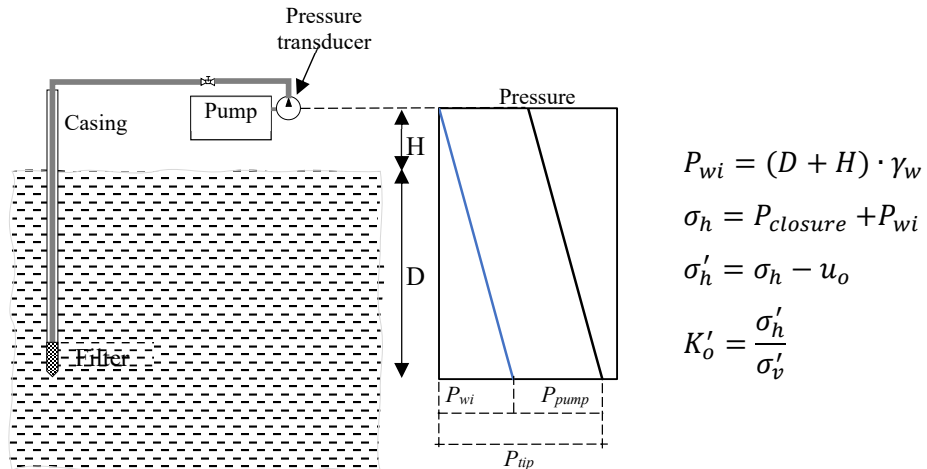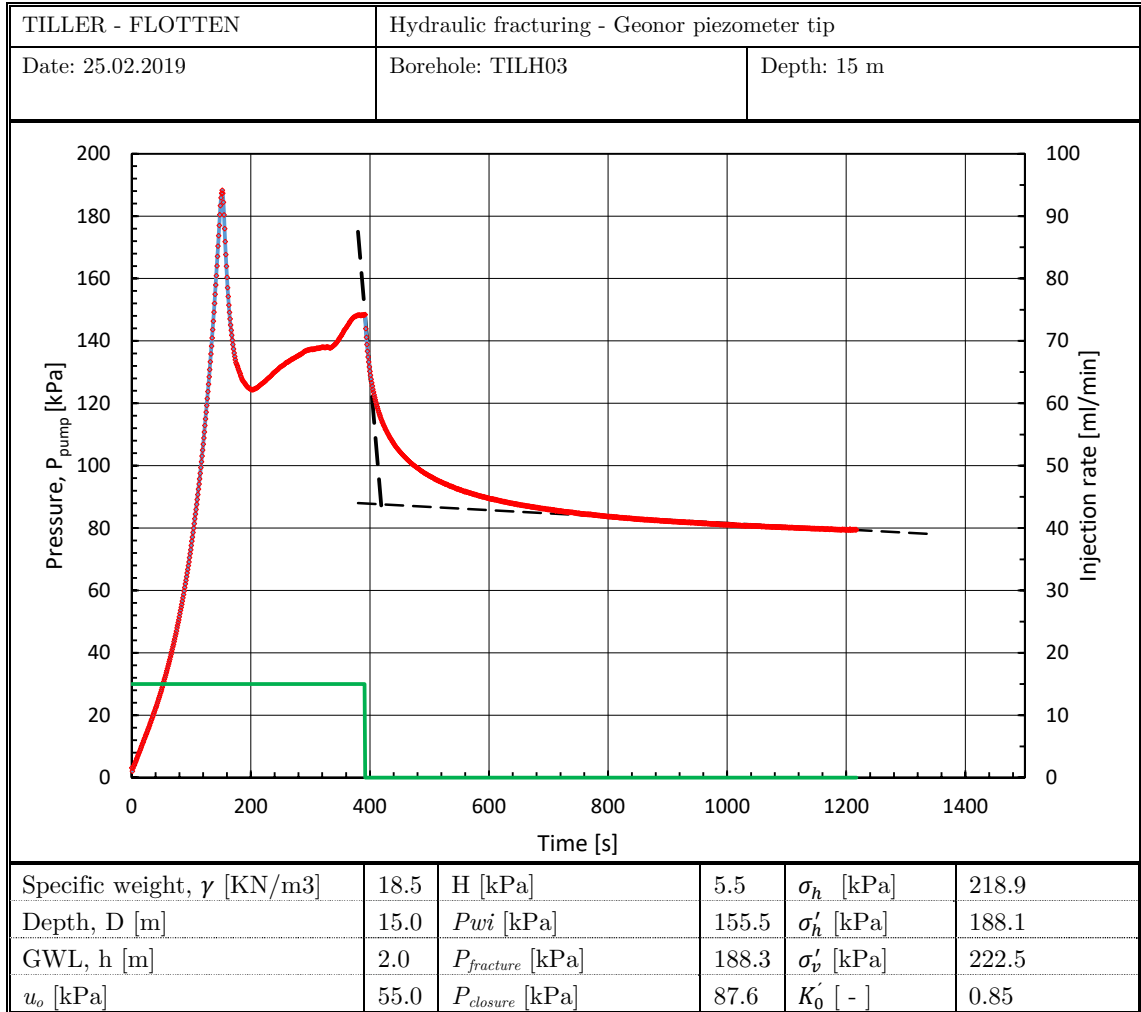
Figure C- 3 Pressure and injection flow rate vs. time record for borehole TILH03 (15m depth)

TILLER - FLOTTEN	Hydraulic fracturing - Geonor piezometer tip	
Date: 26.02.2019	Borehole: TILH04	Depth: 5 m

Specific weight, γ [KN/m3]	18.5	H [kPa]	5.5	σ_h [kPa]	153.1
Depth, D [m]	5.0	Pwi [kPa]	55.5	σ'_h [kPa]	122.1
GWL, h [m]	2.0	$P_{fracture}$ [kPa]	176.1	σ'_v [kPa]	61.5
u_o [kPa]	31.0	$P_{closure}$ [kPa]	97.6	K'_0 [-]	1.99

$$P_{wi} = (D + H) \cdot \gamma_w$$

$$\sigma_h = P_{closure} + P_{wi}$$

$$\sigma'_h = \sigma_h - u_o$$

$$K'_o = \frac{\sigma'_h}{\sigma'_v}$$

Figure C- 4 Pressure and injection flow rate vs. time record for borehole TILH04 (5m depth)

TILLER - FLOTTEN	Hydraulic fracturing - Geonor piezometer tip	
Date: 26.02.2019	Borehole: TILH05	Depth: 10 m

Specific weight, γ [KN/m3]	18.5	H [kPa]	5.5	σ_h [kPa]	233.5
Depth, D [m]	10.0	P_{wi} [kPa]	105.5	σ'_h [kPa]	190.5
GWL, h [m]	2.0	$P_{fracture}$ [kPa]	205.3	σ'_v [kPa]	142.0
u_o [kPa]	43.0	$P_{closure}$ [kPa]	128.0	K'_0 [-]	1.34

$$P_{wi} = (D + H) \cdot \gamma_w$$

$$\sigma_h = P_{closure} + P_{wi}$$

$$\sigma'_h = \sigma_h - u_o$$

$$K'_o = \frac{\sigma'_h}{\sigma'_v}$$
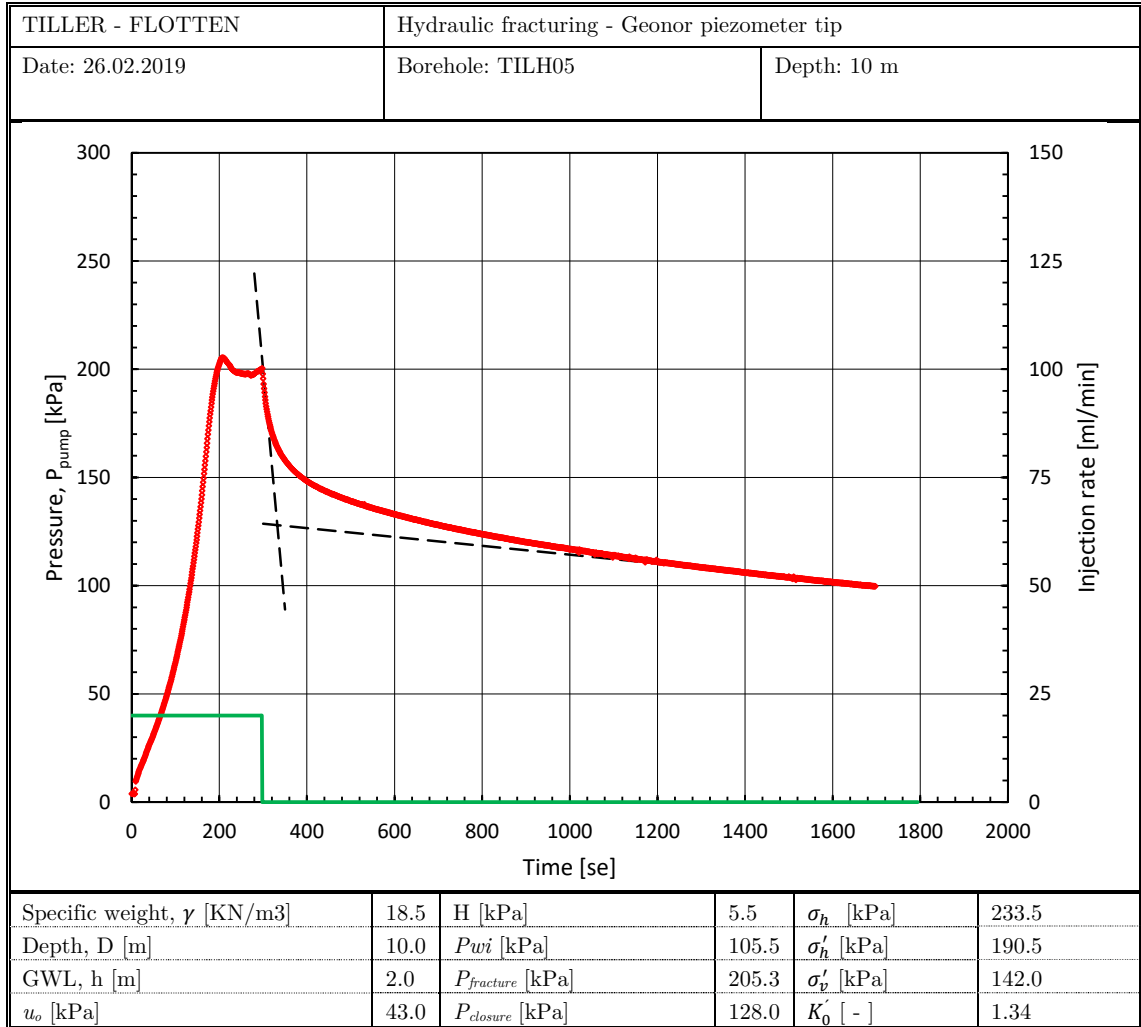
Figure C- 5 Pressure and injection flow rate vs. time record for borehole TILH05 (10m depth)

APPENDIX C: HYDRAULIC FRACTURING

TILLER - FLOTTEN	Hydraulic fracturing - Geonor piezometer tip	
Date: 26.02.2019	Borehole: TILH06	Depth: 15 m

Specific weight, γ [KN/m3]	18.5	H [kPa]	5.5	σ_h [kPa]	319.1
Depth, D [m]	15.0	P_{wi} [kPa]	155.5	σ'_h [kPa]	264.1
GWL, h [m]	2.0	$P_{fracture}$ [kPa]	268.0	σ'_v [kPa]	222.5
u_o [kPa]	55.0	$P_{closure}$ [kPa]	163.6	K'_0 [-]	1.19

$$P_{wi} = (D + H) \cdot \gamma_w$$

$$\sigma_h = P_{closure} + P_{wi}$$

$$\sigma'_h = \sigma_h - u_o$$

$$K'_o = \frac{\sigma'_h}{\sigma'_v}$$

Figure C- 6 Pressure and injection flow rate vs. time record for borehole TILH06 (15m depth)

TILLER - FLOTTEN	Hydraulic fracturing - Geonor piezometer tip	
Date: 21.05.2019	Borehole: TILH01	Depth: 5 m

Specific weight, γ [KN/m3]	18.5	H [kPa]	5.5	σ_h [kPa]	135.2
Depth, D [m]	5.0	Pwi [kPa]	55.5	σ_h' [kPa]	104.2
GWL, h [m]	2.0	$P_{fracture}$ [kPa]	139.2	σ_v' [kPa]	61.5
u_o [kPa]	31.0	$P_{closure}$ [kPa]	79.7	K_0' [-]	1.69

$$P_{wi} = (D + H) \cdot \gamma_w$$

$$\sigma_h = P_{closure} + P_{wi}$$

$$\sigma_h' = \sigma_h - u_o$$

$$K_o' = \frac{\sigma_h'}{\sigma_v'}$$

Figure C- 7 Pressure and injection flow rate vs. time record for borehole TILH01, 2nd attempt (5m depth)

TILLER - FLOTTEN	Hydraulic fracturing - Geonor piezometer tip	
Date: 21.05.2019	Borehole: TILH02	Depth: 10 m

Specific weight, γ [KN/m3]	18.5	H [kPa]	5.5	σ_h [kPa]	194.8
Depth, D [m]	10.0	Pwi [kPa]	105.5	σ_h' [kPa]	151.8
GWL, h [m]	2.0	$P_{fracture}$ [kPa]	188.0	σ_v' [kPa]	142.0
u_o [kPa]	43.0	$P_{closure}$ [kPa]	89.3	K_0' [-]	1.07

$$P_{wi} = (D + H) \cdot \gamma_w$$

$$\sigma_h = P_{closure} + P_{wi}$$

$$\sigma_h' = \sigma_h - u_o$$

$$K_o' = \frac{\sigma_h'}{\sigma_v'}$$

Figure C- 8 Pressure and injection flow rate vs. time record for borehole TILH02, 2nd attempt (10m depth)

APPENDIX C: HYDRAULIC FRACTURING

TILLER - FLOTTEN	Hydraulic fracturing - Geonor piezometer tip	
Date: 21.05.2019	Borehole: TILH03	Depth: 15 m

Specific weight, γ [KN/m3]	18.5	H [kPa]	5.5	σ_h [kPa]	344.4
Depth, D [m]	15.0	Pwi [kPa]	155.5	σ_h' [kPa]	289.4
GWL, h [m]	2.0	$P_{fracture}$ [kPa]	326.0	σ_v' [kPa]	222.5
u_o [kPa]	55.0	$P_{closure}$ [kPa]	188.9	K_0' [-]	1.30

$$P_{wi} = (D + H) \cdot \gamma_w$$

$$\sigma_h = P_{closure} + P_{wi}$$

$$\sigma_h' = \sigma_h - u_o$$

$$K_o' = \frac{\sigma_h'}{\sigma_v'}$$

Figure C- 9 Pressure and injection flow rate vs. time record for borehole TILH03, 2ⁿᵈ attempt
(15m depth)

TILLER - FLOTTEN	Hydraulic fracturing - Geonor piezometer tip	
Date: 22.05.2019	Borehole: TILH04	Depth: 5 m

Specific weight, γ [KN/m3]	18.5	H [kPa]	5.5	σ_h [kPa]	159.8
Depth, D [m]	5.0	Pwi [kPa]	55.5	σ_h' [kPa]	128.8
GWL, h [m]	2.0	$P_{fracture}$ [kPa]	150.0	σ_v' [kPa]	61.5
u_o [kPa]	31.0	$P_{closure}$ [kPa]	104.3	K_0' [-]	2.09

$$P_{wi} = (D + H) \cdot \gamma_w$$

$$\sigma_h = P_{closure} + P_{wi}$$

$$\sigma_h' = \sigma_h - u_o$$

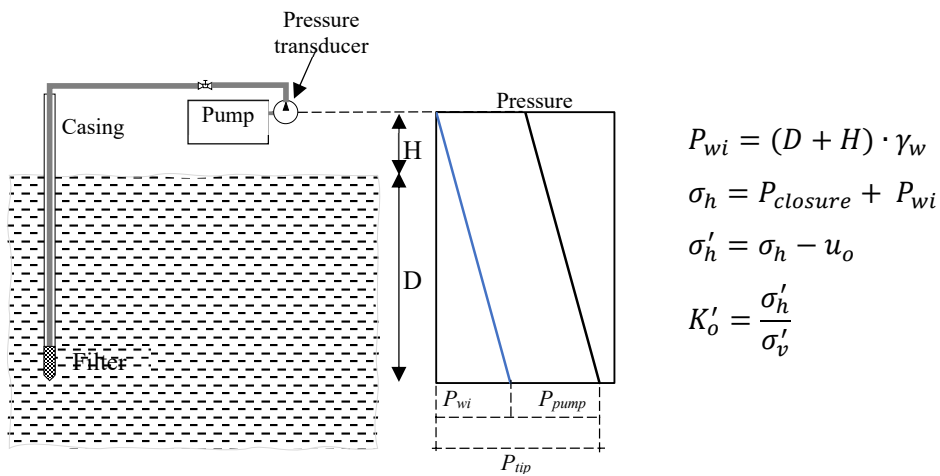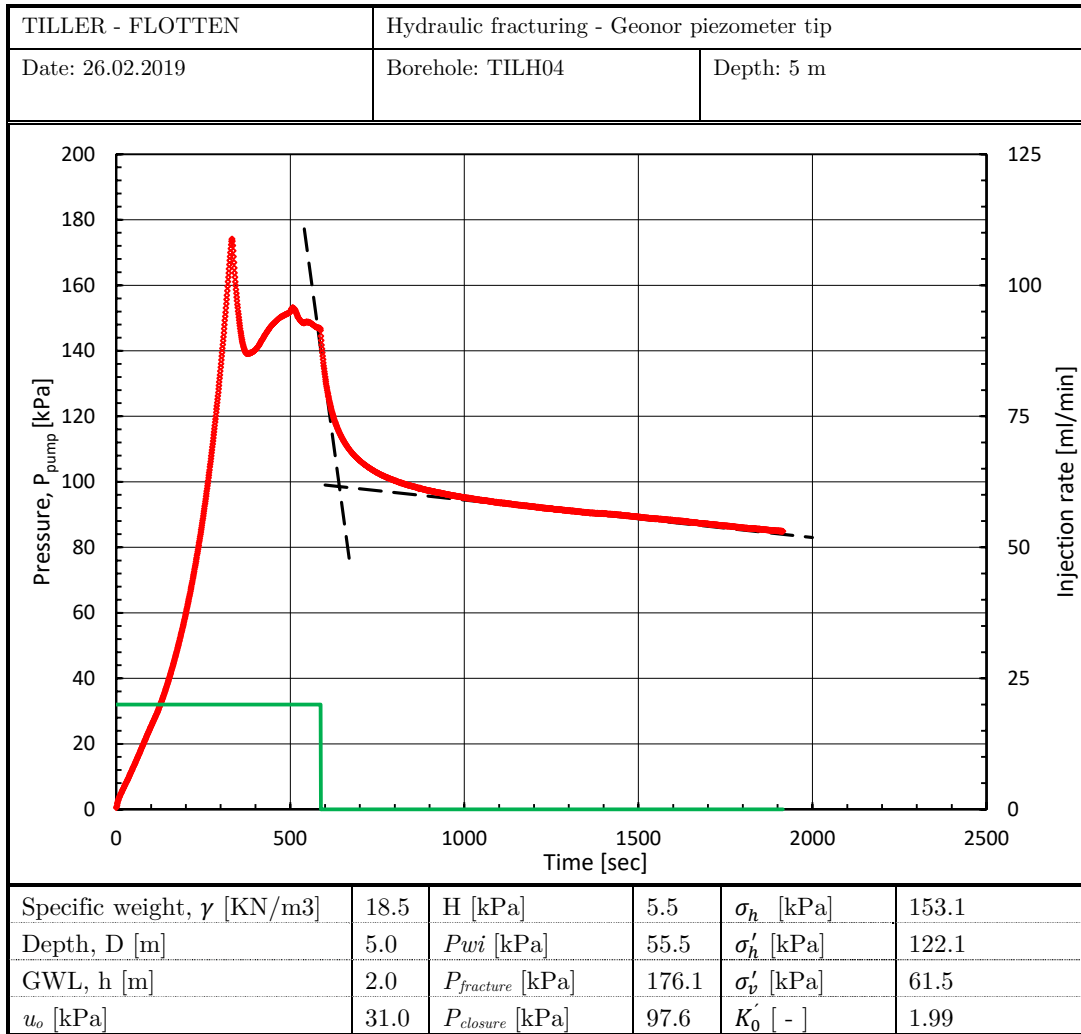$$K_o' = \frac{\sigma_h'}{\sigma_v'}$$
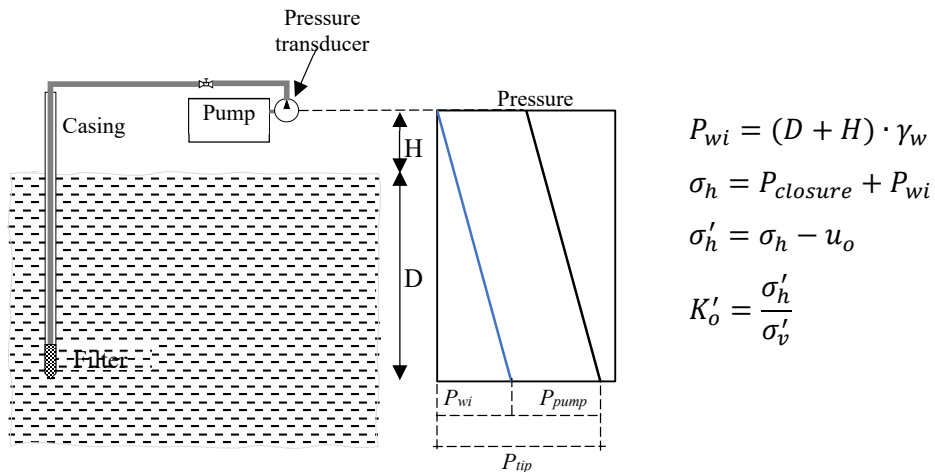
Figure C- 10 Pressure and injection flow rate vs. time record for borehole TILH04, 2ⁿᵈ attempt (5m depth)

APPENDIX C: HYDRAULIC FRACTURING

TILLER - FLOTTEN	Hydraulic fracturing - Geonor piezometer tip	
Date: 26.02.2019	Borehole: TILH05	Depth: 10 m

Specific weight, γ [KN/m3]	18.5	H [kPa]	5.5	σ_h [kPa]	225.5
Depth, D [m]	10.0	Pwi [kPa]	105.5	σ_h' [kPa]	182.5
GWL, h [m]	2.0	$P_{fracture}$ [kPa]	196.0	σ_v' [kPa]	142.0
u_o [kPa]		43.0	$P_{closure}$ [kPa]	120.0	K_0' [-]	1.29

$$P_{wi} = (D + H) \cdot \gamma_w$$

$$\sigma_h = P_{closure} + P_{wi}$$

$$\sigma_h' = \sigma_h - u_o$$

$$K_o' = \frac{\sigma_h'}{\sigma_v'}$$
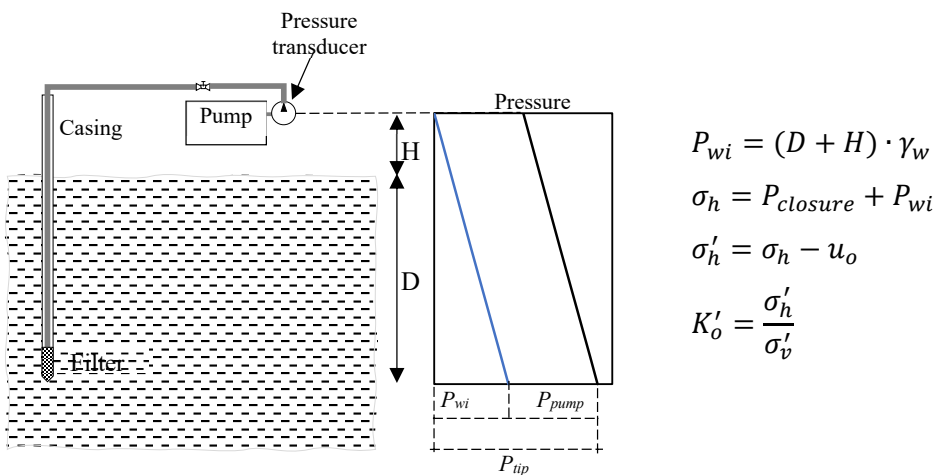
Figure C- 11 Pressure and injection flow rate vs. time record for borehole TILH05, 2ⁿᵈ attempt (10m depth)
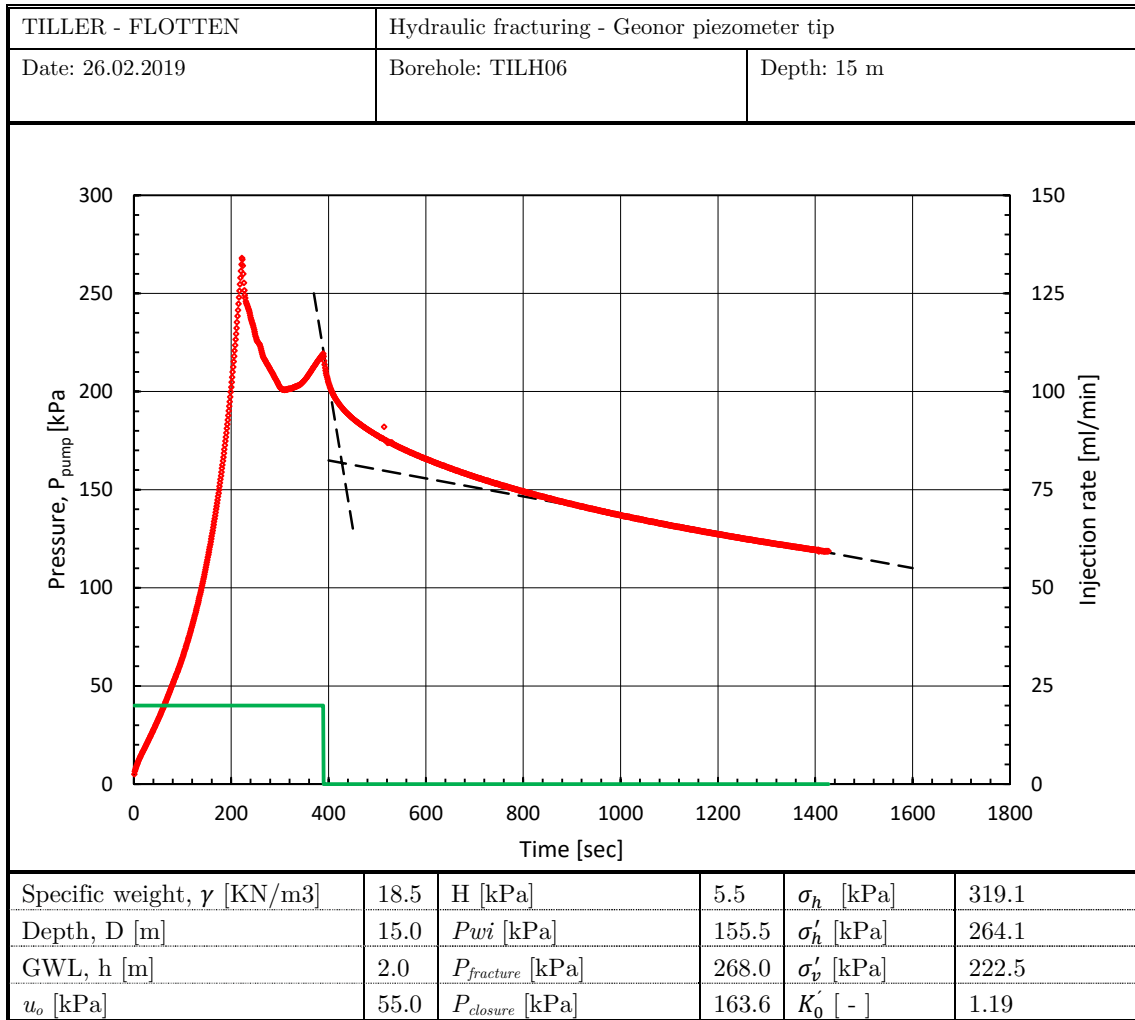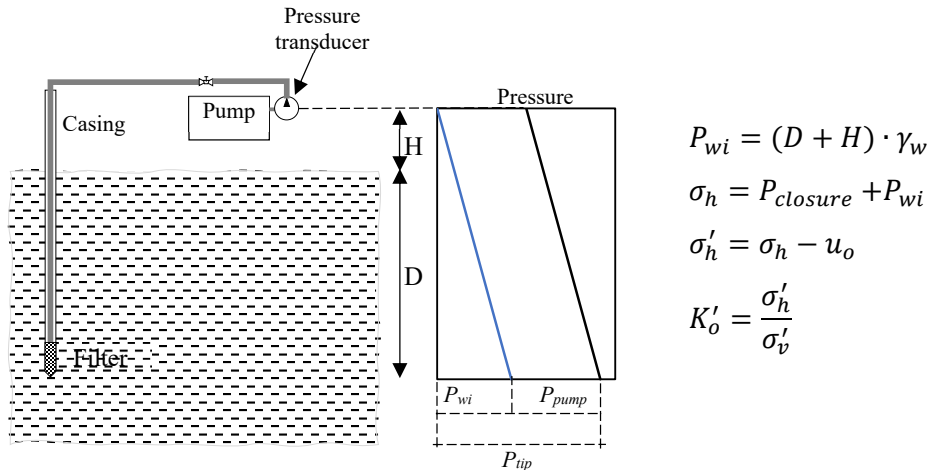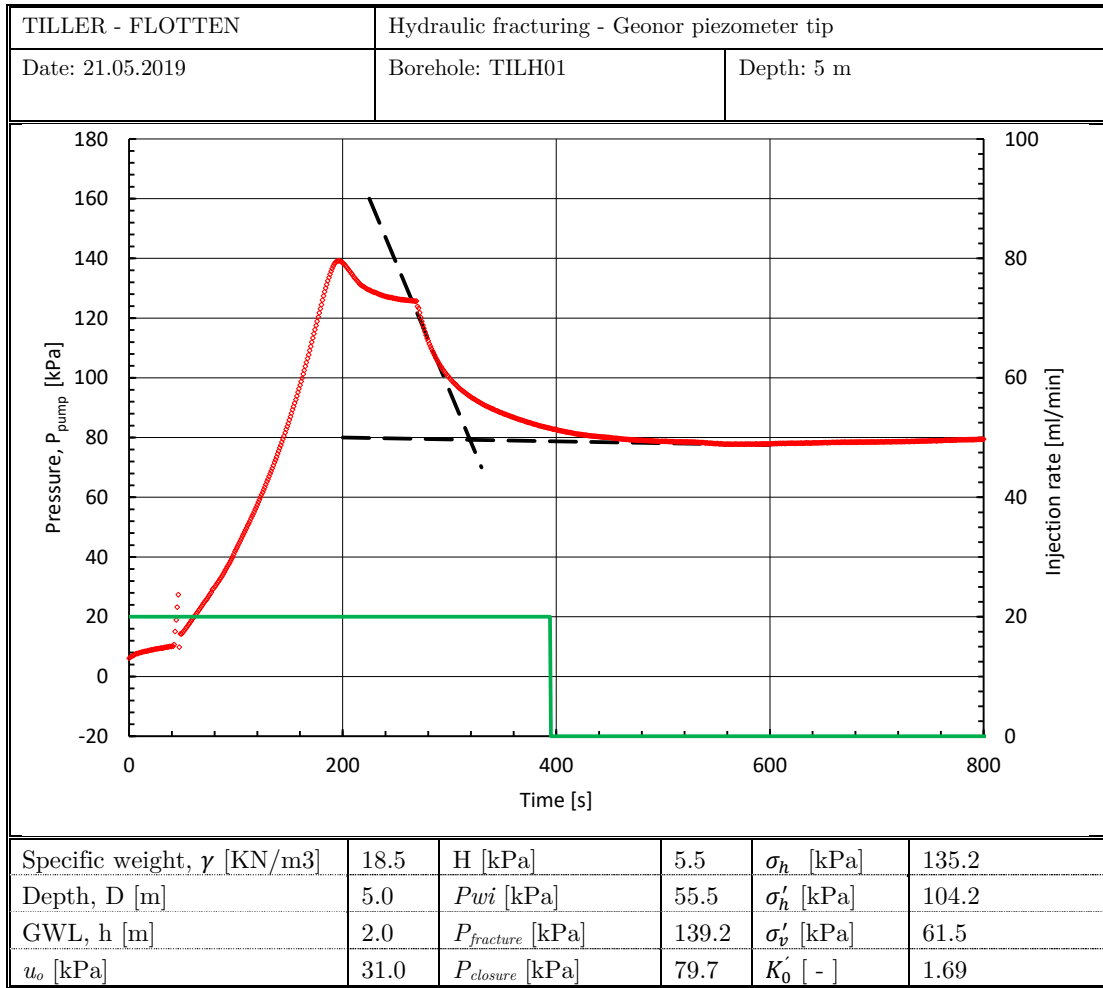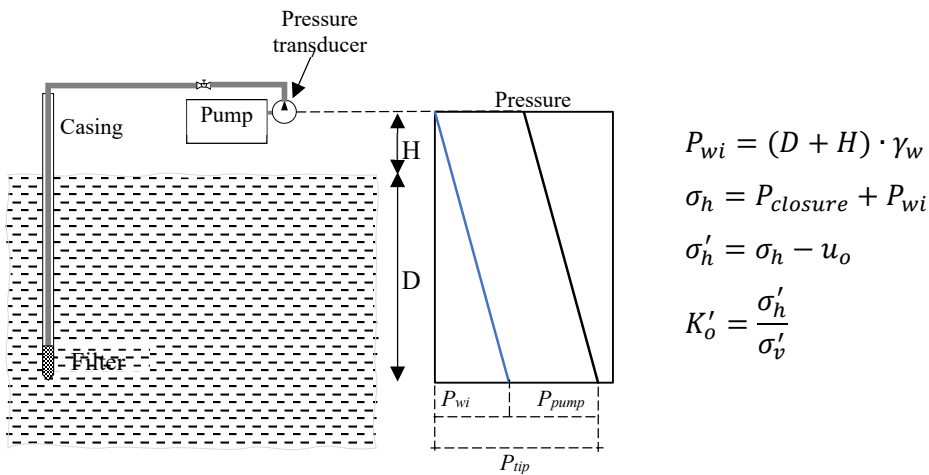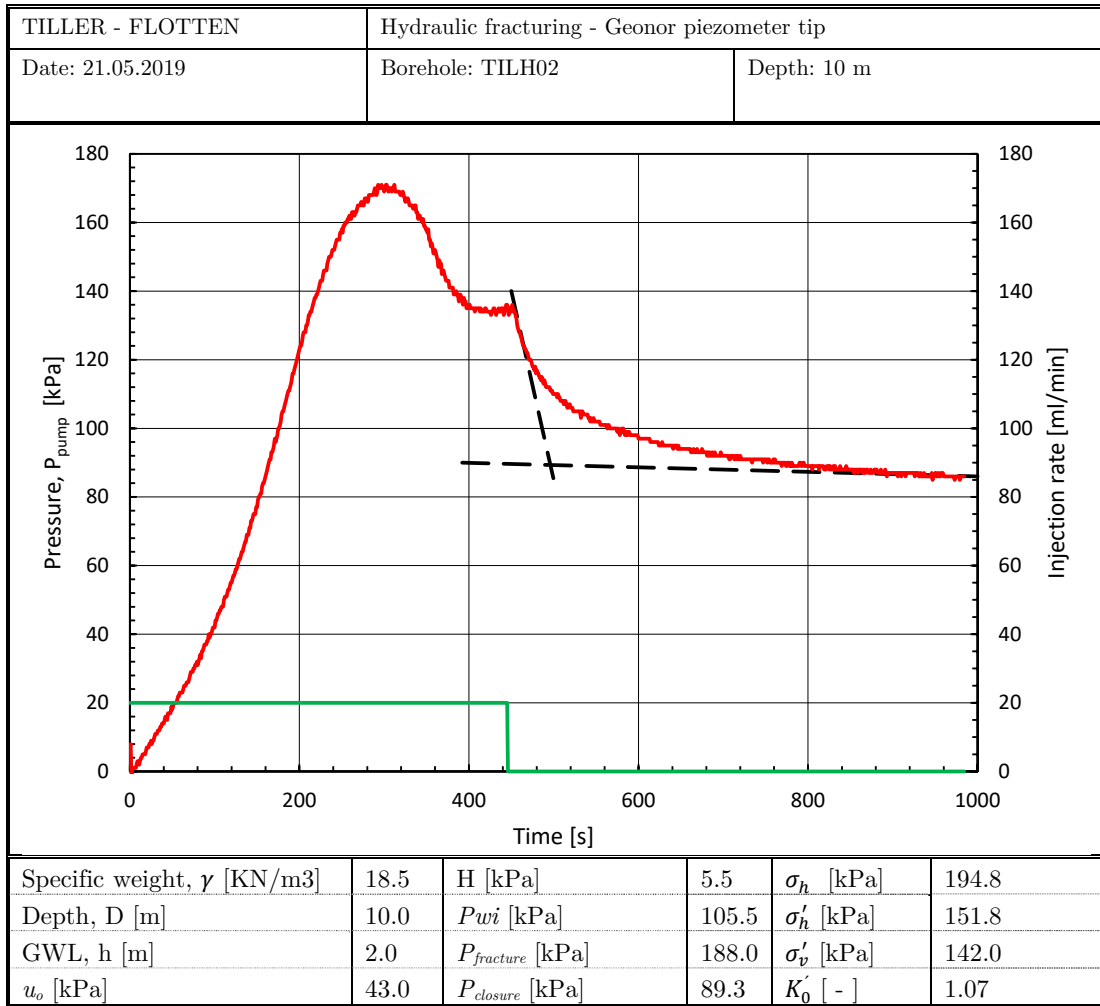
APPENDIX C: HYDRAULIC FRACTURING

TILLER - FLOTTEN	Hydraulic fracturing - Geonor piezometer tip	
Date: 22.05.2019	Borehole: TILH06	Depth: 15 m

Specific weight, γ [KN/m3]	18.5	H [kPa]	5.5	σ_h [kPa]	313.7
Depth, D [m]	15.0	Pwi [kPa]	155.5	σ_h' [kPa]	258.7
GWL, h [m]	2	$P_{fracture}$ [kPa]	266.5	σ_v' [kPa]	222.5
u_o [kPa]	55.0	$P_{closure}$ [kPa]	158.2	K_0' [-]	1.16

$$P_{wi} = (D + H) \cdot \gamma_w$$

$$\sigma_h = P_{closure} + P_{wi}$$

$$\sigma_h' = \sigma_h - u_o$$

$$K_o' = \frac{\sigma_h'}{\sigma_v'}$$

Figure C- 12 Pressure and injection flow rate vs. time record for borehole TILH06, 2nd attempt(15m depth)

TILLER - FLOTTEN	Hydraulic fracturing - Geonor piezometer tip	
Date: 06.06.2019	Borehole: TILH01	Depth: 7 m

Specific weight, γ [KN/m3]	18.5	H [kPa]	5.5	σ_h [kPa]	153.9
Depth, D [m]	7.0	Pwi [kPa]	75.5	σ_h' [kPa]	116.9
GWL, h [m]	2.0	$P_{fracture}$ [kPa]	136.7	σ_v' [kPa]	92.5
u_o [kPa]	37.0	$P_{closure}$ [kPa]	78.3	K_0' [-]	1.26

$$P_{wi} = (D + H) \cdot \gamma_w$$
$$\sigma_h = P_{closure} + P_{wi}$$
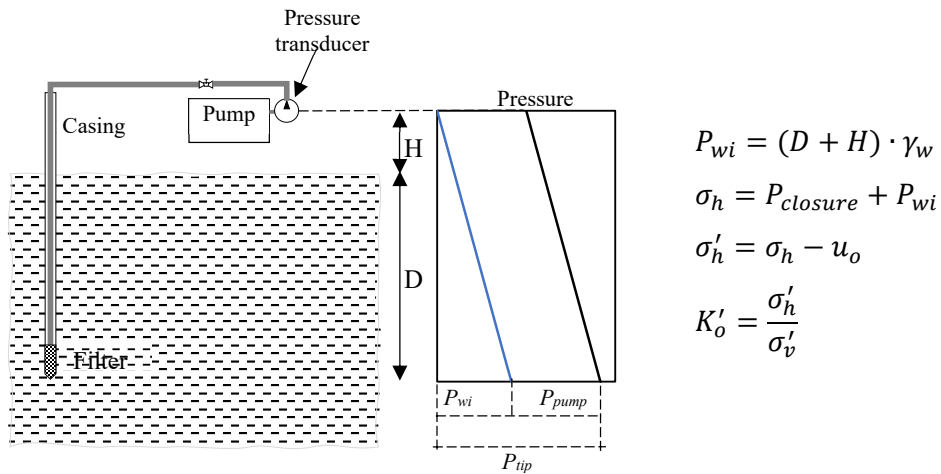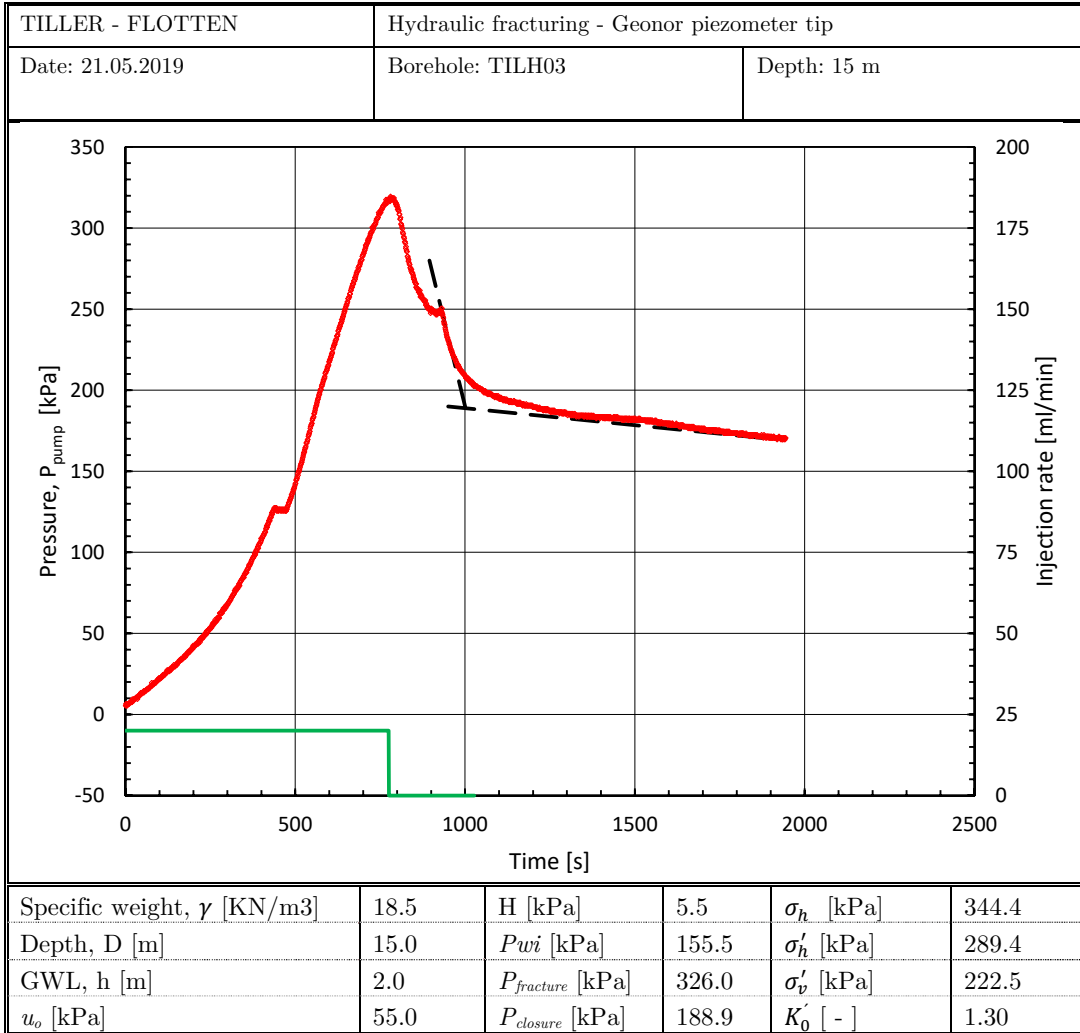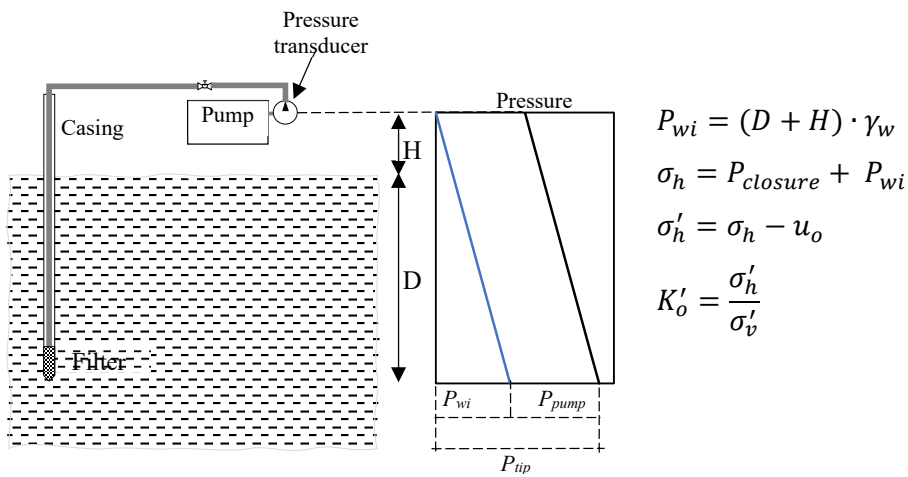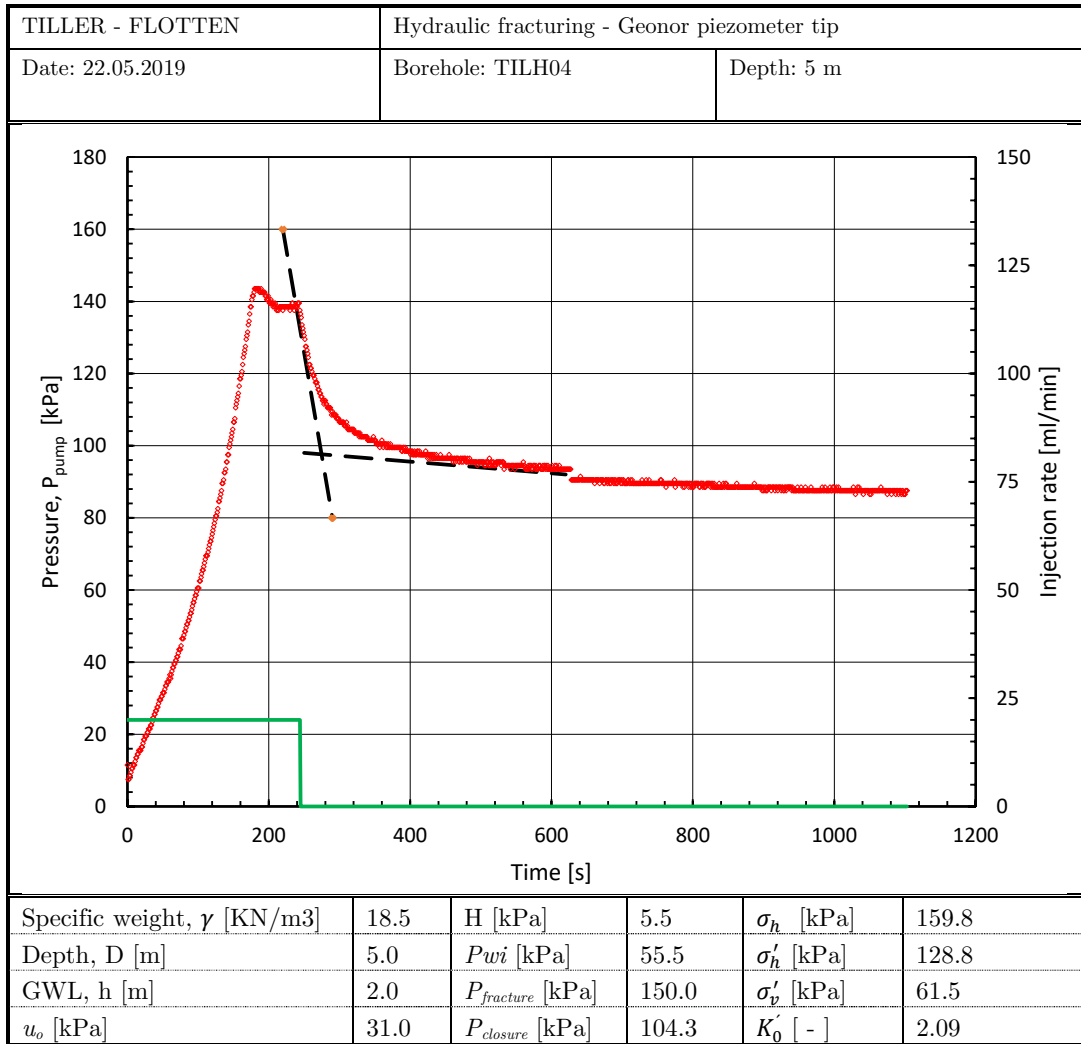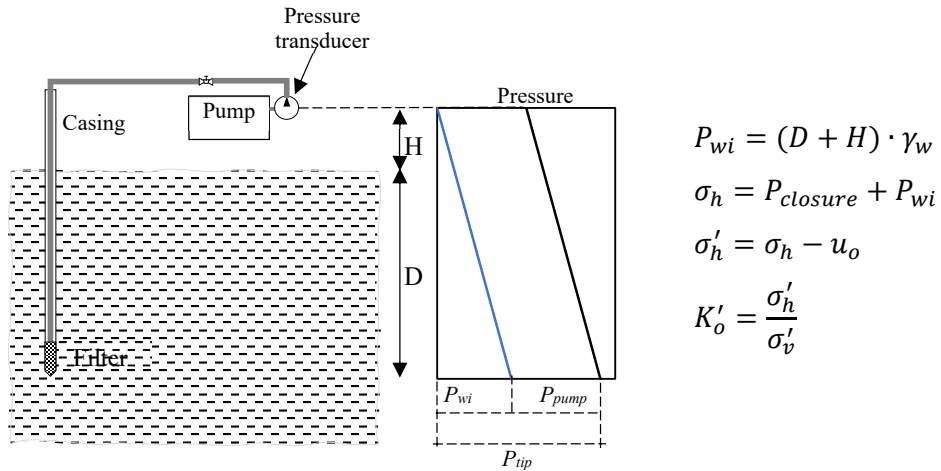$$\sigma_h' = \sigma_h - u_o$$
$$K_o' = \frac{\sigma_h'}{\sigma_v'}$$

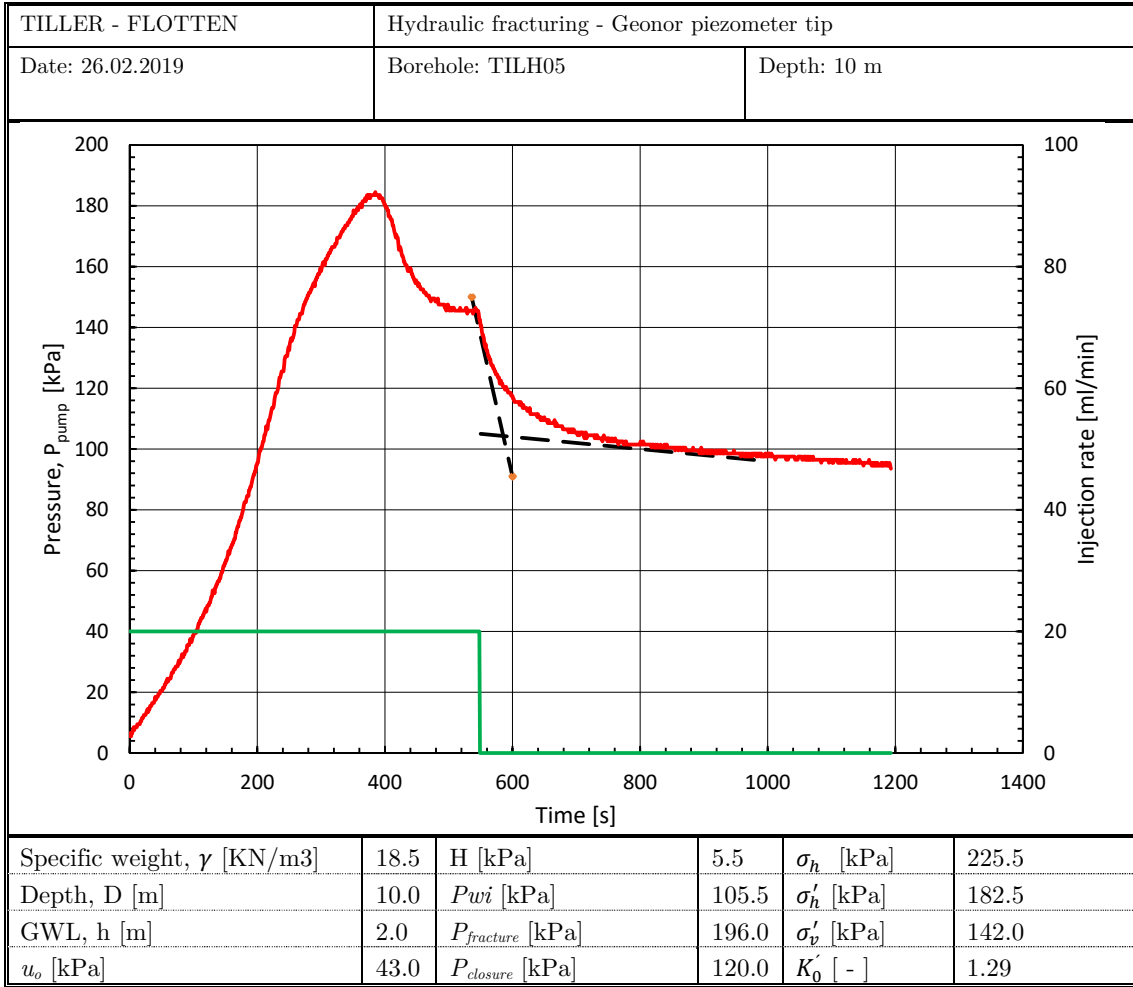*Figure C- 13 Pressure and injection flow rate vs. time record for borehole TILH01 (7m depth)*

APPENDIX C: HYDRAULIC FRACTURING

TILLER - FLOTTEN	Hydraulic fracturing - Geonor piezometer tip	
Date: 06.06.2019	Borehole: TILH02	Depth: 12 m

Specific weight, γ [KN/m3]	18.5	H [kPa]	5.5	σ_h [kPa]	279.5
Depth, D [m]	12.0	P_{wi} [kPa]	125.5	σ_h' [kPa]	231.5
GWL, h [m]	2.0	$P_{fracture}$ [kPa]	211.0	σ_v' [kPa]	174.0
u_o [kPa]	48.0	$P_{closure}$ [kPa]	154.0	K_0' [-]	1.33

$$P_{wi} = (D + H) \cdot \gamma_w$$

$$\sigma_h = P_{closure} + P_{wi}$$

$$\sigma_h' = \sigma_h - u_o$$

$$K_o' = \frac{\sigma_h'}{\sigma_v'}$$

Figure C- 14 Pressure and injection flow rate vs. time record for borehole TILH02 (12m depth)

146

TILLER - FLOTTEN	Hydraulic fracturing - Geonor piezometer tip	
Date: 06.06.2019	Borehole: TILH03	Depth: 17 m

Specific weight, γ [KN/m3]	18.5	H [kPa]	5.5	σ_h [kPa]	386.5
Depth, D [m]	17.0	Pwi [kPa]	175.5	σ_h' [kPa]	320.5
GWL, h [m]	2.0	$P_{fracture}$ [kPa]	297.4	σ_v' [kPa]	248.5
u_o [kPa]	66.0	$P_{closure}$ [kPa]	211.0	K_0' [-]	1.29

$$P_{wi} = (D + H) \cdot \gamma_w$$

$$\sigma_h = P_{closure} + P_{wi}$$

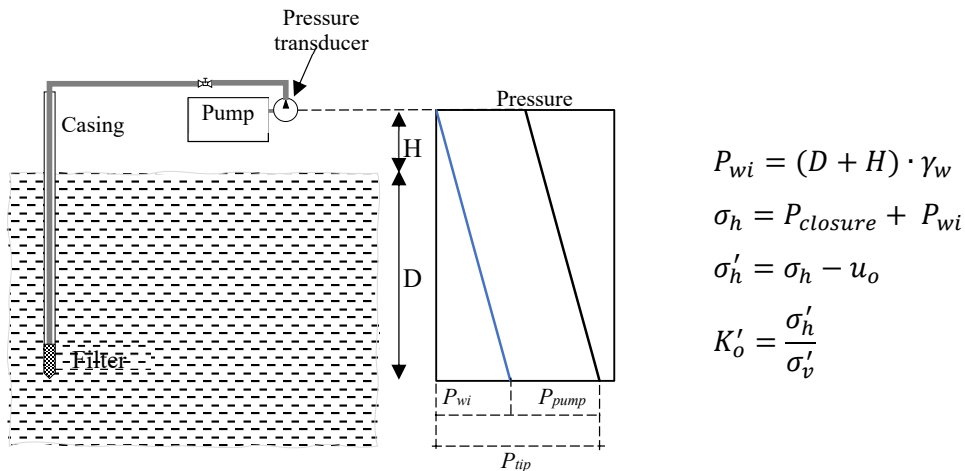$$\sigma_h' = \sigma_h - u_o$$

$$K_o' = \frac{\sigma_h'}{\sigma_v'}$$
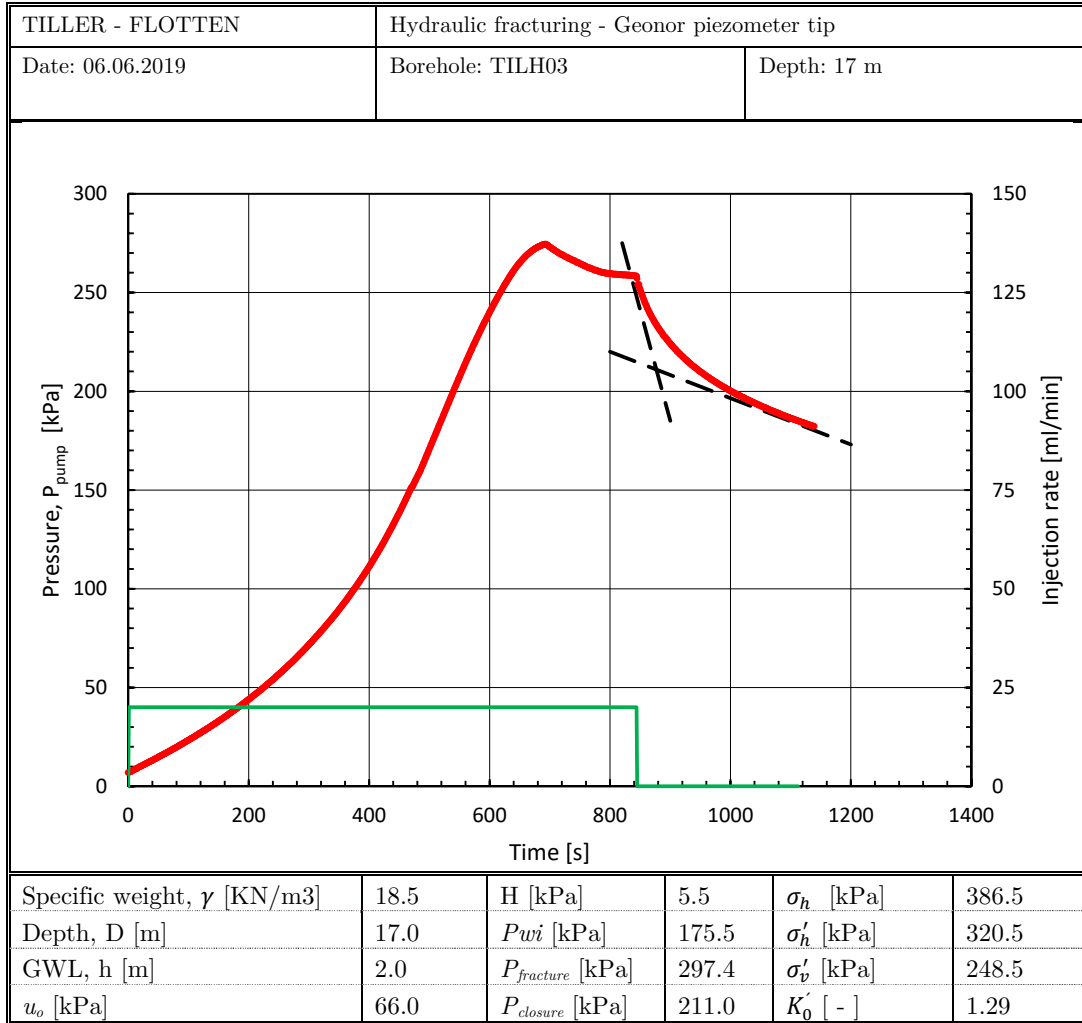
Figure C- 15 Pressure and injection flow rate vs. time record for borehole TILH03 (17m depth)
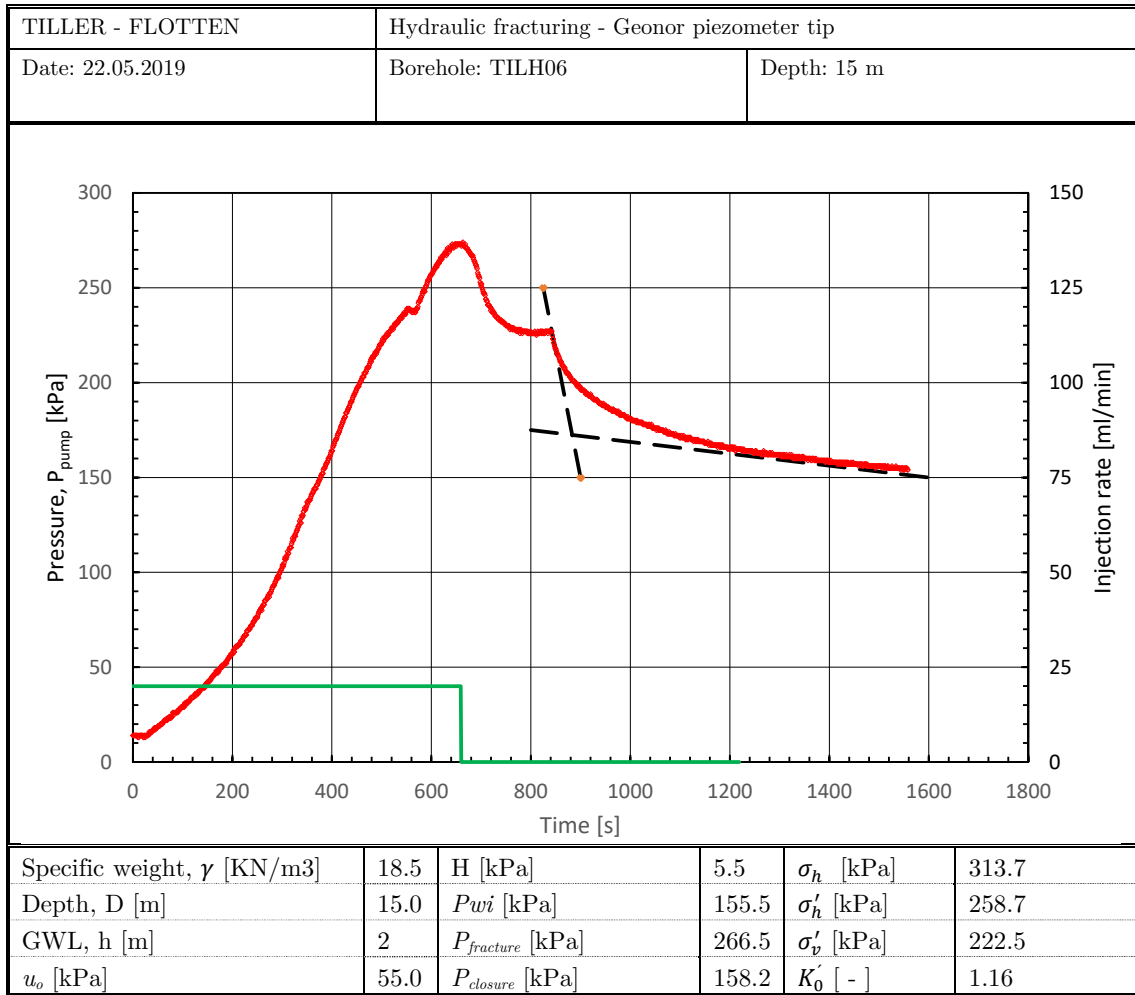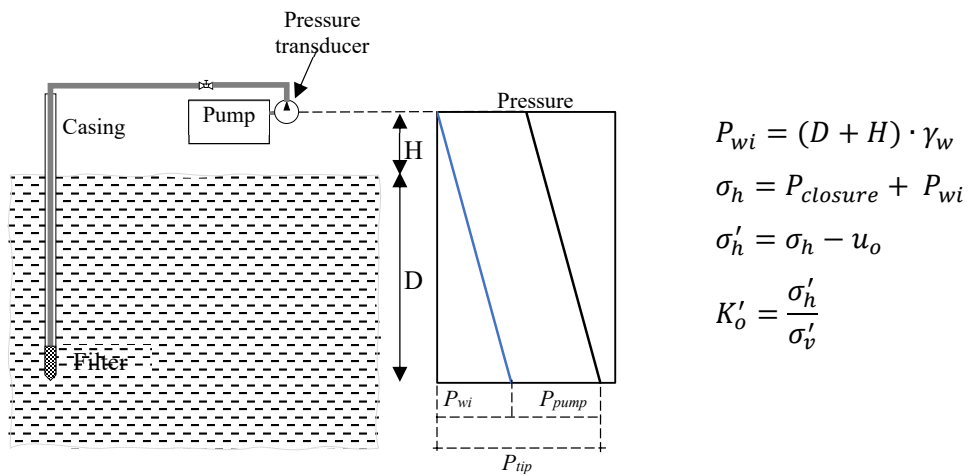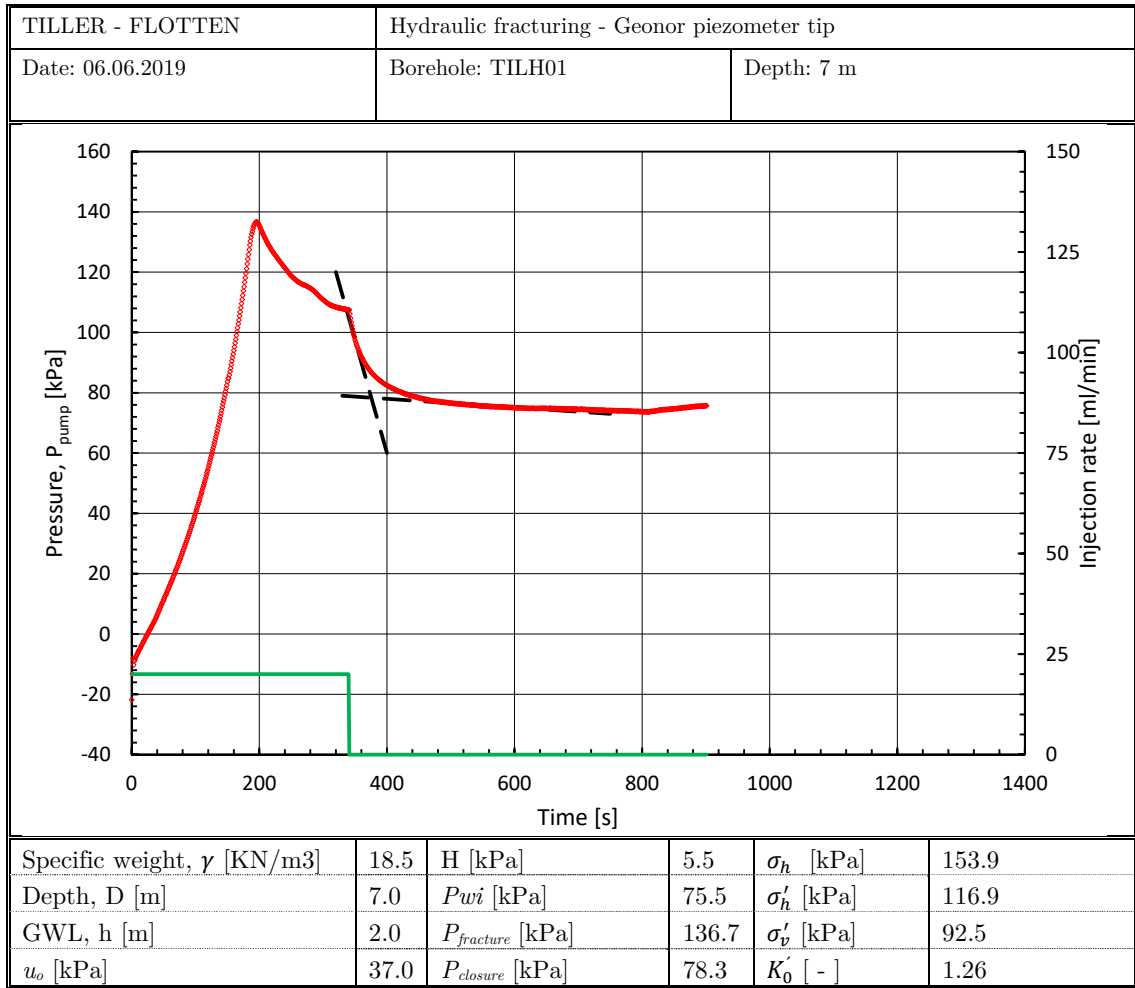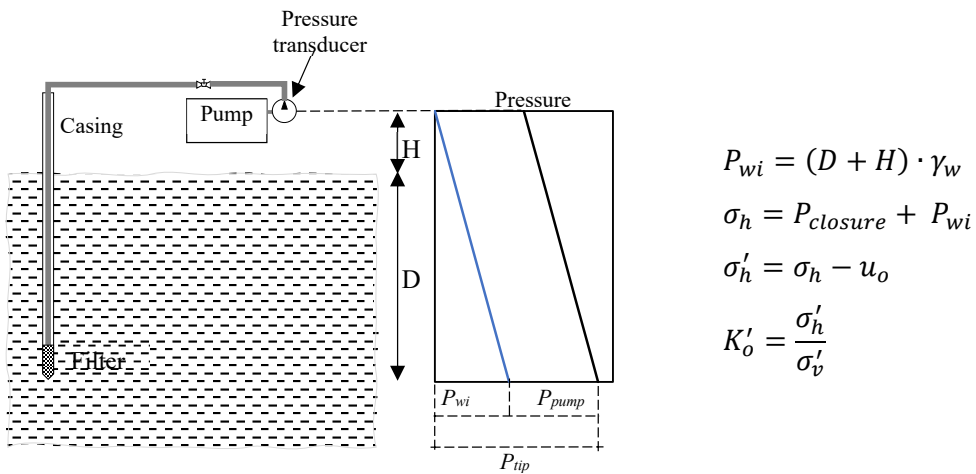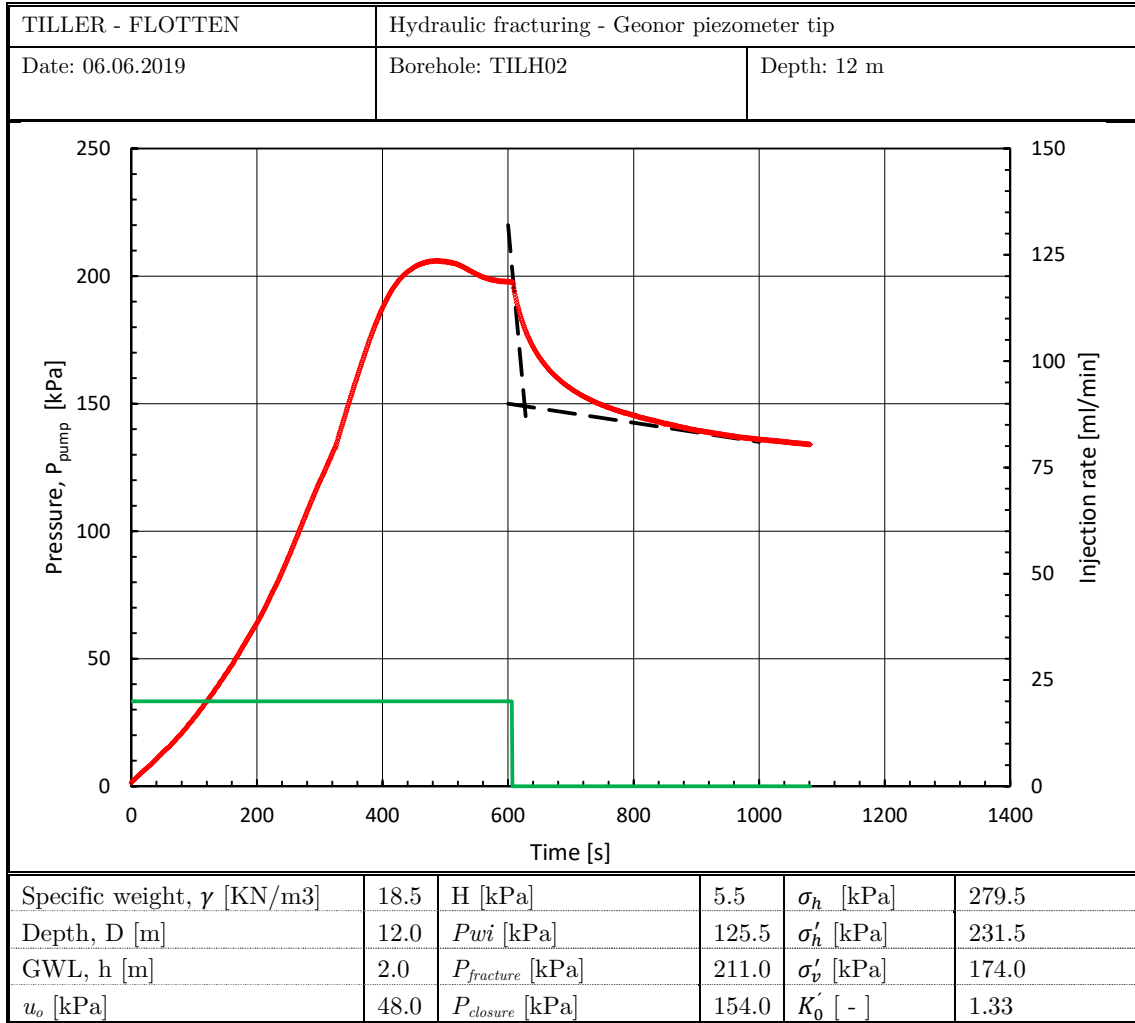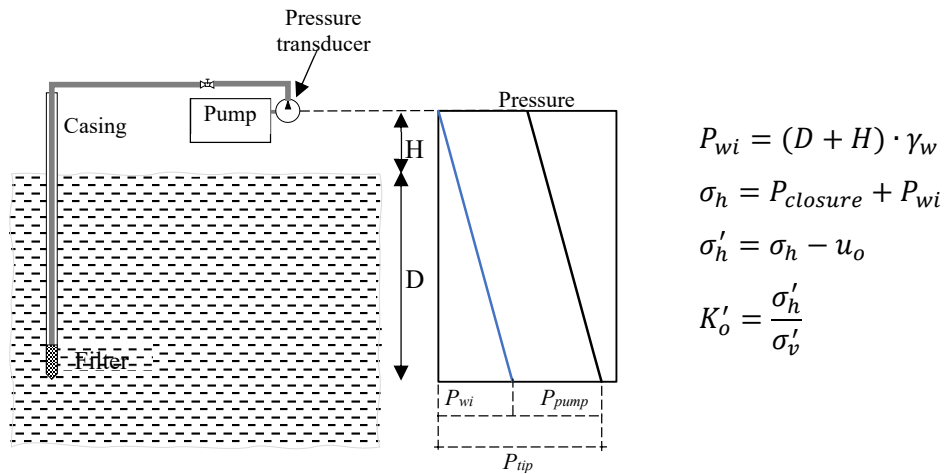
APPENDIX C: HYDRAULIC FRACTURING

TILLER - FLOTTEN	Hydraulic fracturing - Geonor piezometer tip	
Date: 06.06.2019	Borehole: TILH04	Depth: 7 m

Specific weight, γ [KN/m3]	18.5	H [kPa]	5.5	σ_h [kPa]	170.3
Depth, D [m]	7.0	Pwi [kPa]	75.5	σ_h' [kPa]	133.3
GWL, h [m]	2.0	$P_{fracture}$ [kPa]	161.6	σ_v' [kPa]	92.5
u_o [kPa]	37.0	$P_{closure}$ [kPa]	94.8	K_0' [-]	1.44

$$P_{wi} = (D + H) \cdot \gamma_w$$

$$\sigma_h = P_{closure} + P_{wi}$$

$$\sigma_h' = \sigma_h - u_o$$

$$K_o' = \frac{\sigma_h'}{\sigma_v'}$$
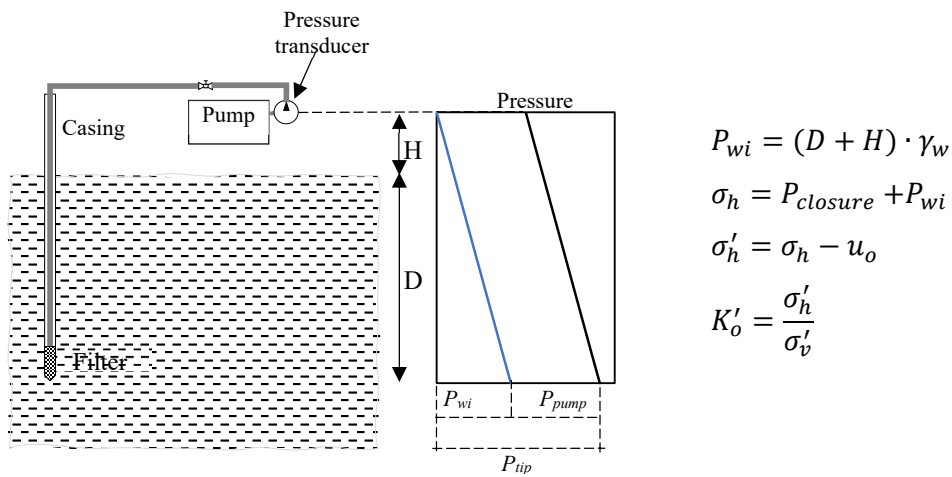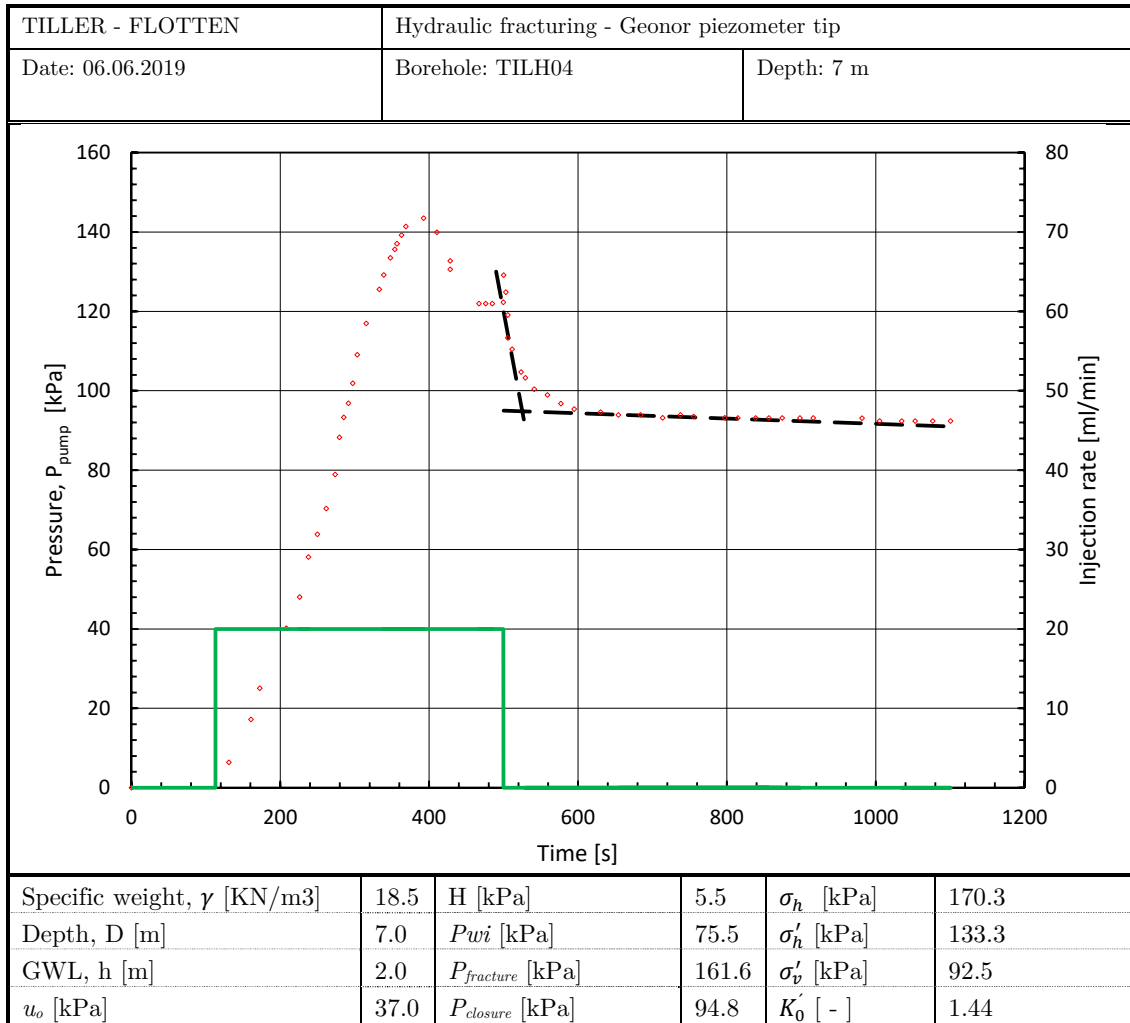
Figure C- 16 Pressure and injection flow versus time record for TILH04 (7 m depth)

148

TILLER - FLOTTEN	Hydraulic fracturing - Geonor piezometer tip	
Date: 06.06.2019	Borehole: TILH05	Depth: 12 m

Specific weight, γ [KN/m3]	18.5	H [kPa]	5.5	σ_h [kPa]	263.9
Depth, D [m]	12.0	Pwi [kPa]	125.5	σ_h' [kPa]	215.9
GWL, h [m]	2.0	$P_{fracture}$ [kPa]	236.7	σ_v' [kPa]	174.0
u_o [kPa]	48.0	$P_{closure}$ [kPa]	138.4	K_0' [-]	1.24

$$P_{wi} = (D + H) \cdot \gamma_w$$

$$\sigma_h = P_{closure} + P_{wi}$$

$$\sigma_h' = \sigma_h - u_o$$

$$K_o' = \frac{\sigma_h'}{\sigma_v'}$$
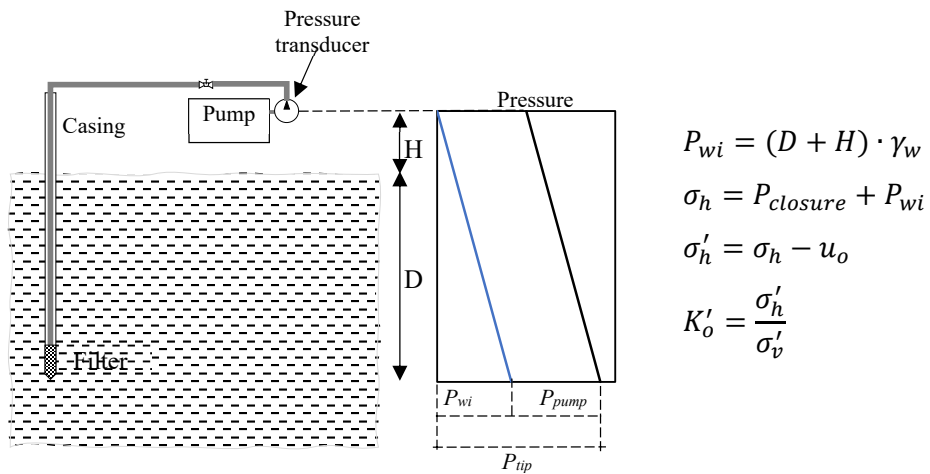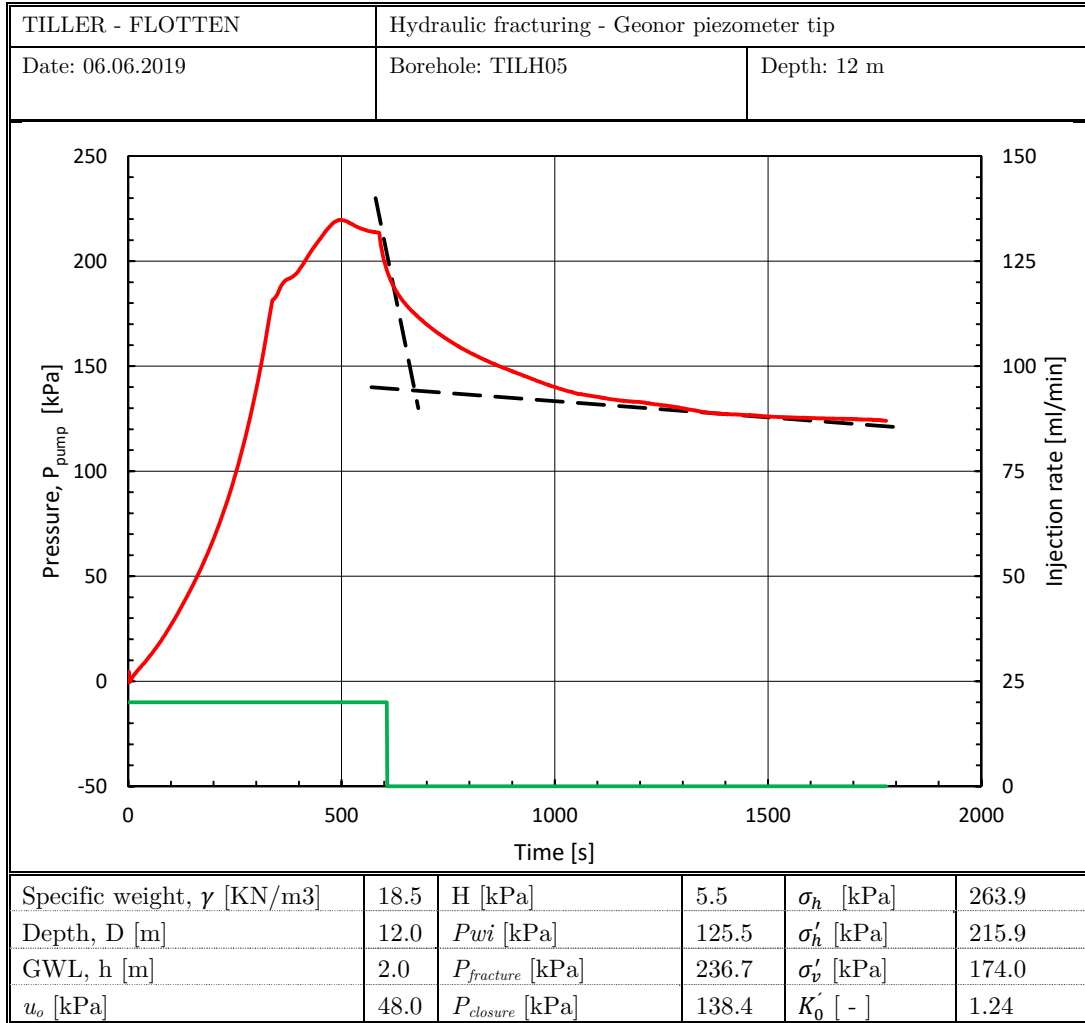
Figure C- 17 Pressure and injection flow versus time record for TILH05 (12m depth)

TILLER - FLOTTEN	Hydraulic fracturing - Geonor piezometer tip	
Date: 06.06.2019	Borehole: TILH06	Depth: 17 m

Specific weight, γ [KN/m3]	18.5	H [kPa]	5.5	σ_h [kPa]	359.6
Depth, D [m]	17.0	Pwi [kPa]	175.5	σ_h' [kPa]	293.6
GWL, h [m]	2	$P_{fracture}$ [kPa]	284.2	σ_v' [kPa]	248.5
u_o [kPa]	66.0	$P_{closure}$ [kPa]	184.1	K_0' [-]	1.18

$$P_{wi} = (D + H) \cdot \gamma_w$$

$$\sigma_h = P_{closure} + P_{wi}$$

$$\sigma_h' = \sigma_h - u_o$$

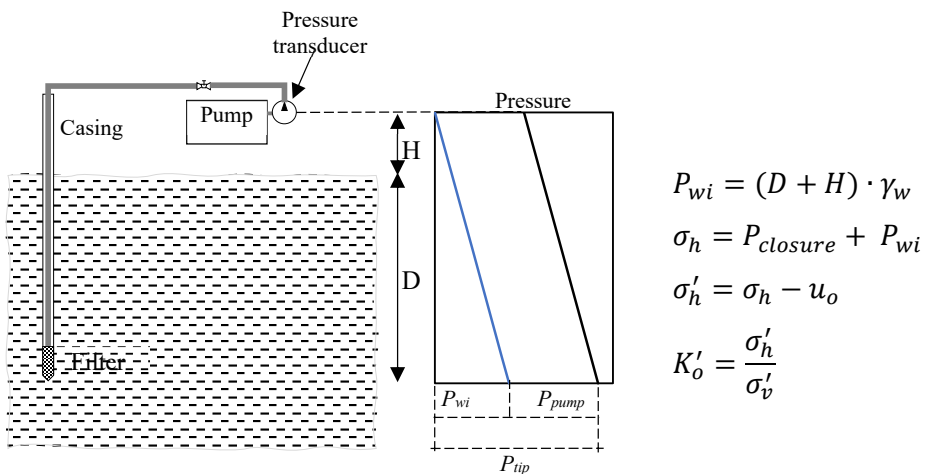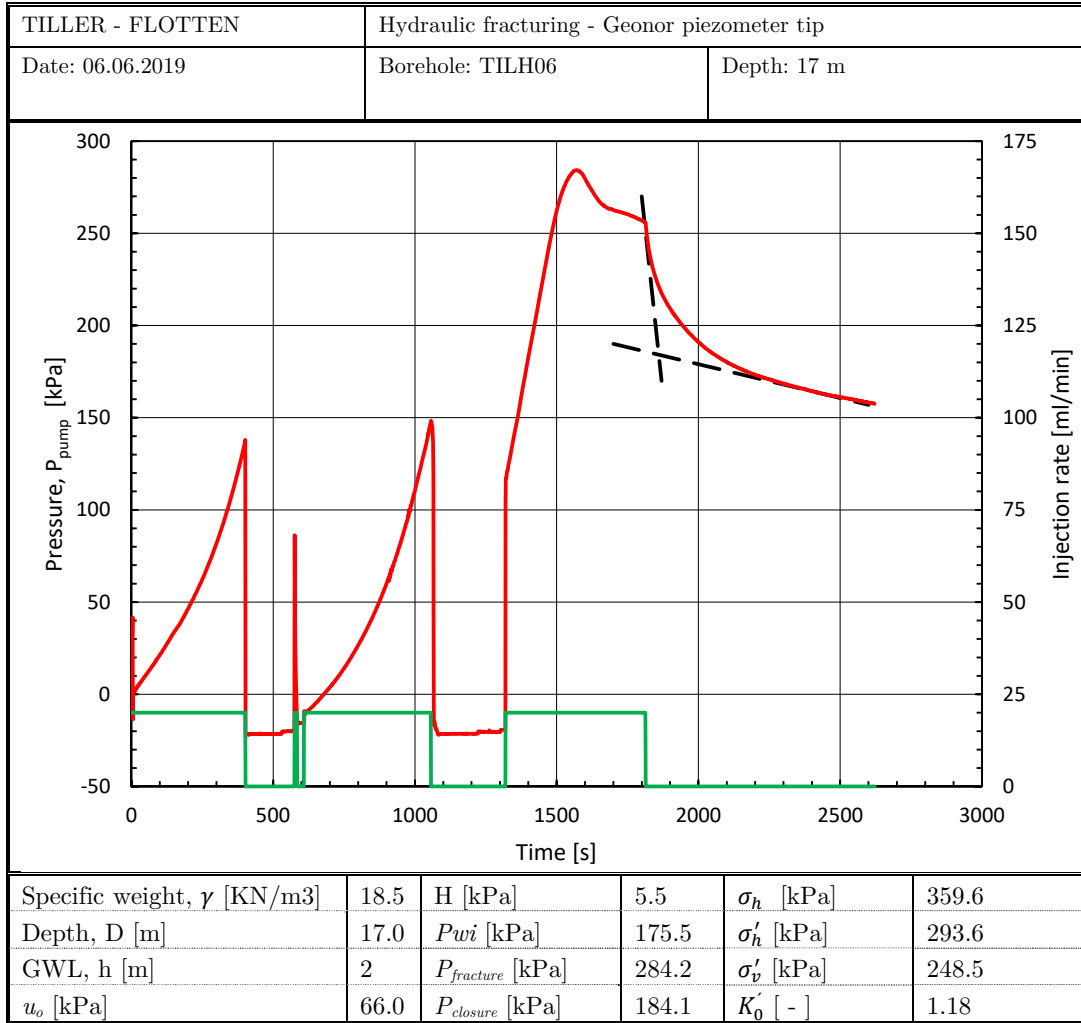$$K_o' = \frac{\sigma_h'}{\sigma_v'}$$

Figure C- 18 Pressure and injection flow versus time record for TILH06 (17m depth)
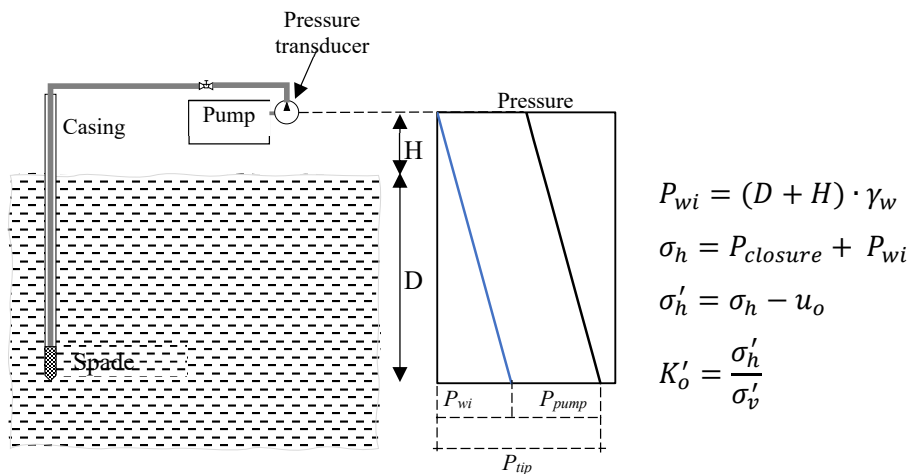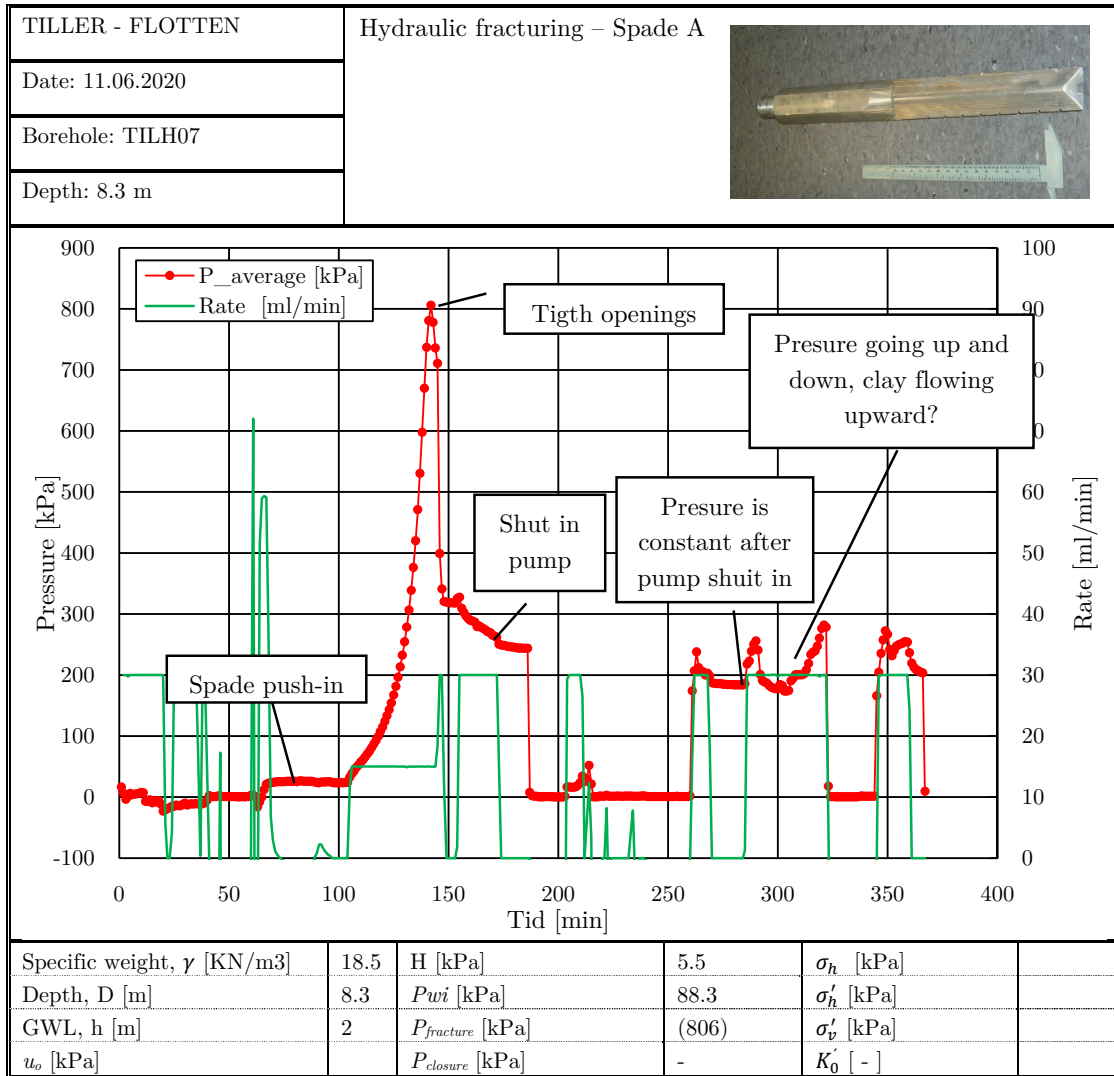
150

C.2 Raw data pilot testing with new nozzles

TILLER - FLOTTEN	Hydraulic fracturing – Spade A	
Date: 11.06.2020		
Borehole: TILH07		
Depth: 8.3 m		

Specific weight, γ [KN/m3]	18.5	H [kPa]	5.5	σ_h [kPa]
Depth, D [m]	8.3	Pwi [kPa]	88.3	σ_h' [kPa]
GWL, h [m]	2	$P_{fracture}$ [kPa]	(806)	σ_v' [kPa]
u_o [kPa]		$P_{closure}$ [kPa]	-	K_0' [-]

$$P_{wi} = (D + H) \cdot \gamma_w$$

$$\sigma_h = P_{closure} + P_{wi}$$

$$\sigma_h' = \sigma_h - u_o$$

$$K_o' = \frac{\sigma_h'}{\sigma_v'}$$

Figure C- 19 Pressure and injection flow versus time record for TILH07 (8.3m depth)

151

TILLER - FLOTTEN	Hydraulic fracturing – Spade B
Date: 17.06.2020	
Borehole: TILH07	
Depth: 9.3 m	

Specific weight, γ [KN/m3]	18.5	H [kPa]	5.5	σ_h [kPa]	167.2
Depth, D [m]	8.3	Pwi [kPa]	98.3	σ'_h [kPa]	126.2
GWL, h [m]	2	$P_{fracture}$ [kPa]	203	σ'_v [kPa]	131.05
u_o [kPa]	41	$P_{closure}$ [kPa]	68.9	K'_0 [-]	0.96
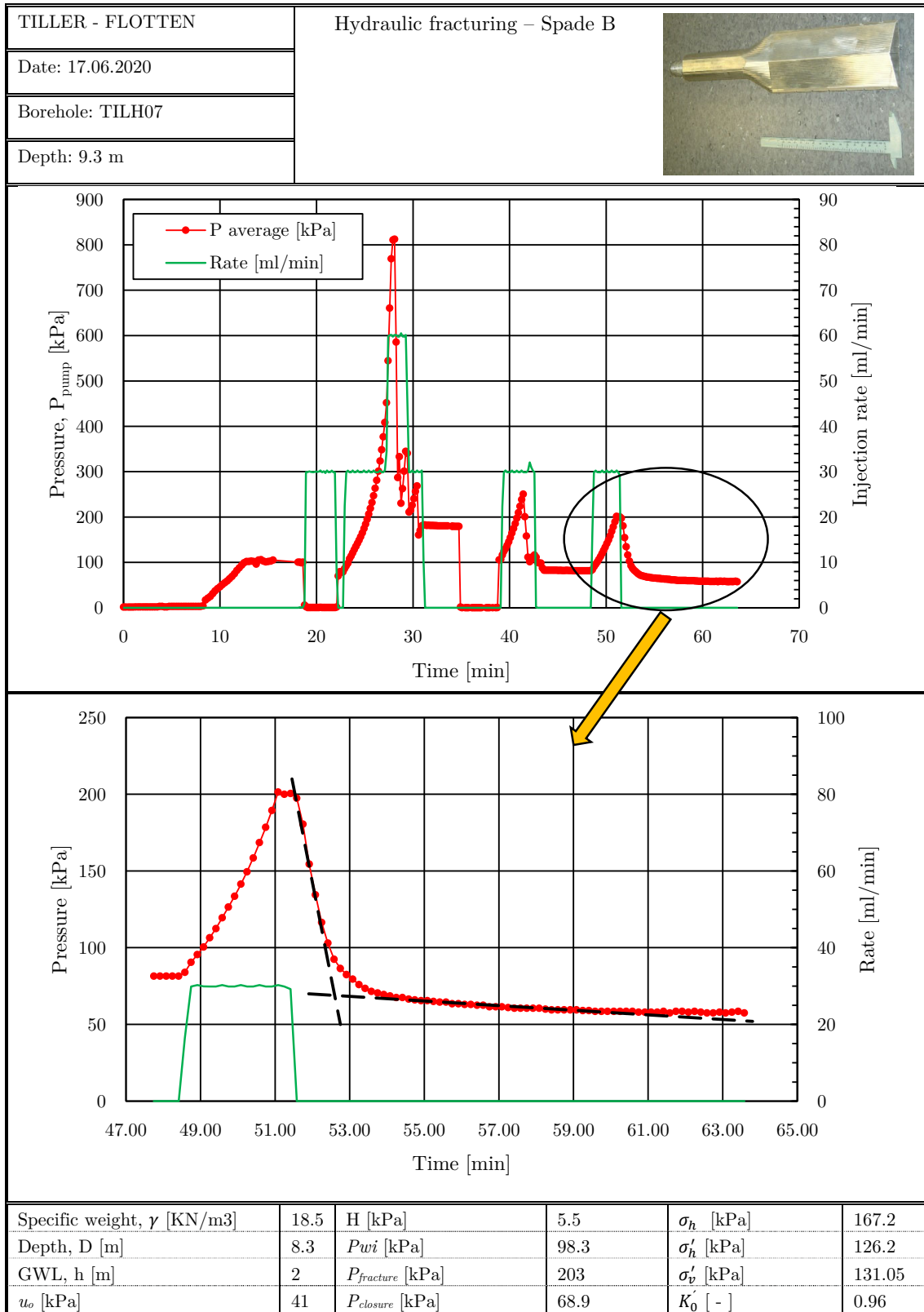
Figure C- 20 Pressure versus time record for nozzle type B

Appendix D

Drawings

In this appendix drawings of the new injection nozzles are attached.

APPENDIX D: DRAWINGS

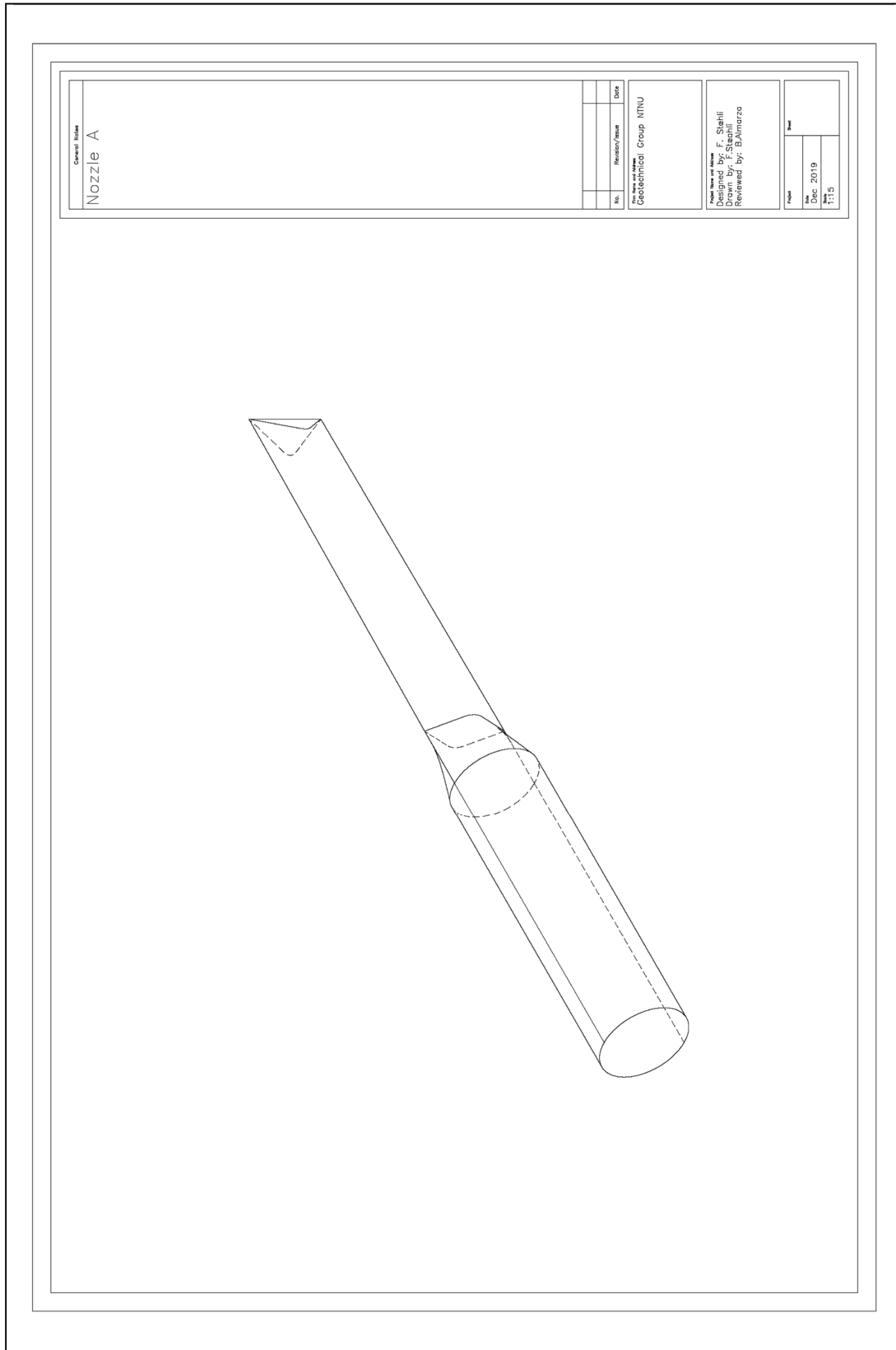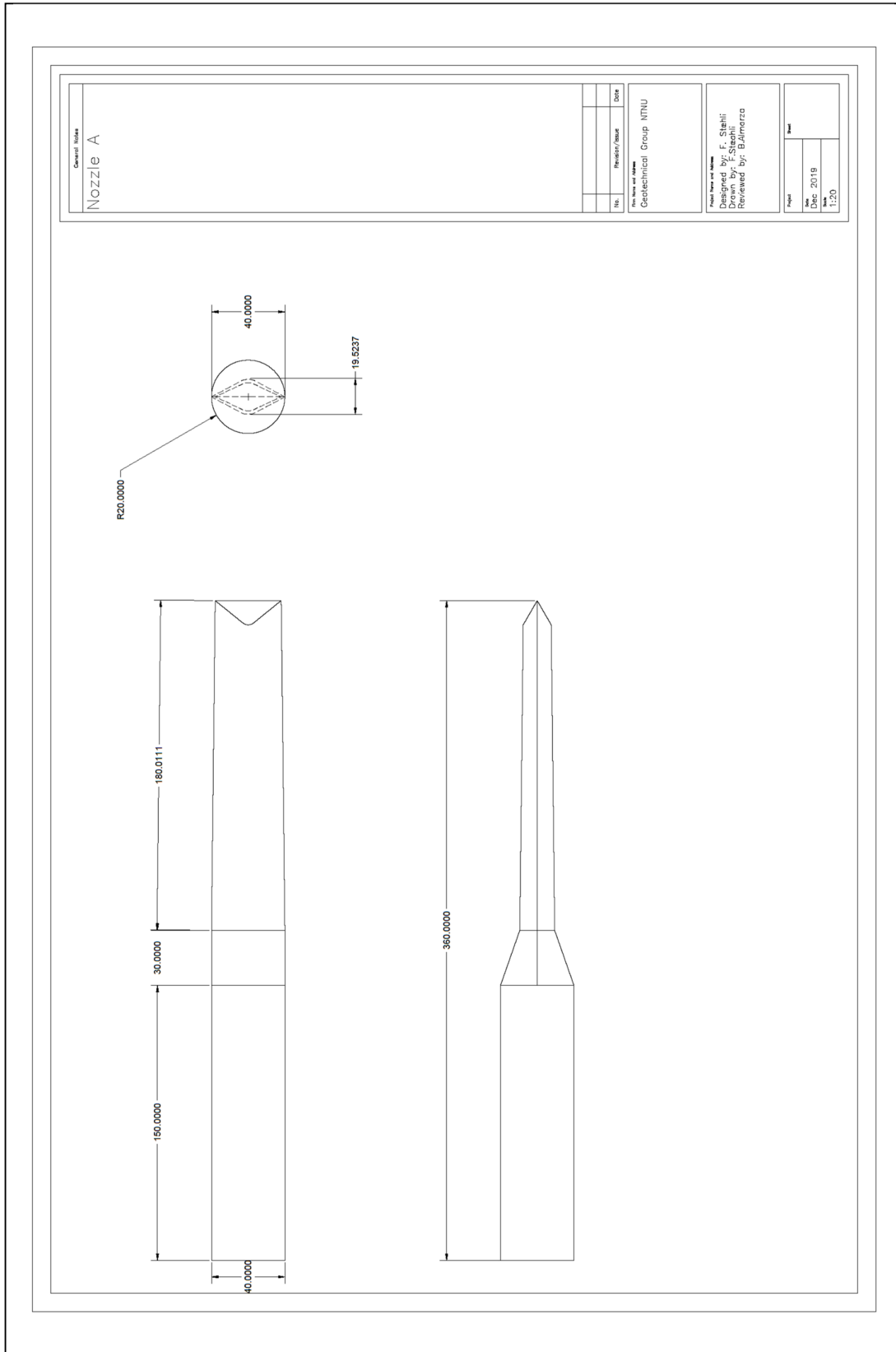*Figure D. 1 3D representation of injection nozzle A (thin spade)*

Figure D. 2 Views representation of injection nozzle A (thin spade)

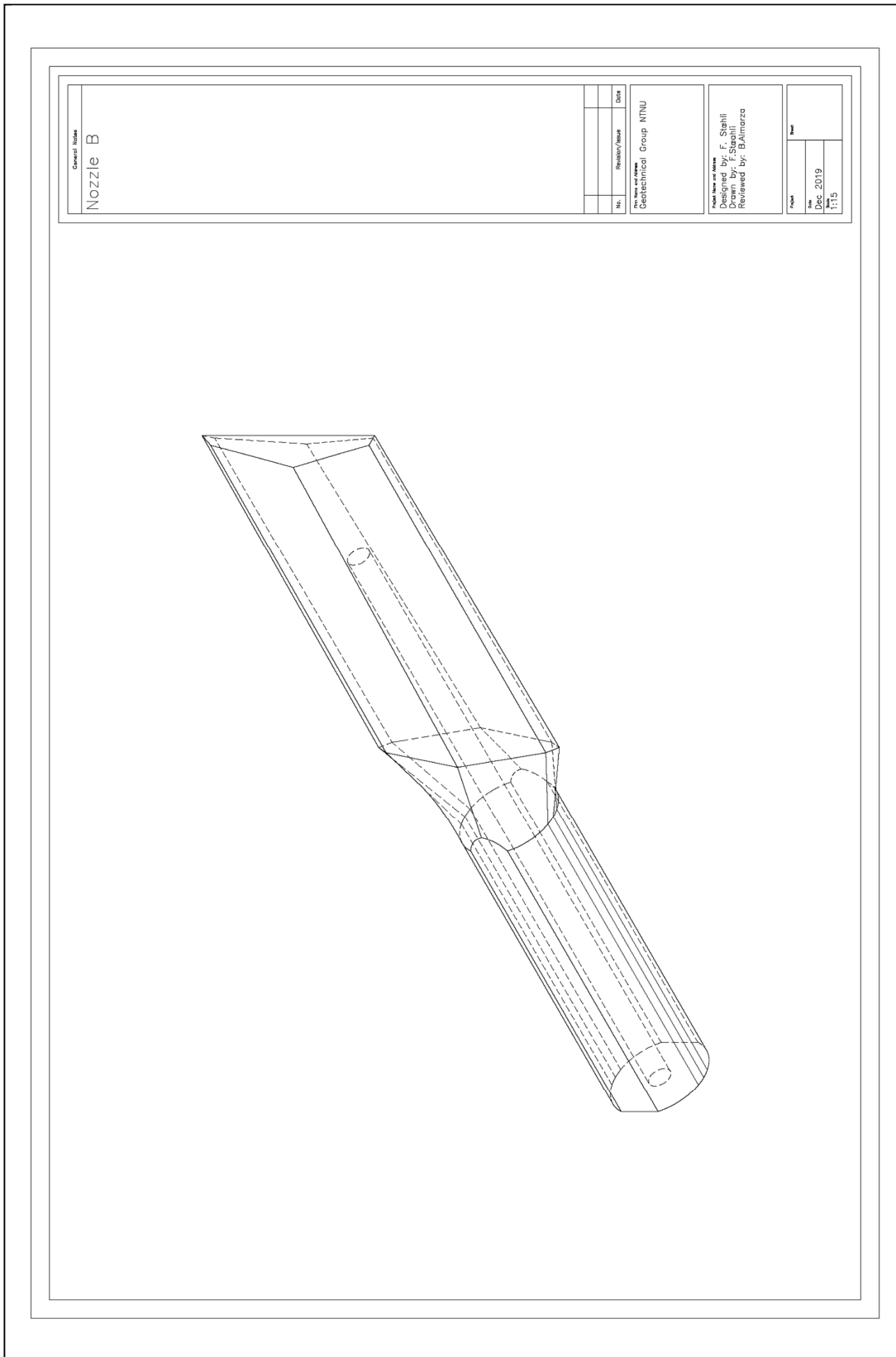*Figure D. 3 3D representation of injection nozzle B (wide spade)*

Figure D. 4 Views representation of injection nozzle B (wide spade)

Beatriz María Almarza Galdón

An evaluation of in situ measurement methods of K₀ in sensitive clays

NTNU
Norwegian University of
Science and Technology